

Copyright
by
Thomas A. Deetjen
2018

The Dissertation Committee for Thomas A. Deetjen
certifies that this is the approved version of the following dissertation:

**The benefits and challenges of renewables on the electric
grid and opportunities for systems integration and demand
side management**

Committee:

Michael E. Webber, Supervisor

Ross Baldick

Robert E. Hebner

Benjamin D. Leibowicz

**The benefits and challenges of renewables on the electric
grid and opportunities for systems integration and demand
side management**

by

Thomas A. Deetjen,

DISSERTATION

Presented to the Faculty of the Graduate School of
The University of Texas at Austin
in Partial Fulfillment
of the Requirements
for the Degree of

DOCTOR OF PHILOSOPHY

THE UNIVERSITY OF TEXAS AT AUSTIN

May 2018

Dedicated to my wife, Katie.

Thank you for your encouragement through all of the ups and downs
and your counsel through all of the decisions that brought us here.

You bless me each day with your wisdom, optimism, and faith.

Acknowledgments

I could not have completed this dissertation without the advice, input, troubleshooting, and brainstorming help from multiple people. Thanks to my adviser, Michael Webber, for your honesty, generosity, and candidness, and for providing me with opportunities to develop in so many ways beyond just learning how to perform robust academic research. Thanks to Jared Garrison for quickly orienting me to graduate school and helping me get started on a meaningful research trajectory. Thanks to Joshua Rhodes for your frequent feedback, editing, and brainstorming. Thanks to Kazunori Nagasawa, Scott Vitter, and Andrew Reimers for your camaraderie and collaborative spirit. Thanks to Ross Baldick and Benjamin Leibowicz for your career and research advice and to Bob Hebner for serving on my dissertation committee. Thanks to Matthias Huber and Henry Martin for your hospitality, collaboration, and candid European perspective. Thanks to Kevin Hanson, Doug Murray, and Paul Wattles for your helpfulness and responsiveness. Thanks to God for granting me some talents and some opportunities to apply them.

Thank you to the sponsors who funded my graduate research: the Electric Reliability Council of Texas, the U.S. Department of Energy, the National Science Foundation's Integrative Graduate Education and Research Traineeship, the Virginia and Ernest Cockrell, Jr. Endowed Graduate Fellowship in Engineering, and the University of Texas Graduate School. Thank you to my wife, Katie, for being the breadwinner of the family.

The benefits and challenges of renewables on the electric grid and opportunities for systems integration and demand side management

Publication No. _____

Thomas A. Deetjen, Ph.D.
The University of Texas at Austin, 2018

Supervisor: Michael E. Webber

Environmental policies, reduced manufacturing costs, and technology improvements have all contributed to the growing installation of wind turbines and solar photovoltaic arrays in the electric grid. While these new sources of renewable electrical power provide environmental and economic benefits to the electric grid, they also complicate the balancing of supply and demand required to reliably operate the grid. The seasonal, daily, and sub-hourly fluctuations in the energy output of wind and solar generators must be compensated by operating the existing power plant fleet more flexibly or by providing more flexible sources of electricity demand. This dissertation categorizes and quantifies this compensation by studying the “flexibility requirements” imposed by wind and solar generation, approximates the economically optimal capacities of regional wind and solar resources in the grid, and explores the ability of a central utility plant to add a flexible source of demand

to the electric grid system. These topics are covered in the four chapters described below.

Chapter 3 utilizes a unit commitment and dispatch (UC&D) model to simulate large solar generation assets with different geographic locations and orientations. The simulations show the sensitivity of the wholesale energy price, reserve market prices, total dispatch cost, fuel mix, emissions, and water use to changes in net load flexibility requirements. The results show that generating 22,500 GWh of solar energy in a 2011 simulation of the Electric Reliability Council of Texas (ERCOT) reduces total dispatch cost by approximately \$900 Million (a 10.3% decrease) while increasing ancillary services costs by approximately \$10 Million (a 3% increase). The results also show that solar PV reduces water consumption, water withdrawals, and CO₂, NO_x, and SO_x emissions. Installing sufficient solar panel capacity to generate that much electricity also reduces peak load by 4% but increases net load volatility by 40–79% and ramping by 11–33%. In addition, west-located, west-oriented solar resources reduce total dispatch cost more than the other simulated solar scenarios. The west-located, west-oriented solar simulation required greater system flexibility, but utilized more low-cost generators and fewer high-cost generators for energy production than other simulated scenarios. These results suggest that the mix of energy provided by different generation technologies influences the dispatch cost more than the net load flexibility requirements.

Chapter 4 develops a quantitative framework for calculating flexibility requirements and performs a statistical analysis of load, wind, and solar data from the Electric Reliability Council of Texas (ERCOT) to show how wind and solar capacity

impacts these grid flexibility requirements. Growing wind capacity shows only minor correlation with increasing flexibility requirements, but shows some correlation with ramp down rates and daily volatility in the net load. Growing solar capacity shows a direct correlation with increasing flexibility requirements if load patterns do not change. While adding 15.7 GW of wind power had only minor effects on system flexibility requirements, adding 14.5 GW of solar to the ERCOT grid increases maximum 1-hr ramp rates by 135%, 3-hr ramp rates by 30%, ramp factors by 140%, 1-hr volatility by 100%, and 1-day volatility by 30%. Wind and solar impact flexibility requirements at different times of the day: wind tends to intensify demand-driven flexibility events by ramping up energy production at night when demand is decreasing and ramping down energy production in the morning when demand is increasing, while solar tends to intensify flexibility requirements due to its quick changes in energy output driven by the rising and setting sun. Adding wind to a system with large amounts of solar does not tend to increase flexibility requirements except for the daily volatility. The geographic location and orientation of solar arrays also influences flexibility requirements, with fixed, southeast-facing panels providing a significant reduction. These results can inform strategies for managing the grid flexibility requirements created by growing renewable capacity.

Chapter 5 develops a model for calculating the optimal amount of transmission, wind, and solar capacity that should be built in a grid's different regions. It also presents a framework for choosing CO₂ prices by balancing increasing system cost and flexibility requirements with CO₂ emissions reductions. In a simulation of the ERCOT grid, the model suggests a 60 \$/ton CO₂ price and an optimal investment

of 27.0 GW of transmission capacity to five different regions. These regions install a total of 26.6 GW of wind and 11.1 GW of solar, representing a grid with about 60% thermal and 40% renewable capacity. This renewable mix produces 110 TWh of energy per year, 34% of the total electricity demand. The grid emits 82.2 million tons of CO₂ per year under this scenario, a 65% reduction from the 237 million tons produced when no renewable capacity is installed. At the optimal renewable development solution, all coal and natural gas boiler generators have capacity factors less than 20% with many of them not being dispatched at all. While these results are specific to ERCOT, the methods and model can be used by any grid considering renewable energy capacity expansion.

Chapter 6 develops a mixed-integer linear program for modeling the optimal equipment capacity and dispatch of a central utility plant (CUP) in a residential neighborhood and its ability to improve rooftop solar integration. The CUP equipment includes a microturbine, battery, chiller plant, and cooling storage. The CUP model is exposed to a variety of electricity rate structures to see how they influence its operation. The model finds the optimal capacity for each piece of CUP equipment, optimizing their hourly dispatch to meet neighborhood cooling and electric demand while maximizing profit. In an Austin, TX, USA base case, the neighborhood benefits economically by including the CUP, although the CUP demonstrates limited potential to integrate high penetrations of rooftop solar resources. While peak demand and reverse power flows are reduced under all tested rate structures, the CUP worsens net demand ramp rates. A time-of-use rate with no demand charge and moderate differences between off-peak and on-peak prices balances the output

parameters, reducing reverse power flows by 43%, peak demand by 51%, and annual cost by 9.1% versus the “No CUP” base case while limiting net demand ramp rate increase to 84% more than the base case.

Building a clean, resilient, and reliable electric grid for the future is a worthwhile endeavor that will require innovative supply-side and demand-side solutions for integrating the intermittent power output of renewable generation into the electric grid. As a cohesive document, this dissertation communicates the scale and severity of the flexibility requirements that will be required to operate systems with large amounts of wind and solar generation and explores one demand-side method for providing that needed flexibility. There are many opportunities to expand these analyses and explore new sources of grid flexibility in future work.

Table of Contents

Acknowledgments	v
Abstract	vi
List of Tables	xv
List of Figures	xviii
Chapter 1. Introduction	1
1.1 Purpose and motivation	1
1.2 Scope and organization	8
1.3 Major findings	10
Chapter 2. Background	13
2.1 Electric Reliability Council of Texas	13
2.2 Merit Order and Flexibility	14
2.2.1 Flexibility Requirement Calculations	20
2.2.1.1 1-Hour Ramp Rate	21
2.2.1.2 3-Hour Ramp Rate	21
2.2.1.3 Ramp Factor	22
2.2.1.4 Ramp Acceleration	22
2.2.1.5 1-Hr Volatility	23
2.2.1.6 1-Day Volatility	23
2.3 Literature Review	24
2.3.1 Grid-Integration of Solar	24
2.3.2 Influence of Renewable Generation on Flexibility Requirements	26
2.3.3 Wind and Solar Capacity Expansion	28
2.3.4 Microgrids for Renewable Energy Integration	31

Chapter 3. Solar PV integration cost variation due to array orientation and geographic location in the Electric Reliability Council of Texas	36
3.1 Methods	36
3.2 Results and Discussion	42
3.2.1 Prices and Total Dispatch Cost	43
3.2.2 Net Load Reduction	46
3.2.3 Net Load Flexibility Requirements	50
3.2.4 Generation by Generator Type	52
3.2.5 Emissions & Water Use	54
3.3 Conclusions	57
Chapter 4. The impacts of wind and solar on grid flexibility requirements in the Electric Reliability Council of Texas	61
4.1 Methods	61
4.1.1 Peak Output Calculation	62
4.1.2 Data Generation	63
4.1.3 Limitations	73
4.2 Results and Discussion	75
4.2.1 Wind and Solar Peak Output Comparison	76
4.2.1.1 1-Hr Ramp Rates	76
4.2.1.2 3-Hr Ramp Rates	79
4.2.1.3 Ramp Factors	80
4.2.1.4 1-Hr Volatility	86
4.2.1.5 1-Day Volatility	86
4.2.1.6 Section 4.2.1 Results Summary	89
4.2.1.7 Wind and Solar Confounding	93
4.2.2 Solar Array Orientation and Location Comparisons	99
4.2.2.1 Orientation Comparison	99
4.2.2.2 Location Comparison	100
4.3 Conclusions	103

Chapter 5. Modeling the optimal mix and location of wind and solar with transmission and carbon pricing considerations	107
5.1 Methods	107
5.1.1 System cost minimization theory	108
5.1.2 Transmission regions	111
5.1.3 Model optimization process	114
5.1.4 Economic costs and prices	117
5.1.5 Limitations	118
5.2 Results and discussion	120
5.2.1 Base case scenario	120
5.2.2 Model vs existing ERCOT renewables	129
5.2.3 CO ₂ price sensitivity	130
5.2.4 Minimum net load constraint sensitivity	139
5.2.5 Natural gas price sensitivity	139
5.2.6 Existing power plant capacity factors	141
5.3 Conclusions	144
Chapter 6. Optimal dispatch and equipment sizing of a residential central utility plant for improving rooftop solar integration	149
6.1 Model background	149
6.1.1 Neighborhood and solar models	152
6.1.2 Central utility plant equipment models	155
6.1.3 Electricity rate structures	168
6.1.4 CO ₂ emissions calculations	172
6.2 Optimization description	174
6.2.1 Linear program description	175
6.3 Results and discussion	176
6.4 Conclusions	186

Chapter 7. Summary	189
7.1 Solar PV integration cost variation due to array orientaiton and geographic location in the Electric Reliability Council of Texas	190
7.2 The impacts of wind and solar on grid flexibility requirements in the Electric Reliability Council of Texas	190
7.3 Modeling the optimal mix and location of wind and solar with transmission and carbon pricing considerations	191
7.4 Optimal dispatch and equipment sizing of a residential central utility plant for improving rooftop solar integration	191
7.5 Overall considerations	192
7.6 Future work	193
Appendices	195
Appendix A. Statistical Tables for Chapter 4	196
Appendix B. Interest Rate Sensitivity Figures for Chapter 5	199
Bibliography	202

List of Tables

3.1	Input data used to generate the solar PV hourly generation curves for the different scenarios. All parameters were set to the default values except the weather data set and array azimuth.	40
3.2	The results for each of the four 8,760-hour UC&D simulations of the ERCOT electricity market are shown below. The information is categorized into smaller tables corresponding to each of the “Results & Discussion” sub-sections in this report.	44
4.1	Different data sets acquired from ERCOT and the National Renewable Energy Laboratory (NREL) [130] were used to create the “Model Data” described in this table.	65
4.2	Since portions of the data are created by connecting December 31 to January 1 of the same year, discontinuities will arise, as shown here for the load. The discontinuity between the actual load at 12/31 23:45 and 1/1 0:00 leads to an artificial ramp rate of -2,792 MW/15min. Adjusting the load to the indicated values removes the artificial ramp rate and creates continuity between the data.	66
4.3	The installed solar capacity increases according to the top portion of this table. The bottom portion of this table describes the different solar location and orientation scenarios used for comparison in this study.	66
4.4	Solar data from 19 different cities is used in this study [130]. The solar profile for each “location comparison” scenario is built from the indicated fractions of each city’s solar profile.	67
4.5	The results for Section 4.2.1 are summarized in this table.	94
4.6	The statistical distribution for each flexibility requirement and orientation scenario is shown below. Dark green and dark red cell shading indicates when a the absolute value of a cell is 20% less or more than the average value of the six scenarios. Light green and light red cell shading indicates when a the absolute value of a cell is 10% less or more than the average value.	101

4.7	The statistical distribution for each flexibility requirement and location scenario is shown below. Dark green and dark red cell shading indicates when a the absolute value of a cell is 20% less or more than the average value of the three scenarios. Light green and light red cell shading indicates when a the absolute value of a cell is 10% less or more than the average value.	102
5.1	During the first optimization step, the model extends 500 MW of transmission to each of the 15 regions and finds the wind and solar capacity for each region that will minimize system cost. Based on these optimization results, the model will choose to build transmission to the region that reduces system cost the most (“11 Big Bend” in this example, highlighted green). The model repeats this process until adding 500 MW of new transmission to the grid can no longer reduce system costs.	116
5.2	Table of annualized capital costs used in the model.	118
5.3	Table of fuel and CO ₂ prices used in the base case model.	118
5.4	Uncertainty analysis showing alternate solutions to the base case scenario.	128
5.5	A model solution approximating ERCOT’s existing renewable capacity build-out (column 2) is compared with a model solution run from scratch (column 3). Each solution uses a 0 \$/ton CO ₂ price, 2,750 \$/kW solar capital costs, and a 15 \$/MWh wind production tax credit in addition to the base case market conditions.	131
6.1	Nomenclature: Exogenous Variables	150
6.2	Nomenclature: Decision Variables	151
6.3	Data summary for the Austin, TX neighborhood case study with 750 houses and 1.2 MW solar.	153
6.4	CUP operation and efficiency equations.	157
6.5	CUP capital cost and the operation and maintenance (O&M).	157
6.6	Rate structures with demand charges are created by lowering the energy price of a medium TOU rate and introducing a demand charge. A 1 MW constant load will pay the same annual cost under each rate structure.	172
6.7	Linear program constraints	177
6.8	Results for optimal CUP operation under flat, time-of-use (TOU), and real-time-price (RTP) electricity rate structures (see Section 6.1.3).	178
6.9	Results for 1.2 MW solar under different demand charges.	183

A.1 The following table shows the maximum, 95th percentile, median, 5th percentile, and minimum values for each flexibility requirement over each year. 197

A.2 The following table shows the maximum, 95th percentile, median, 5th percentile, and minimum values for each flexibility requirement over each year if wind generation is removed from the analysis. 198

List of Figures

1.1	Aggregated demand for a 750-house neighborhood in Austin, TX, USA on August 14, 2015. Solar and cooling contribute to high peak demand, and steep net demand ramp rates (changes in the net demand in MW/hr).	5
1.2	Aggregated demand for a 750-house neighborhood in Austin, TX, USA on October 26, 2015. Solar and cooling contribute to reverse power flow (negative net demand), and steep net demand ramp rates (changes in net demand in MW/hr).	6
2.1	Wind resources in Texas are strongest in the northwest part of the state with some strong resources in the central-west as well [128]. . .	15
2.2	Solar resources in Texas are strongest in the west part of the state and generally degrade to the east [128].	15
2.3	The merit order curve sorts an electricity market’s power plants by their marginal cost, visualizing how the power plants with least expensive marginal cost will be dispatched first. Zero-marginal-cost resources (wind, solar, water) are added to the front of the merit order curve, pushing thermal generators (nuclear, coal, natural gas) later in the order. This shift reduces wholesale prices. This figure shows an example of how 15 GW of renewable generation might reduce wholesale market prices from 50 \$/MWh to 35 \$/MWh.	17
2.4	Projected demand, wind, and solar data for June 19, 2022 in the ERCOT electric grid. Changes in the net demand can be quantified using the flexibility requirement calculations described in Section 2.2.1.	18
3.1	The normalized generation curves for the three different solar scenarios show the typical variation in the timing of their electricity generation during the course of a summer day. The East and West scenarios peak approximately three hours apart from each other and represent the bounds of solar generation timing in ERCOT [129].	38
3.2	This figure shows the State of Texas with the ERCOT boundary shaded in blue. The cities associated with the East, South, and West scenarios are indicated.	40
3.3	The monthly energy output of the different arrays is influenced by seasonal shifts in weather and the sun’s path through the sky as well as the installed capacity of the arrays.	42

3.4	The monthly price averages and standard deviations change depending on the solar scenario. Solar tends to increase monthly price standard deviation in the winter and decrease it in the summer. It also decreases energy prices more in the summer than in the winter.	47
3.5	Each solar scenario reduces the monthly total dispatch cost when compared to the No Solar scenario. Summer months see more savings due to greater solar output and the alignment of solar generation with peak demand.	48
3.6	The net load duration curve with insets magnifying the highest and lowest net load values shows the number of hours per year experienced at different net loads by each scenario. During the highest net load hours of the year, the West net load is generally smaller than the South net load which is smaller than the East net load. However, all three solar scenarios have similar maximum net loads for the year. During the lowest net load hours of the year, the West net load is larger than the South net load which is larger than the East net load.	49
3.7	These charts show each scenario’s hourly fuel mix during a typical summer day. The net load is represented by the bottom of the wind generation area. The “duck curve” is not as apparent during the summer season when solar generation is aligned with peak demand.	53
3.8	These charts show each scenario’s hourly fuel mix during a typical spring day. The net load is represented by the bottom of the wind generation area. The “duck curve” manifests itself in ERCOT during the shoulder seasons when there is abundant spare capacity. ISOs have expressed concern about accommodating the steep evening ramp rates shown here.	55
3.9	The top two charts show the hourly output of natural gas combined cycle (NGCC) and open cycle gas turbine (OCGT) generators averaged over the year for each scenario. The bottom two charts show the annual average hourly dispatch of a solar scenario minus the annual average hourly dispatch of the No Solar scenario where negative values indicate hours of the day when the generator category is being dispatched less than in the No Solar scenario.	56
4.1	Growth of the wind and solar peak output can be organized into the 2008–2015 “wind era” and the 2016–2025 “solar era”.	63
4.2	This chart shows the net load for each 15-minute interval, averaged over all the days in January for each year. January exhibits the two-peak net load often seen during the winter and shoulder season months in ERCOT. The years 2008 to 2015 are a period of rapid growth in wind capacity. From 2016–2025, as more solar is added to the grid, it generates power from 8:00 to 18:00, reducing the net load and creating steep ramp rates as the sun rises and sets.	68

4.3	The net load is shown for each 15-minute interval on February 8th of each year after 2016, when solar capacity begins to trend upward. These profiles strongly exhibit the tendency for solar generation to increase the ramping and volatility of the net load as discussed later in this study.	69
4.4	This chart shows the net load for each 15-minute interval, averaged over all the days in June for each year. June exhibits the dramatic single-peak net load seen during the summer months in ERCOT where peak net load is driven significantly by air conditioning demand. The years 2008 to 2015 are a period of rapid growth in wind capacity. From 2016–2025, as more solar is added to the grid, it generates power from 6:30 to 18:30, reducing the net load and creating steep ramp rates as the sun rises and sets.	70
4.5	This chart shows load, wind, and solar capacity factors averaged over the months of January (winter), April (shoulder season), and August (summer). Peak demand, wind output, and solar output are 80.0, 13.1, and 11.1 GW, respectively.	72
4.6	The 1-hr ramp rate becomes wider as the solar peak output increases while remaining relatively centered on 0 MW/hr.	77
4.7	The small changes in median 1-hr ramp rate do not appear to be correlated with season or year, remaining relatively centered on 0 MW/hr.	77
4.8	The maximum 1-hr ramp rate increases with solar peak output, especially between November and April.	78
4.9	The median 1-hr ramp rate does not appear to be correlated with wind or solar peak output.	78
4.10	The maximum 1-hr ramp rate appears to be positively correlated with peak solar output, while the first additions of wind peak output might have slightly reduced the maximum.	78
4.11	The minimum 1-hr ramp rate worsens slightly with increasing wind and solar peak output.	79
4.12	The 3-hr ramp rate becomes wider as the solar peak increases while shifting slightly towards the right.	80
4.13	The median 3-hr ramp tends to be greater during the shoulder seasons and less during the summer and winter. Increased solar peak output appears to increase the summer median and reduce the winter and spring median.	81
4.14	Increased wind peak output appears to increase maximum 3-hr ramp rates during the summer. Increased solar peak output appears to increase maximum 3-hr ramp rates from November through April.	81

4.15	The median 3-hr ramp rate does not show a strong correlation with wind peak output, and appears to increase slightly with initial increases in solar peak output.	82
4.16	The maximum 3-hr ramp rate increases with wind peak output, especially at higher wind penetrations, and increases slightly with solar peak output.	82
4.17	The minimum 3-hr ramp rate worsens steadily with increasing wind peak output and slightly with increased solar output.	82
4.18	The ramp factor distribution becomes wider as the solar peak increases while shifting towards the left.	83
4.19	The median ramp factor tends to be greater during April–June and September–November. Increased wind peak output appears to slightly increase the median in the summer while increased solar peak output tends to reduce it.	84
4.20	Maximum ramp factors are lowest in the summer when large amounts of online generation can more easily handle ramping from the net load. Increasing solar peak output increases the ramp factor, especially from October–May where ramp factors can reach over 0.20.	84
4.21	The median ramp factor tends to increase with wind peak output and decrease with solar peak output, though it doesn’t stray far from 0.00.	85
4.22	The maximum ramp factor tends to decrease slightly with wind peak output and increase with solar peak output.	85
4.23	Increasing solar peak output widens the 1-hr volatility density curve and shifts it to the right.	87
4.24	Wind does not show a strong correlation with the median 1-hr volatility, while adding solar tends to increase it.	87
4.25	Increased solar peak output strongly correlates with increased maximum 1-hr volatility, especially from February through August. Note 2011, an outlier year, which shows strong maximum 1-hr volatility.	88
4.26	Increased wind peak output does not correlate strongly with the median 1-hr volatility except at high penetrations. In the 9,500+ MW wind peak output range, a small amount of solar peak output (150-1,000 MW) might contribute to the sharp increase in median 1-hr volatility. Additional solar peak capacity slightly increases the median 1-hr volatility.	88
4.27	Wind does not appear to be correlated with maximum 1-hr volatility except at high penetrations, while peak solar output shows a strong direct relationship.	89
4.28	Increasing solar peak output widens the 1-day volatility density curve and shifts it to the right.	90

4.29	Increased solar peak output tends to raise the median 1-day volatility, especially from February through September.	90
4.30	Increased solar peak output strongly correlates with increased maximum 1-day volatility, especially from January through September. Note 2011, an outlier year, which shows strong maximum 1-day volatility.	91
4.31	Increased wind peak output does not correlate strongly with the median 1-day volatility except at high penetrations. In the 9,500+ MW wind peak output range, a small amount of solar peak output (150-1,000 MW) might contribute to the sharp increase in median 1-day volatility. Additional solar peak capacity increases the median 1-day volatility. .	91
4.32	Wind does not appear to be correlated with maximum 1-day volatility except at high penetrations, while peak solar output shows a strong direct relationship.	92
4.33	As solar capacity increases, the timing of the maximum 1-hour ramp rate shifts from the morning (6:00–9:00, driven by increasing demand and decreasing wind output) to the evening (17:00–19:00, driven by decreasing solar output) especially between November and March when lower demand contributes less to net demand ramp rates.	95
4.34	As solar capacity increases, the timing of the minimum 1-hour ramp rate shifts from the evening (21:00–23:00, driven by decreasing demand and increasing wind output) to the morning (8:00–10:00, driven by increasing solar output) from November through March.	95
4.35	As solar capacity increases, the timing of the maximum 3-hour ramp rate shifts from the morning (5:00–8:00, driven by increasing demand and decreasing wind output) to the evening (17:00–19:00, driven by decreasing solar output) from November through March. Maximum 3-hour ramp rates from May through October continue to occur in the late morning, driven by increasing demand.	96
4.36	As solar capacity increases, the timing of the minimum 3-hour ramp rate shifts from the evening (22:00–24:00, driven by decreasing demand and increasing wind output) to the late morning (9:00–11:00, driven by increasing solar output) from November through March. Minimum 3-hour ramp rates from April through November continue to occur in the late evening, driven by decreasing demand and increasing wind output.	96
4.37	As solar capacity increases, the timing of the maximum 1-hour volatility shifts from occurring throughout the day to occurring during the evening (17:00–18:00, driven by decreasing solar output).	97
4.38	Comparison of annual maximum and minimum flexibility requirements in all-solar and solar-plus-wind systems.	98

5.1	“Thermal Cost” is the integral of the merit order curve bounded by the net load. Renewable generation pushes the merit order curve to the right, reducing the thermal cost.	109
5.2	The regions of ERCOT are designed according to Section 5.1.2. The underlying population density map (green - sparsely populated to red - densely populated) indicates the approximate location of the loads. The five “Competitive Renewable Energy Zones” (CREZ) used by ERCOT in their own transmission expansion planning are bubbled in for comparison.	113
5.3	This flow chart visualizes the model optimization process described in Section 5.1.3.	115
5.4	Transmission investments in the base case scenario are split among five different regions, with three regions receiving the majority of the investment.	121
5.5	Each region that is connected to the transmission network has unique wind and solar generation profiles, and installs the amount of renewable energy capacity that minimizes system cost.	121
5.6	Each region that is connected to the transmission network has a unique wind and solar generation profiles, and installs the mix of wind and solar capacity that minimizes system cost.	122
5.7	The transmission, wind, and solar investments are distributed among different regions in the ERCOT grid. Each region contributes to reducing system costs based on its unique renewable profiles and capacities as wind and solar resources vary throughout Texas.	123
5.8	This figure shows capacity factors for an average day in August. While the interaction between these regions is nuanced, this figure suggests that the model develops regions that produce large amounts of energy during the peak load hours (12:00–20:00) and that complement each other’s minimum and peak output (especially evident from 6:00–12:00).	124
5.9	As transmission and renewables are invested in, system costs fall as falling thermal costs offset rising capital costs until the minimum system cost is reached.	125
5.10	Curtailment occurs when too much renewable energy is being generated to meet the line capacity and/or minimum net load constraints. The model chooses wind and solar capacities that balance the disadvantages of curtailment with the benefits of having greater renewable generation during periods when curtailment is not binding.	126
5.11	As more renewable capacity is installed, traditional thermal generators are pushed higher up in the merit order and are utilized less often, reducing CO ₂ emissions throughout ERCOT.	126

5.12	As the CO ₂ price rises, the marginal cost of any CO ₂ emitting generators increases, and the thermal and system costs increase as a result.	132
5.13	Adding even a small CO ₂ price to the market greatly reduces CO ₂ emissions, while large prices have a diminishing return. For reference, the model calculates 237 million tons of CO ₂ emissions with no renewables and a 0 \$/ton CO ₂ price.	132
5.14	The comprehensive system cost at a 100 \$/ton social price of CO ₂ experiences diminishing reductions at higher CO ₂ prices.	133
5.15	Even at a 250 \$/ton social price of CO ₂ , higher CO ₂ prices tend to have diminishing returns on reducing the comprehensive system cost.	133
5.16	Increasing CO ₂ price causes (a): more wind and solar capacity, (b): larger capital and CO ₂ cost, but lower thermal cost, and (c): lower CO ₂ emissions and comprehensive system cost, but higher system cost.	134
5.17	Increasing CO ₂ price changes the regions the model chooses to invest in, and the optimal wind/solar mix in those regions.	135
5.18	As the CO ₂ price increases and more renewables are built, the annual peak net load is reduced as well. CO ₂ prices higher than 70 \$/ton have a diminishing effect on reducing the peak net load.	137
5.19	The maximum 1-Hour Ramp Rate is relatively consistent for lower CO ₂ prices, but begins increasing for prices of 70 \$/ton and higher.	137
5.20	The maximum 3-Hour Ramp Rate is greatest for CO ₂ prices of 30, 40, and 70+ \$/ton.	138
5.21	The maximum 2-Hour Volatility is relatively consistent for lower CO ₂ prices, but begins increasing for prices of 60 \$/ton and higher.	138
5.22	Increasing the minimum load constraint causes (a): lower flexibility requirements, (b): less wind and solar capacity, (c): larger thermal and CO ₂ cost, but lower capital cost, and (d): higher CO ₂ emissions and system cost.	140
5.23	Increasing the natural gas price causes (a): more wind and solar capacity, (b): larger thermal and capital cost, but lower CO ₂ cost, and (c): higher system costs and lower CO ₂ emissions (up to 7.00 \$/MMBtu).	142
5.24	At a CO ₂ price of 60 \$/ton and 0.0 GW of transmission to renewable energy regions, all of the demand is met by the existing generator fleet. Most of the generators are dispatched during the year, with 36 GW of capacity experiencing a 40% or better capacity factor.	143
5.25	At a CO ₂ price of 60 \$/ton and 27.0 GW of transmission at the optimal solution, less of the demand is met by the existing generator fleet. Only 24 GW of the existing generator fleet experiences a 40% or better capacity factor.	143

5.26	A CO ₂ price of 60 \$/ton creates a merit order curve that dispatches natural gas combined cycle generators (left) before a coal and less-efficient natural gas generators (right).	144
5.27	At a CO ₂ price of 20 \$/ton and 17.0 GW of transmission at the optimal solution, 30 GW of the existing generator fleet experiences a 40% or better capacity factor.	145
5.28	A CO ₂ price of 20 \$/ton begins to move coal power plants higher up the merit order curve in favor of cleaner natural gas combined cycle generators. Coal still has a lower marginal cost than natural gas boilers and simple cycle generators.	145
5.29	At a CO ₂ price of 100 \$/ton and 33.0 GW of transmission at the optimal solution, only 20.5 GW of the existing generator fleet experiences a 40% or better capacity factor.	146
5.30	A CO ₂ price of 100 \$/ton moves coal power plants towards the end of the merit order. Their CO ₂ emissions are too large to justify their dispatch at such a high CO ₂ price.	146
6.1	Daily sums for the 750-house neighborhood model with 1.2 MW solar.	153
6.2	Hourly ambient temperature in Austin, TX, USA in 2015.	154
6.3	CUP flowchart. A microturbine, battery, chiller plant, and CTES system comprise a CUP that acts as an intermediary between the electric grid and the neighborhood's electric demand, cooling demand, and solar generation.	156
6.4	Manufacturer data indicate a lack of correlation between rated capacity and rated efficiency for microturbines in the 0 to 4 MW capacity range.	159
6.5	Microturbine normalized fuel consumption versus normalized electrical output under part-load operation. Results from Malinowski [117], Ismail [99], Milan [121], and Gilette [73] support a linear relationship between fuel consumption and electrical output.	160
6.6	Data indicate a lack of correlation between rated capacity and rated COP for air-cooled chillers of various models and sizes manufactured by the Trane corporation [172].	164
6.7	Data support a one-to-one relationship between part-load chiller cooling output and power demand [173].	165
6.8	Chiller COP varies directly with ambient temperature [173] and whether the chiller is in cooling or ice-making mode [97].	166
6.9	A rudimentary design for the neighborhood chilled water distribution system using design guidelines from [165] helps estimate the capital cost of the piping network at \$2.9 Million.	168

6.10	Energy only rate structures for electricity purchased during peak season (June 1–September 30). Real time prices vary hourly, based on the historic wholesale market.	170
6.11	Energy only rate structures for electricity purchased during off-peak season (October 1–May 31). Real time prices vary hourly, based on the historic wholesale market.	171
6.12	Hourly wholesale prices for the ERCOT market, 2015.	173
6.13	Dispatch of the CUP equipment for August 14, 2015, one of the hottest days of the summer (see Fig 1.1). The “Electric Grid” series is equivalent to the net demand.	181
6.14	Dispatch of the CUP equipment for October 26, 2015, a day where solar output exceeds total neighborhood demand and should lead to reverse power flow (see Fig 1.2). The “Electric Grid” series is equivalent to the net demand.	182
6.15	Sensitivity of the results to demand charges. “No CUP” is the neighborhood at flat energy rates and no CUP. “Demand 0” through “Demand 4” are TOU energy rates with increasing demand charges as shown in Table 6.6.	184
6.16	Hours per year that each CUP component spends at different output levels under the Medium TOU scenario. While the microturbine seldom operates at low part-loads, the chiller plant regularly operates at low output. An actual CUP design might use multiple chiller units to achieve the dispatch schedule in these results.	186
B.1	Annual system cost for different capital investment interest rates. . .	199
B.2	Annual CO ₂ emissions for different capital investment interest rates. .	200
B.3	Comprehensive system cost at a 100 \$/ton social price of CO ₂ for different capital investment interest rates.	200
B.4	Renewable capacity installed for different capital investment interest rates.	201

Chapter 1

Introduction

1.1 Purpose and motivation

Wind and solar generation offer opportunities to provide clean, domestic, and affordable power in the future [140]. Driven by environmentally-minded regulations, such as the United States' Production Tax Credit and Investment Tax Credit (PTC & ITC) [31] or the European Commission's 2020 climate and energy package [36], the installed capacities of wind and solar are on the rise globally [18]. Many of these policies, including the EU 2020 and renewable portfolio standards (RPS) in many states in the U.S., have specific goals for renewable energy capacity development, either in terms of actual capacity or percentage of annual energy production. However, these goals seldom consider how renewable generation will influence the flexibility and reliability of the electric grid, where new renewable generation and transmission capacity should be installed, or which technologies and strategies can be used to integrate renewable resources into the grid. This dissertation explores each of these questions to improve our understanding of renewable integration issues and explore technology and policy solutions for improving them.

The variability and timing of renewable energy generation can make its output difficult to balance and integrate [21, 111]. These variability and timing issues exac-

erbate “flexibility requirements”, such as ramp rates (the change in net demand over a period of time) [90, 91]. Flexibility is normally provided by dispatchable thermal power plants and ancillary services [91]. Requiring greater flexibility from the grid can cause increased cycling and ramping at power plants, inflating system costs [38]. It can also increase the need for operating reserves [53] and can reduce the stability of the grid’s frequency and voltage [10].

Independent System Operators (ISOs) are especially concerned with accommodating over-generation and increased ramping requirements from solar generation as illustrated by the California ISO experience with the so called “duck curve” (where low net loads are followed by steep ramp rates) [21] and Germany’s experience with widespread negative wholesale prices [76]. These experiences illustrate how existing electricity markets might struggle to provide the operational flexibility required for the successful integration of renewable generation. The view that renewable generation can reduce the total dispatch cost and environmental impacts of the electric grid must be considered in context with the understanding that increasing wind and solar capacities might also bring integration costs, grid-balancing challenges, and stability issues.

Moreover, these issues cannot be effectively studied without considering how the geographic location of renewable energy resources influences their generation profiles. Wind and solar generation produce electricity intermittently depending on wind speed and solar radiation. Thus, different climates and seasons will experience different generation profiles, and the generation timing for different locations in an electric grid will also vary. Whether these generation profiles coincide with the load

and with each other influences grid flexibility requirements and the market value of that wind and solar resource [188].

While a geographically-sensitive understanding of utility-scale wind and solar generation can help grid operators anticipate future flexibility requirements, it is also valuable to understand renewable energy integration issues at the distribution level, particularly in reference to rooftop solar generation in residential neighborhoods. Three issues deserve special attention. First, when distributed solar generation exceeds local demand, it reverses power flow toward the substation and can create control and protection problems at the transformer [16]. Reverse power flow also incurs losses at the transformer and power lines [103] and requires additional distribution hardware and controls for managing reactive power and voltage regulation [109]. In response, many utilities are moving towards rate structures that will reduce compensation for selling excess solar generation to the grid [16].

Second, since maximum solar output is not always coincident with peak demand, solar capacity does little to reduce local peak demand [38] and, thus, contributes to the under-utilization of grid infrastructure. Electric grids are built to handle a peak system demand that seldom occurs, leaving some of the grid's infrastructure sitting idle for much of the year. In the Electric Reliability Council of Texas (ERCOT, the system operator of the electric grid covering about 90% of Texas' population), for example, the annual utilization (average demand/peak demand) is just 55%, and only 1,000 hours each year exceed 75% of the peak demand [59]. Adding more solar, which reduces average demand without strongly influencing peak demand, can reduce the capital investment efficiency of an already over-built

infrastructure.

Third, as solar output ramps up and down with sunrise, sunset, and cloud cover variation, net demand ramp rates can be quite steep in local grids. Large ramp rates in distribution networks increase the need for flexibility both locally and in the bulk transmission grid, which can further exacerbate power plant cycling and ramping, ancillary service shortages, and grid stability issues.

These adverse, solar-related effects can be even more pronounced for residential neighborhoods, where solar penetration can be quite high [11], and in cooling-dominated climates, where cooling demand creates strong diurnal demand spikes. For example, Figs 1.1 and 1.2 show the August 14 and October 26, 2015, aggregated electricity demand for a 750-house neighborhood in Austin, Texas, USA, with 1.2 MW of rooftop solar (approximately 30% penetration). These figures show the influence of solar and cooling on the net demand (demand minus solar). Solar does little to reduce peak demand, creates steep net demand ramp rates (derivative of the net demand in MW/hr), and can create reverse power flow (negative net demand).

Improving these issues in residential neighborhoods would benefit the whole grid, especially in systems like ERCOT where over 50% of the annual peak demand comes from the residential sector [149]. Specifically, residential distribution feeders could add value to the grid by selling less power (decreasing their reverse power flows), lowering their peak demand (reducing infrastructure needs), and decreasing their ramp rates (simplifying reliable grid operation).

While many strategies aim to improve these issues for individual houses [152],

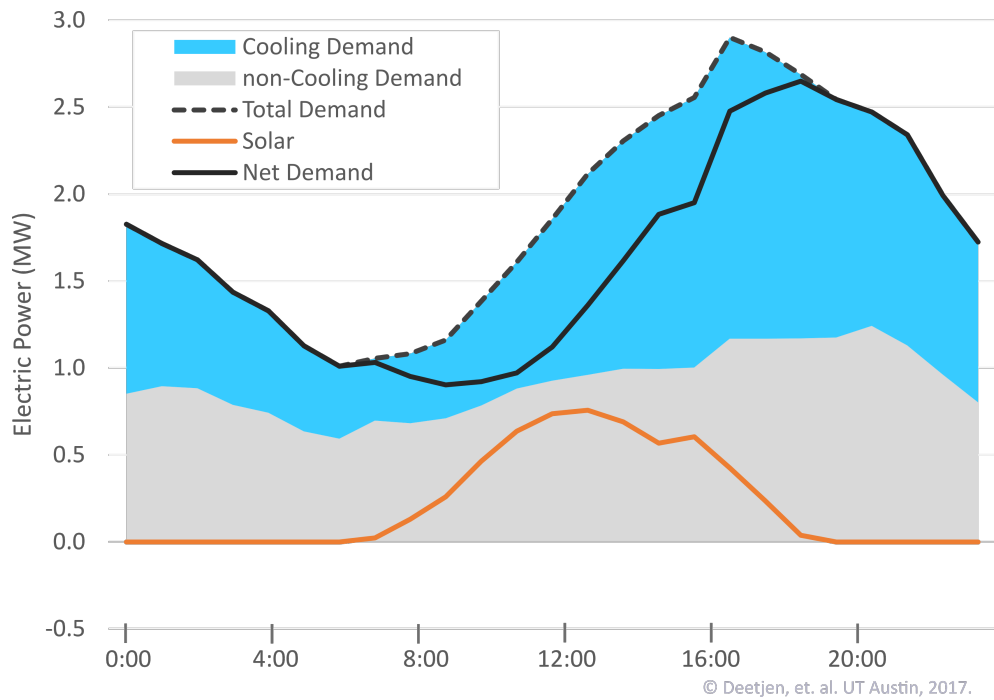


Figure 1.1: Aggregated demand for a 750-house neighborhood in Austin, TX, USA on August 14, 2015. Solar and cooling contribute to high peak demand, and steep net demand ramp rates (changes in the net demand in MW/hr).

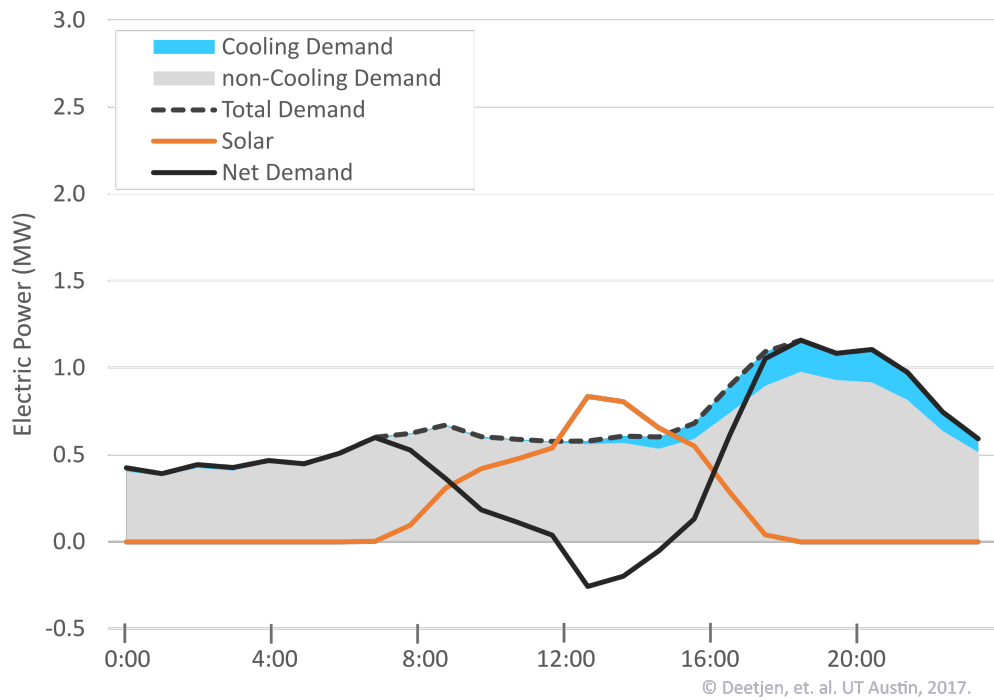


Figure 1.2: Aggregated demand for a 750-house neighborhood in Austin, TX, USA on October 26, 2015. Solar and cooling contribute to reverse power flow (negative net demand), and steep net demand ramp rates (changes in net demand in MW/hr).

it can be more effective to coordinate multiple loads simultaneously [25]. This coordination can be achieved by virtually organizing the behavior of load, generation, and storage resources spread across the electric grid. Examples include demand response, where a regulator uses price or command signals to influence load shifting, or energy aggregation, where a community of distributed resources act collaboratively to appear as a single power plant or load to the grid operator [139]. Alternatively, the coordination of multiple loads can be achieved by physically connecting them via a microgrid or central utility network, where electricity, cooling, and heating are produced in a central plant and delivered to multiple buildings via local infrastructure.

Central utility networks have been implemented in commercial and industrial settings such as hospitals [132] and university campuses [167], and could be applied in a residential setting. Compared to using small equipment at individual buildings, a central utility plant (CUP) can take advantage of economies of scale resulting in lower operation and maintenance cost [132]. Though these operational benefits are the primary reason for constructing a CUP, there is growing interest in the added benefit of using CUPs for providing grid services that improve the flexibility of the electric grid and the integration of renewables [167].

In summary, wind and solar generation require greater system flexibility to maintain stability in both local distribution networks and larger transmission grids. Traditional strategies, such as ancillary services and the flexible operation of the dispatchable power plant fleet, can provide some flexibility at the transmission level. Energy aggregation and centralized utility services in the residential sector can pro-

vide transmission-level grid services while also improving rooftop solar integration at the local level.

1.2 Scope and organization

This dissertation explores these topics in four chapters addressing the following objectives:

- *Objective 1: Explore the effects of adding large amounts of solar generation to the grid and assess the importance of array orientation and geographic location.* Chapter 3 contributes to the growing area of research on the grid-integration of renewable energy by providing a holistic study of how generator dispatch, system flexibility requirements, environmental considerations, and market dispatch costs are influenced by the orientation and geographic location of solar generation assets. The information in this study can encourage utilities, grid operators, and other entities involved with influencing the development of the electric grid to develop renewable energy portfolios, tax incentives, and investment plans that consider the comprehensive costs of integrating solar into the grid.
- *Objective 2: Determine how growing wind and solar capacities correlate with increasing flexibility requirements.* Chapter 4, in response to a lack of consensus in the existing literature [113], illustrates a framework for quantifying flexibility requirements by analyzing the correlation of increasing wind and solar generation with grid flexibility requirements in ERCOT. The trends discussed in this

study are intended to provide meaningful insight for grid planners as they anticipate the growth of renewable energy resources and the strategies they should implement to maintain reliability and manage integration costs. This insight is especially valuable for grids with rapid penetrations of renewables already underway or looming, such as Germany, China, Australia, Ireland, ERCOT, and many others.

- *Objective 3: Project the amount of wind and solar capacity that should be installed in different regions of the electric grid.* Chapter 5 builds a model that recommends the optimal investment of wind, solar, and transmission capacity in the different regions of an electric grid and develops a framework for balancing system costs, flexibility requirements, and CO₂ emissions. Improving over existing capacity expansion models that tend to develop wind and solar based on their capacity factors alone, this model values regional wind and solar resources based on their time coincidence with the load and with the renewable energy profiles of other grid regions as well as considering the available export capacity of the region's transmission infrastructure. This analysis uses ERCOT as a demonstration case, but its methods are applicable to other grids.
- *Objective 4: Analyze opportunities for system integration and demand-side management to add flexibility to the electric grid.* Chapter 6 hypothesizes that a central utility plant (CUP) could economically improve rooftop solar integration in a residential neighborhood and support grid-wide operational stability. It contributes novel research by bridging a gap in the academic literature between distributed, residential solar integration and micro-grid/CUP

optimization. It adds to the micro-grid/CUP modeling literature by developing a generalized, linear model to optimize CUP equipment capacity and hourly dispatch simultaneously and by analyzing a microgrid's ability to integrate rooftop solar in the residential sector of a cooling-dominated climate.

1.3 Major findings

The major findings from this dissertation are summarized below, and are explored in greater detail in the following chapters.

1. In an electric grid with large amounts of solar generation, the percentage savings in dispatch cost exceeds the percentage of annual energy produced by solar generation.
2. Solar generation increases ancillary service prices, though the increase is small relative to dispatch cost savings.
3. Solar generation intensifies net load ramp rates and volatility while doing little to reduce peak demand.
4. Solar generation reduces emissions and water consumption in the electric grid.
5. During the daytime, solar generation tends to reduce utilization of high-cost generators and increase utilization of fast ramping generators.
6. Total dispatch cost in a high-penetration solar system is influenced more by the efficient use of thermal generation assets than by costs associated with flexibility requirements.

7. Increased wind capacity does not correlate strongly with increased flexibility requirements, except for 1-hr and 3-hr ramp down rates.
8. Increased solar capacity correlates strongly with increased flexibility requirements in systems with large amounts of wind generation, especially net load volatility and ramp up rates.
9. Solar tracking arrays increase energy production and exacerbate grid flexibility requirements, while fixed, southeast facing panels impact flexibility requirements much less with only minor reductions in energy production.
10. A 60 \$/ton CO₂ price incentivizes 40% renewable capacity (71% wind, 29% solar) and reduces annual CO₂ emissions by 65% in ERCOT.
11. Increasing wind and solar penetration beyond 40% total capacity is not economically optimal in ERCOT, even with a 60 \$/ton CO₂ price, unless renewable energy capital costs decrease or the minimum amount of on-line thermal generation required to maintain system stability is reduced.
12. Optimal renewable capacity expansion results are most sensitive to solar capital cost, wind capital cost, and the operating costs of the existing generator fleet, and least sensitive to transmission cost.
13. The grid experiences diminishing returns from increasing the CO₂ price as steadily rising costs produce fewer reductions in CO₂ emissions.
14. Reducing the grid's minimum stable net load can significantly increase the optimal capacity of wind and solar generation.

15. Renewable generation will greatly reduce the need for high marginal cost generators in the electric grid.
16. A central utility plant with microturbine, chiller plant, and cooling storage could operate economically in a residential neighborhood under a time-of-use electricity rate structure.
17. Battery capital costs are currently too high to economically justify using them for load shifting in a residential neighborhood setting if microturbine or thermal storage alternatives are available.
18. A residential central utility plant can increase demand flexibility, but incentivizing CUP operational behavior that benefits the electric grid will require appropriately designed electricity rate structures or plant control schemes.

In concert, these findings suggest that future wind and solar development in the electric grid will provide economic and environmental benefits while also increasing the need for greater operational flexibility of the electricity system. A residential central utility plant with cooling thermal storage might economically provide some of that needed operational flexibility from a demand-side source. The following chapters explore and support these findings in greater detail.

Chapter 2

Background

This background section provides information for understanding the methods and analyses presented in Chapters 3–6 and places the academic contributions of this dissertation in the context of the existing scholarly literature. Section 2.1 discusses characteristics of the Electric Reliability Council of Texas, which this dissertation uses frequently as a case study. Section 2.2 describes how renewable generation integrates with the existing power plant fleet. Section 2.3 summarizes the academic literature relevant to this dissertation.

2.1 Electric Reliability Council of Texas

While the analysis and modeling methods used in this dissertation are generally applicable to different electric grids, the Electric Reliability Council of Texas (ERCOT, the system operator serving 90% of Texas' load) is used to demonstrate the functionality and output of those methods. This section provides some background information about the ERCOT electric grid.

There are a number of characteristics about ERCOT that make it a useful case study. It is an isolated grid with a competitive wholesale energy market and a diverse set of existing generators [38]. It also has significant wind and solar resources covering

a large geographic area that is generally distinct from its load locations. Fig 2.1 [128] shows that Texas' best wind resources are in the northwest and central-west parts of the state. Fig 2.2 [128] shows that Texas' best solar resources exist in the west part of the state, with resources generally degrading to the east. The majority of Texas' electricity load is located in the east third of the state.

The ERCOT test cases used in this dissertation are based on data from the 2011, 2012, and 2015 market. For reference, in 2016, ERCOT experienced a peak demand of 71.1 GW with a total energy consumption of 351 TWh. It procured roughly 44% of that energy from natural gas, 29% from coal, 15% from wind, and 12% from nuclear generators [58]. The ERCOT load is driven by summer cooling demand with more than a quarter of its peak load coming from residential air conditioning [149], so it experiences the effects of renewable energy penetration during both high-demand (summer and early-autumn) and low-demand (late-winter and spring) seasons.

2.2 Merit Order and Flexibility

Wind and solar energy resources bring an interesting new aspect to the operation of electricity markets. Since wind and solar have low operational costs, they can bid into the day-ahead electricity market at a zero price [34] moving them to the front of the merit order (the list of dispatchable generators arranged by their energy bid price, see Fig 2.3). This favorable bid position means that it is economically desirable (and sometimes required per feed-in regulations [34]) to integrate all available wind and solar generation into the electric grid. In response to this integration, the remaining dispatchable generation must transition from simply meeting

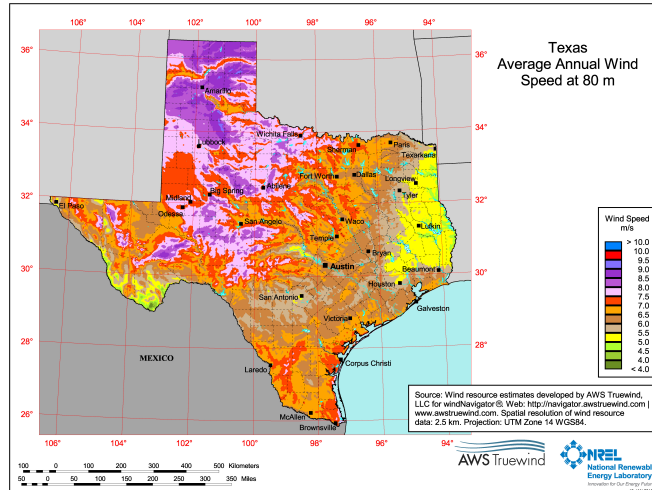


Figure 2.1: Wind resources in Texas are strongest in the northwest part of the state with some strong resources in the central-west as well [128].

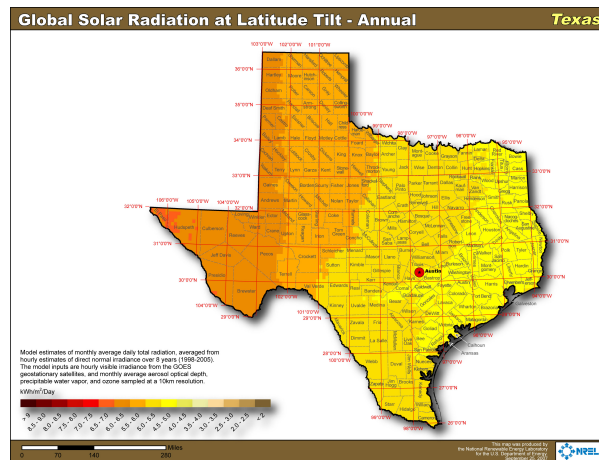


Figure 2.2: Solar resources in Texas are strongest in the west part of the state and generally degrade to the east [128].

the load to balancing the residual load or net load (load minus wind, solar, and other intermittent renewable generation) [133]. This requirement exposes the generation fleet to additional ramping (quick changes in generator power output), cycling (powering down and up in short time periods), and other operational difficulties called “flexibility requirements” [38, 91].

These flexibility requirements can be observed in the electric grid’s net demand, as shown in Fig 2.4. Many different methods can provide the flexibility needed to integrate wind and solar into the electric grid and match dispatchable supply to the net demand. Currently, grid operators respond to flexibility requirements primarily by utilizing the capabilities of the generation fleet [113], where net load ramping is balanced by quick changes in the generator fleet’s power output, and large swings between daily or sub-daily minimum and maximum net loads are balanced by turning power plants on and off. Additionally, using ancillary services to procure reserve capacity is a common market tool for responding to flexibility requirements [32, 72]. It has been hypothesized that these strategies will lose their efficacy at higher renewable energy levels and require additional support, such as energy storage [44] or demand response from interruptible loads.

Storage technologies are capable of providing many services to the grid that would improve the integration of variable renewable generation, such as bulk energy storage, energy management, power quality management, and intermittency mitigation, but are likely to see limited use until they become more economical [63, 79]. Another growing opportunity for meeting flexibility requirements is the use of demand response, whereby flexible loads, such as water treatment that can be ramped

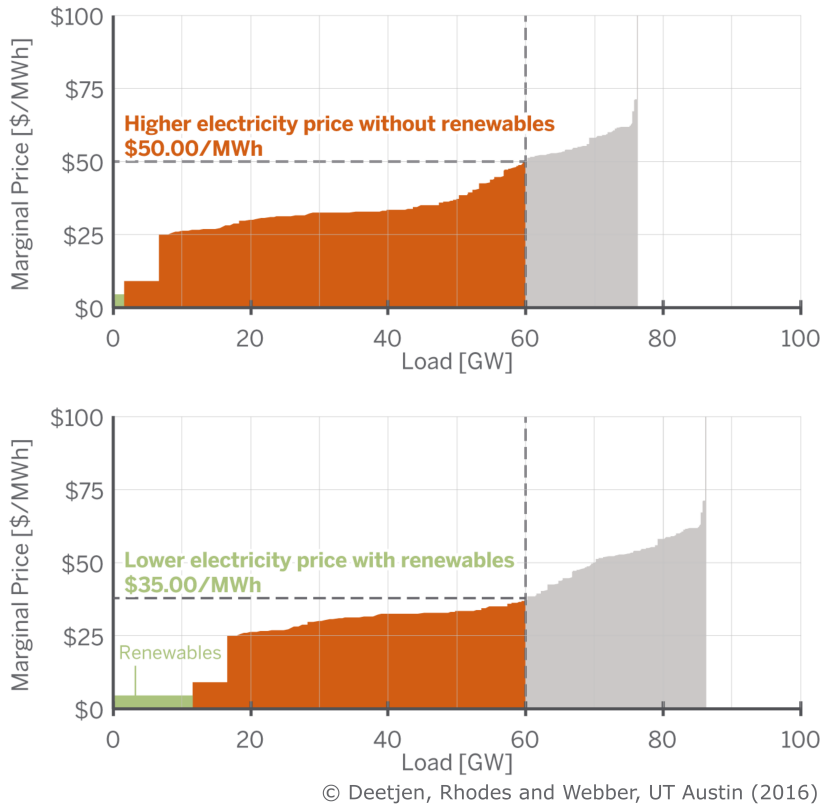


Figure 2.3: The merit order curve sorts an electricity market’s power plants by their marginal cost, visualizing how the power plants with least expensive marginal cost will be dispatched first. Zero-marginal-cost resources (wind, solar, water) are added to the front of the merit order curve, pushing thermal generators (nuclear, coal, natural gas) later in the order. This shift reduces wholesale prices. This figure shows an example of how 15 GW of renewable generation might reduce wholesale market prices from 50 \$/MWh to 35 \$/MWh.

up and down [33], adjust their consumption in response to signals from the grid, allowing the grid to soften demand spikes or large ramping events [24, 143]. Additional grid-supporting strategies continue to be developed, including the dispatch of grid-connected electric vehicles [102], transmission restructuring, and market re-design [113].

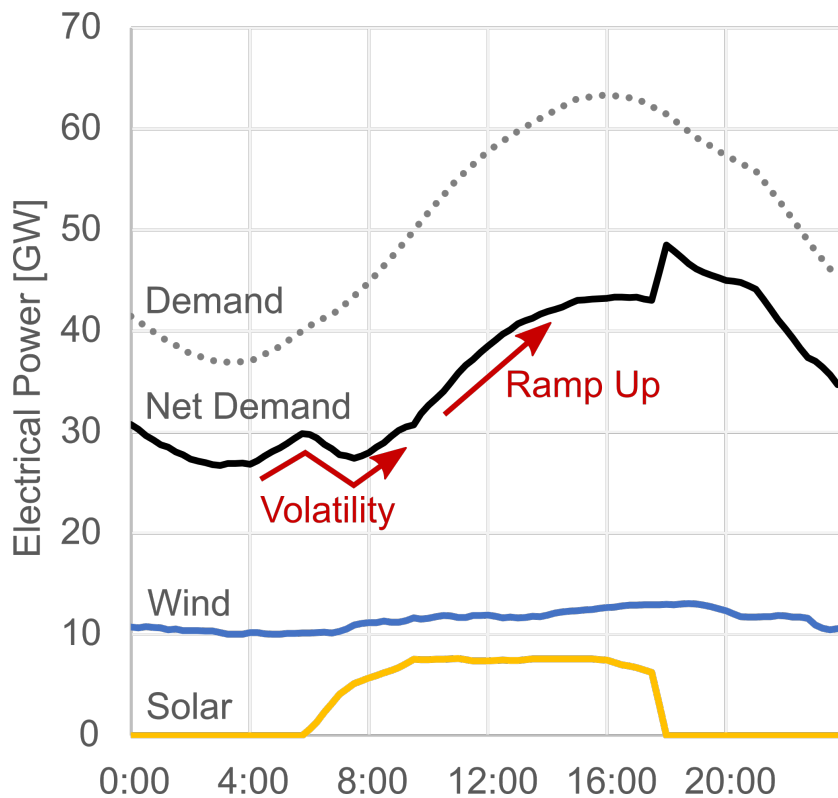


Figure 2.4: Projected demand, wind, and solar data for June 19, 2022 in the ERCOT electric grid. Changes in the net demand can be quantified using the flexibility requirement calculations described in Section 2.2.1.

An inability to provide the necessary grid flexibility, i.e. to match supply with demand, can destabilize the electric grid as evidenced by changes in the alternating

current frequency. Grid frequency needs to be kept within certain bounds. Otherwise, generators, motors, and other electrical equipment will automatically initiate safety protocols that disconnect them from the grid, which can lead to cascading black outs in severe cases [57].

The North American Electric Reliability Corporation (NERC) quantifies a Balancing Authority’s ability to match supply and demand by calculating its Area Control Error (ACE) and quantifies a grid Interconnection’s ability to manage frequency excursions by calculating its Control Performance Standard 1 (CPS1). According to NERC,

“Over-generation makes ACE go positive and puts upward pressure on Interconnection frequency. A large negative ACE causes Interconnection frequency to drop. Highly variable, or noisy, ACE tends to contribute similarly to noisy frequency [1].”

Increased flexibility requirements caused by intermittent renewable generation can make it more difficult for Balancing Authorities to match supply and demand, which complicates the management of Interconnection frequency and leads to poorer ACE and CPS1 scores.

The correlation between larger flexibility requirements and increased difficulty in regulating grid frequency might be highly situational and vary from grid to grid, so the question of “When do net load ramp rates and volatility become too large for the grid to handle?” can be difficult to answer quantitatively. Some analyses have used historical data in actual electric grids to imply causation between intense

ramping or volatility events and significant changes in system frequency [50]. This dissertation assumes that frequency regulation in the electric grid will become increasingly difficult as flexibility requirements grow larger, though it does not model or quantify frequency directly.

2.2.1 Flexibility Requirement Calculations

To adequately analyze and discuss electric grid flexibility requirements, it is helpful to define a framework for how they should be quantified. Existing literature lacks consensus on how flexibility should be calculated [113], though there is some agreement on the importance of ramp rate calculations with respect to the ramping abilities of generators [72, 92]. In addition to ramp rate calculations, this chapter also proposes “volatility” as a useful measure of net load flexibility that is being underrepresented in the current literature. Volatility is the absolute value of the net load curve’s second derivative, summed over various time frames. It describes the amount of “chatter” or “noise” of the net load curve as it ramps up and down over short time spans. These quick fluctuations can influence the grid to dispatch faster-ramping resources [43], even though large ramp rates are not necessarily being experienced. To encourage more consensus on the quantification of flexibility requirements, this dissertation proposes the calculations described below, which are quantitatively illustrated using information from Fig 2.4.

2.2.1.1 1-Hour Ramp Rate

The 1-hr ramp rate is calculated by subtracting the net load 1 hour prior from the current net load as shown in equation 2.1, where t is time in 15-minute intervals. For example, the June 19, 2022 net load changes from 36,996 MW at 11:00 to 39,752 MW at 12:00 for a 1-hr ramp rate of 2,756 (39,752 – 36,996). It is measured in units of MW/hr and describes short-term ramping events that might be handled by ancillary services. Thus, an increase in 1-hr ramp rates might indicate the need for improved ancillary services or fast-response ramping resources on the grid.

$$1HrRampRate(t) = NetLoad(t) - NetLoad(t - 4) \quad (2.1)$$

2.2.1.2 3-Hour Ramp Rate

The 3-hr ramp rate is calculated by subtracting the net load 3 hours prior from the current net load as shown in equation 2.2, where t is time in 15-minute intervals. For example, the June 19, 2022 net load changes from 36,996 MW at 11:00 to 41,900 MW at 14:00 for a 3-hr ramp rate of 4,904 (41,900 – 36,996). It is measured in units of MW/3hr and describes medium-term ramping events that might be handled by dispatching additional capacity rather than relying on ancillary services. Thus, an increase in 3-hr ramp rates might indicate the need to displace slow-ramping base load generators with faster resources.

$$3HrRampRate(t) = NetLoad(t) - NetLoad(t - 12) \quad (2.2)$$

2.2.1.3 Ramp Factor

The ramp factor is calculated by dividing the 15-minute ramp rate by the net load of the previous 15-minute interval as shown in equation 3.2, where t is time in 15-minute intervals. It normalizes the ramp rate in terms of online capacity, where a ramp factor of 0.10 indicates that the dispatchable generation fleet must increase its output by 10% in the next 15 minutes. For example, the June 19, 2022 net load changes from 36,996 MW at 11:00 to 37,637 MW at 11:15 for a ramp factor of 0.017 $((37,637 - 36,996) / 36,996)$. It is measured in units of $(\text{MW}/15\text{min})/(\text{MW online})$. An increase in ramp factors might indicate the need to commit additional generators but dispatch them at partial-capacity to increase the amount of reserve capacity on the grid.

$$\text{RampFactor}(t) = (\text{NetLoad}(t) - \text{NetLoad}(t - 1)) / (\text{NetLoad}(t - 1)) \quad (2.3)$$

2.2.1.4 Ramp Acceleration

As noted in prior work, the ramp acceleration is calculated by subtracting the previous interval's 15-minute ramp rate from the current interval's 15-minute ramp rate and taking the absolute value of the result [38] as shown in equation 2.4, where t is time in 15-minute intervals. For example, the June 19, 2022 net load changes from 39,752 MW at 12:00 to 40,422 MW at 12:15 and 40,276 MW at 12:30 for 15-minute ramp rates of 670 MW/15min $(40,422 - 39,752)$ at 11:15 and -146 MW/15min $(40,276 - 40,422)$ at 11:30 and a ramp acceleration of 816 MW/(15min·15min) $(\text{abs}(-146 - 670))$ at 11:30. It's sole use in this study is for calculating volatility.

$$\text{RampAccel.}(t) = \text{abs}(15\text{MinRampRate}(t) - 15\text{MinRampRate}(t - 1)) \quad (2.4)$$

2.2.1.5 1-Hr Volatility

The 1-hr volatility is calculated by summing the ramp accelerations over the previous hour as shown in equation 2.5, where t is time in 15-minute intervals. For example, the June 19, 2022 net loads for each 15 minute period from 12:00 to 13:30 are 39,752, 40,422, 40,276, 40,136, 40,681, and 41,369 MW. These net loads yield ramp accelerations of 816, 6, 685, and 143 MW/(15min·15min) for each 15 minute period from 12:30 to 13:30. Adding these ramp accelerations together yields a volatility of 1,650 (816 + 6 + 685 + 143) at 13:30. The 1-hr volatility is measured in units of MW/(15min·hr) and describes the intensity of short-term “chatter” in the net load profile that might be handled by faster-ramping resources. Thus, an increase in 1-hr volatility might indicate a temporary need to commit more fast-response resources to the grid.

$$1HrVolatility(t) = \sum_{t=1}^{t-4} RampAcceleration(t) \quad (2.5)$$

2.2.1.6 1-Day Volatility

The 1-day volatility is calculated by summing the ramp accelerations over the previous 24 hours as shown in equation 2.6, where t is time in 15-minute intervals. This calculation is similar to the example calculation for subsection 2.2.1.5 except that 96 ramp accelerations (24 hours’ worth) are summed together instead of 4 (1 hour’s worth). It is measured in units of MW/(15min·day) and describes the intensity of long-term “chatter” in the net load profile that might be handled by faster-ramping resources. Thus, an increase in 1-day volatility might indicate a semi-permanent need

to commit more fast-response resources to the grid.

$$1DayVolatility(t) = \sum_{t=1}^{t-96} RampAcceleration(t) \quad (2.6)$$

2.3 Literature Review

This dissertation discusses how new renewable generation assets will be integrated into the electric grid, quantifies their impact on grid flexibility requirements, and tests the ability of a residential central utility plant to add flexibility to the grid. Consequently, the dissertation covers a number of different sections of the academic literature, including the grid-integration of solar, the influence of renewable generation on flexibility requirements, wind and solar capacity expansion, micro-grid optimization, and rooftop solar integration. This dissertation contributes novel research towards each of those areas as discussed below.

2.3.1 Grid-Integration of Solar

Existing research about integration costs shows that the value of solar capacity decreases as more of it is installed [45, 66]. Research also shows that larger amounts of renewable energy generation require greater flexibility from dispatchable generation assets [46, 66] while also reducing their utilization and potentially having little impact on the overall peak demand [87]. Other studies use duration curves and merit order analyses to show how renewable energy resources affect the spot price of electricity [114, 161]. Because solar production varies based on astronomical and meteorological conditions, gaining a deeper understanding of the impact of renew-

able energy sources requires considering the time of day and season during which it is produced [134, 153]. Historical data on renewable energy generation can be compared with historical prices to gain a more temporal understanding of the impact of renewable energy on wholesale prices [100, 190]. However, the impact of large solar resources, or aggregations of many smaller units, can be better understood by simulating their participation in the electricity market.

Electricity market operators decide how to dispatch their generation assets by using unit commitment and dispatch (UC&D) algorithms that optimize the dispatch to produce the lowest total dispatch cost [69]. UC&D models can be used to estimate the value of renewable energy resources in electricity markets [82, 86], observe how renewable generation influences the utilization of power plants [93, 155, 174], test how different market structures can facilitate the integration of renewable energy sources into the electric grid [164], and to assess transmission investments necessary for meeting renewable energy goals [68].

The generation profile of a solar array is largely dependent on its geographic location and azimuth orientation. Studies show that an owner can maximize the value of a small solar array by optimizing its orientation and tilt according to historical prices, peak demand timing, and pricing structures rather than simply maximizing its annual energy output [20, 153, 156, 158]. However, since large installations of solar generation influence wholesale prices, generator dispatch, and net demand timing, these studies provide limited insight regarding the optimal orientation for large penetrations of solar generation in the grid.

Building on the existing literature above, which communicates many individ-

ual, generalized aspects about integrating solar generation into the grid, Chapter 3 of this dissertation undertakes a comprehensive assessment of how large amounts of solar generation might influence the system-wide flexibility requirements, hourly generation fleet dispatch, and resulting dispatch costs and emissions in an actual electricity market. This dissertation extends solar integration cost research by using an advanced and calibrated UC&D model to simulate the hourly dispatch of the ERCOT generator fleet under different solar penetration scenarios. The simulation results provide novel information about how grid-scale solar integration costs change depending on the daily and seasonal timing of the solar generation profile, as influenced by the location and orientation of solar assets.

2.3.2 Influence of Renewable Generation on Flexibility Requirements

An important consequence of the grid-integration of intermittent renewables is an increased need for flexibility in the electric grid. While there are many viable options for meeting this need, choosing the best strategies for improving grid flexibility begins with understanding how wind and solar generation influence grid flexibility requirements in the first place [91]. Different studies have worked to advance this knowledge. Hirth et al. [89] use economic analysis to dissect how variable renewable generation adds costs to the operation of the grid. One major cost category, “profile costs”, derives from the temporal variability of renewable generation. These costs are driven by the flexibility effect (the increased ramping and cycling of power plants) and the utilization effect (the generators’ distribution of fixed annual capital costs over fewer annual hours of energy production profit). Hirth shows how more

renewable generation leads to larger ramp rates, increased power plant cycling, and reduced thermal utilization, which all add costs to the system.

Huber et al. [92] give a general look at how flexibility requirements change across different European countries as their renewable generation and share of solar generation increase. Using 1-hour resolution, simulated, wind and solar data, the study uses time series analysis to calculate ramp rates on a 1 to 12 hour time scale. They show that flexibility requirements will greatly increase at renewable generation penetrations greater than 30%, especially with significant amounts of solar generation. They conclude that grid size and renewable generation full load hours (FLH) also contribute to changing flexibility requirements.

Additionally, a consulting report published by GE Energy in 2008 [72] conducts time series variability analysis of simulated wind data in ERCOT and assesses the ability of ancillary services to accommodate growing flexibility needs. It is an interesting counterpart to this dissertation as it was written in 2008 with a future-looking perspective, while Chapter 4 of this dissertation utilizes historic 2008–2014 data, and both focus on the ERCOT grid. Key takeaways from the report show that increased wind generation is correlated with increased ramp rates over all 1-minute to 60-minute time spans, and that increasing 15-minute and 60-minute ramp rates are driven by net load variability rather than stochastic variation. It also suggests that the larger ramp rates created by significant wind penetration will increase the maximum amount of regulation reserves that will need to be provided for maintaining grid stability.

This dissertation improves on the aforementioned flexibility requirement stud-

ies in a number of ways. It utilizes 15-minute data in Chapter 4 to perform calculations on a short time scale. While it does utilize simulated solar data, the majority of its wind flexibility analysis is based on actual historical data from ERCOT. It also discusses the influence of solar array orientation and geographic location on flexibility requirements. The dissertation is novel in both its proposal of a framework for calculating flexibility requirements, and its further development of the concept of net load “volatility” as shown in Section 2.2.1.

2.3.3 Wind and Solar Capacity Expansion

It is helpful to analyze how flexibility requirements change with growing wind and solar generation scenarios. However, the actual flexibility requirements of a grid’s future net load depends on the timing coincidence of wind output, solar output, and electric demand. That timing coincidence depends on the regional development of wind and solar capacity, which can be modeled using a capacity expansion model with detailed geographic resolution.

Existing literature recognizes the significance of wind and solar timing coincidence with the load, though a majority of studies seem to focus on the optimization of small-scale hybrid systems [163, 193], or small utility districts [183]. However, some studies have addressed the value of grid-level wind and solar based on their generation timing coincidence. One publication stresses the need to study renewable sources in combination when discussing future grid scenarios [188]. By analyzing different mixes of wind and solar capacity that produce 10 TWh of annual energy (7% of the total annual Swedish supply), the study uses statistical analysis to calculate the

correlation between wind and solar resources in different locations. It concludes that wind and solar are negatively correlated, especially on monthly timescales, meaning that their generation is out of phase with each other. Thus, system-wide renewable electricity output will be more evenly distributed by combining both resources.

Heide et. al. [85] developed a model for choosing wind and solar capacity locations around Europe that minimize the annual need for energy storage. Their model predicts the optimal wind and solar mix given a certain amount of renewable capacity, but does not recommend a total renewable capacity or argue that storage minimization is the best objective for optimizing the renewable capacity mix. A follow-up study expands this work to include different storage methods and discusses the trade-off between energy storage and excess generation [84].

Schaber et. al [160] focuses on extending the European transmission grid to reduce overproduction, storage, and reserve requirements. The study assumes that wind and solar resources will be installed in locations and capacities proportional to their power production potential (in Full Load Hours). Under this assumption, a European grid dispatch model is used to find optimal transmission grid extensions, depending on the wind and solar mix, for balancing overproduction, backup capacity, emissions, and other factors. A follow-up study uses their model to quantify the regional economic effects of projected wind and solar capacities in Europe [159].

Hirth [88] uses a grid dispatch model to analyze the optimal wind and solar mix for maximizing social welfare. This analysis looks at the impacts of temporal variability, forecast errors, storage, increased system flexibility, and climate policy. One shortcoming is its lack of geographic capabilities. Consequently, it does not im-

plement transmission congestion curtailment. It also does not optimize the renewable capacity of different regions in the grid, but models wind and solar as having a fixed geographic dispersion across Europe.

The market valuation of renewable energy generation also depends on CO₂ emissions policies. Since Finland introduced the world's first carbon tax in 1990, many CO₂ emissions taxes and commodity trading schemes have developed in power market across the world [148]. Many more electricity markets, including those in the United States, are likely to adopt some form of CO₂ pricing in the future if they haven't already done so [110]. While there are many methods for pricing CO₂ emissions, carbon taxes (where policy dictates a CO₂ price) and emissions trading schemes (where markets determine a CO₂ price) are particularly popular [17]. In the U.S., CO₂ prices using either method could range from 25 to 53 \$/ton by 2030, and be as high as 120 \$/ton by 2050 [110]. The social price of carbon, an approximation of the agricultural, property, health and other damages that might be attributable to CO₂ emissions, is predicted to fall in a similar range [191]. Economic theory suggests that emissions costs should be considered as a marginal cost of producing electricity [184], and economic literature suggests that CO₂ prices are passed down into electricity prices [65]. Consequently, CO₂ prices could have a significant impact on electricity markets and decisions about renewable energy investment.

As electric grids establish future renewable energy goals and market structures or standards that will achieve them, it is important to consider how much transmission, wind, and solar capacity there ought to be, and where it ought to be built. Existing studies provide important analyses regarding the effects of different

wind and solar mixes on the electrical grid, but they do not satisfactorily address these grid planning questions. Chapter 5 of this dissertation expands on the existing literature by using regional wind and solar generation profiles, existing generator fleet data, market prices, capital costs, and grid flexibility considerations to model the optimal wind, solar, and transmission capacity for each region in the grid. It also provides a framework for balancing increasing system costs and flexibility requirements with reductions in CO₂ emissions to choose an appropriate CO₂ price for the market.

2.3.4 Microgrids for Renewable Energy Integration

Literature on wind and solar capacity expansion, renewable generation flexibility requirements, and the grid-integration of solar all contribute to our understanding of how renewable generation will influence the operation of the electric grid. Many strategies can be used to provide the needed flexibility for integrating renewables into the electric grid. This dissertation provides analysis of one specific strategy - using a central utility plant (CUP) in a residential neighborhood to improve solar integration - by developing an optimization model.

Two bodies of research are especially significant when discussing the application of a residential CUP for improving rooftop solar integration. The first identifies issues caused by distributed solar generation and explores solutions for mitigating them. The second discusses the operation, modeling, and optimization of microgrid/CUP equipment while considering their interactions with the electric grid.

A significant strategy for improving rooftop solar integration in the distri-

bution grid revolves around the concept of “demand-side management,” where consumers change their demand profiles to provide some service to the grid. The application of batteries, thermal energy storage, building thermal mass, and demand response are particularly well-discussed in the literature. For example, Alam et. al. develop a new charge-discharge control strategy for distributed battery resources to show how residential battery systems can help manage peak demand, reverse power flow, and voltage-rise issues in residential neighborhoods with large solar resources [9]. Arteconi et. al. review thermal energy storage applications for demand-side management and renewable energy integration. They conclude that only ice storage for air conditioning has a good market in the US, though better policies could expand thermal storage in other sectors and incentivize their use for peak demand shaving and other beneficial behavior for the grid [13]. Hao et. al. explore the provision of ancillary services using the thermal mass of a commercial building to act as short-term cooling storage for shifting cooling demand [78]. Demand response is analyzed using detailed bottom-up approaches such as using building energy models to assess the impacts of thermostat set-point changes for shifting cooling demand [182], or using top-down models where appliances are generalized based on their demand magnitude and time-shifting capabilities [15].

These demand-side management studies often focus on single technologies and/or modeling individual buildings. Under this focus, they fail to capture the benefits of managing the demand of many buildings and coordinating multiple technologies to meet that demand. These topics, however, are regularly discussed in the microgrid/CUP literature.

The microgrid literature covers the economics and operational strategies of central utility plant equipment in great detail. These analyses are typically accomplished using optimization models, often with the objective of minimizing operating costs by optimizing the dispatch of a microturbine, battery, chiller plant, and/or other centralized equipment [122]. Some studies will also test the sensitivity of the results to a parameter of interest, such as errors in load, solar, and temperature forecasts [169].

A relevant study analyzes the economics and operation costs for commercial building, hospital, and large campus microgrids in California. The results show favorable economics for using a microturbine, solar panels, and purchased electricity to meet demand. The CUP uses some battery capacity to shift electricity demand, and is integrated with a centralized cooling plant and storage to help shift cooling demand. While the CUP's economic benefit is positive, the study shows that the microturbine increases greenhouse gas emissions. The ability of the microgrid to provide grid services or improve solar integration is not analyzed [77].

The microgrid/CUP literature often focuses on combined-heat-and-power (CHP, where power plant waste heat is used to meet heating demand) in industrial or commercial settings, and is somewhat sparse on residential applications, especially in cooling dominated climates. A study by Ondeck et. al. builds a detailed engineering model of a CHP plant with solar generation and a chiller plant for a 5,600-house, residential neighborhood in Austin, TX [136]. While that model provides some new insights about the applicability of a residential CUP, it lacks some important features. It does not utilize storage of any kind or purchase electricity from the grid,

and only simulates the equipment dispatch for a few weeks of the year.

Some microgrid studies do look more specifically at interactions between CUPs and the broader electric grid, especially focusing on market signals and incentives. Siler-Evans et. al. present CHP in commercial buildings as an economical way to improve the efficiency of the electric grid. They note, however, that flat rate structures, where electricity prices do not vary with time or season, do not provide strong enough signals for CUP development, and that buildings have yet to significantly participate in demand response and regulation markets, though strong economic possibilities exist [162]. Another study analyzes the University of California San Diego CUP's ability to provide load shifting, solar PV firming (managing intermittent solar generation), and grid support. Though the CUP is capable of providing those services, existing tariff structures and market prices don't incentivize it to do so [167].

In summary, the academic literature recognizes the issues caused by large amounts of distributed, rooftop, solar generation. It proposes a number of solutions focused on individual customers and/or individual technologies including batteries, thermal storage, and demand response. These solutions overlook the benefits of aggregating demand management and utility equipment on a larger scale.

While the microgrid/CUP literature looks more at this aggregation concept, it has little to say about the management of solar issues in residential neighborhoods, especially in cooling climates where peak grid-wide demand is driven by residential consumption. Many microgrid studies deal with industrial or commercial processes in heating dominated climates where CHP is the technology of interest. The few studies

that do look at residential CUPs in cooling climates provide little analysis regarding solar integration or grid interactions. Microgrid studies that do focus on electric grid interactions show that CUPs could contribute to grid efficiency, solar integration, load shifting, and grid support, but that existing markets don't incentivize that behavior.

Chapter 6 of this dissertation adds to the literature by expanding the conversation on rooftop solar integration to look beyond individual technologies and buildings towards integrated sets of technology and aggregated loads coordinated by a single CUP/microgrid. It adds to the microgrid literature by providing additional analysis of the under-examined sector of residential neighborhoods in cooling climates and by explicitly evaluating the microgrid as a strategy for improving rooftop solar integration. It also examines the influence of different electricity rate structures on the microgrid's effectiveness, expanding the discussion on what market incentives are necessary for incentivizing microgrid behavior that improves solar integration.

Chapter 3

Solar PV integration cost variation due to array orientation and geographic location in the Electric Reliability Council of Texas

This chapter of the dissertation contributes to the growing area of research on the grid-integration of renewable energy by providing a holistic study of how generator dispatch, system flexibility requirements, and market dispatch costs are influenced by the orientation and geographic location of solar generation assets. The information in this study can encourage utilities, grid operators, and other entities involved with influencing the development of the electric grid to develop renewable energy portfolios, tax incentives, and investment plans that consider the comprehensive costs of integrating solar into the grid.

This chapter is an updated study of “Solar PV integration cost variation due to array orientation and geographic location in the Electric Reliability Council of Texas” as published by *Applied Energy* in 2016 [38].

3.1 Methods

This study utilizes a UC&D model of the ERCOT electricity market developed by Garrison, et al. [69]. The model is built in the PLEXOS Integrated Energy

Model (PLEXOS) software. The model includes each generator in the ERCOT grid, and assigns them unique variable marginal heat rates, maximum capacities, and performance parameters based on their fuel type and technology. It utilizes hourly load, wind generation, and solar generation profiles, along with other system parameters to calculate the hourly dispatch of each generator, hourly prices, the total dispatch cost, and other market information. These calculations are performed by a mixed-integer linear program that includes the operating costs of each generator in its objective function. The total dispatch cost includes generator start-up costs and the cost of purchasing reserve capacity from the generators, but its largest portion is calculated by multiplying the hourly energy price (\$/MWh) by the total amount of generation needed in each hour. The energy price is determined by the marginal operating cost of the most expensive dispatched generator. With this calculation in mind, the program chooses the hourly dispatch for each generator that minimizes the total daily dispatch cost of the ERCOT system, provides enough hourly generation and reserves to meet the hourly demand, and respects ramping, capacity, and other generator operational constraints. This optimization is performed for each day of the year producing an hourly dispatch schedule for all 8,760 hours of the year.

The ERCOT UC&D model has been calibrated to historical 2011 data for wholesale prices, ancillary service prices, and fuel use, and can accurately reproduce the historical 2011 ERCOT market [69]. While the model can produce accurate results, its current version has several limitations. It does not include transmission constraints treating ERCOT as a single node, assumes marginal cost bidding behavior by the generators, and uses perfect load and renewable electricity generation

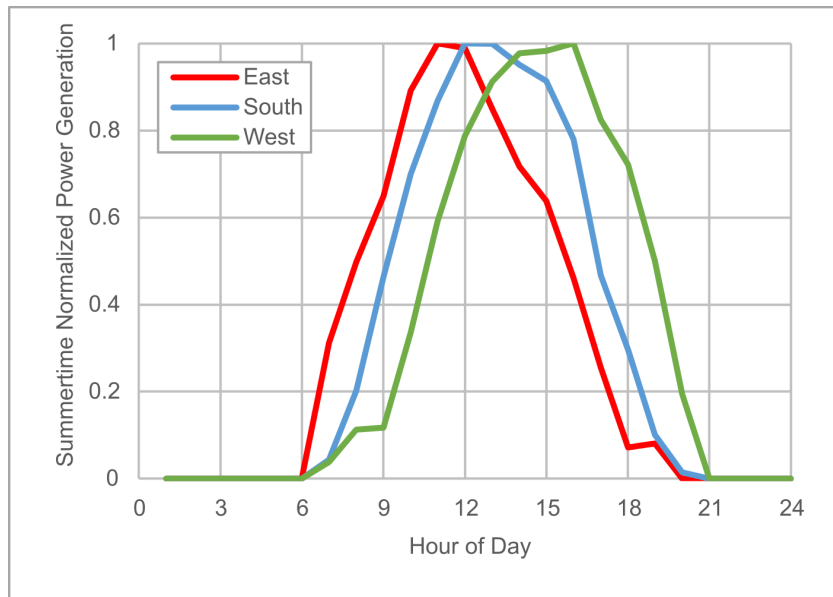


Figure 3.1: The normalized generation curves for the three different solar scenarios show the typical variation in the timing of their electricity generation during the course of a summer day. The East and West scenarios peak approximately three hours apart from each other and represent the bounds of solar generation timing in ERCOT [129].

forecasts. The primary impact of these limitations is a poor representation of non-marginal bidding behavior by the generators, which leads to an inability to reproduce price spikes under scarcity conditions. Additional details on the development of this ERCOT UC&D model can be found in Garrison’s doctoral dissertation [69].

The primary analysis in this study involves the comparison of different solar arrays in Texas based on their geographic location and orientation. Rather than compare dozens of scenarios with different locations and orientations around the state of Texas, this study limits its scope to observing the extremes of possible solar output profiles. An east-facing (90 degree) solar array installed in east Texas

(Longview, Texas) and a west-facing (270 degree) solar array installed in west Texas (El Paso, Texas) represent the range of solar generation possibilities in ERCOT. Though El Paso is not connected to the ERCOT grid, it is the closest weather data location for approximating far west ERCOT solar PV output in the PV generation calculator utilized in this study. Figure 3.1 illustrates the normalized generation profiles for a maximum-output summer day for each scenario showing that their peak production times occur approximately 3 hours apart. The generation profile of any other configuration of solar assets in ERCOT will fall within the timing bounded by these two profiles. A south-facing (180 degree) solar array installed in central Texas (Abilene, Texas) was also added to provide additional insight to the results. All times are reported in Central Standard Time. The three solar scenarios will be referred to as “East”, “South”, and “West” in this report as indicated in the map of ERCOT shown in Figure 3.2.

The hourly output data for the East, South, and West solar generation curves were created by utilizing the PVWatts Calculator developed by the National Renewable Energy Laboratory (NREL) [129]. This calculator uses solar insolation information from typical meteorological year (TMY) data to estimate the hourly electricity generation of a solar array based on its location, orientation, and other input criteria. Each array is tilted at 20 degrees above horizontal, a common tilt used to favor summer-time electricity generation, and the default value used by the PVWatts Calculator. Default PVWatts data were also used for the array type, system loss, DC to AC size ratio, inverter efficiency, and ground cover ratio values. The criteria chosen for the East, South, and West scenarios are summarized in Table 3.1.

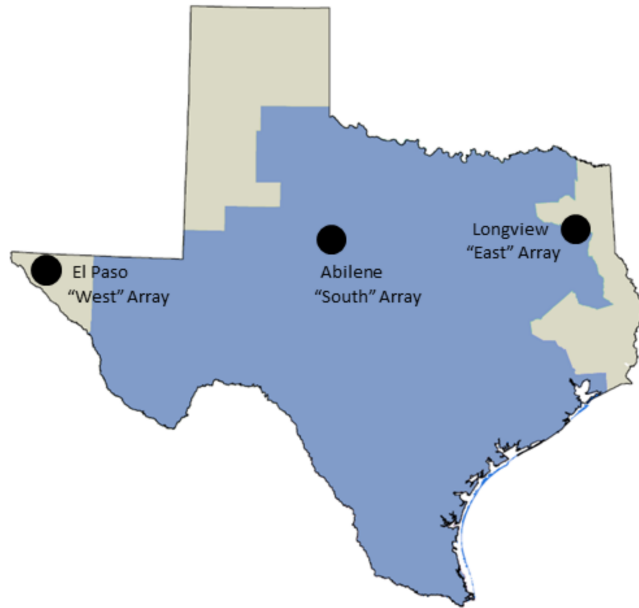


Figure 3.2: This figure shows the State of Texas with the ERCOT boundary shaded in blue. The cities associated with the East, South, and West scenarios are indicated.

Table 3.1: Input data used to generate the solar PV hourly generation curves for the different scenarios. All parameters were set to the default values except the weather data set and array azimuth.

Scenario	Weather Data Set	Array Azimuth (deg)	Array Tilt (deg)	Array Type	System Loss	DC to AC Size Ratio	Inverter Efficiency	Ground Cover Ratio
East	TMY3 Longview Gregg County Airport, TX	90	20	fixed	14%	1.1	96%	0.4
South	TMY3 Abilene Regional Airport, TX	180	20	fixed	14%	1.1	96%	0.4
West	TMY3 El Paso International Airport, TX	270	20	fixed	14%	1.1	96%	0.4

Rather than assigning the same installed capacity to each of the solar arrays for the different scenarios, each array's capacity was sized to generate 22,500 GWh of annual energy, about 6.8% of annual generation in 2011. While specifying an identical capacity for each of the arrays would provide a more straightforward comparison of their net load profiles and flexibility requirements (see sections 4.2 and 4.3), the scenarios would produce different amounts of annual solar energy - an aspect that would greatly complicate the comparison of their dispatch costs, generator dispatch, and emissions calculations (see sections 4.1, 4.4, and 4.5). Sizing the arrays to produce the same annual solar energy allows their dispatch and emissions to be easily compared while still allowing a reasonable opportunity to compare their net load profiles and flexibility requirements. Based on trial-and-error model simulations, 22,500 GWh of energy generation was selected because it is large enough to impact the market, but small enough to eliminate solar curtailment and avoid low net loads, which can be difficult for the model to optimize. The East, South, and West arrays were sized at 18.3 GW, 14.2 GW, and 15.0 GW, respectively to match this generation level. The monthly energy production for each solar array is presented in Figure 3.3. The shapes of these energy generation profiles are influenced by seasonal shifts in weather and the sun's path through the sky as well as the installed capacity of the arrays. The one-year hourly generation data for each of these scenarios was incorporated into the ERCOT UC&D model with historical 2011 hourly load and 2011 hourly wind generation data. All 8,760 hours of the year are simulated for each solar scenario and for a base case that does not include solar.

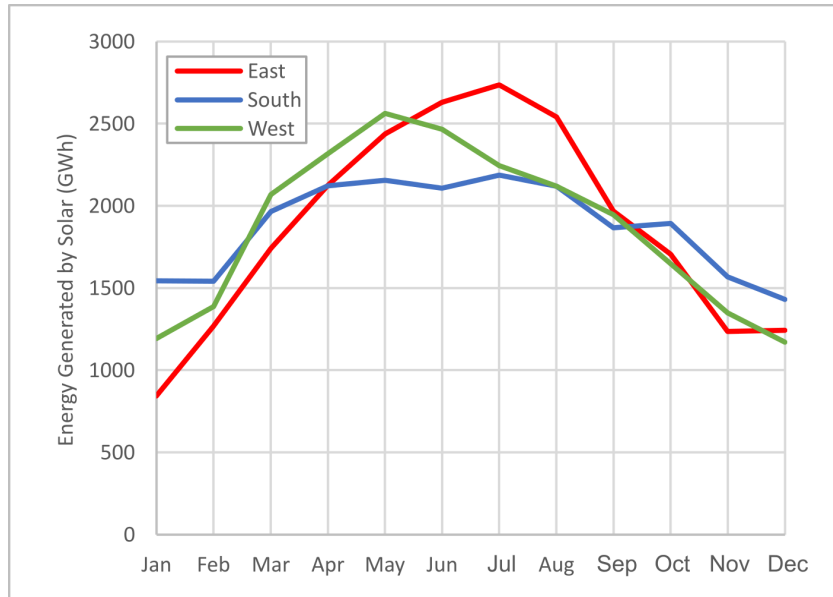


Figure 3.3: The monthly energy output of the different arrays is influenced by seasonal shifts in weather and the sun’s path through the sky as well as the installed capacity of the arrays.

3.2 Results and Discussion

Solar arrays with different locations and orientations will require different capacities to generate the same amount of annual energy. While the South and West array capacities are within 5% of each other, the East array has over 20% more capacity than either of the other scenarios due to orientation and different meteorological conditions that yield less overall solar insolation [189]. A system with greater capacity can produce greater instantaneous generation and ramping. This distinction should be kept in mind when analyzing the results. Additionally, while this UC&D model can accurately simulate the ERCOT day-ahead market, it does not completely predict all of the market behavior that affects prices and dispatch in the

real-time market, such as extremely high prices caused by competitive bidding during times of high grid stress. The results presented in this study are not meant to make detailed predictions but to illustrate big-picture trends and intuitions. The results show how total dispatch cost, net load reduction, net load flexibility requirements, fuel use, and emissions vary between the different scenarios. Most of the results are summarized in Table 3.2.

3.2.1 Prices and Total Dispatch Cost

The wholesale energy price is the compensation (\$/MWh) paid to all generators for the amount of energy they produced for the wholesale electricity market during a given time frame. Table 3.2 shows that solar generation reduces the average energy price over the entire year. When comparing the solar scenarios, the East scenario has the lowest average annual energy price and the South scenario has the highest. The simulation results also show that, when compared with the No Solar scenario, solar generation reduces energy prices more in the summer than in the winter. It also increases price volatility in the winter and reduces price volatility in summer as shown in Figure 3.4.

In addition to purchasing energy generation, electricity markets also purchase ancillary services that provide reserve generation capacity and grid stability features. The 2011 ERCOT model developed for this work uses four types of ancillary services. “Regulation Up” and “Regulation Down” services require on-line generators to raise or lower their generation within five minutes. “Responsive” services require on-line generators to raise their generation within ten minutes. “Non-Spinning” services re-

Table 3.2: The results for each of the four 8,760-hour UC&D simulations of the ERCOT electricity market are shown below. The information is categorized into smaller tables corresponding to each of the “Results & Discussion” sub-sections in this report.

Solar Data	Array Size	(GW Capacity)	East 18.3	South 14.2	West 15.0	No Solar 0.0
	Annual Total Solar Generation	(GWh) (% of Annual Energy Demand)	22,500 6.8%	22,500 6.8%	22,500 6.8%	- -
4.1 Prices & Total Dispatch Cost	Annual Total Dispatch Cost	(\$ Billion)	7.98	7.94	7.90	8.81
		(% reduction vs. No Solar)	9.4%	9.9%	10.3%	-
	Average Yearly Prices	Ancillary Services Cost (\$ Billion)	0.308	0.306	0.306	0.297
		Energy (\$/MWh)	33.73	33.92	33.80	35.53
		Regulation Up (\$/MWh)	10.55	10.51	10.59	10.23
		Regulation Down (\$/MWh)	6.85	6.66	6.28	5.09
		Responsive (\$/MWh)	12.94	12.96	13.03	12.88
Non-Spinning (\$/MWh)	2.40	2.40	2.40	2.40		
4.2 Net Load Red.	Maximum Net Load	(GW)	62.9	62.6	63.2	65.8
	Hours Net Load Above 60 GW	(Hours)	50	28	12	204
	Minimum Net Load	(GW)	9.1	11.4	12.3	15.4
	Hours Net Load Below 15 GW	(Hours)	61	36	13	0
4.3 Net Load Flexibility Req.	Ramp Down Requirement	Average(GW/hr)	4.4	3.9	3.9	3.5
		Std. Dev. (GW/hr)	1.3	1.1	1.0	1.1
	Ramp Up Requirement	Average(GW/hr)	4.5	4.1	4.6	3.6
		Std. Dev. (GW/hr)	1.5	1.5	1.5	1.3
	Ramp Up Factor Requirement	Average(GW/hr per GW)	0.16	0.14	0.16	0.12
		Std. Dev. (GW/hr per GW)	0.06	0.05	0.07	0.03
		Year Max. (GW/hr per GW)	0.51	0.42	0.47	0.22
		Year # Hrs Ramp Fact.> 0.35	5	2	5	0
	Volatility Requirement	Average(GW/(hr*day))	36.1	28.3	32.6	20.2
Std. Dev. (GW/(hr*day))		10.5	8.7	9.4	4.0	
4.4 Generation by Generator Type	Coal	(GWh)	123,800	123,500	124,100	128,700
		(% Reduction vs. No Solar)	3.8%	4.0%	3.6%	-
	Hydroelectricity	(GWh)	815	815	815	820
		(% Reduction vs. No Solar)	0.6%	0.6%	0.6%	-
	Nat. Gas Boiler	(GWh)	3,580	3,050	2,350	5,310
		(% Reduction vs. No Solar)	32.6%	42.6%	55.7%	-
	Nat. Gas Combined Cycle	(GWh)	106,300	106,800	107,300	121,700
		(% Reduction vs. No Solar)	12.7%	12.2%	11.8%	-
	Nat. Gas Internal Combustion	(GWh)	700	700	680	740
		(% Reduction vs. No Solar)	5%	5%	8%	-
	Nuclear	(GWh)	40,000	40,000	40,000	40,000
		(% Reduction vs. No Solar)	0%	0%	0%	-
	Open Cycle Gas Turbine	(GWh)	3,630	3,700	3,440	3,920
		(% Reduction vs. No Solar)	7.4%	5.6%	12.2%	-
Wind	(GWh)	31,000	31,000	31,000	31,000	
	(% Reduction vs. No Solar)	0%	0%	0%	-	
4.5 Emissions & Water Use	CO ₂	(million tons)	193	192	192	207
		(% Reduction vs. No Solar)	6.8%	7.2%	7.2%	-
	NO _x	(thousand tons)	99.6	99.1	98.9	105.5
		(% Reduction vs. No Solar)	5.6%	6.1%	6.3%	-
	SO _x	(thousand tons)	321	319	321	336
		(% Reduction vs. No Solar)	4.5%	5.1%	4.5%	-
	Water Consumption	(billion gallons)	106	106	106	112
		(% Reduction vs. No Solar)	5.4%	5.4%	5.4%	-
	Water Withdrawals	(billion gallons)	8,440	8,420	8,410	8,720
		(% Reduction vs. No Solar)	3.2%	3.4%	3.6%	-

quire off-line generators to come online and provide generation within thirty minutes. New ancillary service markets being designed by ERCOT [177] will affect future iterations of the model used for this study, but the model does not currently account for these pending market updates.

While prices communicate some information about how solar generation affects the electricity market, total dispatch cost (the cost of providing energy and ancillary services for the electric grid) is a more useful metric for judging the overall impact of solar generation. Total dispatch cost amounted to \$8.81 Billion for the No Solar scenario. This amount was reduced in the East, South, and West scenarios by 9.4%, 9.9%, and 10.3%, respectively - a reduction of approximately \$900 Million. A 10% reduction in total dispatch cost resulting from solar energy producing only 6.8% of total energy demand indicates a high value for the electricity generated by solar. Figure 3.5 shows how each solar scenario reduces the monthly total dispatch cost throughout the year. When comparing the solar scenarios with each other, the East scenario reduces total dispatch costs most in July and August, the South scenario most from October through February, and the West scenario most for March through June and for September. Many factors influence the difference in total dispatch costs between the solar scenarios, but there is a strong correlation between the dispatch costs and the seasonal solar output of the arrays shown in Figure 3.3. Noticeably, the East array only reduces the July and August dispatch costs slightly compared to the other scenarios, though it produces significantly more energy during those months. This result speaks to the lower quality of the East array's production as its peak power output occurs a few hours before peak demand and it introduces higher

flexibility requirements as discussed in Section 3.2.3.

While solar generation reduces total dispatch cost, it increases the cost of procuring ancillary services. As seen in Table 2, solar generation causes the average yearly ancillary services prices to increase by 2.7–3.5% for Regulation Up, 23–35% for Regulation Down, and 1% or less for the other ancillary services. The West array increases Regulation Up prices and the East array increases Regulation Down prices more than the other scenario, a result that correlates with the Ramp Up and Ramp Down Requirements discussed in Section 3.2.3, where a system with greater Ramp Down Requirements might be expected to pay more for Regulation Down services. Ancillary services cost, the annual amount paid to generators for procuring ancillary services, amounted to \$297 Million for the No Solar scenario. This amount increased by approximately 3.1%, or \$10 Million, for the solar scenarios. Since this cost accounts for only 3.4–3.9% of the total dispatch cost, a 3.1% increase in ancillary services cost has a small effect on the market as a whole. The \$900 Million reduction in total dispatch cost created by solar generation is much more substantial than the \$10 Million increase in ancillary services cost.

3.2.2 Net Load Reduction

Since wind and solar electricity resources have zero marginal costs, they are usually dispatched first (unless there is curtailment because of transmission congestion or oversupply), and dispatchable generation resources meet the remaining demand. This tendency is captured in the net load, where net load is equal to the total load minus the electricity generated by solar and wind resources. The peak-period

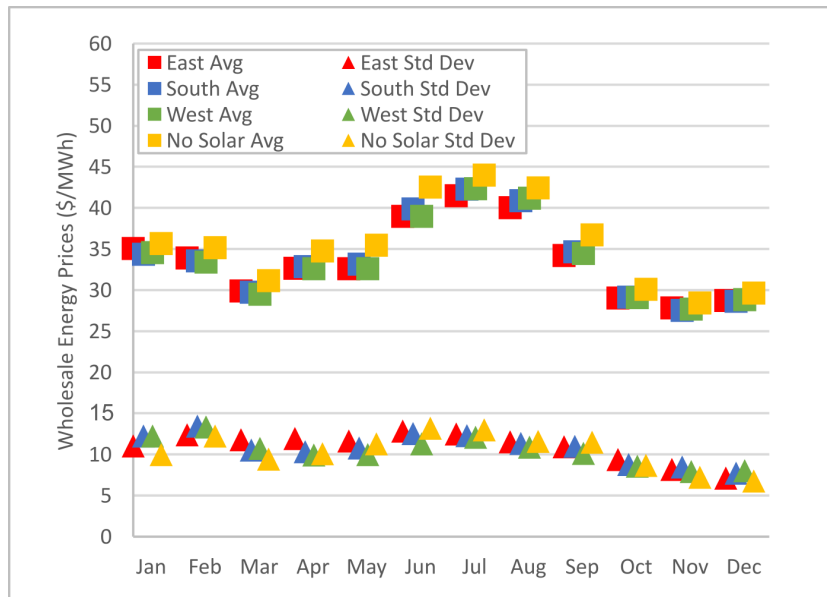


Figure 3.4: The monthly price averages and standard deviations change depending on the solar scenario. Solar tends to increase monthly price standard deviation in the winter and decrease it in the summer. It also decreases energy prices more in the summer than in the winter.

and off-peak net loads encountered during the UC&D simulation are useful tools for comparing the different solar scenarios. Smaller peak-period net loads indicate that fewer dispatchable resources are needed to meet demand and suggest that peak-load generation assets might be dispatched less often. Smaller off-peak net loads indicate that more dispatchable resources must be turned off or operate at their minimum capacities. This situation can increase dispatch costs by incurring more generator start-up costs and causing generators to operate at less-efficient capacities. Wind and solar resources can also be curtailed to balance low net loads, though this study uses a no-curtailment constraint.

The net loads for each scenario are illustrated in the Figure 3.6 duration curve.

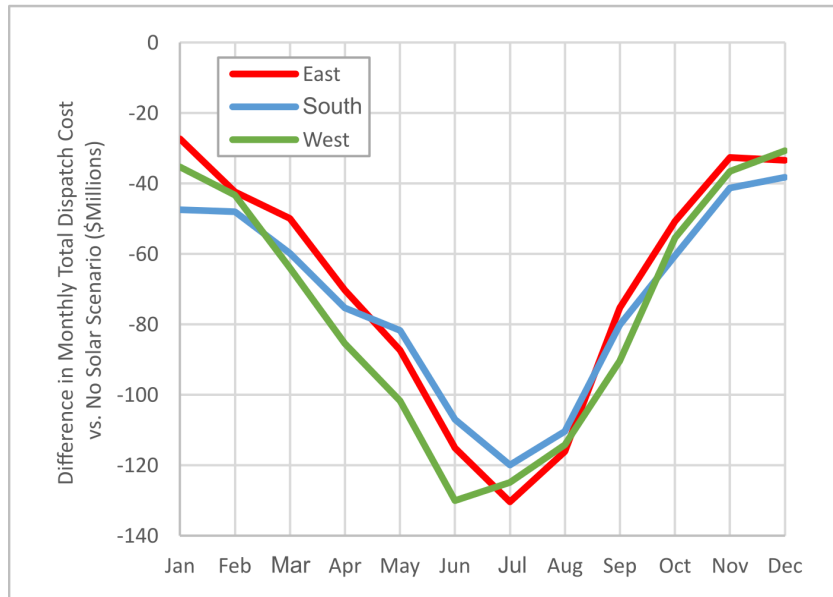


Figure 3.5: Each solar scenario reduces the monthly total dispatch cost when compared to the No Solar scenario. Summer months see more savings due to greater solar output and the alignment of solar generation with peak demand.

This figure indicates that the West array will generally reduce the highest net load values more than the South or East arrays. These results suggest that electricity generation from the West array is more aligned with peak summer demand than the other scenarios and will require less energy generation from peak-load generators. However, all three scenarios have similar maximum net loads for the year requiring similar dispatchable generation capacity to meet maximum net demand. The figure also indicates that the East array will create the lowest net loads of the three arrays. These results suggest that electricity generation from the East array is more aligned with minimum shoulder-season demand than the other scenarios and will force base-load generators to shut-down or operate at minimum capacity more often.

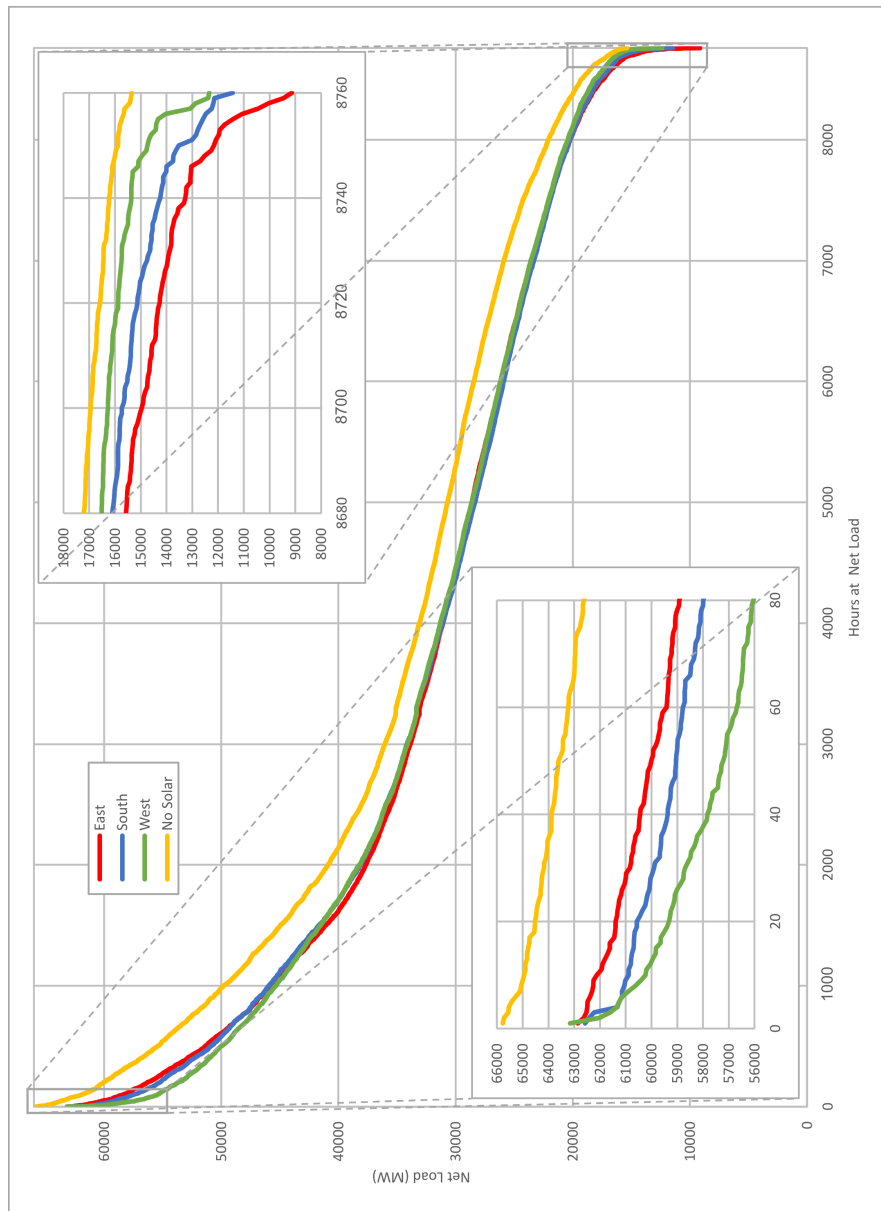


Figure 3.6: The net load duration curve with insets magnifying the highest and lowest net load values shows the number of hours per year experienced at different net loads by each scenario. During the highest net load hours of the year, the West net load is generally smaller than the South net load which is smaller than the East net load. However, all three solar scenarios have similar maximum net loads for the year. During the lowest net load hours of the year, the West net load is larger than the South net load which is larger than the East net load.

3.2.3 Net Load Flexibility Requirements

The hourly profile of the net load indicates the load and ramp rates that must be met by dispatchable resources to accommodate the full solar and wind capacity. Increased volatility and ramping in the net load curve imply the need for more flexible generation resources or renewable energy curtailment. The flexibility requirements of the different scenarios can be compared by calculating a number of net load ramping characteristics.

Ramp rates are calculated by subtracting the previous hour’s net load from the current hour’s net load as shown in equation 3.1, where t is time in hours. “Average Ramp Down Requirements” are calculated by taking the steepest negative ramp rate during each day of the year and averaging these 365 ramp rates together. Similarly, “Average Ramp Up Requirements” are derived by averaging the largest positive ramp rates for each day of the year.

$$RampRate(t) = NetLoad(t) - NetLoad(t - 1) \quad (3.1)$$

“Ramp Factors” are calculated by dividing the 1-hour net load ramp rate by the previous hour’s net load as shown in equation 3.2. A ramp factor of 0.50 means that the generation fleet must increase its generation output by 50% over the next hour. “Average Ramp Up Factor Requirements” are calculated by taking the maximum ramp factor during each day of the year and averaging these 365 ramp factors together. While ramp requirements communicate the megawatt-per-hour changes needed from the generation fleet, ramp up factor requirements anticipate the difficulties of quickly

ramping up a generator fleet with limited on-line capacity.

$$RampFactor(t) = \frac{RampRate(t)}{NetLoad(t-1)} \quad (3.2)$$

Finally, “Volatility” is used to observe the effects of intermittent solar output on the net load. First, “Ramp Acceleration” is calculated by subtracting the previous hour’s ramp rate from the current hour’s ramp rate and taking the absolute value of the result as shown in equation 3.3. Then, the “Daily Volatility” is calculated by summing the 24 ramp acceleration values for each hour in a day. “Average Volatility Requirements” are calculated by taking the volatility for each day of the year and averaging these 365 volatilities together.

$$RampAcceleration(t) = abs(RampRate(t) - RampRate(t-1)) \quad (3.3)$$

Average ramp down and ramp up requirements are 11–28% greater, average ramp up factor requirements are 17–33% greater, and average volatility requirements are 40–79% greater for the solar scenarios than for the No Solar base case. The maximum annual ramp up factors are 91–132% greater for the solar scenarios than for the No Solar base case. Though these maximum values indicate extreme ramping situations that might occur only once per year, the generation fleet must be capable of providing that flexibility to meet reliability expectations.

The results in Table 2 show that the East scenario has the greatest average ramp down and volatility requirements, the South scenario has the lowest requirements in all of the categories, and the West scenario has the greatest average maximum ramp up requirements. The scenarios can be listed in order of greatest flexibility requirements as East > West > South.

3.2.4 Generation by Generator Type

The ERCOT UC&D model utilized in this study tracks the hourly energy production of each generator in the fleet. Categorizing these generators based on their fuel type and technology reveals which types of generators will be dispatched more or less often with greater solar penetration. Table 3.2 shows the total energy (GWh) produced by each generator type for each of the four scenarios. Among the solar scenarios, energy generation from natural gas boilers was greatly reduced, and energy generation from natural gas combined cycle (NGCC) resources was reduced by a greater percentage than for open cycle gas turbines (OCGT) even though OCGT resources are more expensive to operate. Figure 3.7 shows the 24-hour generator mix for July 25th. It illustrates how the net load and generation fuel mix changes for each scenario during a day of maximum solar output in the summer and shows how solar can reduce maximum net load in the summer displacing the most expensive generators in the bid stack.

In addition to reducing the maximum net load, solar generation also changes the way generators are dispatched by utilizing them to handle the increased net load ramp rates and volatility. Figure 3.8 shows the 24-hour generator mix for March 5th. It illustrates how the net load and generation fuel mix changes for each scenario during a day of maximum solar output in the spring and shows how solar can create low net loads followed by steep ramp rates requiring dispatchable generation to operate more flexibly. Figure 3.9 charts the average hourly dispatch for NGCC (slow-ramping, mid-load) and OCGT (fast-ramping, peak-load) generators during the year. While fast-ramping generators (e.g. OCGT) help compensate for solar PV

generation by ramping up in the evening, slow-ramping, mid-load generators (e.g. NGCC) play an important role by absorbing much of the mid-day solar generation as well as providing ramping support. In most markets, where mid-load capacity greatly exceeds fast-ramping capacity, the mid-load generation will compensate for large, bulk changes to the net load, while fast-ramping generation will act to increase short-term ramping capabilities.

While utilization of the least expensive generation resources (hydroelectricity, nuclear, wind) is almost unchanged, the dispatch of slow-ramping generators is reduced by percentages roughly corresponding to their marginal cost (i.e. natural gas boilers, having greater marginal costs than coal, are dispatched less than coal overall). Alternatively, fast ramping, expensive, peak-load generators such as open cycle gas turbines are also displaced during peak solar generation hours but recover some of their utilization by providing ramping support in the evening.

3.2.5 Emissions & Water Use

Since solar generation displaces existing thermal generation resources without producing emissions or using cooling water, it has a significant impact on the amount of emissions produced and water utilized in the electricity market. The production of CO₂, NO_x, and SO_x emissions as well as the withdrawal and consumption of water are calculated in the model. Water withdrawals denote the total amount of water entering the cooling system of a power plant (much of which is returned to a water body) and water consumption denotes the amount of water lost to evaporation during the cooling process.

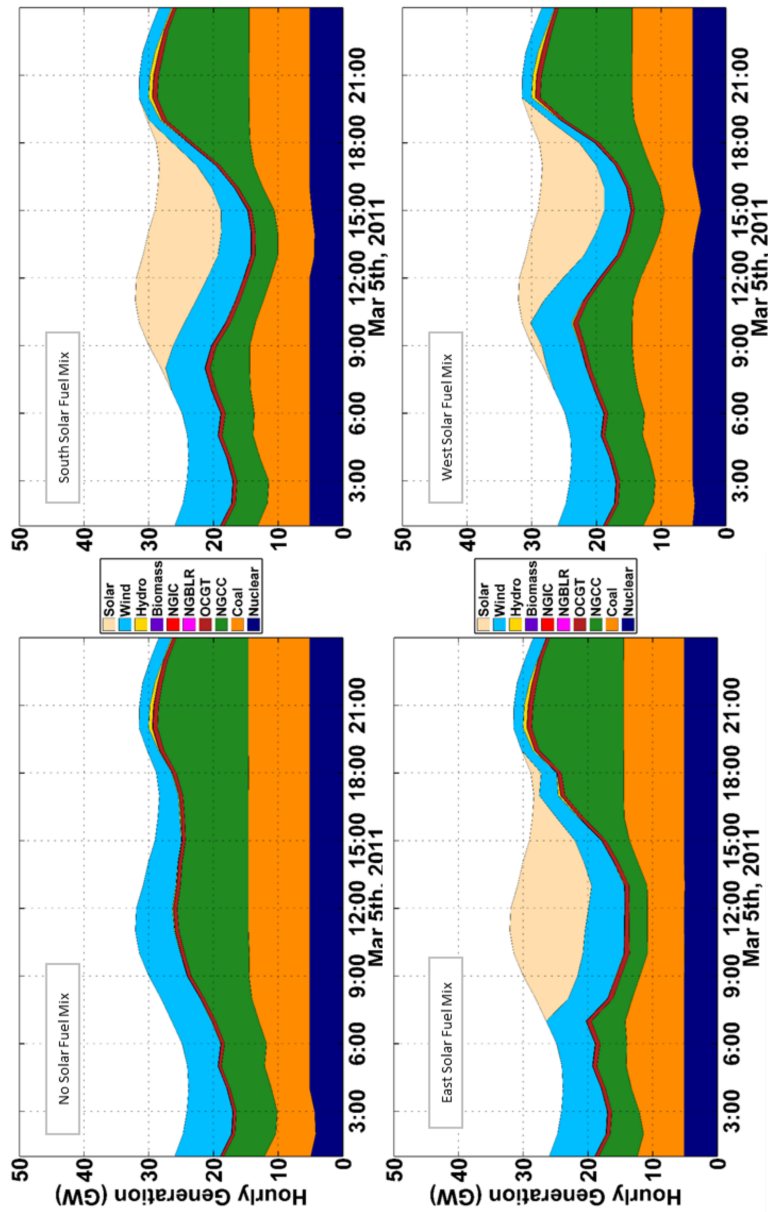


Figure 3.8: These charts show each scenario’s hourly fuel mix during a typical spring day. The net load is represented by the bottom of the wind generation area. The “duck curve” manifests itself in ERCOT during the shoulder seasons when there is abundant spare capacity. ISOs have expressed concern about accommodating the steep evening ramp rates shown here.

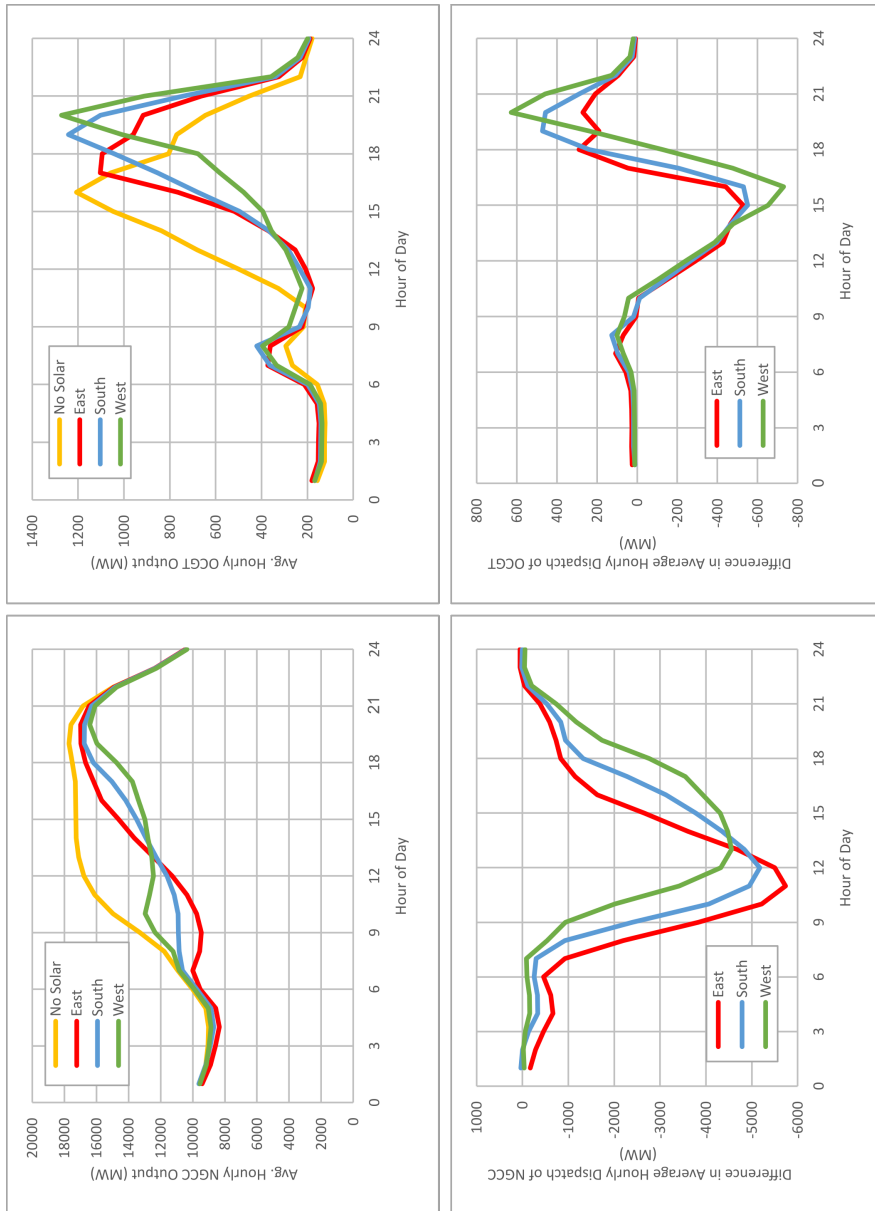


Figure 3.9: The top two charts show the hourly output of natural gas combined cycle (NGCC) and open cycle gas turbine (OCGT) generators averaged over the year for each scenario. The bottom two charts show the annual average hourly dispatch of a solar scenario minus the annual average hourly dispatch of the No Solar scenario where negative values indicate hours of the day when the generator category is being dispatched less than in the No Solar scenario.

The results in Table 3.2 show that increased solar generation leads to reductions in emissions and water. The West scenario reduces NO_x emissions and water withdrawals more than the other scenarios while the South Scenario reduces SO_x emissions more. The East scenario has a lower impact on CO_2 emissions, NO_x emissions, and water withdrawals than the other scenarios.

3.3 Conclusions

While the four scenarios produce different results, they all support some generalizations about solar penetration in ERCOT. First, 22,500 GWh of solar generation reduces the total dispatch cost in the ERCOT market by approximately \$900 Million per year. The cost reduction percentages in all three scenarios (9.4–10.3%) exceed the percentage of total energy provided by the arrays (6.8%), which is a non-obvious result. This result occurs partly because the energy that is being displaced by low-cost solar tends to come from higher-than-average cost generators rather than from lower-than-average cost generators. The solar arrays in this study also increased ancillary services costs by approximately \$10 Million per year. This 3% increase is small when compared to the overall reduction in total dispatch cost.

Second, 22,500 GWh of solar generation reduces peak demand by 2.6–3.2 GW and increases net load flexibility requirements. Solar generation is not always closely aligned with load, but it is aligned enough to reduce the amount of thermal generation capacity needed by the electricity system during peak demand. However, the solar PV arrays only reduce annual peak demand by 15–23% of their installed capacity. Solar will eliminate the need for some existing dispatchable capacity, however most

of the generators in the generator fleet will still be needed to meet peak summer demand, though they will be utilized for fewer hours during the year. Solar will also intensify ramping and volatility, particularly during shoulder seasons, requiring spare capacity to be available to provide increased system flexibility.

Third, solar affects how dispatchable generation is utilized in ERCOT. There appear to be two effects that influence this utilization. One, solar tends to reduce day-time net load which displaces higher-cost generators and reduces total dispatch cost. Slow-ramping, mid-load generation provides much of the flexibility needed to accommodate this net load reduction. Two, solar requires greater system flexibility, and, without broader system changes, needs dispatchable generators to support its large-scale integration, some of which are expensive faster-ramping generators that increase total dispatch cost. This dichotomy along with relatively small reductions to the annual maximum net load are notable characteristics of an electric grid with large solar penetration. This situation presents opportunities for demand response, electricity storage, and other supporting technologies to gain additional value by reducing solar integration costs.

Fourth, solar generation reduces emissions and water consumption. If carbon dioxide emission reductions, water conservation, and other environmental considerations continue to gain support, solar technology could be an important contributor for realizing those goals. For instance, if CO₂ were priced at \$10/ton and SO_x and NO_x at \$10k/ton, the emissions reductions from these solar scenarios would contribute an additional \$350 million in value.

The differences in the value of solar generation based on location and ori-

entation can be explained by comparing the integration costs of the different solar scenarios. The integration costs from the UC&D simulations can be categorized as flexibility costs and thermal utilization costs. Transmission constraints, which can also contribute to integration costs, are ignored in this model. When compared to the other scenarios, the East scenario did not excel in efficient power plant utilization or reduced flexibility requirements and was the worst scenario at minimizing total dispatch cost. Even though the East array is better aligned with the seasonal load of the ERCOT market, its daily summer generation peaks a few hours before the peak demand. This incongruence should be examined in future studies to see if solar arrays with both seasonal and daily correlations with peak demand can be employed. When comparing the South and West scenarios, the South array produces a net load profile with lower ramp rates and less volatility, which translates to lower flexibility requirements and lower costs. However, the West array utilizes the existing thermal resources more effectively by dispatching more of the efficient coal and natural gas combined cycle resources and less of the inefficient natural gas boiler and open cycle gas turbine resources as shown in Table 3.2. This efficient use of the thermal generation fleet also translates to lower costs. The West scenario reduces dispatch costs more than the South scenario by a non-trivial amount. This comparison strongly suggests that the total dispatch cost is influenced more by the efficient use of thermal generation assets than by flexibility requirements.

A number of these conclusions should be insightful as electric grids plan for future capacity expansion. Encouraging the growth of solar energy generation can be a good step towards achieving sustainability goals, but it must be done with

care. The orientation and geographic location of solar panels within an electric grid not only affects emissions, but influences the generator dispatch, total dispatch cost, system flexibility requirements, and other parameters that grid developers might not have considered. This study aims to contribute new knowledge about the holistic affects of integrating solar generation into the grid that will help inform these grid development decisions.

Chapter 4

The impacts of wind and solar on grid flexibility requirements in the Electric Reliability Council of Texas

Chapter 4 illustrates a framework for quantifying flexibility requirements by analyzing the correlation of increasing wind and solar generation with grid flexibility requirements in ERCOT. The trends discussed in this study are intended to provide meaningful insight for grid planners as they anticipate the growth of renewable energy resources and the strategies they should implement to maintain reliability and manage integration costs. This insight is especially valuable for grids with rapid penetrations of renewables already underway or looming, such as Germany, China, Australia, Ireland, ERCOT, and many others.

This chapter is an updated study of “The impacts of wind and solar on grid flexibility requirements in the Electric Reliability Council of Texas” as published by *Energy* in 2017 [41].

4.1 Methods

The methods for this study are presented in three separate subsections. Section 4.1.1 discusses the calculation of the peak output, a proxy for installed capacity,

and illustrates the renewable energy capacity growth used in this analysis. Section 4.1.2 discusses the data sources used for this study and the methods used to expand them. Section 4.1.3 discusses the limitations of the analysis.

4.1.1 Peak Output Calculation

Portions of this paper compare the flexibility requirements with the amount of renewable energy installed on the grid. Rather than using the installed capacity, this study compares the flexibility requirements with the greatest demonstrated wind and solar output up to the date being analyzed, referred to now as the “peak output”. While installed capacity does not account for capacity factors or solar resource efficacy, these properties are inherent in the peak output, which simplifies its comparison between grids with different solar resources. Additionally, the peak output, being calculated directly from the data used in this study, is more quantitatively robust than the approximate installed capacity numbers shown herein. Fig 4.1 shows the growing installed capacity and peak output for wind and solar from 2008–2025. As seen in the figure, the peak output can be roughly divided into the 2008–2015 “wind era” where wind output grows steadily and solar output remains negligible and the 2016–2025 “solar era”, which is a simulated forward-looking era during which wind output is held constant and solar output grows steadily. This capacity growth scenario is not meant to suggest that wind capacity will not grow in ERCOT in the future; it simply provides a useful analytical scenario. Thus, this study assumes that changes in flexibility requirements during the wind era are driven by increasing wind output, and changes in flexibility requirements during the solar era are driven by

increasing solar output.

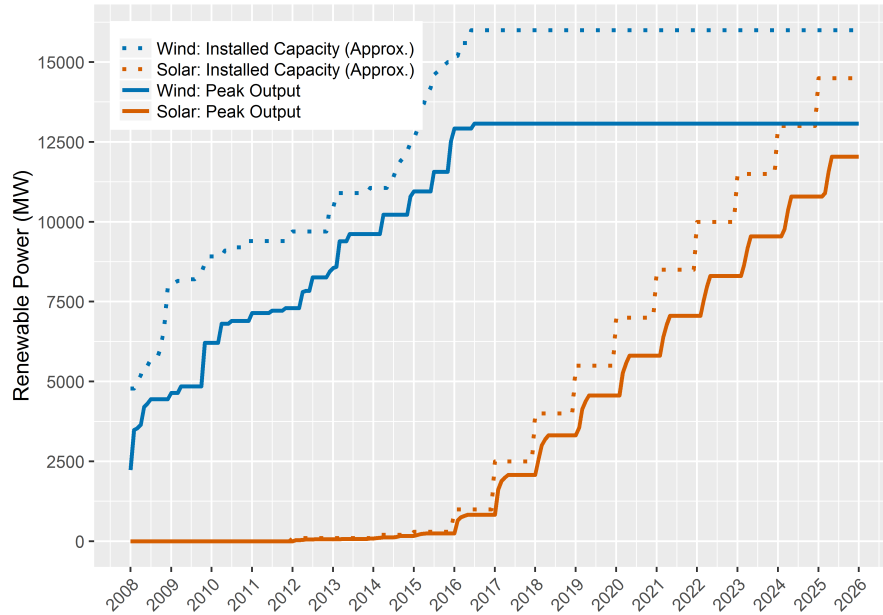


Figure 4.1: Growth of the wind and solar peak output can be organized into the 2008–2015 “wind era” and the 2016–2025 “solar era”.

4.1.2 Data Generation

This study analyzes a set of 15-minute resolution, load, wind, and solar data from 2008–2025. This data set was created using different data sets acquired from ERCOT and NREL as described in Table 4.1. When creating the data, discontinuities between the first interval of any calculated year of load, wind, or solar data and the last interval of the previous year’s data are connected by a linear interpolation with a slight slope (less than 500 (MW/15min)) until the discontinuity has been removed. This adjustment preserves continuity between years without creating artificial periods of significant ramping. See Table 4.2 for an example of this calculation.

By basing all load, wind, and solar projections off of a single year of data (2012), potential weather-related correlations between load, wind, and solar are preserved. ERCOT advised the authors to use 2012 as a base year due to their perception of 2012 as a typical grid operation year without extreme weather, outage, or other outlier events.

Portions of the 15-minute resolution 2008–2025 load, wind generation, and solar generation data are visualized in Figs 4.2-4.4. Fig 4.2 shows the net load for each 15-minute interval, averaged over all the days in January for each year. It exhibits the two-peak net load often seen during the winter and shoulder seasons in ERCOT. From 2016–2025, an increase in projected load drives the load curve upward each year, but increasing solar generation drives the net load down from 8:00 to 18:00 when solar generation is producing electricity. This reduction of the daytime net load creates steep ramp rates around 10:00 and 17:00 and moves the minimum net load to the middle of the day. Fig 4.3 shows the net load at each 15-minute interval on February 8th of each year after 2016, when solar capacity begins to trend upward. In addition to steeper ramp rates, this figure also shows the increasing volatility of the net load curve as solar penetration increases. Fig 4.4 shows the net load for each 15-minute interval, averaged over all the days in June for each year. It exhibits the large mid-day peak driven significantly by air conditioning demand. From 2016–2025, an increase in projected load drives the net load curve upward each year. As solar generation turns on around 6:30, it reduces the net load, creating steep downward ramp rates. As solar generation falls off around 18:30, the net load quickly rises, creating steep upward ramp rates.

Table 4.1: Different data sets acquired from ERCOT and the National Renewable Energy Laboratory (NREL) [130] were used to create the “Model Data” described in this table.

	Name	Resolution	Description	Source
Source Data	ERCOT 2008–2014	15-minute	Load and wind data from 2008–2014. Solar data from 2012–2014 (solar generation was not tracked until 2012).	ERCOT
	ERCOT 2015	60-minute	Load, wind, and solar data.	ERCOT
	ERCOT Load Projections	60-minute	Projected load data for 2016–2025, based on 2012 weather data.	ERCOT
	NREL NSRDB [130]	30-minute	Historical weather data and calculated solar insolation data, such as global horizontal radiation (GHI), needed to calculate solar panel power output.	NREL
Model Data	2008–2014 Load, Wind, Solar	15-minute	Taken verbatim from “ERCOT 2008–2014” data set.	
	2015 Load	15-minute	The 2012 load data from the “ERCOT 2008–2014” data set was multiplied by a constant scaling factor. The resulting load profile has the same annual peak demand as the “ERCOT 2015” data set.	
	2015 Wind	15-minute	The 2012 wind data from the “ERCOT 2008–2014” data set was multiplied by a linear scaling factor. The resulting wind profile has the same January installed wind capacity as January 2015, and the same December installed wind capacity as December 2015.	
	2016–2025 Wind	15-minute	The 2012 wind data from the “ERCOT 2008–2014” data set was multiplied by a linear scaling factor. The resulting wind profile has the same January installed wind capacity as December 2015, and the same December installed wind capacity as December 2015. This wind profile is repeated annually for 2016–2025, assuming that the installed wind capacity at the end of 2015 (15.7 GW) remains constant through 2025 with no additional wind being installed.	
	2015–2025 Solar	15-minute	Using the “NREL NRSDB” database, 2012 weather profiles for eleven locations across west and central Texas were compiled. These eleven weather profiles are read into the NREL System Advisor Model software [127], which translates the weather profiles and solar array properties into 30-minute resolution, 1-axis tracking, solar generation profiles. By weighting these profiles to accentuate west and central Texas, normalizing the output to the installed capacity, and averaging each pair of adjacent, 30-minute interval data points to create 15-minute interval data points, a 15-minute solar generation profile is created. Each year in the 2015-2025 solar data set is created by multiplying this normalized generation profile by the installed capacities in Table 4.3.	
	2015–2025 Comparison Solar	15-minute	The method for creating the “2015–2025 Solar” data set is used to create a variety of different solar installation scenarios as shown in Table 4.3. The flexibility requirements of these scenarios are compared against each other in the analysis.	

Table 4.2: Since portions of the data are created by connecting December 31 to January 1 of the same year, discontinuities will arise, as shown here for the load. The discontinuity between the actual load at 12/31 23:45 and 1/1 0:00 leads to an artificial ramp rate of -2,792 MW/15min. Adjusting the load to the indicated values removes the artificial ramp rate and creates continuity between the data.

	12/31 23:15	12/31 23:30	12/31 23:45	1/1 0:00	1/1 0:15	1/1 0:30	1/1 0:45	1/1 1:00	1/1 1:15
Actual Load	29,860	29,570	29,313	26,521	26,441	26,358	26,269	26,058	25,892
Actual Ramp		-290	-257	-2,792	-80	-83	-89	-211	-166
Adjusted Load	29,860	29,392	28,892	28,392	27,892	27,392	26,892	26,392	25,892
Adjusted Ramp		-468	-500	-500	-500	-500	-500	-500	-500

Table 4.3: The installed solar capacity increases according to the top portion of this table. The bottom portion of this table describes the different solar location and orientation scenarios used for comparison in this study.

Installed Solar Capacity	2015	300 MW total
	2016	1,000 MW total
	2017–2024	+1,500 MW of new capacity added each year ⁷
	2025	14,500 MW total
Solar Scenarios	Location Comparisons (all 1-axis tracking arrays) (see Table 4.4 for detailed geographic information)	West: emphasis on west and central Texas (best solar resource locations)
		Central: emphasis on central Texas (best proximity to population centers and transmission infrastructure)
		South: emphasis on south and central Texas (another good solar resource location)
	Orientation Comparisons (all West located; 20-deg above-horizontal tilt for all fixed panels)	Fixed West: all solar is fixed, west-facing panels
		Fixed Southwest: all solar is fixed, southwest-facing panels
		Fixed South: all solar is fixed, south-facing panels
		Fixed Southeast: all solar is fixed, southeast-facing panels
		1-axis: all solar is 1-axis tracking (identical to the West scenario)
2-axis: all solar is 2-axis tracking panels		

Table 4.4: Solar data from 19 different cities is used in this study [130]. The solar profile for each “location comparison” scenario is built from the indicated fractions of each city’s solar profile.

Solar Array Location (City)	Location Comparisons		
	West	Central	South
Abilene	0.08	0.08	0
Alpine	0.13	0	0
Amarillo	0.08	0	0
College Station	0	0.08	0.06
Del Rio	0	0	0.14
Fort Worth	0.04	0.2	0
Guthrie	0.08	0	0
Houston	0	0.2	0.06
Laredo	0	0	0.14
Longview	0	0.08	0
Lubbock	0.08	0	0
Lufkin	0	0.04	0
McAllen	0	0	0.14
Midland	0.13	0.08	0.06
Pecos	0.13	0	0
San Antonio	0.04	0.16	0.14
Sheffield	0.13	0	0.06
Sonora	0.08	0.04	0.06
Victoria	0	0.04	0.14

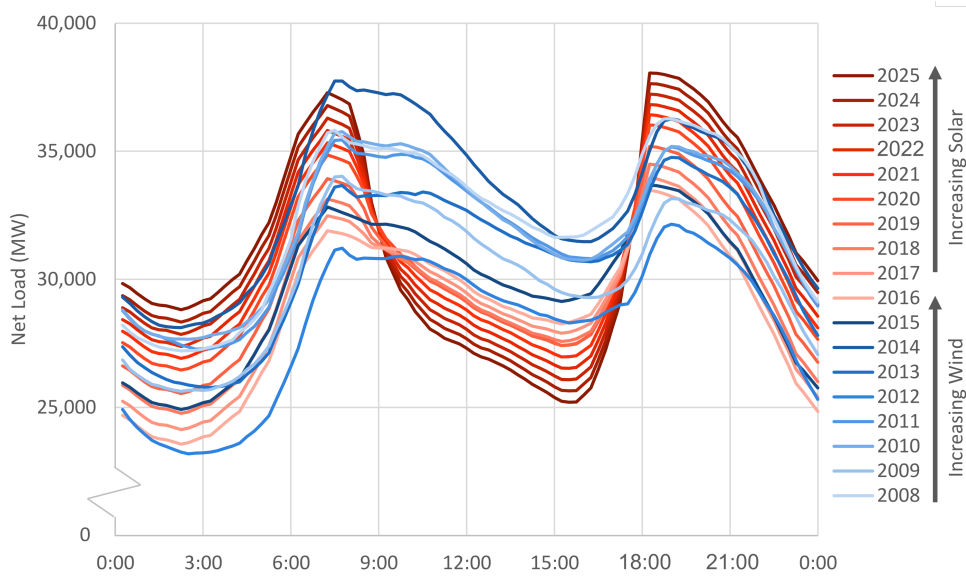


Figure 4.2: This chart shows the net load for each 15-minute interval, averaged over all the days in January for each year. January exhibits the two-peak net load often seen during the winter and shoulder season months in ERCOT. The years 2008 to 2015 are a period of rapid growth in wind capacity. From 2016–2025, as more solar is added to the grid, it generates power from 8:00 to 18:00, reducing the net load and creating steep ramp rates as the sun rises and sets.

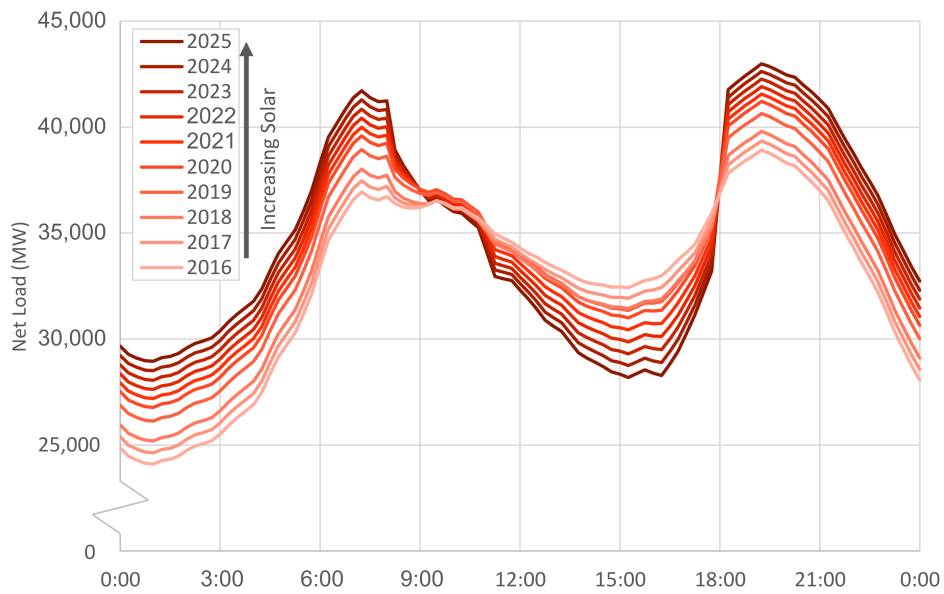


Figure 4.3: The net load is shown for each 15-minute interval on February 8th of each year after 2016, when solar capacity begins to trend upward. These profiles strongly exhibit the tendency for solar generation to increase the ramping and volatility of the net load as discussed later in this study.

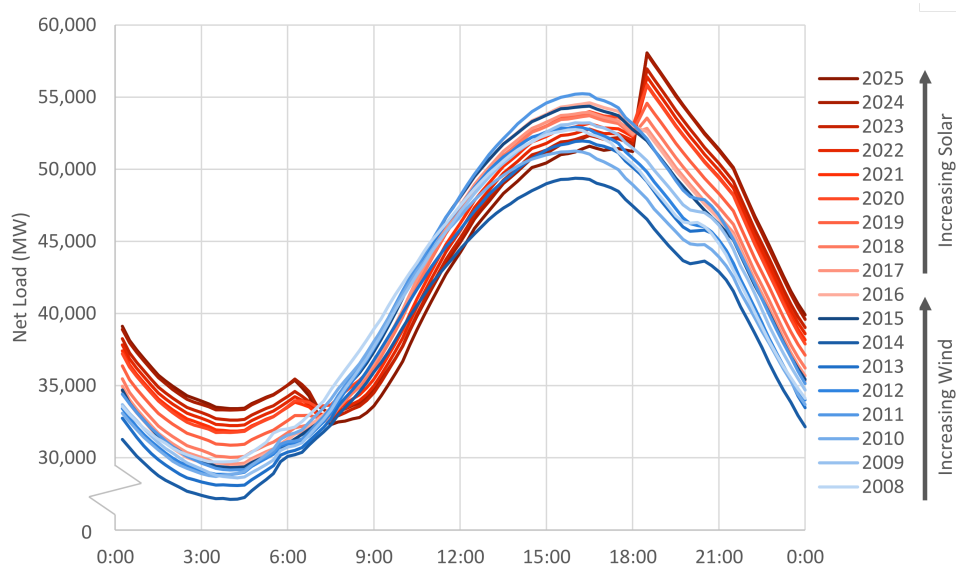


Figure 4.4: This chart shows the net load for each 15-minute interval, averaged over all the days in June for each year. June exhibits the dramatic single-peak net load seen during the summer months in ERCOT where peak net load is driven significantly by air conditioning demand. The years 2008 to 2015 are a period of rapid growth in wind capacity. From 2016–2025, as more solar is added to the grid, it generates power from 6:30 to 18:30, reducing the net load and creating steep ramp rates as the sun rises and sets.

A hypothesis can be developed by observing the general timing, ramping, and volatility of the curves in Fig 4.5, which shows the capacity factors for the load, wind, and solar profiles in 2025 averaged over the months of January (winter), April (shoulder season), and August (summer). Considering that peak demand (80.0 GW) is six to seven times greater than the peak wind (13.1 GW) and solar (11.1 GW) output, it is likely that flexibility requirements will be driven by changes in the demand profile, where the maximum ramp up rates tend to occur in the morning and the most severe ramp down rates tend to occur in the evening. Renewable generation will accentuate these demand-driven flexibility requirements whenever changes in renewable output are asynchronous with demand, e.g. flexibility requirements caused by simultaneously decreasing demand and increasing wind output will exceed the flexibility requirements caused by decreasing demand alone. Alternatively, abrupt changes in renewable output might create flexibility requirements of greater magnitude than the existing demand-driven flexibility requirements, e.g. large amounts of solar capacity might ramp up and down with the sun quickly enough to create net demand ramp rates that are greater than the demand-driven ramp rates.

Wind output shows some asynchronization with the demand profile, which might cause correlations between increasing wind capacity and increasing flexibility requirements. On average, wind output undergoes sustained, multiple-hour ramp ups as demand is ramping down in the evening, particularly in the winter and summer, suggesting that greater wind capacity might cause minimum 1-hour and 3-hour ramp down rates to worsen. However, wind output is somewhat flatter during the morning as demand is ramping up, suggesting that additional wind capacity will not

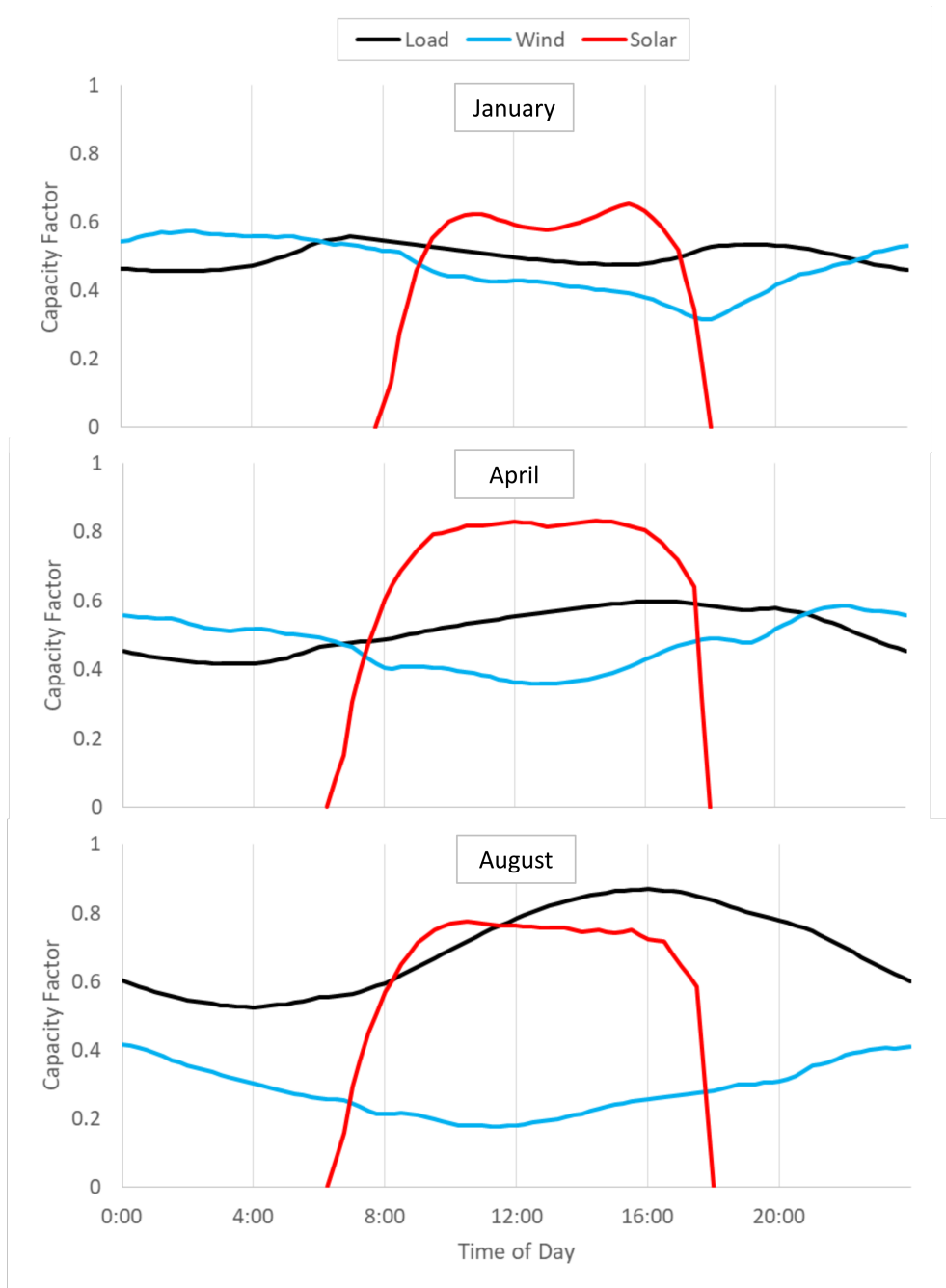


Figure 4.5: This chart shows load, wind, and solar capacity factors averaged over the months of January (winter), April (shoulder season), and August (summer). Peak demand, wind output, and solar output are 80.0, 13.1, and 11.1 GW, respectively.

significantly impact maximum 1-hour or 3-hour ramp up rates.

Solar output tends to be more synchronized with the demand profile, meaning that it has a limited ability to intensify the existing demand-driven flexibility requirements. However, solar output does change dramatically with sunrise and sunset. These quick changes in solar output suggest that large amounts of solar capacity might cause a shift from demand-driven to solar-driven flexibility requirements. In this case, the largest net demand ramp up rates will occur in the evening as solar output falls off with the setting sun and the most severe net demand ramp down rates will occur in the morning as solar output spikes with the rising sun.

Both the wind and solar output curves exhibit chatter or noisiness that will contribute to net demand volatility. This chatter is unrelated to the noisiness of the demand profile, meaning that the net demand curve will likely have more volatility than the demand profile, and increasing wind and solar capacity might both cause greater net load volatility.

4.1.3 Limitations

While this study offers some improvements over previous flexibility analyses as discussed in Section 6.1, it also experiences some limitations. First, this study fails to address the contribution of random stochastic noise to the overall flexibility requirements. Random noise contributes to flexibility requirements, especially in the 5-minute or less time scale [72]. Forecast errors due to the weather-related uncertainties of renewable energy power output also contribute to flexibility requirements [89]. Since this study assumes perfect knowledge of 15-minute resolution renewable energy

generation, it ignores forecast errors and overlooks much of the random variation that can increase flexibility requirements on shorter timescales.

Additionally, the quality of the solar data might fail to capture extreme flexibility requirements caused by infrequent weather events. While this study uses multiple solar generation locations to simulate the smoothing effect of geographic diversity as recommended by Lettendre et al. [107], data collection over a larger geographic area might better represent this effect. Additionally, while converting the solar data from 30-minute to 15-minute intervals allows this study to be performed on a 15-minute time frame, thus preserving the resolution of the load and wind data, it produces a solar curve that is smoother than actual 15-minute data would be. Higher resolution solar data would improve the model's ability to observe its variability at this time interval. Historical solar generation data would also be an improvement over the calculated solar data used in this study. Still, a large degree of solar variability results from the path of the sun through the sky, a variable that is easily anticipated [107] and is captured in the data used in this analysis. With these limitations in mind, the results from this study will be used to communicate the general flexibility trends associated with increased renewable energy generation, rather than analyzing specific dates or events.

Finally, though this study quantifies flexibility requirements using five different ramping and volatility metrics, there are numerous other calculations that could be used to discuss changing flexibility requirements [113]. Some of these metrics, such as the range in daily net load, have been excluded either due to their limited correlation with wind and solar peak output or with the brevity of this paper in

mind.

4.2 Results and Discussion

The majority of the results are visualized using three different chart types. Density charts, as shown in Fig 4.6, plot the density function of the flexibility requirements calculated for each 15-minute interval of each year. The area under each density curve sums to 1. The x-axis is truncated to highlight the changing shape and center of the density curves. The maximum values, being excluded during these truncations, are shown in other chart types.

Contour charts, as shown in Figs 4.7 and 4.8, plot the median or maximum value of the flexibility requirements for each week of each year. Moving up the y-axis shows how increasing wind and solar peak output changes the flexibility requirements (since the wind and/or solar output increases each year per Subsection 4.1.2). Moving across the x-axis shows how flexibility requirements change throughout the seasons.

Scatter charts, as shown in Figs 4.9 and 4.10, plot wind and solar peak output on the x-axis and flexibility units on the y-axis. These charts give a sense of the flexibility requirement quantities being experienced during each week. The solar section of the chart has a constant wind peak output of 13.1 GW while solar increases annually per Subsection 4.1.2. The regression lines suggest whether increased wind or solar peak output is noticeably correlated with flexibility requirements. Additional statistical analysis of the results can be found in the Appendix (Chapter A).

4.2.1 Wind and Solar Peak Output Comparison

The following subsection analyzes the changes to the net load caused by increasing wind and solar peak output. The analysis is performed using the West scenario described in Subsection 4.1.2. Detailed results are presented in subsections 4.2.1.1-4.2.1.5 with a summary of the results shown in Table 4.5. In each subsection, the results will be discussed in consideration of both the wind era, where wind peak output increases from 2.4 GW to 13.1 GW during 2008–2015, and the solar era, where solar peak output increases from 0.6 to 12.0 GW during 2016–2025.

4.2.1.1 1-Hr Ramp Rates

The 1-Hr ramp rate requirements for 2008–2025 are summarized in Figs 4.6 through 4.11. As wind peak output increases, the density curves in Fig 4.6 show no discernible trend and the median stays relatively centered on 0 MW/hr. Fig 4.8 shows a possible correlation between increasing wind peak output, decreasing December–March ramping, and increasing June–August ramping, but the effect is minor. Based on Fig 4.11 lower minimums seem to be the only 1-hr ramp rate statistic that correlates with increasing wind penetration.

As solar peak output increases, the density curves in Fig 4.6 tend to widen, showing fewer ramp rates in the -1,000 to 2,000 MW/hr range and more in the <-1,000 and >3,000 MW/hr range with the median staying near 0. Fig 4.8 shows a noticeable correlation between maximum 1-hr ramp rates and solar peak output, especially from November to May. February 2023–2025 experiences some 1-hr ramp rates in excess of 12,000 MW/hr, the highest in this study. Figs 4.10 and 4.11 suggests

that the minimum and maximum 1-hr ramp rates both correlate with increasing peak solar output.

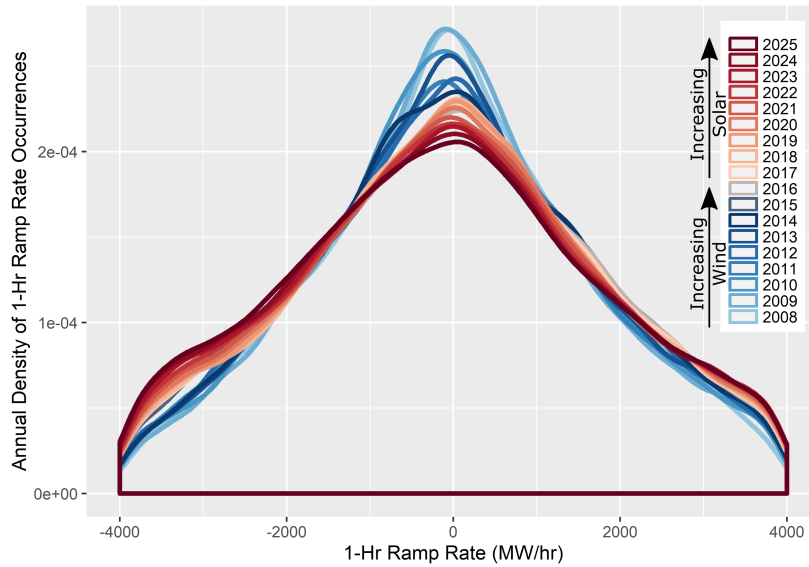


Figure 4.6: The 1-hr ramp rate becomes wider as the solar peak output increases while remaining relatively centered on 0 MW/hr.

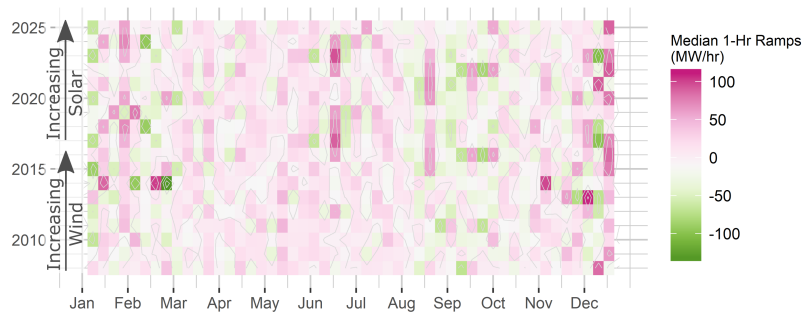


Figure 4.7: The small changes in median 1-hr ramp rate do not appear to be correlated with season or year, remaining relatively centered on 0 MW/hr.

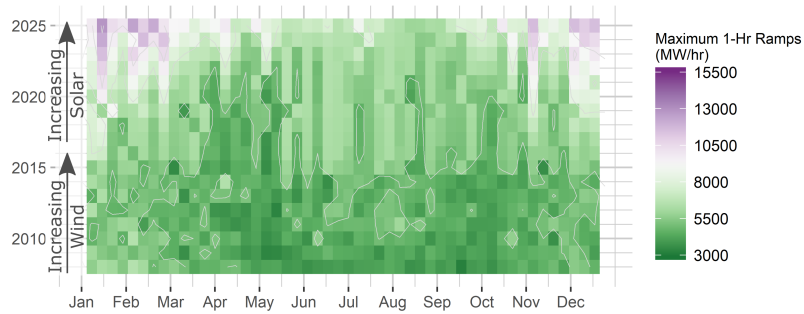


Figure 4.8: The maximum 1-hr ramp rate increases with solar peak output, especially between November and April.

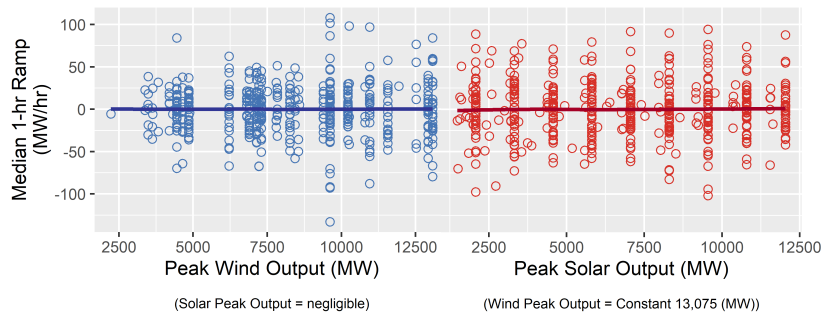


Figure 4.9: The median 1-hr ramp rate does not appear to be correlated with wind or solar peak output.

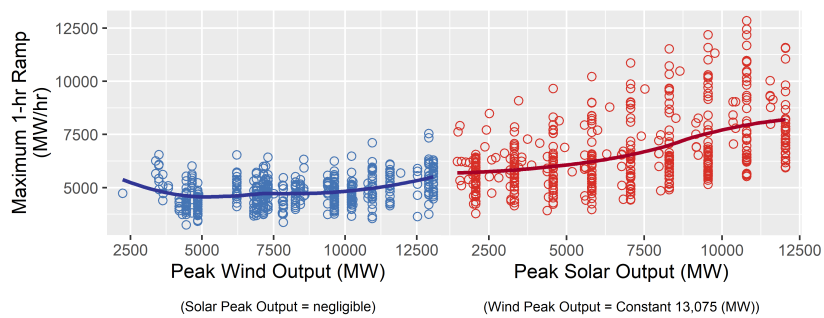


Figure 4.10: The maximum 1-hr ramp rate appears to be positively correlated with peak solar output, while the first additions of wind peak output might have slightly reduced the maximum.

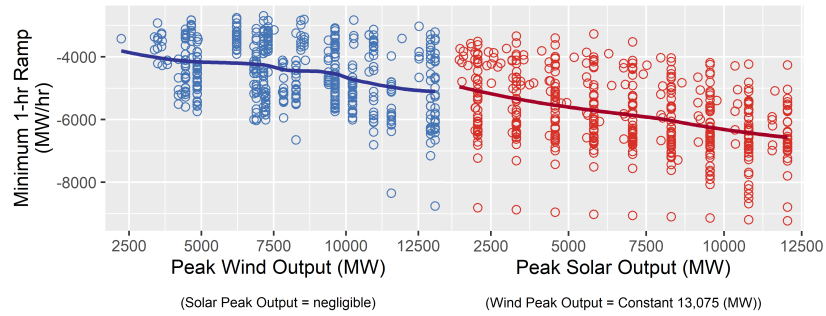


Figure 4.11: The minimum 1-hr ramp rate worsens slightly with increasing wind and solar peak output.

4.2.1.2 3-Hr Ramp Rates

The 3-Hr ramp rate requirements for 2008–2025 are summarized in Figs 4.12 through 4.17. As wind peak output increases, the density curves in Fig 4.12 show no discernible trend, though Fig 4.13 suggests higher medians during the shoulder seasons in general. Fig 4.14 shows an increase in summer 3-Hr ramp rates as wind peak output increases, but the effect seems to level off. Figs 4.16 and 4.17 suggest that greater wind peak output correlates with worsening minimum and maximum 3-Hr ramp rates.

As solar peak output increases, the density curves in Fig 4.12 tend to widen, showing fewer ramp rates in the -1,500 to 6,000 MW/3hr range and more in the <-1,500 and >6,000 MW/3hr range with the median shifting to the right. In Fig 4.13, the median summer 3-hr ramp rates change from negative to positive. Fig 4.14 shows a noticeable correlation between maximum 3-hr ramp rates and solar peak output from November through April. The maximum 3-hr ramp rates in the summer, being dominated by trends in the load, are not significantly altered by adding solar peak

output. January and February 2023–2025 experiences some 3-hr ramp rates in excess of 18,000 MW/3hr, the highest in this study. Figs 4.15, 4.16, and 4.17 suggests that 3-hr ramp rate medians, maximums, and minimums tend to worsen with peak solar output.

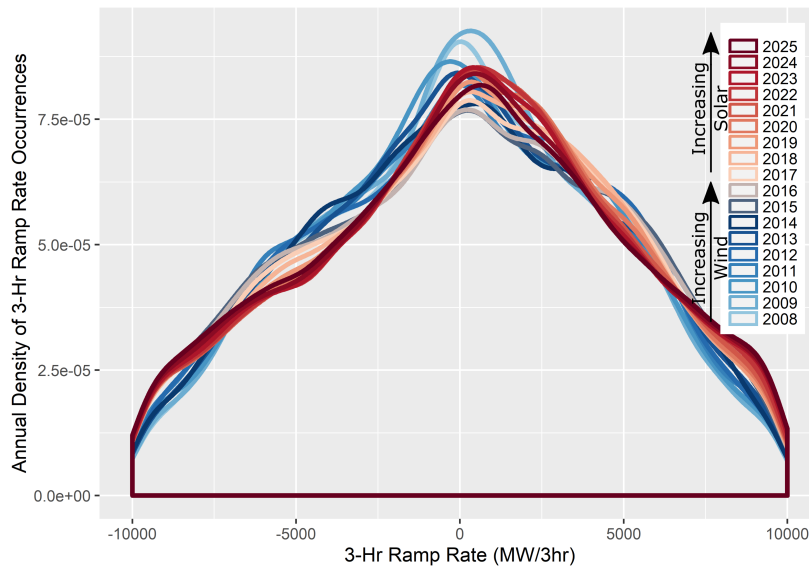


Figure 4.12: The 3-hr ramp rate becomes wider as the solar peak increases while shifting slightly towards the right.

4.2.1.3 Ramp Factors

The ramp rate requirements for 2008–2025 are summarized in Figs 4.18 through 4.22. As wind peak output increases, Figs 4.19 and 4.21 suggest that median ramp factor increases slightly. Figures 4.20 and 4.22 show that maximum ramp factor may tend to slightly decrease as wind peak output increases.

As solar peak output increases, the density curves in Fig 4.18 tend to widen

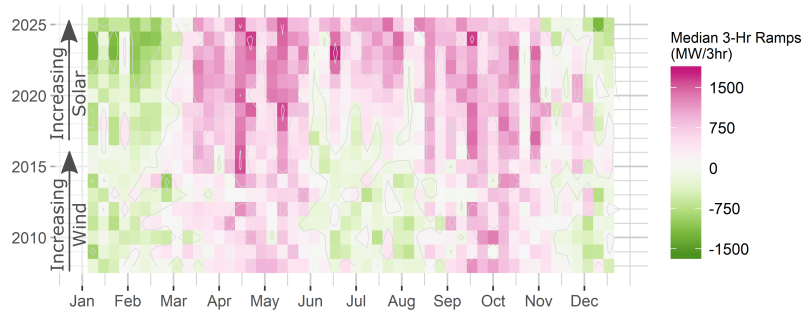


Figure 4.13: The median 3-hr ramp tends to be greater during the shoulder seasons and less during the summer and winter. Increased solar peak output appears to increase the summer median and reduce the winter and spring median.

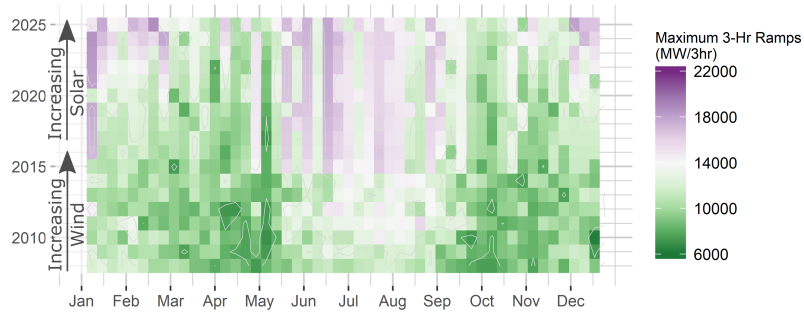


Figure 4.14: Increased wind peak output appears to increase maximum 3-hr ramp rates during the summer. Increased solar peak output appears to increase maximum 3-hr ramp rates from November through April.

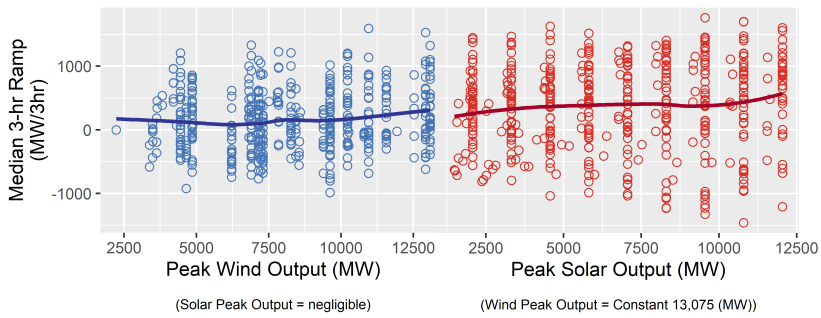


Figure 4.15: The median 3-hr ramp rate does not show a strong correlation with wind peak output, and appears to increase slightly with initial increases in solar peak output.

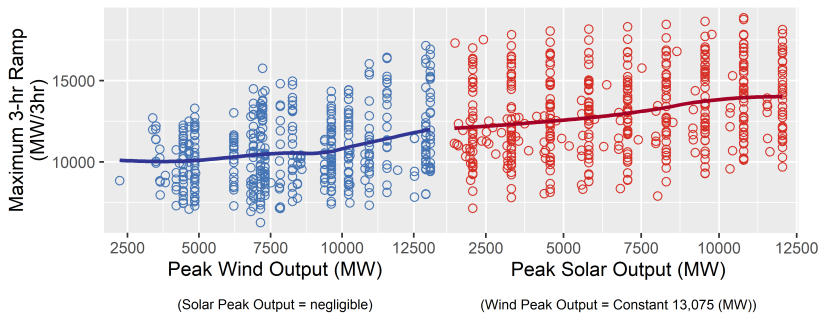


Figure 4.16: The maximum 3-hr ramp rate increases with wind peak output, especially at higher wind penetrations, and increases slightly with solar peak output.

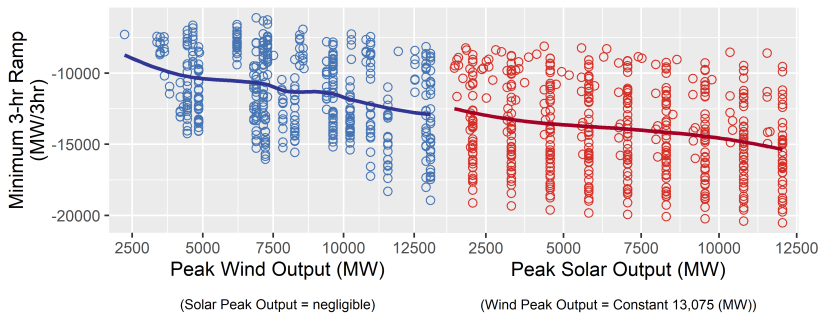


Figure 4.17: The minimum 3-hr ramp rate worsens steadily with increasing wind peak output and slightly with increased solar output.

and shift to the left, showing fewer ramp factors in the -0.005 to 0.025 ((MW/15min)/(MW online)) range and more in the <-0.005 range with the median shifting to the left. Fig 4.20 shows a noticeable correlation between maximum ramp Factors and solar peak output, especially from November to April. February 2025 experiences some ramp factors near 0.25 when 4.9 GW/15min ramp rates occur after net loads of just over 20 GW, situations where total dispatchable generation would need to increase by almost 25% during a 15-minute interval. Figs 4.21 and 4.22 suggest that ramp factor medians tend to decrease and maximums tend to increase with peak solar output.

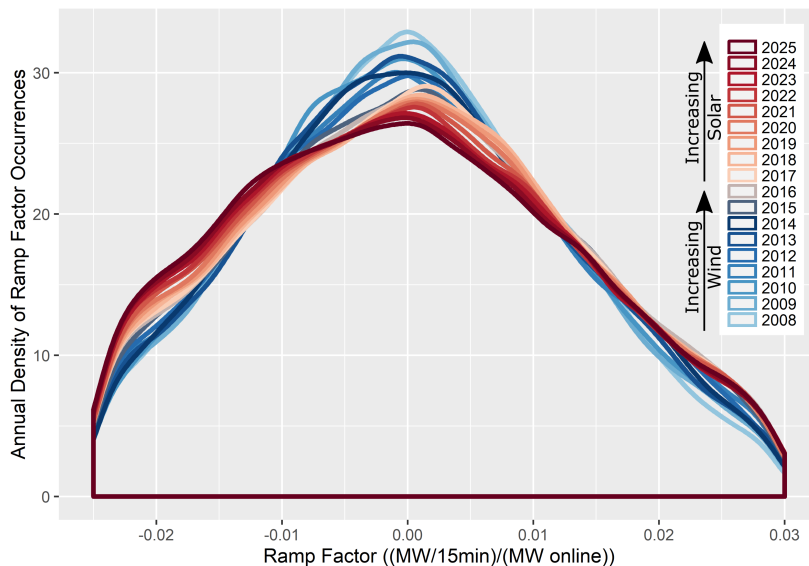


Figure 4.18: The ramp factor distribution becomes wider as the solar peak increases while shifting towards the left.

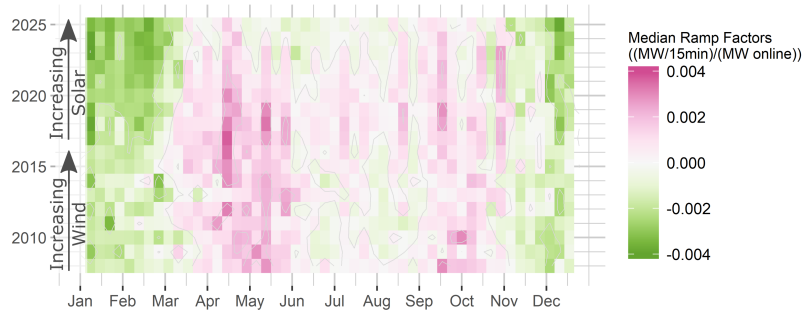


Figure 4.19: The median ramp factor tends to be greater during April–June and September–November. Increased wind peak output appears to slightly increase the median in the summer while increased solar peak output tends to reduce it.

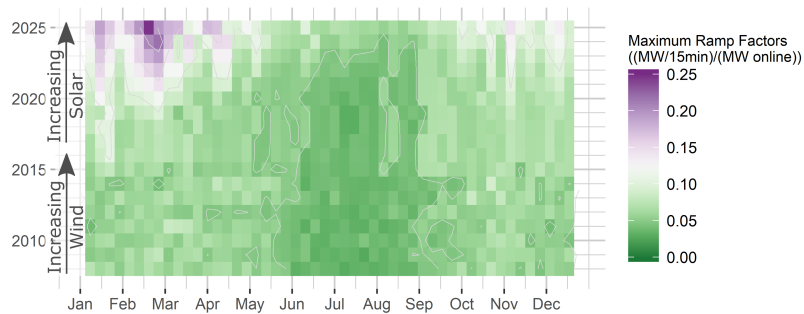


Figure 4.20: Maximum ramp factors are lowest in the summer when large amounts of online generation can more easily handle ramping from the net load. Increasing solar peak output increases the ramp factor, especially from October–May where ramp factors can reach over 0.20.

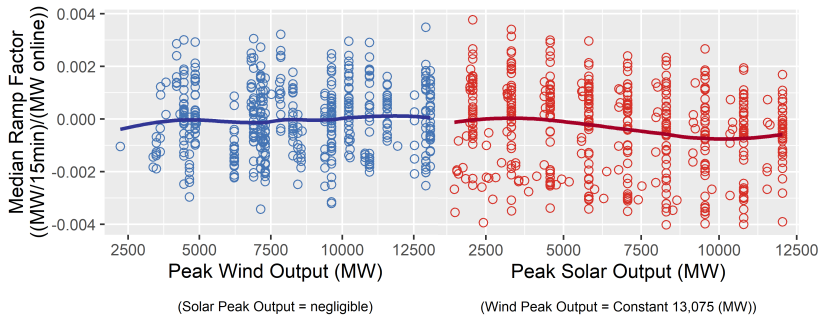


Figure 4.21: The median ramp factor tends to increase with wind peak output and decrease with solar peak output, though it doesn't stray far from 0.00.

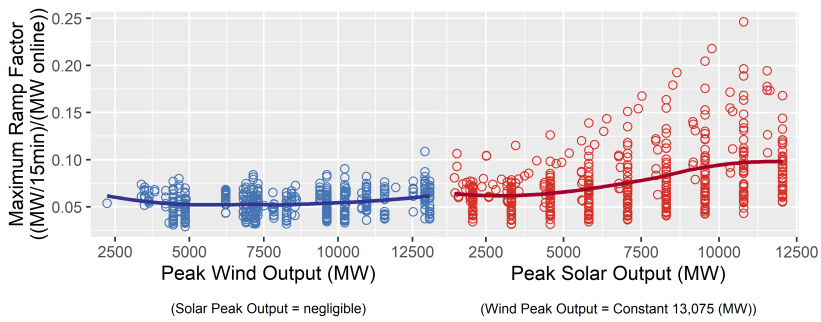


Figure 4.22: The maximum ramp factor tends to decrease slightly with wind peak output and increase with solar peak output.

4.2.1.4 1-Hr Volatility

The 1-hr volatility requirements for 2008–2025 are summarized in Figs 4.23 through 4.27. As wind peak output increases, Figs 4.26 and 4.27 suggest a small correlation with 1-hr volatility that increases at higher wind penetrations.

As solar peak output increases, the 1-hr volatility density curves in Fig 4.23 widen and shift to the right, suggesting that the solar in ERCOT increases the median and maximum 1-hr volatilities. This result is corroborated by Figs 4.24 through 4.27, with the contour charts suggesting a seasonal shift towards higher volatility from February through August and lower volatility from September through January. April–June of 2024–2025 experience some 1-hr volatilities in excess of 9,500 MW/(15min·hr), the highest in this study.

The year 2011, one the hottest and driest years in Texas history, shows uncharacteristically high maximum volatilities in the range of 6,500 MW/(15min·hr). While this year might be considered an outlier, it might provide a historical case study for future work on observing the effects of volatility on prices and dispatch costs.

4.2.1.5 1-Day Volatility

The 1-day volatility requirements for 2008–2025 are summarized in Figs 4.28 through 4.32. As wind peak output increases, Figs 4.26 and 4.27 suggest a small correlation with 1-day volatility that increases at higher wind penetrations.

As solar peak output increases, the 1-day volatility density curves in Fig 4.28

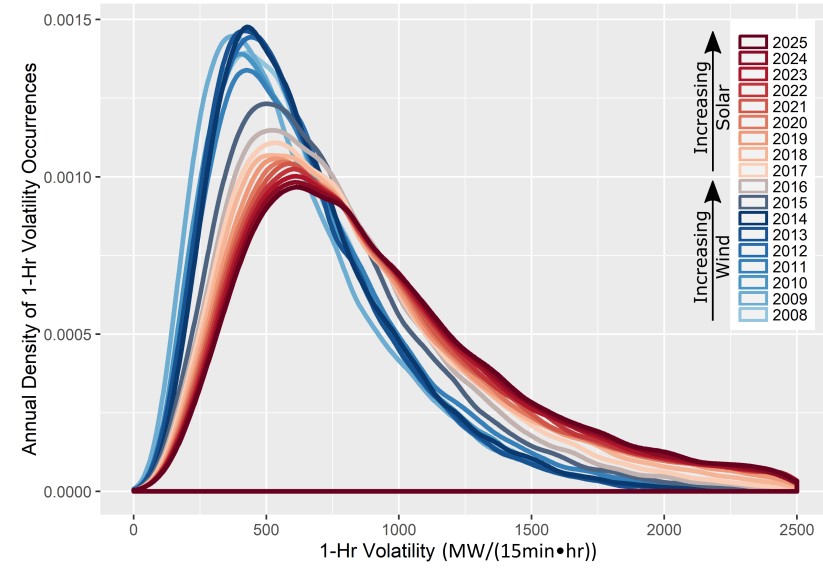


Figure 4.23: Increasing solar peak output widens the 1-hr volatility density curve and shifts it to the right.

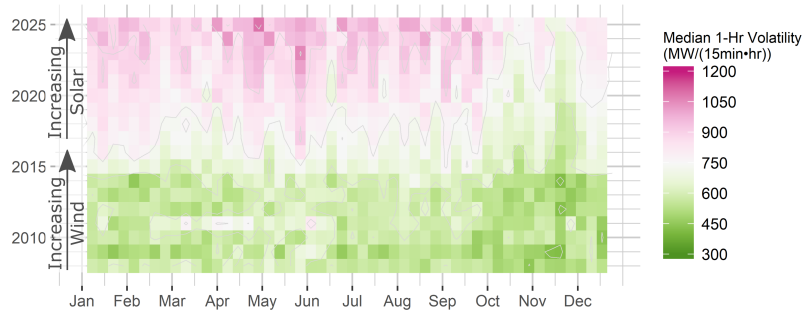


Figure 4.24: Wind does not show a strong correlation with the median 1-hr volatility, while adding solar tends to increase it.

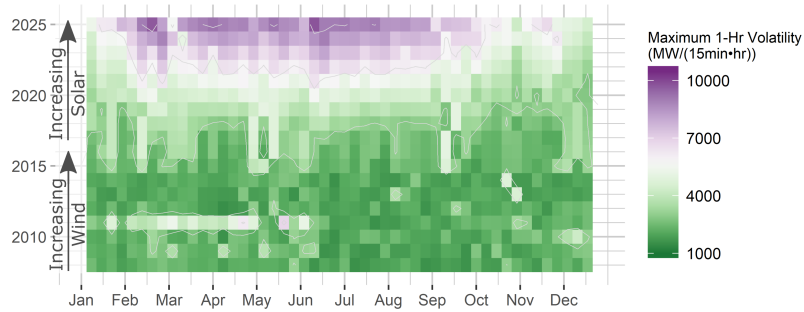


Figure 4.25: Increased solar peak output strongly correlates with increased maximum 1-hr volatility, especially from February through August. Note 2011, an outlier year, which shows strong maximum 1-hr volatility.

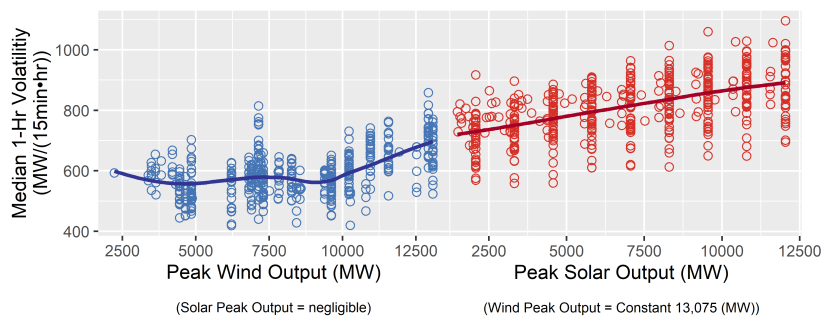


Figure 4.26: Increased wind peak output does not correlate strongly with the median 1-hr volatility except at high penetrations. In the 9,500+ MW wind peak output range, a small amount of solar peak output (150-1,000 MW) might contribute to the sharp increase in median 1-hr volatility. Additional solar peak capacity slightly increases the median 1-hr volatility.

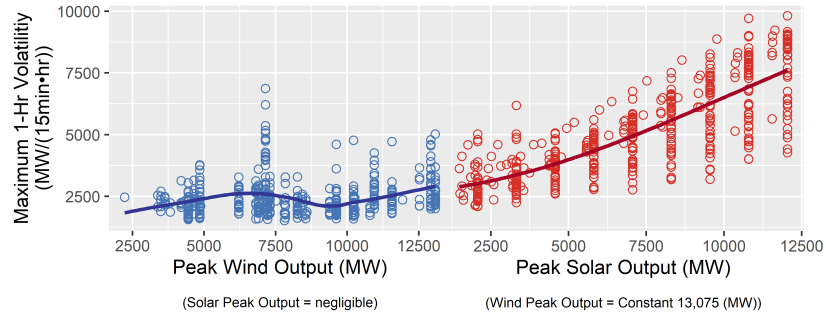


Figure 4.27: Wind does not appear to be correlated with maximum 1-hr volatility except at high penetrations, while peak solar output shows a strong direct relationship.

widen and shift to the right, suggesting that solar shows a strong correlation with increased 1-day volatility. This result is corroborated by Figs 4.29 through 4.32, with the contour charts suggesting a seasonal shift towards higher volatility from January through September and lower volatility from October through December. February and March of 2024–2025 experience some 1-day volatilities in excess of 40,000 MW/(15min·day), the highest in this study.

4.2.1.6 Section 4.2.1 Results Summary

A summary of the results presented in subsections 4.2.1.1–4.2.1.5 is shown in Table 4.5. Table A.1, in the appendix (Chapter A), shows a more complete picture of the results for each year. The results indicate a number of significant correlations between solar capacity and the flexibility requirements analyzed in this study, while wind capacity tends to show only a few slight correlations. Based on Table A.1, adding 14.5 GW of solar (from 2016–2025) to the ERCOT grid increases maximum 1-hr ramp rates by 135%, 3-hr ramp rates by 25%, ramp factors by 125%, 1-hr

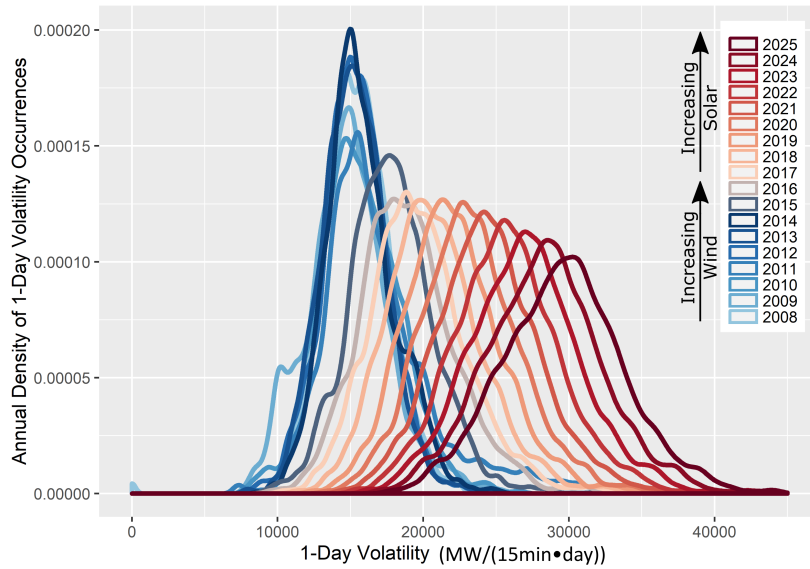


Figure 4.28: Increasing solar peak output widens the 1-day volatility density curve and shifts it to the right.

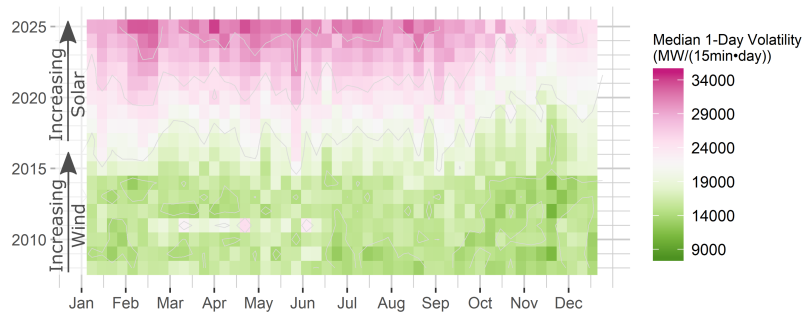


Figure 4.29: Increased solar peak output tends to raise the median 1-day volatility, especially from February through September.

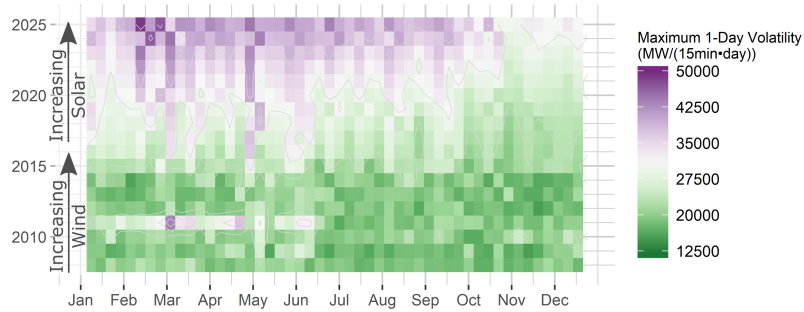


Figure 4.30: Increased solar peak output strongly correlates with increased maximum 1-day volatility, especially from January through September. Note 2011, an outlier year, which shows strong maximum 1-day volatility.

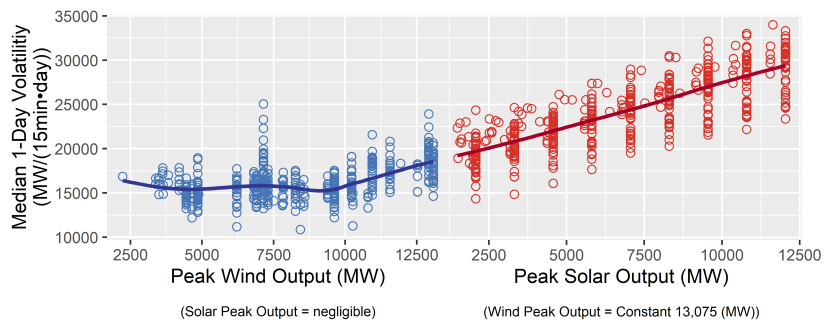


Figure 4.31: Increased wind peak output does not correlate strongly with the median 1-day volatility except at high penetrations. In the 9,500+ MW wind peak output range, a small amount of solar peak output (150-1,000 MW) might contribute to the sharp increase in median 1-day volatility. Additional solar peak capacity increases the median 1-day volatility.

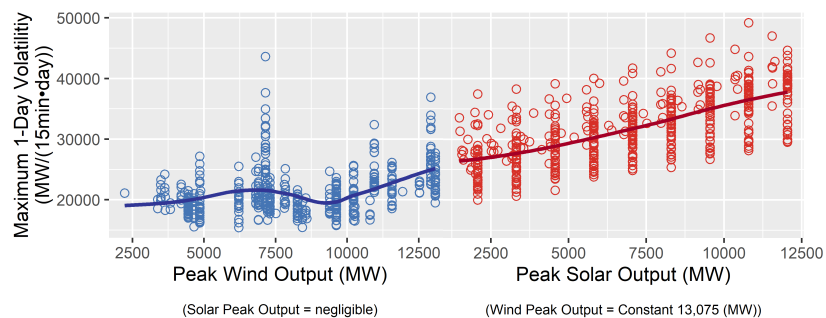


Figure 4.32: Wind does not appear to be correlated with maximum 1-day volatility except at high penetrations, while peak solar output shows a strong direct relationship.

volatility by 100%, and 1-day volatility by 30%. Solar tends to influence ramp rates most strongly from November to April and volatility from February through August. Since ERCOT’s load is lowest in January, February, and March, it is likely that the most significant ramping and flexibility events will occur when fewer generators are on-line to provide flexibility resources and many generators are traditionally shut down for maintenance. Grid operators will need to anticipate these difficult flexibility situations and procure more flexibility resources on the grid as needed.

Likewise, scaling wind up to 16.1 GW of capacity from 2008 to 2016 increases maximum 1-hr volatility by 65% and maximum 1-day volatility by 40% and decreases minimum 1-hr ramp rates by 50% and minimum 3-hr ramp rates by 26% without significantly impacting other flexibility requirements.

The lack of correlation between wind capacity and flexibility requirements contrasts with the results from the GE Energy study [72] discussed in Section 2. The GE Energy study predicts that ramp rates on all time frames from 1 minute to 1

hour will increase as wind capacity increases. The disagreement between these results and those presented in subsections 4.2.1.1–4.2.1.5 could be due to the GE Energy study’s use of modeled weather data to produce calculated wind generation curves. This method for wind data generation might fail to capture the smoothing effects of geographic dispersion of renewable capacity [107] or other factors that influence wind variability. The GE Energy study does conclude that increasing ramp rates caused by wind generation will drive up the maximum amount of regulation reserves that will need to be provided for maintaining grid stability. If this conclusion holds for solar-induced ramp rate increases, then a more robust ancillary services market might be a necessary market response to increasing flexibility requirements.

4.2.1.7 Wind and Solar Confounding

The results indicate that increasing solar capacity correlates strongly with increasing flexibility requirements in a system that already has significant amount of wind generation. To test whether the impact of wind and solar on flexibility requirements are confounded, it is helpful to observe the timing of the different flexibility requirements as shown in Figs 4.33–4.37. As solar capacity grows, the timing of the maximum ramp rates shift from morning to evening, the timing of the shoulder season minimum ramp rates shift from late evening to morning, and the timing of the maximum 1-hour volatility shifts from an assortment of times to evening. These timing shifts represent a system whose largest flexibility requirements are shifting from being driven by the mismatch of demand and wind output to being driven by the daily ramp up and ramp down of solar generation due to the rising

Table 4.5: The results for Section 4.2.1 are summarized in this table.

		Effect of Increasing Wind Capacity	Cause	Effect of Increasing Solar Capacity	Cause
1-Hr Ramp Rate	Min.	Consistent decrease	Simultaneous rising wind output and falling demand in the evening	Consistent decrease	Rising solar output in the morning
	Med.	No correlation	Demand drives ramp rates during most times	No correlation	Demand drives ramp rates during most times
	Max.	Slight or negligible correlation	Falling wind output not generally synchronized with rising demand in the morning	Significant increase, especially in November–April	Falling solar output in the evening
3-Hr Ramp Rate	Min.	Consistent decrease	Simultaneous rising wind output and falling demand in the evening	Slight decrease	Rising solar output in the morning occurs on a shorter timescale than 3 hours, which limits its impact
	Med.	Negligible correlation	Demand drives ramp rates during most times	Slight correlation, increase in June–September, decrease in December–March	Summer from 10:00–16:00, solar output falls slowly during rising demand. Winter from 10:00–14:00, solar output falls slowly during falling demand
	Max.	Slight increase, especially in June–September	Falling wind output not generally synchronized with rising demand in the morning	Moderate increase, especially in November–April	Falling solar output in the evening occurs on a shorter timescale than 3 hours, which limits its impact
Ramp Factor	Med.	No correlation	Demand drives ramp rates during most times	Negligible correlation	Demand drives ramp rates during most times
	Max.	Slight increase, especially June–September	Falling wind output not generally synchronized with rising demand in the morning	Significant increase, especially in November–April	Falling solar output in the evening, accentuated by low net demand in November–April
1-Hr Volatility	Med.	Moderate increase	Noisiness of wind output	Moderate increase	Noisiness of solar output plus quick changes in morning and evening solar output
	Max.	Slight increase	Noisiness of wind output	Significant increase, especially in February–September	Noisiness of solar output plus quick changes in morning and evening solar output
1-Day Volatility	Med.	Moderate increase	Noisiness of wind output	Significant increase	Noisiness of solar output plus quick changes in morning and evening solar output
	Max.	Moderate increase	Noisiness of wind output	Significant increase, especially in February–September	Noisiness of solar output plus quick changes in morning and evening solar output

and setting sun.

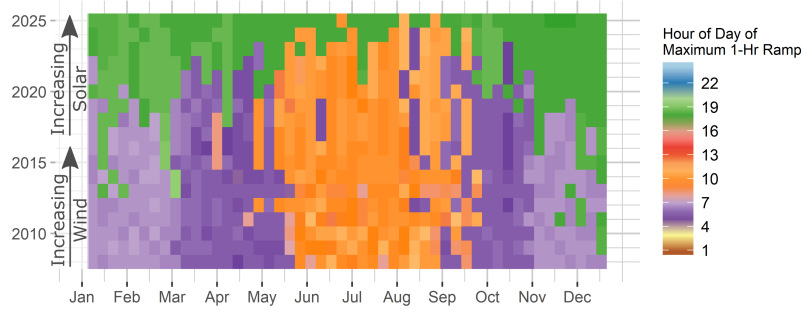


Figure 4.33: As solar capacity increases, the timing of the maximum 1-hour ramp rate shifts from the morning (6:00–9:00, driven by increasing demand and decreasing wind output) to the evening (17:00–19:00, driven by decreasing solar output) especially between November and March when lower demand contributes less to net demand ramp rates.

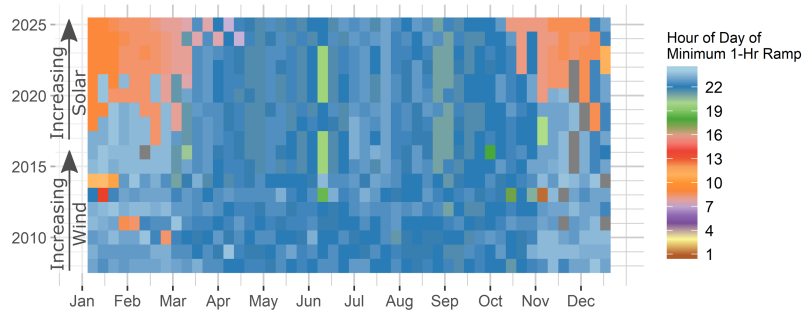


Figure 4.34: As solar capacity increases, the timing of the minimum 1-hour ramp rate shifts from the evening (21:00–23:00, driven by decreasing demand and increasing wind output) to the morning (8:00–10:00, driven by increasing solar output) from November through March.

Removing the wind generation from the system and recalculating the results provides another useful comparison between an all-solar system and a solar-plus-wind system. The results of this additional analysis are shown in detail in Table A.2

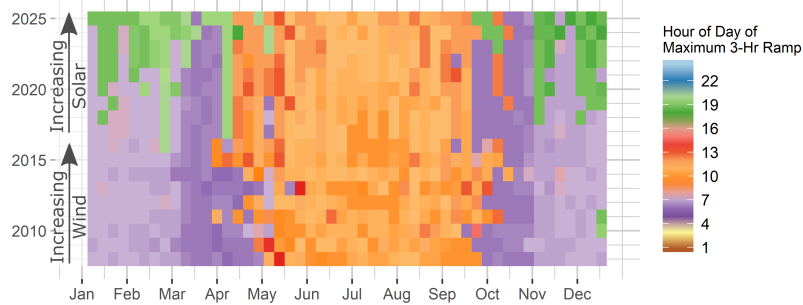


Figure 4.35: As solar capacity increases, the timing of the maximum 3-hour ramp rate shifts from the morning (5:00–8:00, driven by increasing demand and decreasing wind output) to the evening (17:00–19:00, driven by decreasing solar output) from November through March. Maximum 3-hour ramp rates from May through October continue to occur in the late morning, driven by increasing demand.

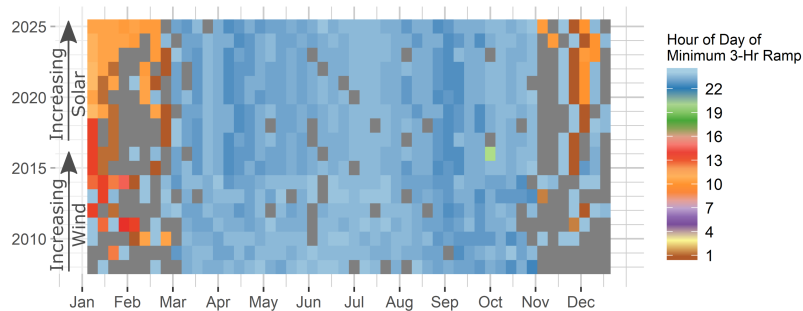


Figure 4.36: As solar capacity increases, the timing of the minimum 3-hour ramp rate shifts from the evening (22:00–24:00, driven by decreasing demand and increasing wind output) to the late morning (9:00–11:00, driven by increasing solar output) from November through March. Minimum 3-hour ramp rates from April through November continue to occur in the late evening, driven by decreasing demand and increasing wind output.

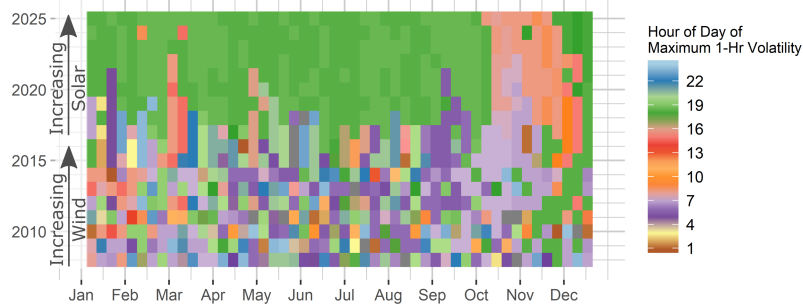


Figure 4.37: As solar capacity increases, the timing of the maximum 1-hour volatility shifts from occurring throughout the day to occurring during the evening (17:00–18:00, driven by decreasing solar output).

in the appendix (Chapter A) and summarized in Fig 4.38. Additional wind capacity has a trivial impact on the annual maximum ramp rates and maximum 1-hour volatility. These annual maximums are driven by the diurnal ramp up and ramp down of solar power, with wind slightly increasing them if it is ramping in sync with solar capacity. Fig 4.11 shows that the minimum 1-hour ramp rate might be a bit of an outlier, though Fig 4.34 and the tightening gap between the “Min. 1-hr Ramp” lines in Fig 4.38 suggests that the minimum 1-hour ramp rate, initially caused by falling demand and rising wind output, will eventually be driven by solar generation ramping up in the morning, in which case additional wind capacity will not significantly impact the flexibility requirement. Wind capacity does appear to significantly increase the maximum 1-day volatility and minimum 3-hour ramp rate versus a solar only system.

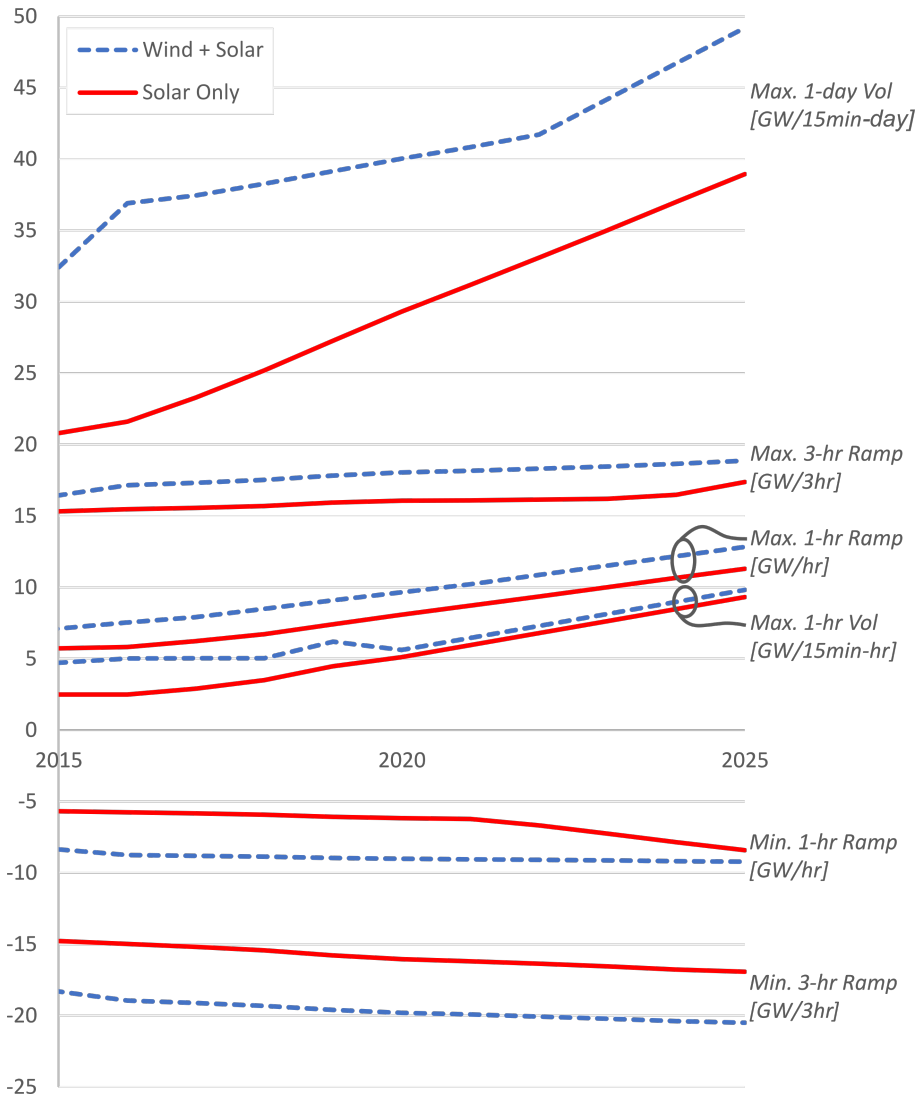


Figure 4.38: Comparison of annual maximum and minimum flexibility requirements in all-solar and solar-plus-wind systems.

4.2.2 Solar Array Orientation and Location Comparisons

The following subsection analyzes the changes to the net load caused by changing the solar array orientation or location. The analysis is performed for the year 2025 using the scenarios described in Subsection 4.1.2. A table has been created for each scenario comparison listing the maximum, 95th percentile, median, 5th percentile, and minimum values for each flexibility requirement and each scenario. Dark green and dark red cell shading indicates when the absolute value of a cell is 20% less or more than the average value. Light green and light red cell shading indicates when the absolute value of a cell is 10% less or more than the average value. By this convention, green cells represent easier-to-manage flexibility requirements, while red cells represent more-difficult ones, and darker shading represents a stronger sense of that definition.

4.2.2.1 Orientation Comparison

Table 4.6 lists the flexibility requirement statistics for the different solar array orientation scenarios in 2025. For example, reading across the “1-Hr Ramp Rate; Max” row, averaging the maximum 1-hr ramp rates of the six scenarios yields 12,401 MW/hr. The “Fixed W” and “Fixed SW” maximum values are within 10% of this average value and do not warrant special attention. The “Fixed S” maximum of 10,546 MW/hr is more than 10% lower than the average and is shaded light green to indicate this benefit. Additionally, the “Fixed SE” maximum of 7,568 MW/hr is more than 20% lower than the average and is shaded dark green to indicate this benefit. Likewise, the “1-Axis Tr.” and “2-Axis Tr.” maximums of 14,854 and 16,869

MW/hr are more than 10% and 20% greater than the average, respectively, and are shaded light and dark red to indicate this difficulty.

The cell shading indicates a strong tendency for tracking arrays to introduce more difficult-to-manage flexibility requirements to the grid. Among the fixed panel arrays, the south- and southeast-facing arrays show noticeable benefits over the west- and southwest- facing arrays.

There is a give-and-take between energy production, which is maximized by using tracking arrays, and flexibility requirements, which are minimized by using fixed arrays. Grid planners might consider these effects when thinking strategically about future solar capacity, especially as it might pertain to balancing commercial, 1-axis tracking arrays and distributed, roof-top arrays.

Additionally, there is little support here for the theory that west-facing panels might better align with load and reduce flexibility requirements [176]. The other fixed orientations analyzed in this study all produce greater energy with lower flexibility requirements than the west-facing scenario.

4.2.2.2 Location Comparison

Table 4.7 lists the flexibility requirement statistics for the different solar array location scenarios in 2025. The cell shading indicates less diversity in flexibility requirements than shown for the orientation scenarios in Table 4.6. There is a slight tendency for the arrays that generate less energy to require less flexibility from the grid, but this tendency could simply be due to the amount of energy being generated rather something inherent in the geographic location.

Table 4.6: The statistical distribution for each flexibility requirement and orientation scenario is shown below. Dark green and dark red cell shading indicates when a the absolute value of a cell is 20% less or more than the average value of the six scenarios. Light green and light red cell shading indicates when a the absolute value of a cell is 10% less or more than the average value.

		Avg	Fixed W	Fixed SW	Fixed S	Fixed SE	1-Axis Tr.	2-Axis Tr.
Energy Gen.	(TWh)	26.2	20.8	23.5	24.7	23.8	29.9	34.4
1-Hr Ramp Rate	Max	12,401	12,152	12,417	10,546	7,568	14,854	16,869
	95%	3,801	3,538	3,515	3,444	3,535	4,323	4,449
	Med	-7	51	59	55	6	-114	-100
	5%	-3,839	-3,669	-3,722	-3,760	-3,791	-3,936	-4,156
	Min	-8,895	-8,375	-8,375	-8,375	-8,375	-8,873	-10,997
3-Hr Ramp Rate	Max	20,384	19,839	20,838	19,861	17,344	21,096	23,328
	95%	9,412	8,389	8,578	8,960	9,457	10,196	10,892
	Med	294	577	515	413	190	55	15
	5%	-10,320	-10,083	-10,286	-10,365	-10,331	-10,221	-10,634
	Min	-18,866	-18,523	-18,523	-18,523	-18,523	-18,523	-20,581
Ramp Factor	Max	0.18	0.15	0.15	0.10	0.09	0.24	0.32
	95%	0.03	0.03	0.03	0.03	0.03	0.03	0.03
	Med	0.00	0.00	0.00	0.00	0.00	0.00	0.00
	5%	-0.03	-0.02	-0.03	-0.03	-0.03	-0.03	-0.03
	Min	-0.10	-0.07	-0.07	-0.08	-0.09	-0.13	-0.18
1-Hr Volatility	Max	7,943	8,333	7,037	5,184	5,184	10,405	11,518
	95%	2,605	2,216	2,209	1,810	1,601	3,491	4,300
	Med	614	581	589	597	599	651	667
	5%	203	195	201	206	205	206	206
	Min	7	7	7	7	7	7	7
1-Day Volatility	Max	41,319	37,526	37,670	38,011	38,509	44,268	51,933
	95%	28,295	26,410	26,252	25,083	24,236	32,323	35,467
	Med	20,482	18,871	18,652	17,420	16,821	23,852	27,276
	5%	14,451	12,751	12,769	11,923	11,294	17,206	20,765
	Min	9,226	7,557	7,583	7,096	8,251	10,253	14,613

Table 4.7: The statistical distribution for each flexibility requirement and location scenario is shown below. Dark green and dark red cell shading indicates when a the absolute value of a cell is 20% less or more than the average value of the three scenarios. Light green and light red cell shading indicates when a the absolute value of a cell is 10% less or more than the average value.

		Avg	West	Central	South
Energy Gen.	(TWh)	27.5	29.9	24.8	27.9
1-Hr Ramp Rate	Max	13,259	14,854	12,044	12,879
	95%	4,174	4,323	4,036	4,163
	Med	-91	-114	-58	-100
	5%	-3,847	-3,936	-3,771	-3,834
	Min	-9,676	-8,873	-9,660	-10,496
3-Hr Ramp Rate	Max	19,460	21,096	18,422	18,862
	95%	9,924	10,196	9,742	9,833
	Med	86	55	127	75
	5%	-10,093	-10,221	-10,010	-10,049
	Min	-18,632	-18,523	-18,523	-18,851
Ramp Factor	Max	0.20	0.24	0.15	0.21
	95%	0.03	0.03	0.03	0.03
	Med	0.00	0.00	0.00	0.00
	5%	-0.03	-0.03	-0.03	-0.03
	Min	-0.11	-0.13	-0.09	-0.10
1-Hr Volatility	Max	9,312	10,405	7,951	9,579
	95%	3,077	3,491	2,699	3,040
	Med	671	651	682	681
	5%	208	206	210	210
	Min	7	7	7	7
1-Day Volatility	Max	44,856	44,268	46,034	44,268
	95%	31,975	32,323	31,277	32,323
	Med	23,481	23,852	22,738	23,852
	5%	16,894	17,206	16,268	17,206
	Min	10,364	10,253	10,588	10,253

4.3 Conclusions

The primary goal of this study is to quantitatively assess the correlation of growing wind and solar peak output with changing flexibility requirements. When observing the effects of solar generation on the net load flexibility, this study finds a number of strong correlations. In relation to ramp rates, solar significantly increases maximum ramp factors and 1-hr and 3-hr ramp rates, especially during the winter and spring. It flips the median 3-hr summer ramp rates from negative to positive. These trends indicate that grids with growing solar capacity should anticipate their ability to double or triple their historical peak ramp up rates, especially during low-demand seasons (winter and spring), and to ramp up more regularly during seasons of high demand (summer).

In relation to volatility, solar shows even stronger tendencies to increase flexibility requirements. The median and maximum 1-hr and 1-day volatilities show a significant correlation with increased peak solar output. While this effect is less intense during the fall and winter, increased volatility during the spring and summer can be quite severe. The increasing maximum values require some consideration, though ERCOT experienced a few events with very high volatility in 2011 that it was able to accommodate. But the fact that median volatility also increases means that extreme volatility will be a much more regular occurrence. Based on the results in this study, adding 8+ GW of solar to ERCOT could create a grid where almost every week will be more volatile than the majority of weeks to date.

When observing the effects of wind generation on the net load flexibility, however, this study discovers only minor correlations. Greater wind peak generation does

correlate with reduced 1-hr and 3-hr ramp rates and might slightly increase 3-hr ramp rates, 1-hr volatility, and 1-day volatility, particularly at higher wind capacities, but in most other metrics its influence is either very small or does not follow a consistent trend. This independence is surprising as it contradicts correlations suggested by the GE Energy study discussed in Section 2 [72]. Perhaps the GE Energy study’s use of modeled weather data and calculated wind generation profiles might have failed to reproduce the smoothing effects of geographic dispersion of wind farms or other factors that influence the variability of wind. The GE Energy study’s conclusion that increasing ramp rates will drive up the need for regulation reserves insinuate that a more robust ancillary services market might be a necessary response to the increasing flexibility requirements discussed in Section 4.2.1 of this paper.

Comparing the general shapes of the demand, wind, and solar profiles explains why greater wind and solar capacity might cause certain flexibility requirements to increase. Solar generation follows a predictable pattern of daily ramping with the rising and setting sun punctuated by periods of cloudiness that add noise to its generation profile. The intensity of this daily pattern causes significant, solar-driven flexibility requirements that supersede the existing demand-driven flexibility requirements. Wind output does not generally change as quickly as solar, but it is often asynchronous with the demand profile. This anti-correlation means that wind output causes some flexibility requirements to increase by intensifying the existing demand-driven flexibility trends. Additionally, daily and seasonal trends in wind profile shape are not as consistent or as predictable as the daily solar generation profile [185]. This unpredictability suggests that, while solar output will more regularly cause the flexi-

bility requirement increases indicated in this study, wind output will vary more from day to day and might not impact flexibility requirements as consistently.

The results in Section 4.2.1.7 show that wind and solar influence the flexibility requirements in different ways. Since wind output tends to negatively correlate with demand, it can intensify some of the flexibility requirements inherent to the demand profile, such as increasing morning net load ramp rates when its reduced output coincides with increased demand. As solar capacity grows, the dominating flexibility events are no longer driven by this wind/demand anti-correlation but are driven by diurnal solar output ramping instead. When solar output dominates the flexibility requirements, the existing wind capacity does not appear to intensify the worst flexibility situations, except for the minimum 3-hr ramp rate and the daily volatility.

This study also draws some important conclusions about the influence of solar array orientation and geographic location on flexibility requirements. Tracking arrays, while they produce more energy over the year, also create significantly greater flexibility requirements than fixed arrays. Facing panels to the west, sometimes suggested as an option for decreasing flexibility requirements [176], actually increases them when compared to other fixed orientations and produces less energy as well. Rather unintuitively, southeast-facing panels appear to significantly reduce flexibility requirements with minor reductions in energy generation when compared to other fixed panels. Solar array location only shows small correlations with flexibility requirements, and those correlations might depend solely on their different annual energy generation amounts.

This study gives a specific look at how flexibility requirements might be chang-

ing in the ERCOT marketplace, and a general intuition about how other grids can anticipate the influence of renewable generation on their own net loads. Some of these flexibility requirement issues might be reduced with future shifts in the demand curve or increased geographic diversity of renewable generation. For example, widespread implementation of energy storage and demand response schemes would change the demand curve, which would affect the net load and flexibility requirements. Still, planning for increasing ramping and volatility in the grid is an important aspect of solar capacity expansion. Electric grids that have demonstrated their ability to handle large amounts of wind generation should not assume they can handle large amounts of solar. They should consider their future flexibility requirements in light of their existing flexibility capabilities. In this way, shortcomings can be addressed by adjusting the geographic location and orientation of future solar assets, or by employing energy storage, market redesign, or one of the numerous strategies discussed in Section 6.1, and our electric grids can continue to provide reliable power at the lowest possible cost.

Chapter 5

Modeling the optimal mix and location of wind and solar with transmission and carbon pricing considerations

This dissertation chapter builds a model that recommends the optimal investment of wind, solar, and transmission capacity in the different regions of an electric grid by evaluating wind and solar resources based on their timing coincidence with the load and with the renewable energy output of other grid regions. This chapter also develops a framework for balancing system costs, flexibility requirements, and CO₂ emissions when considering CO₂ prices or other market policies. This analysis uses ERCOT as a demonstration case, but its methods are applicable to other grids.

This chapter is an updated study of “Modeling the optimal mix and location of wind and solar with transmission and carbon pricing considerations” as published by *Renewable Energy* in 2018 [39].

5.1 Methods

The methods for this study are presented in five separate subsections. Section 5.1.1 discusses the system cost minimization technique used in the model optimization process. Section 5.1.2 describes how the ERCOT grid was split into different

transmission regions. Section 5.1.3 outlines the steps that the model takes as it looks for an optimal solution. Section 5.1.4 lists some of the capital costs and market prices used in the model. Section 5.1.5 discusses the model’s limitations.

5.1.1 System cost minimization theory

The optimization calculations performed by the model developed for this study rely on the concept of “system cost minimization”. In this context, “system cost” C_{sys} is the total annual cost of meeting the grid-wide energy load. It is the sum of the annual capital cost C_{cap} and thermal cost C_{th} as described in Equation 5.1, where t is each 30-minute interval of the year (and one year has 17,520 30-minute intervals). Capital cost is the annual amortized cost of financing transmission and renewable generation investments. Thermal cost is the cost of operating the system’s conventional thermal generators during each of the year’s 30-minute intervals to meet the net load (load – renewable generation). As shown in Fig 5.1, the thermal cost at time t is the integral of the merit order curve bounded by the net load at time t , where the merit order curve is the list of dispatchable generators arranged by their marginal cost. Each generator’s marginal cost is a function of its heat rate, CO₂ emission rate and variable operation costs along with the market prices for fuel and CO₂ emissions.

$$C_{\text{sys}} = C_{\text{cap}} + \sum_{t=1}^{17520} C_{\text{th}}(t) \quad (5.1)$$

The system cost is a function of many different factors. Adding renewable capacity to a particular region of the grid will reduce the net load during certain

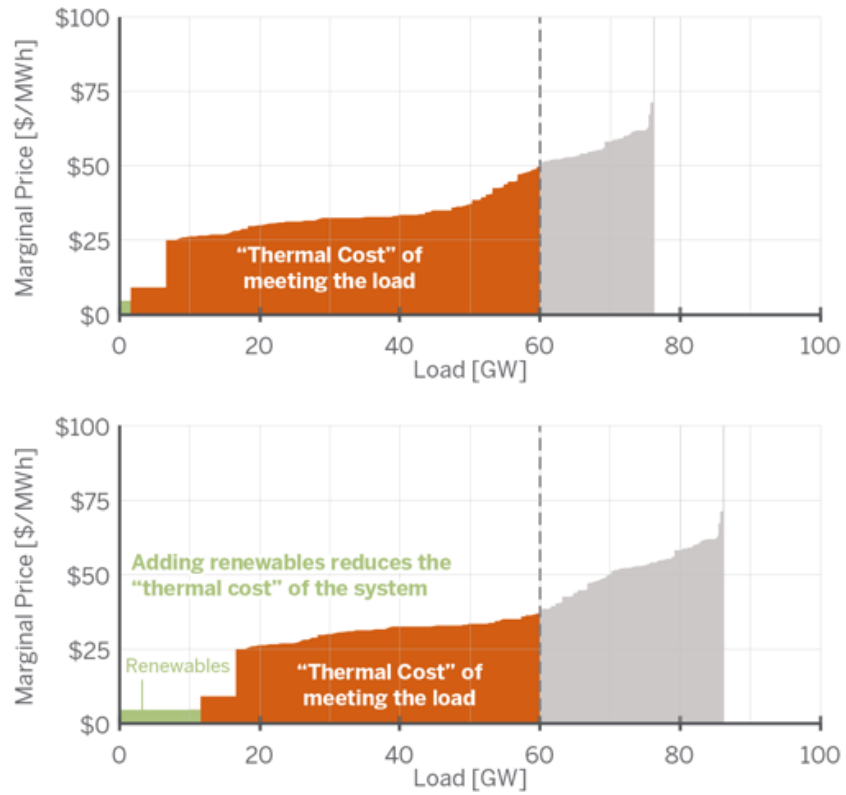


Figure 5.1: “Thermal Cost” is the integral of the merit order curve bounded by the net load. Renewable generation pushes the merit order curve to the right, reducing the thermal cost.

time intervals of the year, which reduces the system’s thermal cost. However, these capacity additions require wind, solar, and transmission investments, which increases the system’s capital cost. Additionally, the ability of a region’s renewable generation to reduce the system net load is constrained by curtailment. The model curtails a region’s renewable generation whenever its renewable energy output exceeds the capacity of the transmission line connecting that region to the load center. Curtailment also occurs to prevent the system net load from falling below a fixed threshold. This requirement comes from an assumption that the total power output of an electric grid’s on-line, inertial generators must exceed a specific percentage of the grid’s maximum annual load to maintain frequency stability [44]. Based on informal guidelines from ERCOT, a minimum net load constraint of 16.45 GW (25% of the 65.8 GW maximum annual ERCOT load in 2012) is used in the base case scenario [56]. The model balances these different factors to choose the mix of wind and solar capacity that minimizes the system cost.

One shortcoming of the system cost calculation is its failure to include CO₂ emissions. Though the merit order curve does change in response to CO₂ prices, higher CO₂ prices only lead to higher system costs. This situation fails to recognize that a market with higher CO₂ prices and, thus, higher system costs, might be more desirable depending on the value of CO₂ emissions reductions. To address this shortcoming, the system cost C_{sys} can be expanded to include the “unaccounted environmental cost” C_{environ} of CO₂ emissions. As shown in Equation 5.2, the unaccounted environmental cost is calculated by multiplying the annual CO₂ emissions $CO_{2,emissions}$ by the difference between the CO₂ price $Price_{CO_2}$ and the social price

of CO₂ emissions SPC (a constant price representing the environmental cost of each ton of CO₂ emissions). For example, society might place a social price of 100 \$/ton on CO₂ emissions even though the market price might be only 20 \$/ton. In this scenario, the 20 \$/ton CO₂ price will influence the merit order curve and market behavior, reducing CO₂ emissions slightly and paying for a portion of the CO₂ environmental cost. The 80 \$/ton residual price (100 \$/ton social price – 20 \$/ton CO₂ price) represents the unaccounted environmental cost of CO₂ emissions. Adding the unaccounted environmental cost to the system cost yields the “comprehensive system cost” C_{compr} , as shown in Equation 5.3. This expanded equation considers the trade-off between higher CO₂ prices (economic cost) and lower CO₂ emissions (economic benefit). While the model works by minimizing the system cost to simulate the market’s response to real prices, the comprehensive system cost is used to process the model results and compare different scenarios.

$$C_{\text{environ}} = CO_{2,\text{emissions}} \times (SPC - Price_{CO_2}) \quad (5.2)$$

$$C_{\text{compr}} = C_{\text{sys}} + C_{\text{environ}} \quad (5.3)$$

5.1.2 Transmission regions

Building transmission to different regions of the electric grid provides access to the unique renewable energy resources in those regions. To simulate this effect, this study has divided ERCOT into a number of independent transmission regions.

These regions were developed using geographic information and line characteristics of the existing ERCOT transmission infrastructure and following the criteria below:

- each region should be well interconnected within itself
- region borders should cut as few transmission lines as possible
- the number of regions should remain small for model tractability
- regions should have higher spatial resolution where renewable resources are abundant to capture differences in renewable generation profile timing

Following these design principles, fifteen notional ERCOT regions were created. Fig 5.2 shows these regions superimposed on a population density map of Texas (representing the location of the load). For comparison, Fig 5.2 also bubbles in the five “Competitive Renewable Energy Zones” (CREZ) used by ERCOT in their own transmission expansion planning [106].

In general, the majority of ERCOT load is located in regions 6, 15, and 16. Regions 5, 10, and 17 show the portions of Texas that are served by electric grids other than ERCOT and are not considered in the model. The remaining regions tend to have lower loads and substantial renewable energy resources. When modeling transmission expansion, it is assumed that the three load regions (6, 15, and 16) are well-connected, and that other regions need only connect to the nearest load region to be integrated into the entire network.

Each of the modeled regions have unique wind and solar generation profiles. The wind profiles are based on the normalized output of the existing wind farms in

each region (data provided by ERCOT). The solar profiles are calculated by feeding solar radiation data [130] into the NREL System Advisor Model software [127], which translates the radiation data and solar array properties into generation profiles. Each region’s solar profile is the normalized output of three different locations within the region using 1-axis tracking solar arrays.

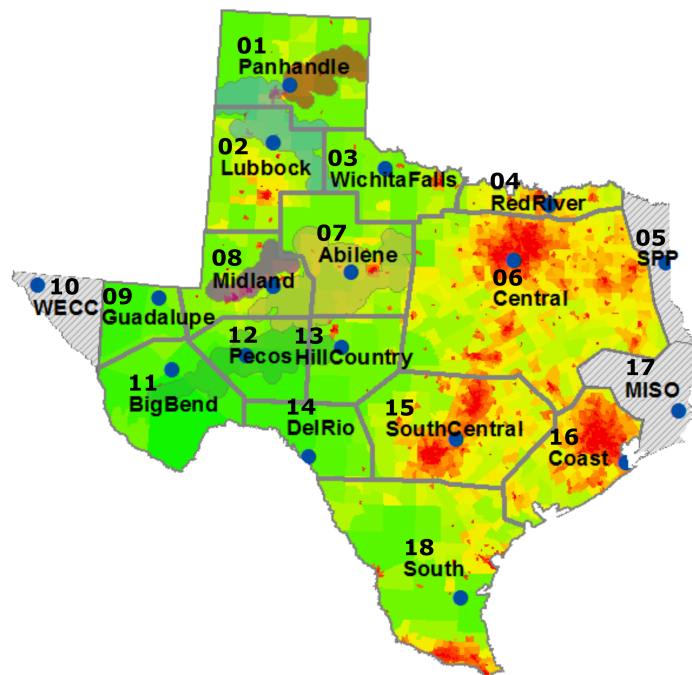


Figure 5.2: The regions of ERCOT are designed according to Section 5.1.2. The underlying population density map (green - sparsely populated to red - densely populated) indicates the approximate location of the loads. The five “Competitive Renewable Energy Zones” (CREZ) used by ERCOT in their own transmission expansion planning are bubbled in for comparison.

5.1.3 Model optimization process

Using the methods discussed in Section 5.1.1, the model begins by calculating the minimum system cost and optimized wind and solar capacities that would result from extending 500 MW of new transmission to a specific region. It performs this calculation for all of the regions in the model. An example of these calculations is shown in Table 5.1. The region that achieves the lowest system cost will receive 500 MW of additional transmission capacity. The model then repeats this process, expanding the transmission network 500 MW at a time, until new transmission investment can no longer reduce the system cost indicating that a grid-wide minimum system cost has been reached. The flow chart in Fig 5.3 visualizes the steps taken by the model optimization process.

When a region is selected for development, the system net load during each time interval is reduced by the corresponding renewable energy output of that region. Consequently, as a region is developed, it cannibalizes its ability to reduce system thermal cost. These diminishing returns increase the attractiveness of regions whose solar and wind profiles are dissimilar from the over-invested region. In this manner, the model tends to invest in a set of regions with solar and wind profiles that complement each other's generation timing, and that collectively coincide with the timing of the load.

There are benefits and disadvantages to solving the model using this sequential/iterative process. The iterative framework helps make the program computationally tractable by separate the large optimization problem into smaller parts that can be parallelized across multiple processors. In addition, analyzing the results

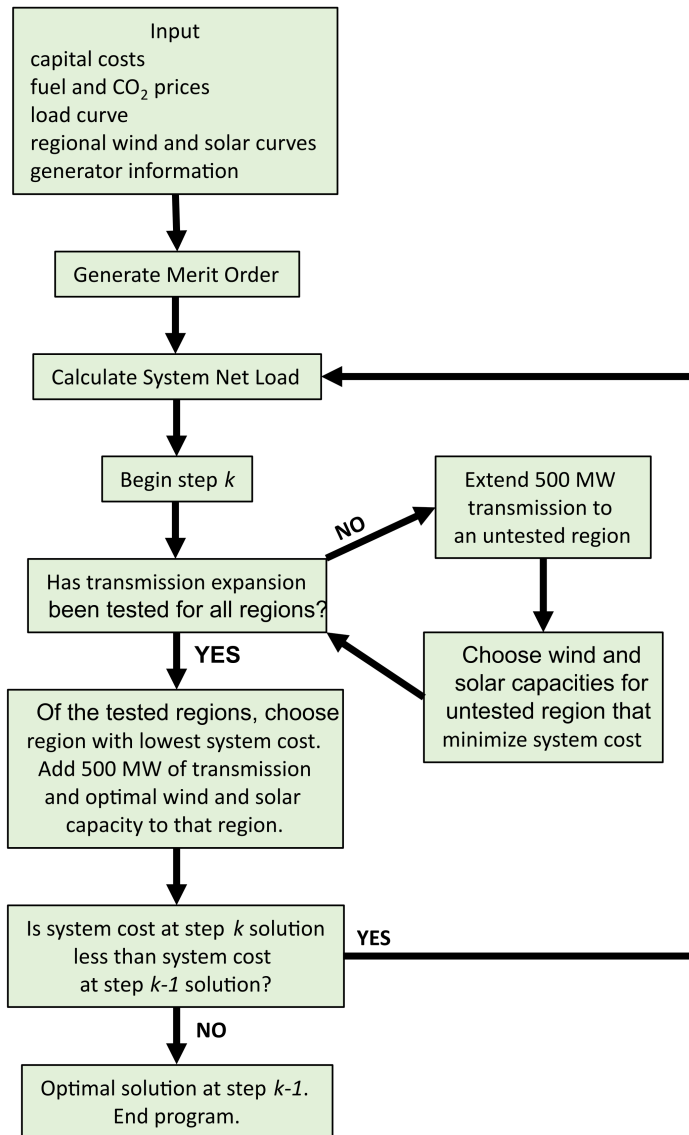


Figure 5.3: This flow chart visualizes the model optimization process described in Section 5.1.3.

Table 5.1: During the first optimization step, the model extends 500 MW of transmission to each of the 15 regions and finds the wind and solar capacity for each region that will minimize system cost. Based on these optimization results, the model will choose to build transmission to the region that reduces system cost the most (“11 Big Bend” in this example, highlighted green). The model repeats this process until adding 500 MW of new transmission to the grid can no longer reduce system costs.

Region Name	Optimal Wind Capacity (GW)	Optimal Solar Capacity (GW)	Transmission Distance (Miles)	Renewable Capital (\$Billion)	Transmission Capital (\$Billion)	Thermal Cost (\$Billion)	System Cost (\$Billion)
01 Panhandle	686	242	325	0.122	0.014	19.433	19.569
02 Lubbock	696	315	300	0.132	0.013	19.426	19.571
03 Wichita Falls	663	348	150	0.132	0.006	19.429	19.567
04 Red River	590	494	75	0.140	0.003	19.451	19.594
06 Central	721	385	0	0.144	0.000	19.435	19.579
07 Abilene	701	389	185	0.142	0.008	19.426	19.576
08 Midland	719	447	265	0.152	0.011	19.414	19.577
09 Guadalupe	566	568	375	0.147	0.016	19.451	19.614
11 Big Bend	637	461	335	0.143	0.014	19.408	19.565
12 Pecos	661	430	250	0.142	0.011	19.423	19.576
13 Hill Country	671	407	150	0.140	0.006	19.421	19.567
14 Del Rio	604	637	150	0.160	0.006	19.468	19.634
15 South Central	590	508	0	0.142	0.000	19.449	19.591
16 Coast	570	593	0	0.150	0.000	19.477	19.627
18 South	813	275	175	0.143	0.008	19.459	19.610

for each step of the solution yields some conclusions that could not be drawn from a non-iterative, global optimization method. However, the solution might not be mathematically optimal since early decisions about transmission, wind, and solar capacity investments cannot be changed during later solving time steps.

5.1.4 Economic costs and prices

The model uses a number of annualized capital costs and market prices when finding a solution, shown in Tables 5.2 and 5.3. Transmission costs were derived from information about the recently completed CREZ transmission project where ERCOT installed 3,600 miles of transmission at a cost of \$7B USD [116]. If the project is mostly 345kV, double-circuit lines, each mile is assumed to have a 1.5 GW capacity [144], and the average cost is 1300 \$/MW-mile. In this study, a more conservative 1500 \$/MW-mile is used. Annual capital costs for solar and wind are based on reports from the National Renewable Energy Laboratory (NREL) [67, 123] and an LCOE calculator developed by the University of Texas at Austin Energy Institute [170]. Overnight construction costs for transmission, wind, and solar are amortized for 25 years at 3.00% interest to translate them into annual costs. (Using 5.00% or 7.00% interest rates for wind and solar capital investment increased the system cost of the solution by 4.5% and 7.5%, respectively. See Appendix Chapter B for interest rate sensitivity charts). By adding fixed annual operation and maintenance costs to these annualized capital costs, an annual cost per MW of capacity is calculated. Fuel prices are based on average historical prices and feedback from ERCOT about typical, conservative, fuel prices used for planning purposes at power

Table 5.2: Table of annualized capital costs used in the model.

	Overnight Cost	Fixed O&M Cost	Annualized Cost
Transmission	1500 (\$/MW-mile)	-	86.14 (\$/MW-mile)
Wind (on-shore)	1710 (\$/kW)	35 (\$/kW-yr)	133,200 (\$/MW)
Solar (1-axis)	1830 (\$/kW)	20 (\$/kW-yr)	123,100 (\$/MW)

Table 5.3: Table of fuel and CO₂ prices used in the base case model.

Fuel Type	Price (\$/MMBtu)
Coal	2.50
Natural Gas	4.50
Uranium	0.50
Biomass	5.00
CO ₂ Emissions	60 (\$/ton)

plants in Texas [56].

5.1.5 Limitations

This study develops a transmission expansion planning model that requires only a merit order curve, regional renewable energy profiles, and a list of capital costs and commodity prices. While this model can produce meaningful results with limited data and computation, its simplifying assumptions introduce some limitations. For example, using the merit order curve (generator marginal cost) as the sole source of thermal costs and electricity prices overlooks many other market characteristics that influence costs, such as reserve requirements and ancillary services. Since the model does not perform unit commitment or dispatch, it overlooks generator operational costs and constraints such as start-up costs and ramping restrictions. Additionally, the integration of renewable energy into the grid might require new ancillary services,

firming power, and frequency support, introducing costs that are not reflected in this model (though previous work from the author suggests that these costs are an order of magnitude smaller than the reductions in wholesale energy costs resulting from renewable investment [38]). Changes in the load profile or load flexibility would also influence the model solution, but are not discussed in this study.

The model results recommend a significant amount of renewable capacity penetration (around 40%) for the ERCOT case study. Getting to such high renewable penetrations complicates the reliable management of the electric grid due to excess power production risk, supply/demand mismatch, transmission flow constraints, and system frequency and voltage security [64]. A recent study of the ERCOT system suggests that some of these issues might begin to manifest when wind power produces 20% of annual energy production [44]. These reliability issues can be managed by increasing the flexibility of the generation fleet [44], adding energy storage to the system [35], extending the transmission network [160], or other methods. These management strategies might influence the operation of the power plant fleet, introduce new system inefficiencies, and add variable and capital costs to the system. These consequences might influence generator fuel consumption, emissions, and market prices. While this study approximates some of these effects by using a minimum net load constraint and performing a qualitative analysis of net load flexibility, it does not explicitly quantify the influence of generator fleet improvements, energy storage, or other system upgrades on the solution.

Another important aspect of electric grid capacity expansion planning is the consideration of future technologies. A grid with high CO₂ prices, for example, might

incentivize investments in low-CO₂-emission technologies other than renewables, such as carbon capture and sequestration or nuclear generation [88]. New investments in storage or demand response capabilities could also influence market dynamics. Since the model considers a static generation fleet, it does not consider how future, non-renewable investments would change the optimal solution.

5.2 Results and discussion

The results for this study are presented in six separate subsections. Section 5.2.1 walks through the base case scenario to demonstrate the model functionality and optimal solution for the ERCOT market. Section 5.2.2 compares ERCOT's existing regional renewable energy capacity with a model solution using the same market conditions. Sections 5.2.3, 5.2.4, and 5.2.5 test the sensitivity of the model solution to CO₂ prices, the minimum net load constraint, and natural gas prices. Section 5.2.6 shows how the utilization of different power plants in the existing generator fleet changes depending on the CO₂ price and the model solution.

5.2.1 Base case scenario

Analyzing the solution of a base scenario with a CO₂ price of 60 \$/ton gives some insight into how the model operates, and shows what a fully developed transmission grid and renewable capacity investment might look like in ERCOT. Figs 5.4, 5.5, and 5.6 show that the model chooses to primarily invest in the Panhandle, Wichita Falls, and Big Bend regions, with minor investments elsewhere. Fig 5.7 shows how these investments are distributed around the ERCOT grid.

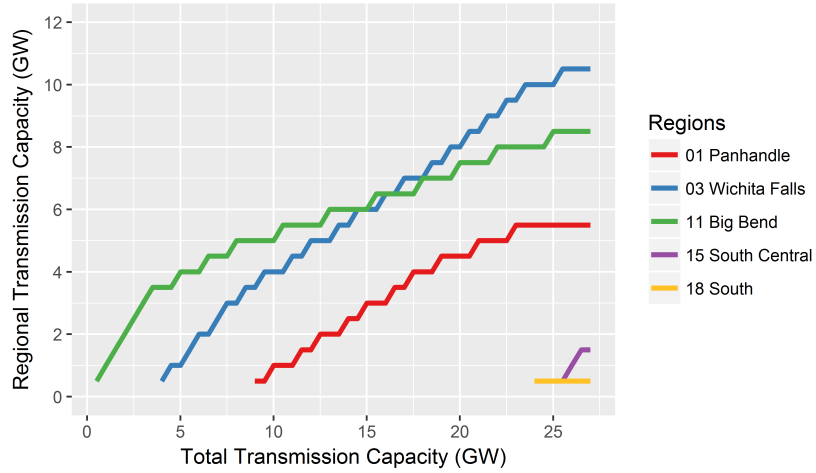


Figure 5.4: Transmission investments in the base case scenario are split among five different regions, with three regions receiving the majority of the investment.

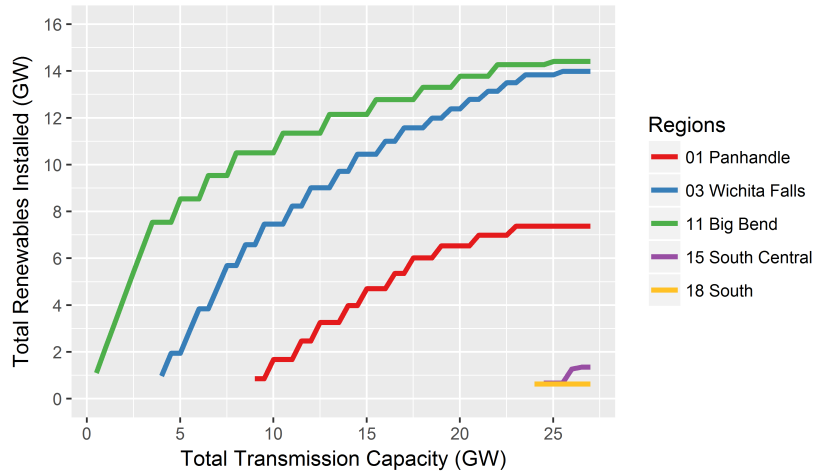


Figure 5.5: Each region that is connected to the transmission network has unique wind and solar generation profiles, and installs the amount of renewable energy capacity that minimizes system cost.

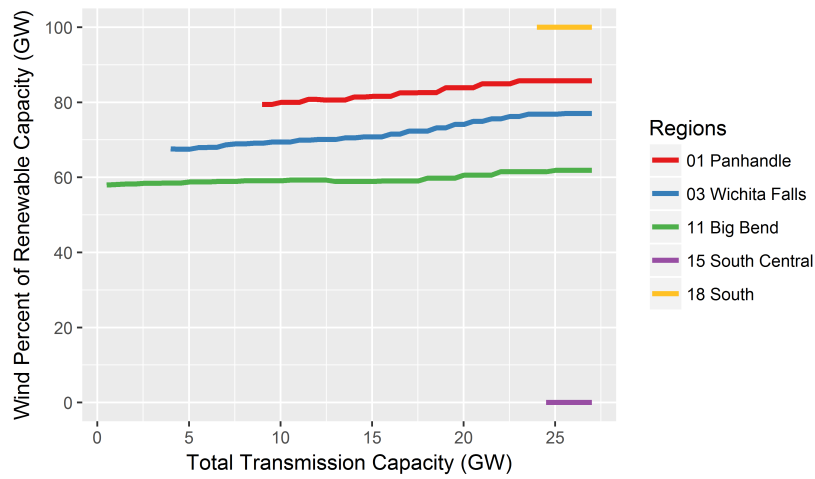


Figure 5.6: Each region that is connected to the transmission network has a unique wind and solar generation profiles, and installs the mix of wind and solar capacity that minimizes system cost.

Dividing the renewable capacity of each region by the transmission capacity, shows that the Panhandle, Wichita Falls, and Big Bend regions install 1.35, 1.33, and 1.69 renewable GW per transmission GW, respectively. Big Bend’s transmission utilization efficiency likely contributes to the model’s tendency to prioritize investment in that region. The geographic dispersion of capacity in the solution suggests that the model capitalizes on the variation of wind and solar resources throughout Texas, prioritizing development in a set of regions that complement each other’s unique generation profiles. This complementary output is illustrated in Fig 5.8, which shows the capacity factors of the renewable output of the three main regions, their combined output, and the load, for an average day in August. Big Bend, the first choice for investment, has good output during the peak load hours (16:00), but less output before and after, and significant output in the morning (7:00-11:00) when wind

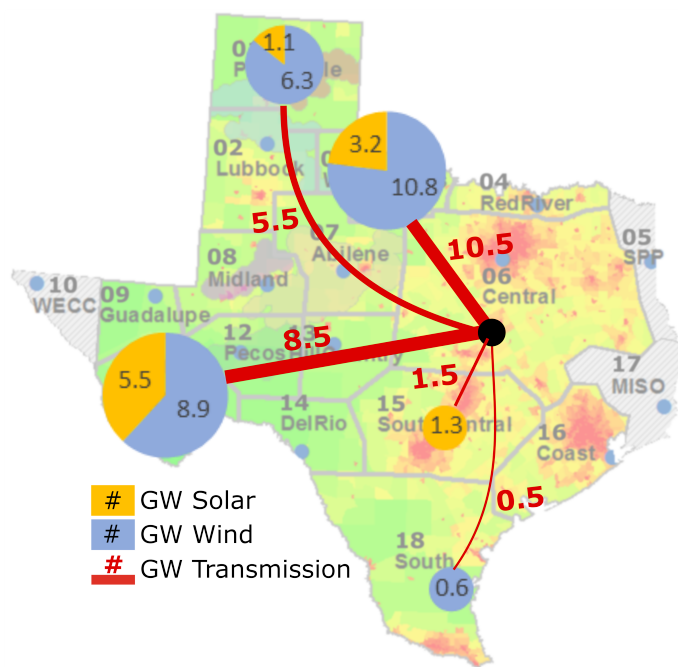


Figure 5.7: The transmission, wind, and solar investments are distributed among different regions in the ERCOT grid. Each region contributes to reducing system costs based on its unique renewable profiles and capacities as wind and solar resources vary throughout Texas.

and solar are both strong. Wichita Falls has its lowest output during the morning, balancing the Big Bend morning generation spike, and has good output during peak load, but it produces a large amount of night time, off-peak energy (22:00-4:00). The Panhandle also has its lowest output during the morning, helping to balance the Big Bend morning generation spike, and adding more output during peak load hours, especially during the early afternoon (12:00-16:00) when the other regions are producing less. The combined output profile is an improvement over the individual regions, producing more renewable energy during the peak load hours (12:00-20:00) and maintaining higher capacity factors overall.

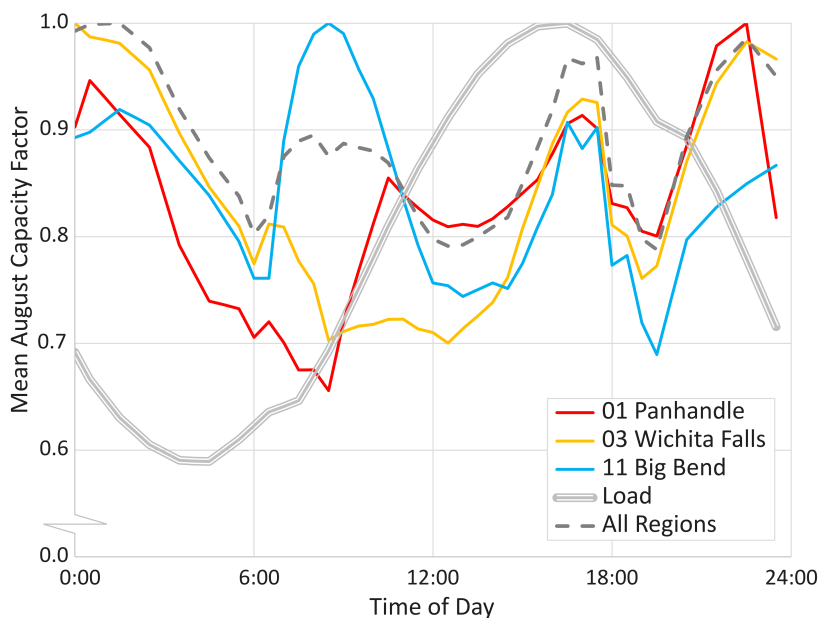


Figure 5.8: This figure shows capacity factors for an average day in August. While the interaction between these regions is nuanced, this figure suggests that the model develops regions that produce large amounts of energy during the peak load hours (12:00–20:00) and that complement each other’s minimum and peak output (especially evident from 6:00–12:00).

Installing more transmission and renewables causes thermal costs to fall as traditional thermal generators are pushed higher up the merit order curve. However, capital costs rise as the new transmission and renewable infrastructure must be paid for. Fig 5.9 shows how this effect influences the overall system cost. Eventually, the capital cost of new investments cannot be recovered by reductions in thermal cost, and the minimum system cost is reached. This minimization occurs as inefficient portions of the merit order curve are used less often, which leaves fewer opportunities for thermal cost reduction, and as curtailment due to the minimum net load constraint makes new renewable capacity less effective, as shown in Fig 5.10. Fig 5.11 shows how CO₂ emissions fall as more transmission and renewables are built.

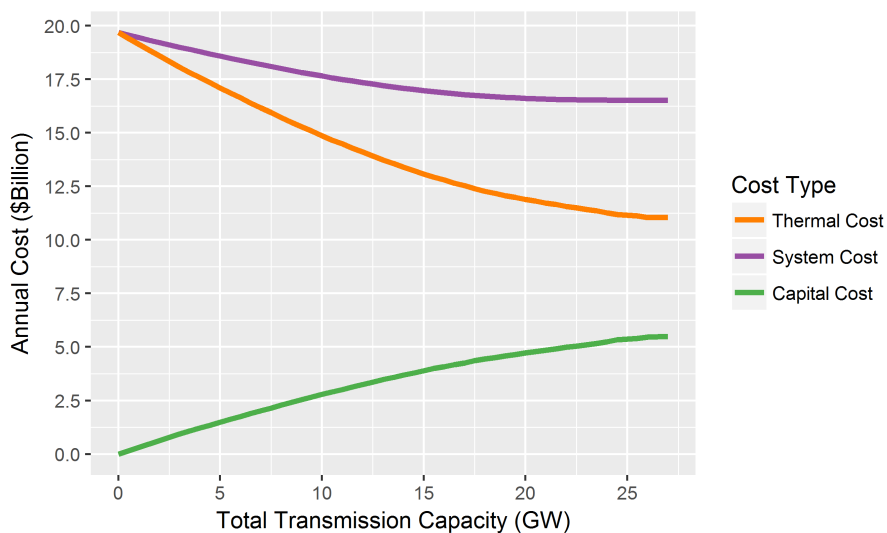


Figure 5.9: As transmission and renewables are invested in, system costs fall as falling thermal costs offset rising capital costs until the minimum system cost is reached.

The solution to the base case recommends a build-out of 27 GW of transmission to five different regions in ERCOT. The model suggests that these regions should

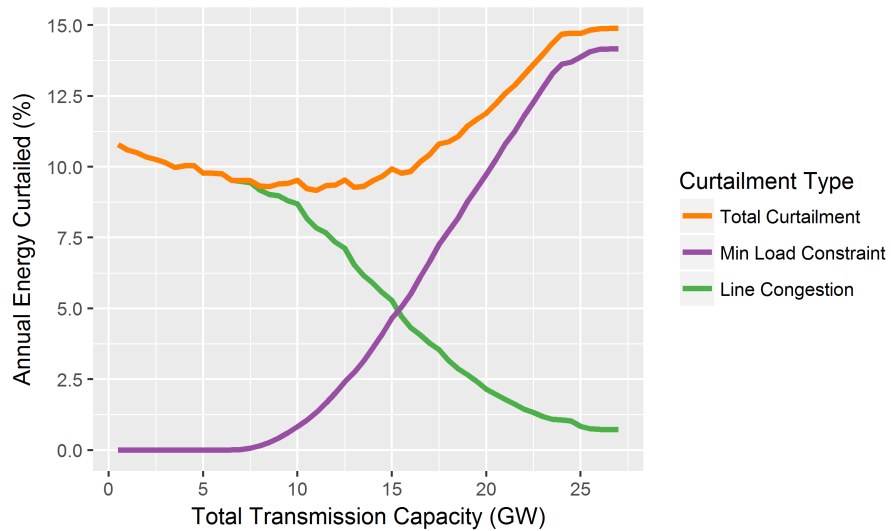


Figure 5.10: Curtailment occurs when too much renewable energy is being generated to meet the line capacity and/or minimum net load constraints. The model chooses wind and solar capacities that balance the disadvantages of curtailment with the benefits of having greater renewable generation during periods when curtailment is not binding.

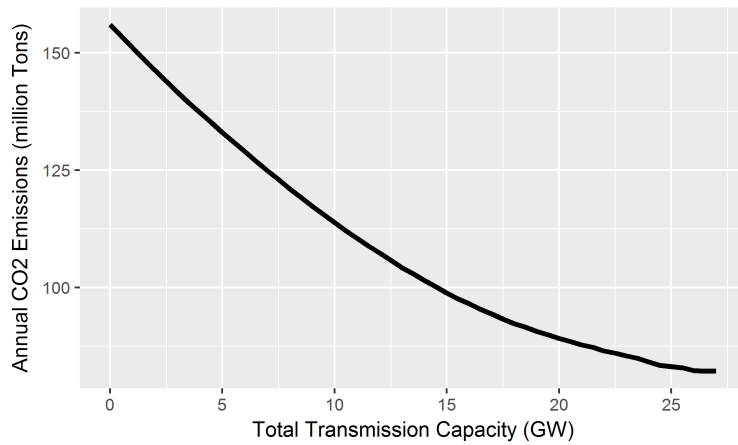


Figure 5.11: As more renewable capacity is installed, traditional thermal generators are pushed higher up in the merit order and are utilized less often, reducing CO₂ emissions throughout ERCOT.

build a total of 26.6 GW and 11.1 GW of wind and solar capacity, respectively, providing 110 TWh of energy (34% of annual electricity demand). Renewable capacity exceeds transmission capacity (regionally and for the whole system) because wind and solar outputs typically peak at different times, so their combined output is usually less than the transmission capacity, or it is curtailed. The 57.0 GW peak annual net load at this renewable build-out would need to be met by traditional thermal generators. Thus, this optimal build-out of renewables represents a grid with 60.2% thermal capacity and 39.8% renewable capacity at a mix of 70.6% wind and 29.4% solar. The results also suggest that the grid will experience diminishing returns from these investments. Thus, if other non-economic factors encouraged fewer renewables on the grid, a less than optimal investment, such as 20 GW of transmission, could be justifiable.

Base Case Uncertainty

The uncertainty of the base case solution depends on the uncertainty of the model inputs, particularly the variables that make up the capital cost and thermal cost components of the system cost objective (see Equation 5.1). These variables include the power plant properties that comprise the thermal cost curve, the transmission capital cost, and the wind and solar capital and operation costs.

Data from the Annual Technology Baseline published by the National Renewable Energy Laboratory [131] indicate large uncertainties in the cost of wind and solar. The study's 2025 projections show solar and wind capital costs falling to 1,200 and 1,400 \$/kW and fixed operation and maintenance cost falling by 26%

and 8%, respectively. These future costs would reduce the annualized capital costs in Table 5.2 by 33.1% for solar and 15.5% for wind.

Transmission costs and power plant properties are derived from historical ERCOT data and should be relatively reliable. An uncertainty of $\pm 25\%$ for transmission cost and $\pm 10\%$ for thermal cost are assumed.

The uncertainty analysis in Table 5.4 shows how the base case results change depending on the different variable uncertainties. Thermal cost uncertainty has a strong influence on all of the results. Wind and solar cost uncertainties also have a significant impact. Transmission cost uncertainty, however, has a limited effect on the solution. Solar capacity is the most uncertain result, with lower solar prices incentivizing solar capacity growth and lower thermal cost discouraging it. When including uncertainty, the base case solution will fall between 24–30 GW of transmission and 31.2–52.5 GW of renewable capacity with wind accounting for 45–81% of the renewable capacity.

Table 5.4: Uncertainty analysis showing alternate solutions to the base case scenario.

Scenario	Transmission		Wind		Solar		System Cost	
	GW	% Change	GW	% Change	GW	% Change	\$Billion	% Change
Low Solar Cost	30.0	+11.1	22.4	-15.8	27.6	+148.6	15.78	-4.5
Low Wind Cost	30.0	+11.1	33.5	+25.9	8.0	-27.9	15.89	-3.9
Low Solar & Low Wind Cost	31.5	+16.7	26.5	-0.4	26.0	+134.2	15.29	-7.5
Low Transmission Cost	27.5	+1.9	27.9	+4.9	9.8	-11.7	16.37	-1.0
High Transmission Cost	26.5	-1.9	25.6	-3.8	12.0	+8.1	16.65	+0.7
Low Thermal Cost	24.0	-11.1	25.1	-5.6	6.1	-45.0	15.35	-7.1
High Thermal Cost	30.0	+11.1	29.1	+9.4	13.7	+23.4	17.60	+6.5

5.2.2 Model vs existing ERCOT renewables

This model can also provide insights about the existing buildout of renewables in ERCOT. First, a model approximation of the existing ERCOT renewable and transmission infrastructure must be made. The existing renewable capacity for each region is given to the model along with the base case fuel prices, a 0 \$/ton CO₂ price, 2,750 \$/kW solar capital costs, and a 15 \$/MWh production tax credit that subtracts \$15 from the system cost for every MWh of wind energy produced. Using these existing market conditions, the model builds out the transmission network shown in column 2 of Table 5.5 with the system performance shown at the bottom of the table.

For comparison, the model is run from scratch using the same market conditions to see where it will invest if allowed to build the same amount of transmission as in the previous simulation. The last column of Table 5.5 shows that the model prefers to invest in the 01 Panhandle and 03 Wichita Falls regions. No investment is made in the 11 Big Bend region as low CO₂ prices and high solar capital costs do not justify investing in that region. This solution yields a lower system cost and comprehensive system cost with less renewable capacity than the existing ERCOT infrastructure. It also creates slightly less CO₂ emissions but greater flexibility requirements.

The difference between these two scenarios shows discrepancy between ERCOT's historical build-out and the model solution. ERCOT likely considers many decision variables when designing transmission expansion projects, such as grid stability, line congestion, and policy factors. While the existing build-out might be

justifiable when considering these factors, the model suggests that it does not minimize the system cost.

5.2.3 CO₂ price sensitivity

As environmental considerations gain importance in the electric grid, it is helpful to test how CO₂ prices might influence the market. The results in this section are calculated by simulating the base case with a variety of CO₂ prices. The CO₂ price herein can be interpreted as a policy-dictated CO₂ tax or the price resulting from an emissions trading system. A comparative analysis of the results uses 100 \$/ton as the social price of CO₂ emissions, based on the ranges reported by [191], though other values could be justifiable.

CO₂ prices can have a large effect on system costs and CO₂ emissions. Increasing the CO₂ price adds to the marginal cost of any CO₂ emitting generators, which increases the thermal and system costs of the grid, as shown in Fig 5.12 along the vertical axis. However, Fig 5.13 shows that CO₂ prices also reduce emissions by reorganizing the merit order curve and encouraging more renewable energy development. For reference, the model calculates 237 million tons of CO₂ emissions with no renewables and a 0 \$/ton CO₂ price. Yet, Fig 5.14 shows that CO₂ price increases have diminishing returns on reducing the comprehensive system cost. This observation holds even when the social price of CO₂ is increased to 250 \$/ton, per Fig 5.15. These results are summarized in Fig 5.16, which shows the various capacity, emissions and cost results at the optimal solution using different CO₂ prices, and Fig 5.17, which shows how the development of different regions changes with the

Table 5.5: A model solution approximating ERCOT’s existing renewable capacity build-out (column 2) is compared with a model solution run from scratch (column 3). Each solution uses a 0 \$/ton CO₂ price, 2,750 \$/kW solar capital costs, and a 15 \$/MWh wind production tax credit in addition to the base case market conditions.

		Modeled Transmission for Existing Renewable Capacity	Model at Existing Market Conditions (stopped at 10 GW Transmission)
Transmission Installed per Region (GW)	01 Panhandle	1.5	1.9
	02 Lubbock	1.2	0
	03 Wichita Falls	0.5	8.0
	04 Red River	0	0
	06 Central	0.9	0
	07 Abilene	2.4	0
	08 Midland	2.2	0
	09 Guadalupe	0	0
	11 Big Bend	0	0
	12 Pecos	0	0
	13 Hill Country	0	0
	14 Del Rio	0	0
	15 South Central	0	0
	16 Coast	0	0
	18 South	1.2	0
All Regions	9.9	10.0	
Total Wind (GW)	13.7	12.9	
Total Solar (GW)	0.0	0.0	
System Cost (\$Billion)	8.345	8.135	
CO ₂ Emissions (Million Tons)	202.9	201.8	
Ext. System Cost (\$Billion)	16.46	16.21	
Max 1-Hr Ramp (MW/hr)	6.36	7.32	
Max 3-Hr Ramp (MW/3hr)	14.84	16.73	
Max 2-Hr Volatility (MW/(30min·2hr))	4.22	7.67	

CO₂ price.

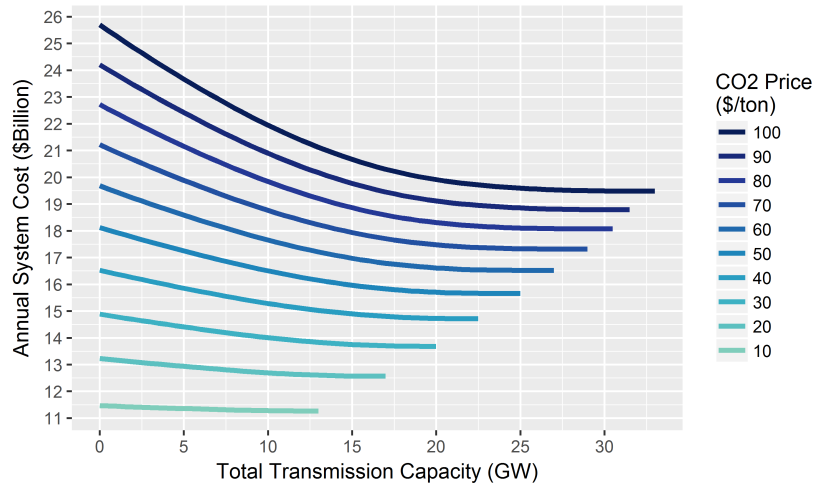


Figure 5.12: As the CO₂ price rises, the marginal cost of any CO₂ emitting generators increases, and the thermal and system costs increase as a result.

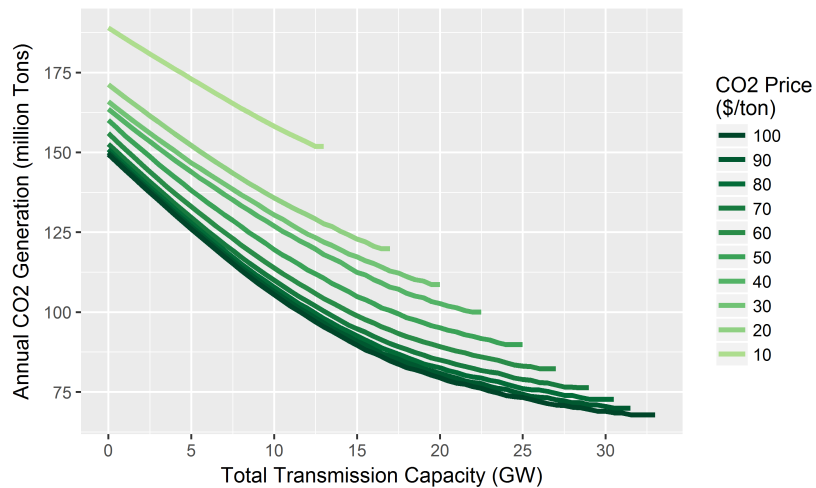


Figure 5.13: Adding even a small CO₂ price to the market greatly reduces CO₂ emissions, while large prices have a diminishing return. For reference, the model calculates 237 million tons of CO₂ emissions with no renewables and a 0 \$/ton CO₂ price.

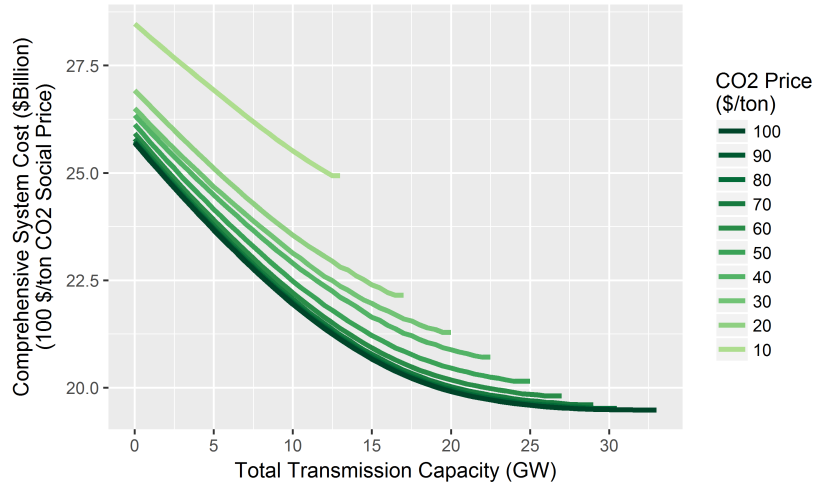


Figure 5.14: The comprehensive system cost at a 100 \$/ton social price of CO₂ experiences diminishing reductions at higher CO₂ prices.

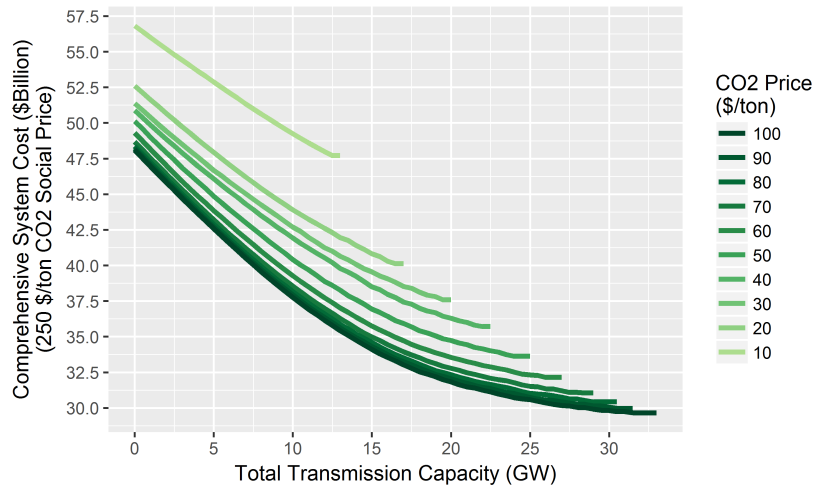


Figure 5.15: Even at a 250 \$/ton social price of CO₂, higher CO₂ prices tend to have diminishing returns on reducing the comprehensive system cost.

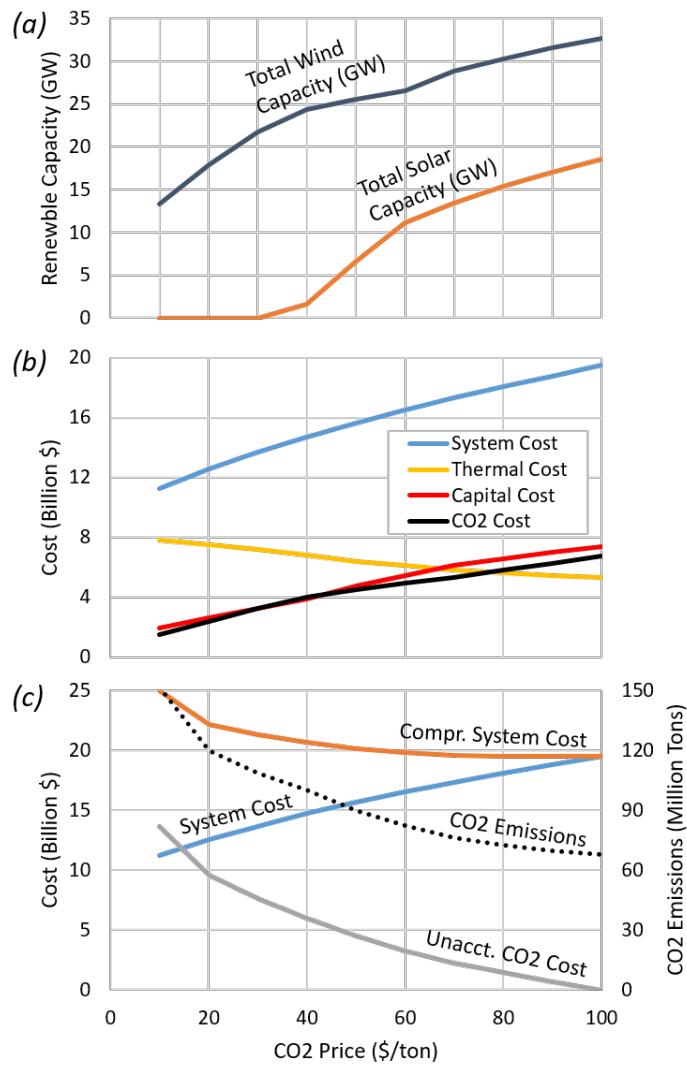


Figure 5.16: Increasing CO₂ price causes (a): more wind and solar capacity, (b): larger capital and CO₂ cost, but lower thermal cost, and (c): lower CO₂ emissions and comprehensive system cost, but higher system cost.

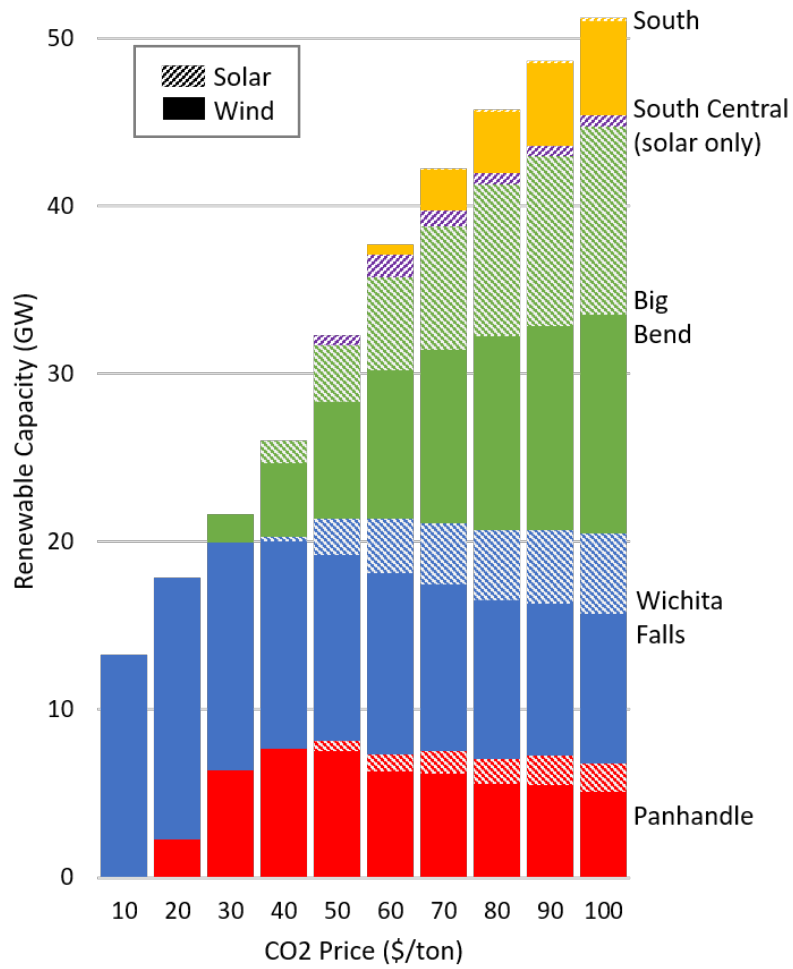


Figure 5.17: Increasing CO₂ price changes the regions the model chooses to invest in, and the optimal wind/solar mix in those regions.

Changes in flexibility requirements provide an additional metric for comparing the solutions under different CO₂ prices. Flexibility requirements refer to aspects of the grid’s net load profile that must be compensated for by dispatchable generators, storage, or other equipment on the grid. These flexibility requirements include ramping, a measurement of how quickly the dispatchable generator fleet must turn their generation capacity up or down, and volatility, a measurement of the “choppiness” of the net load profile [43, 91]. Generally, as flexibility requirements increase, grid maintenance and ancillary service costs increase [38, 89], and grid voltage and frequency stability become more difficult to maintain [10, 19, 145]. Therefore, smaller flexibility requirements are desirable.

Fig 5.18 shows how higher CO₂ prices tend to reduce the annual peak net load with diminishing returns after 70 \$/ton. Figs 5.19–5.21 show how CO₂ prices influence the ramping and volatility of the net load. Larger ramping and volatility maximums require more flexible resources for maintaining the ability of the grid to match supply with demand. In each of Figs 5.19–5.21, CO₂ prices of 70 \$/ton and higher tend to substantially increase flexibility requirements.

This CO₂ sensitivity analysis suggests that an effective CO₂ price might need to strike a balance between system operation costs, environmental benefits, and flexibility requirements. Specifically, the Section 5.2.3 results suggest that a CO₂ price of 60 \$/ton could provide substantial environmental value while keeping flexibility requirements in a familiar, manageable range. Higher CO₂ prices would steadily increase the system cost without any substantial benefit. Consequently, a 60 \$/ton CO₂ price is used in the majority of the simulations in this study.

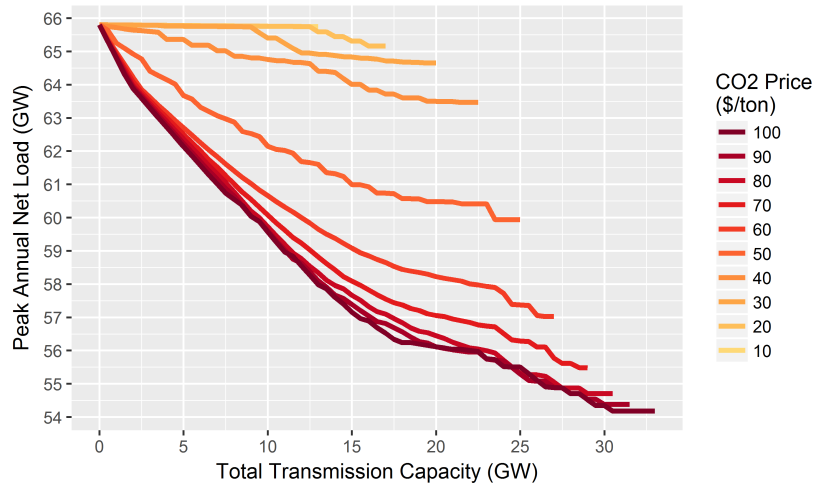


Figure 5.18: As the CO₂ price increases and more renewables are built, the annual peak net load is reduced as well. CO₂ prices higher than 70 \$/ton have a diminishing effect on reducing the peak net load.

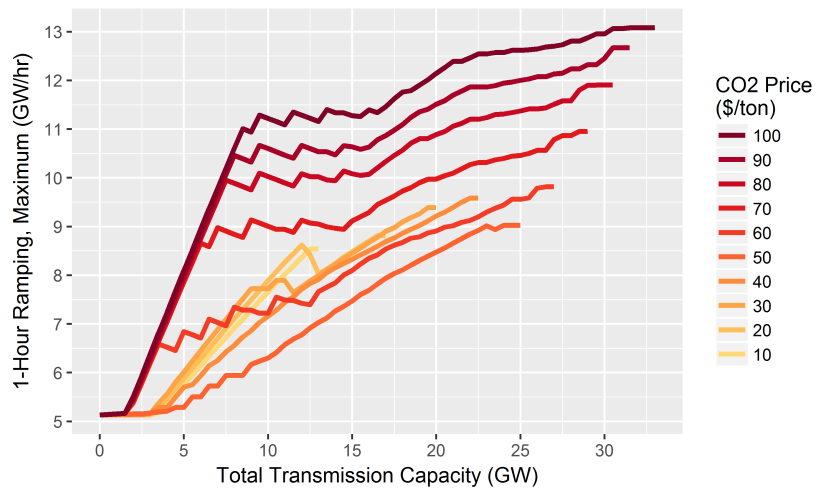


Figure 5.19: The maximum 1-Hour Ramp Rate is relatively consistent for lower CO₂ prices, but begins increasing for prices of 70 \$/ton and higher.

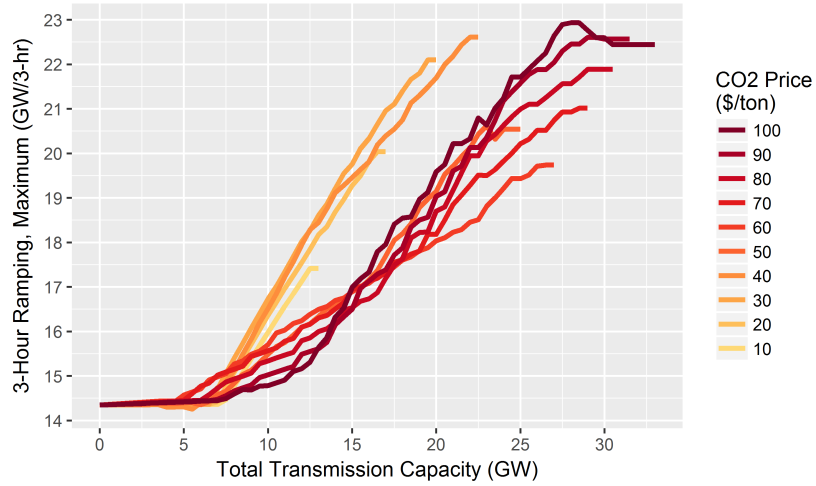


Figure 5.20: The maximum 3-Hour Ramp Rate is greatest for CO₂ prices of 30, 40, and 70+ \$/ton.

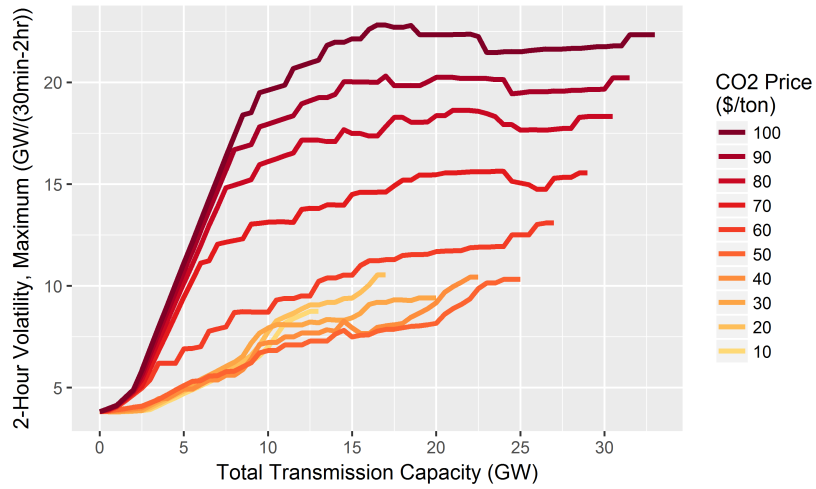


Figure 5.21: The maximum 2-Hour Volatility is relatively consistent for lower CO₂ prices, but begins increasing for prices of 60 \$/ton and higher.

5.2.4 Minimum net load constraint sensitivity

As described in Section 5.1.1, a minimum net load constraint is used by the model to approximate a frequency stability requirement that a certain amount of system power should be generated by traditional, spinning-inertia power plants. The base case model enforces a minimum net load requirement of 25% of peak demand, or 16.45 GW.

Increasing the minimum net load constraint would increase renewable energy curtailment, encouraging less renewable investment, per Fig 5.22(b). Adding fewer renewables to the grid increases costs and emissions, per Figs 5.22(c)&(d), but decreases the flexibility requirements, as shown in Fig 5.22(a). These results suggest that a grid might benefit from investing in technology that can help it maintain frequency stability using less inertial power generation. But if that technology investment does not also increase the system's flexibility, large ramp rates and volatility could be introducing new instabilities to the grid.

5.2.5 Natural gas price sensitivity

Natural gas prices can also have a significant influence on the optimal transmission and renewables investment, as shown in Fig 5.23(a). Rising natural gas prices, like rising CO₂ prices, increase the thermal costs of the system and encourage increasing renewable generation capacity. However, while rising CO₂ prices reorganize the merit order curve to prioritize thermal generators with lower CO₂ emissions, rising natural gas prices tend to do the opposite. This effect occurs as natural gas generators move up higher in the merit order curve, and coal generators take their

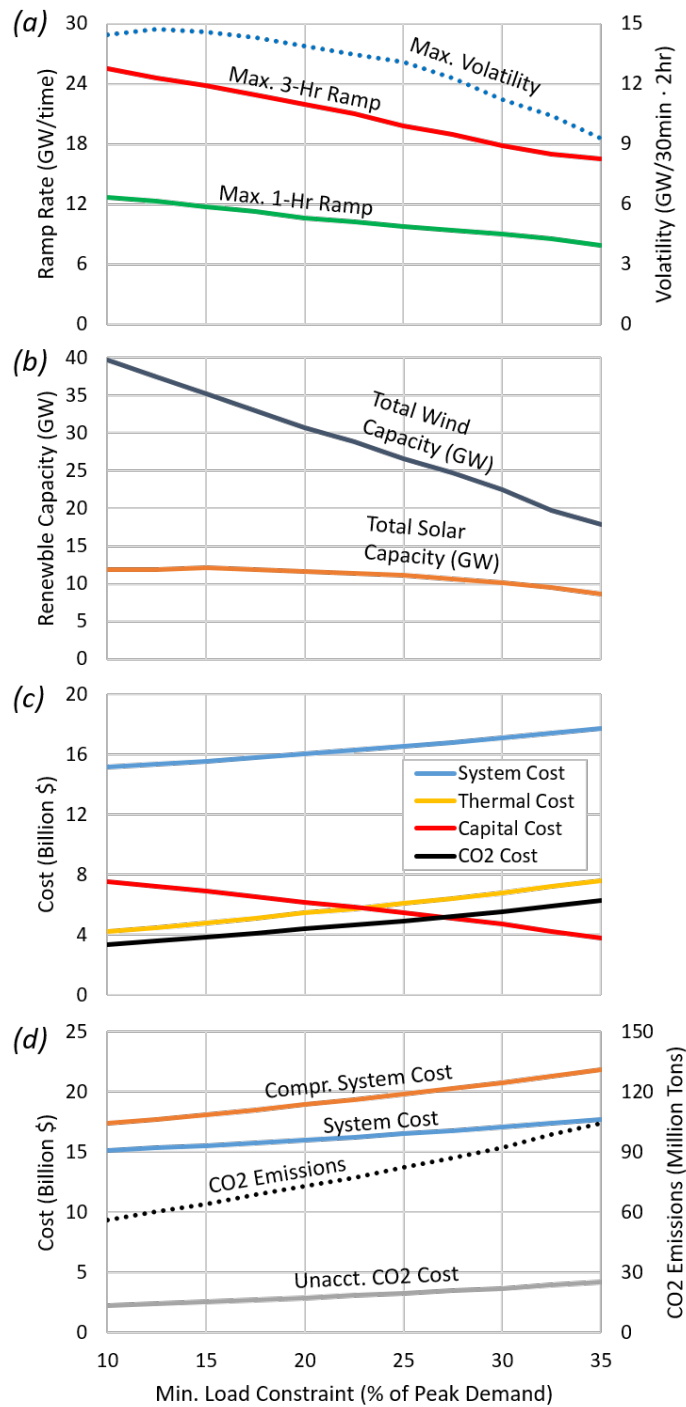


Figure 5.22: Increasing the minimum load constraint causes (a): lower flexibility requirements, (b): less wind and solar capacity, (c): larger thermal and CO₂ cost, but lower capital cost, and (d): higher CO₂ emissions and system cost.

place as the low-cost base load capacity. Therefore, from a CO₂ emissions perspective, higher natural gas prices exhibit a trade-off between encouraging renewable energy development and increasing the CO₂ intensity of the merit order curve. This effect is shown in Fig 5.23(c), where there is little difference between the CO₂ emissions at natural gas prices from 5.00 to 8.00 \$/MMBtu. Nonetheless, according to Fig 5.23(c), if the social price of CO₂ is 100 \$/ton, the system will generally prefer lower natural gas prices.

5.2.6 Existing power plant capacity factors

One consequence of integrating more renewables into the grid is the reduced utilization of existing power plants as renewable energy displaces the need for energy from traditional thermal generators. Fig 5.24 shows the capacity factors of different portions of the merit order at a 60 \$/ton CO₂ price with 0.0 GW of transmission to renewable energy regions. In contrast, Fig 5.25 shows the merit order utilization at the optimal solution of 27.0 GW of transmission investment. The market transitions from the majority of existing power plants being dispatched during some of the year, and 36 GW experiencing capacity factors of 40% or better to a market where the majority of existing generators are dispatched less than 20% of the year, and just 24 GW experience capacity factors of 40% or better. Fig 5.26 shows the different generator types that make up the merit order curve at a 60 \$/ton CO₂ price. In this scenario, all coal and natural gas boiler generators have capacity factors less than 20% with many of them not being dispatched at all. Nuclear and natural gas combined cycle generators provide the majority of non-renewable energy throughout

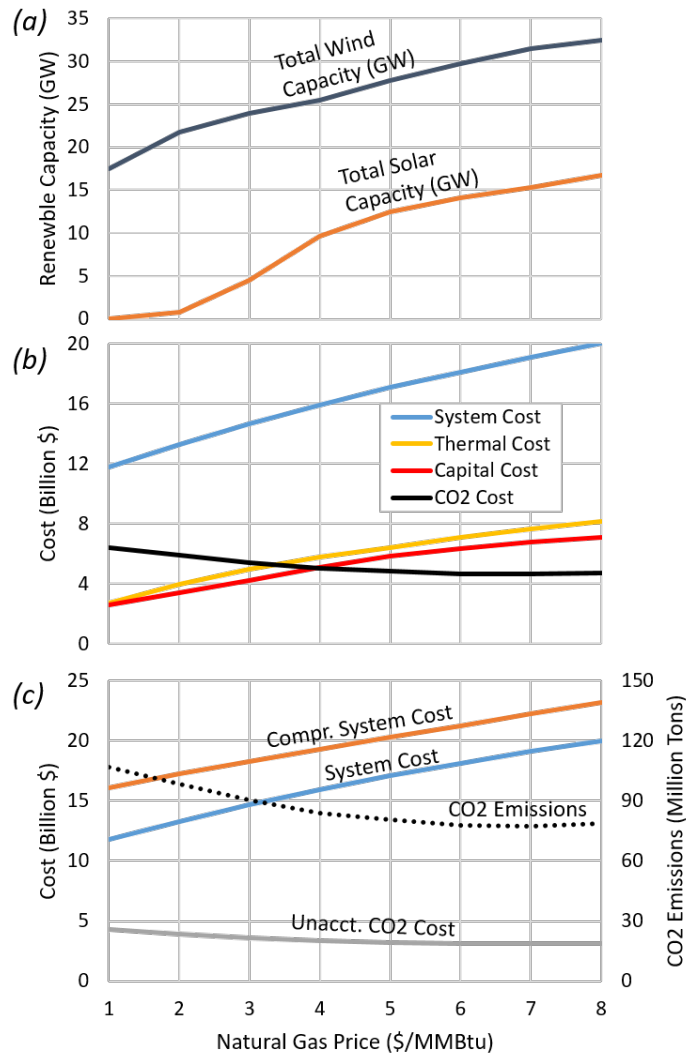


Figure 5.23: Increasing the natural gas price causes (a): more wind and solar capacity, (b): larger thermal and capital cost, but lower CO₂ cost, and (c): higher system costs and lower CO₂ emissions (up to 7.00 \$/MMBtu).

the year.

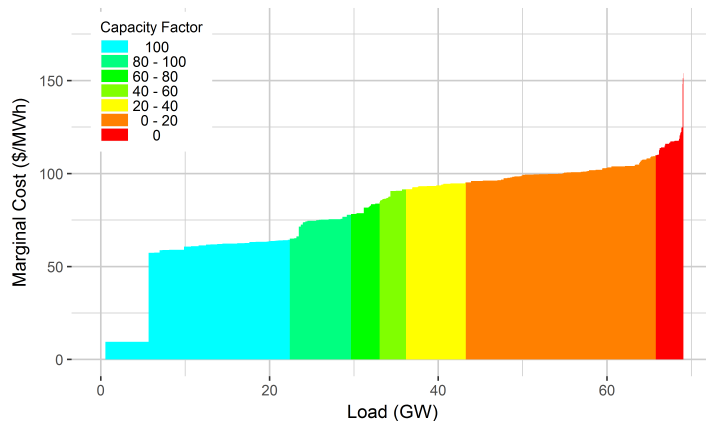


Figure 5.24: At a CO₂ price of 60 \$/ton and 0.0 GW of transmission to renewable energy regions, all of the demand is met by the existing generator fleet. Most of the generators are dispatched during the year, with 36 GW of capacity experiencing a 40% or better capacity factor.

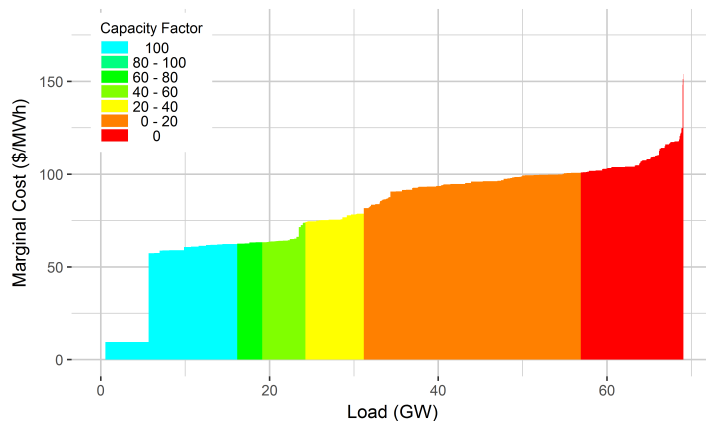


Figure 5.25: At a CO₂ price of 60 \$/ton and 27.0 GW of transmission at the optimal solution, less of the demand is met by the existing generator fleet. Only 24 GW of the existing generator fleet experiences a 40% or better capacity factor.

For comparison, Figs 5.27–5.30 show the merit order makeup and utilization

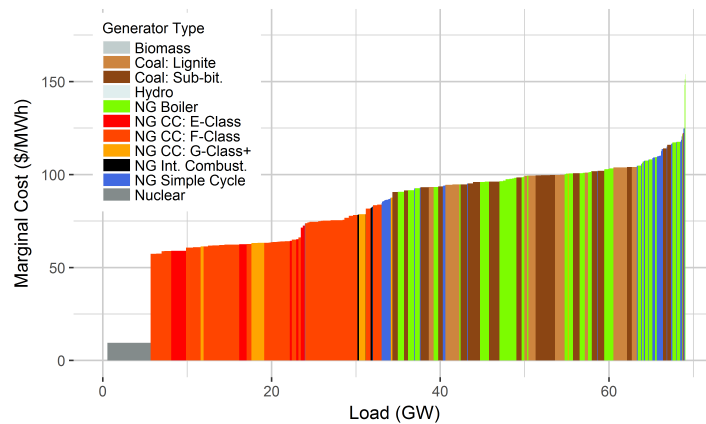


Figure 5.26: A CO₂ price of 60 \$/ton creates a merit order curve that dispatches natural gas combined cycle generators (left) before a coal and less-efficient natural gas generators (right).

at the optimal solutions at CO₂ prices of 20 \$/ton (17.0 GW transmission) and 100 \$/ton (33.0 GW transmission). Rising CO₂ prices push coal generators to the end of the merit order and bring natural gas boiler and simple cycle generators closer to the front. At a 20 \$/ton CO₂ price, all coal generators are dispatched some, and many of them experience capacity factors greater than 20%. At a 100 \$/ton CO₂ price, coal generators are hardly dispatched at all.

5.3 Conclusions

This study shows how system cost minimization is used to develop a model for geographically optimizing regional transmission, wind, and solar investments in an electric grid. This model can also provide useful feedback for setting CO₂ prices and anticipating the changing flexibility requirements that will result from more renewable energy capacity.

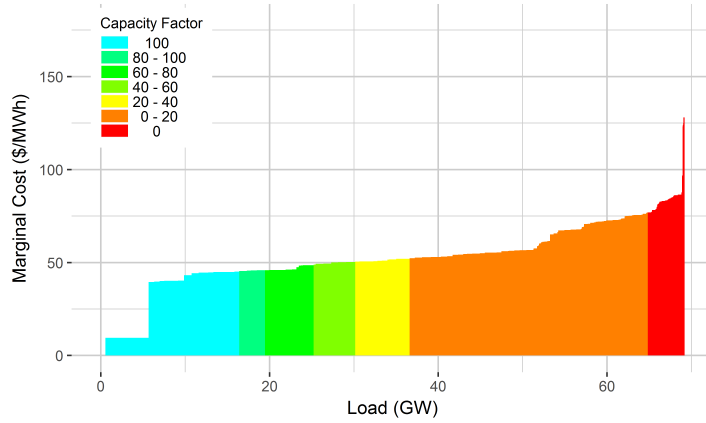


Figure 5.27: At a CO₂ price of 20 \$/ton and 17.0 GW of transmission at the optimal solution, 30 GW of the existing generator fleet experiences a 40% or better capacity factor.

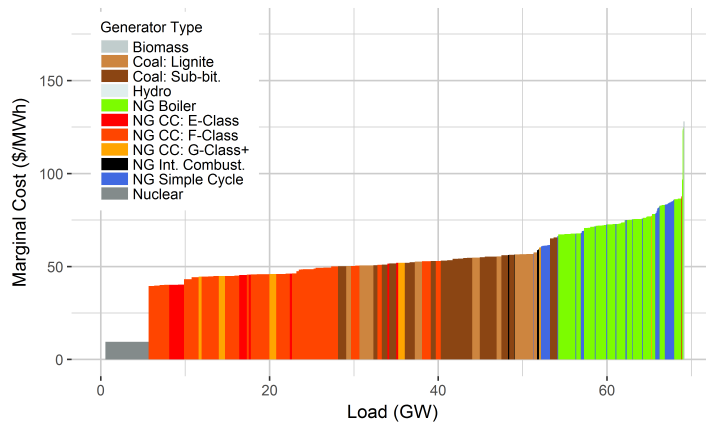


Figure 5.28: A CO₂ price of 20 \$/ton begins to move coal power plants higher up the merit order curve in favor of cleaner natural gas combined cycle generators. Coal still has a lower marginal cost than natural gas boilers and simple cycle generators.

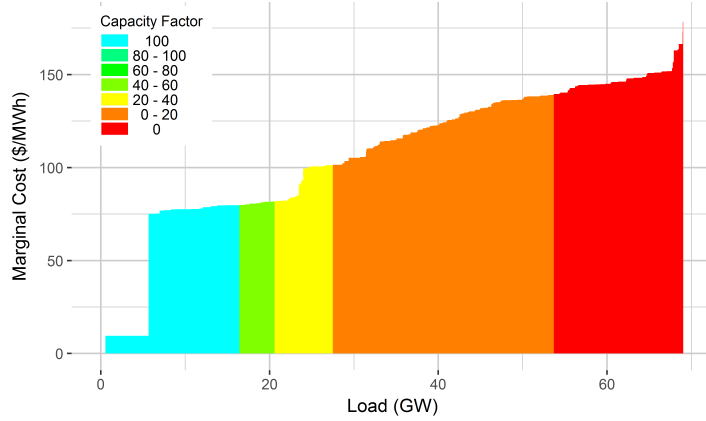


Figure 5.29: At a CO₂ price of 100 \$/ton and 33.0 GW of transmission at the optimal solution, only 20.5 GW of the existing generator fleet experiences a 40% or better capacity factor.

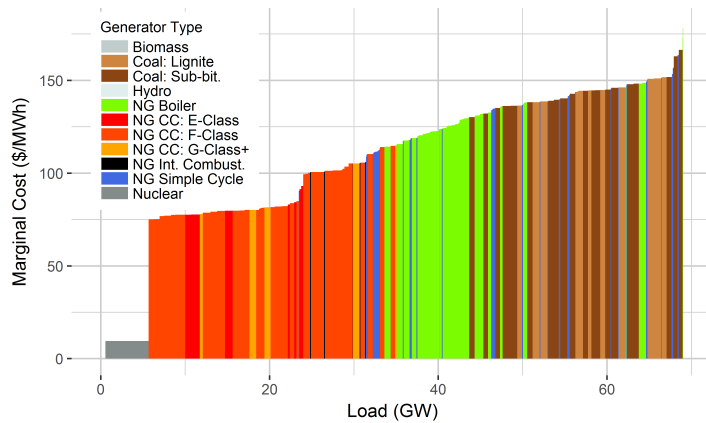


Figure 5.30: A CO₂ price of 100 \$/ton moves coal power plants towards the end of the merit order. Their CO₂ emissions are too large to justify their dispatch at such a high CO₂ price.

In the specific example of ERCOT with a 60 \$/ton CO₂ price, the model results recommended 27.0 GW of transmission capacity to five different ERCOT regions. These regions installed a total of 26.6 GW of wind and 11.1 GW of solar, representing a grid with 60.2% thermal capacity and 39.8% renewable capacity at a mix of 70.6% wind and 29.4% solar. This renewable mix produced 110 TWh of energy meeting 34% of the annual energy demand. The grid emits 82.2 million tons of CO₂ per year under this scenario, a 65% reduction from the 237 million tons produced when no renewable capacity is installed and the CO₂ price is 0 \$/ton.

Uncertainty analysis suggests that changes in thermal cost, solar capital cost, and wind capital cost can significantly impact the solution. Other case studies using this modeling method should use high quality power plant fleet data and define their wind and solar cost assumptions carefully.

Sensitivity analyses suggest that there are diminishing returns for raising the market CO₂ price. At higher CO₂ prices, the small gains in comprehensive system cost attributable to reduced CO₂ emissions might not be justifiable given the steady increase in system cost and flexibility requirements. Since this study does not quantify flexibility costs or provide economic theory for balancing real market costs with unaccounted environmental costs, it does not provide an optimal CO₂ price. However, qualitative assessment points toward a CO₂ price of 60 \$/ton as a good balance between system cost, environmental benefit, and flexibility requirement management, whether implemented as a CO₂ tax or through an emissions trading scheme.

Sensitivity analyses also suggest that the minimum net load constraint in

the model has a significant impact on the optimal solution. This result means that an accurate assessment of this constraint is important for calculating the optimal renewable capacity. It also indicates that technologies that could allow the net load to drop below this requirement without compromising the grid's stability could be valuable additions to the system.

Finally, the results communicate a diminishing need for high marginal cost generators as renewable generation reduces the capacity factor of most of the generators in the merit order curve. Generators with inherently high marginal costs, such as natural gas boilers, or high marginal costs resulting from CO₂ prices, such as coal power plants, will see limited use in an ERCOT market with reasonable CO₂ prices and an optimal investment in renewables.

Chapter 6

Optimal dispatch and equipment sizing of a residential central utility plant for improving rooftop solar integration

This dissertation chapter hypothesizes that a central utility plant (CUP) could economically improve rooftop solar integration in a residential neighborhood and support the stability of the larger electric grid. It contributes novel research by bridging a gap in the academic literature between distributed, residential solar integration and micro-grid/CUP optimization. It adds to the micro-grid/CUP modeling literature by developing a generalized, linear model to optimize CUP equipment capacity and hourly dispatch simultaneously and by analyzing a microgrid’s ability to integrate rooftop solar in the residential sector of a cooling-dominated climate.

This chapter is an updated study of “Optimal dispatch and equipment sizing of a residential central utility plant for improving rooftop solar integration” as published by *Energy* in 2018 [42].

6.1 Model background

While the CUP model’s variables can be adjusted to represent different technology costs, efficiencies, price data, demand data, etc., it is helpful to provide a case

Table 6.1: Nomenclature: Exogenous Variables

Symbol	Description	Bounds
h	Superscript denoting the hour of the year	$\in \mathbb{Z}, \in [0, 8760]$
H	Microturbine generator rated heat rate [$\text{Btu}_{\text{fuel}}/\text{kWh}_{\text{electricity}}$]	-
T^h	Ambient temperature [$^{\circ}\text{C}$] in hour h	-
gen	Equipment subscript denoting the microturbine generator	-
bat	Equipment subscript denoting the battery	-
ch	Equipment subscript denoting the chiller plant	-
$ctes$	Equipment subscript denoting the cooling thermal energy storage	-
$piping$	Subscript denoting the chilled water piping network	-
$solar$	Equipment subscript denoting the neighborhood rooftop solar	-
λ_{e-}^h	Electricity buy price in hour h [$\$/\text{MWh}$]	-
λ_{e+}^h	Electricity sell price in hour h [$\$/\text{MWh}$]	-
λ_d	Electricity peak demand charge [$\$/\text{MW}$]	-
λ_{ng}	Natural gas buy price [$\$/\text{MMBtu}$]	-
$C_{equipment}^0$	Intercept of equipment's capital cost equation (see Table 6.5) [$\$$]	-
$C_{equipment}^1$	Slope of equipment's capital cost equation (see Table 6.5) [$\$/\text{capacity}$]	-
$O_{equipment}$	Equipment's operation and maintenance cost	-
R	Capital amortization factor = 0.0944 (7% interest over 20 years [77])	-
A	Annualized cost of equipment [$\$$]	-
B	Big number = 10,000 (for modeling purposes)	-
η_{bat}	Battery round trip efficiency [%]	-
η_{ctes}	CTES round trip efficiency [%]	-
COP_{cool}^h	Chiller coefficient of performance for cooling in hour h [$\text{MWh}_{\text{th}}/\text{MWh}$]	-
COP_{ice}^h	Chiller coefficient of performance for ice-making in hour h [$\text{MWh}_{\text{th}}/\text{MWh}$]	-
K_{solar}^h	Capacity factor for solar in hour h [%]	-
d_e^h	Neighborhood electric demand in hour h [MWh]	$\in +\mathbb{R}$
d_c^h	Neighborhood cooling demand in hour h [MWh_{th}]	$\in +\mathbb{R}$
$D_{gen,cap}^h$	Ambient de-rating factor for generator capacity in hour h	-
$D_{gen,hr}^h$	Ambient de-rating factor for generator heat rate in hour h	-

Table 6.2: Nomenclature: Decision Variables

Symbol	Description	Bounds
Δ_e^h	Net electric demand in hour h [MWh]	$\in \mathbb{R}$
Δ_{e-}^h	Electricity purchased from the grid in hour h [MWh]	$\in +\mathbb{R}$
Δ_{e+}^h	Electricity sold to the grid in hour h [MWh]	$\in +\mathbb{R}$
F^h	Fuel (natural gas) purchased in hour h [MWh]	$\in +\mathbb{R}$
$F_{gen,on}^h$	Generator fuel consumption if in “on” mode in hour h [MWh]	$\in +\mathbb{R}$
M_Δ	Annual peak electricity demand [MW]	$\in +\mathbb{R}$
$M_{equipment}$	Equipment capacity (maximum output [MW] or [MW _{th}] or storage size [MWh] or [MWh _{th}])	$\in +\mathbb{R}$
P_e^h	Net electricity production in hour h [MWh]	$\in +\mathbb{R}$
$P_{e,gen}^h$	Generator electric output in hour h [MWh]	$\in +\mathbb{R}$
$P_{e,solar}^h$	Solar electric output in hour h [MWh]	$\in +\mathbb{R}$
$P_{e,bat,c}^h$	Electricity charged into battery in hour h [MWh]	$\in +\mathbb{R}$
$P_{e,bat,d}^h$	Electricity discharged from battery in hour h [MWh]	$\in +\mathbb{R}$
$P_{e,ch}^h$	Chiller plant electric demand in hour h [MWh]	$\in +\mathbb{R}$
$P_{c,ch}^h$	Chiller plant cooling output in hour h [MW _{th}]	$\in +\mathbb{R}$
$P_{c,ctes,c}^h$	Cooling charged into CTES in hour h [MW _{th}]	$\in +\mathbb{R}$
$P_{c,ctes,d}^h$	Cooling discharged from CTES in hour h [MW _{th}]	$\in +\mathbb{R}$
S_{bat}^h	Electric energy stored in battery in hour h [MWh]	$\in +\mathbb{R}$
S_{ctes}^h	Cooling energy stored in CTES in hour h [MW _{th}]	$\in +\mathbb{R}$
$y_{gen,on}^h$	Binary equal to “1” when generator is on	$\in \{0, 1\}$
$y_{gen,off}^h$	Binary equal to “1” when generator is off	$\in \{0, 1\}$

study to illustrate how to apply the model to a real world scenario. This section explains the data, equations, and calculations that have been compiled to create the neighborhood and CUP model along with a case study of a residential neighborhood in Austin, TX, USA. Section 6.1.1 presents the data for the neighborhood and solar models. Section 6.1.2 presents the equations for the efficiency, operation, and cost of the CUP equipment. Sections 6.1.3 and 6.1.4 discuss electricity rate structures and CO₂ emissions calculations.

6.1.1 Neighborhood and solar models

The neighborhood model provides an exogenous source of electric demand, cooling demand, and rooftop solar generation for the optimization program. While the model framework can solve for any set of hourly neighborhood data, capital cost, fuel cost, and other inputs, this study uses information from a residential neighborhood in Austin, TX, USA as an illustrative case study. Hourly data from 2015 for 123 houses in Austin are compiled via Pecan Street Incorporated [142], a non-profit entity that collects energy use data and makes it freely available to university researchers [154]. That dataset is scaled up to represent a neighborhood of 750 houses with 1.2 MW of solar capacity. That solar capacity represents approximately 30% rooftop penetration, a value similar to the most solar-dense neighborhoods in California [11]. Table 6.3 summarizes some of the neighborhood data, Figs 1.1, 1.2, and 6.1 show 24-hour and annual profiles for the neighborhood, and Fig 6.2 shows Austin’s hourly ambient temperature in 2015 [186].

While the dataset provides cooling demand in the form of the electrical draw

Table 6.3: Data summary for the Austin, TX neighborhood case study with 750 houses and 1.2 MW solar.

Data Summary Description	Value
Annual cooling demand [MWh _{th}]	8800
Peak cooling demand [MW _{th}]	4.7
Annual electric demand (incl. cooling) [MWh]	9300
Peak electric demand (incl. cooling) [MW]	3.2
Annual net demand (demand – solar) [MWh]	7770
Peak net demand (demand – solar) [MW]	2.98
Minimum net demand ramp rate [MW/hr]	-0.51
Maximum net demand ramp rate [MW/hr]	0.70
Annual CO ₂ emissions [tons]	5920

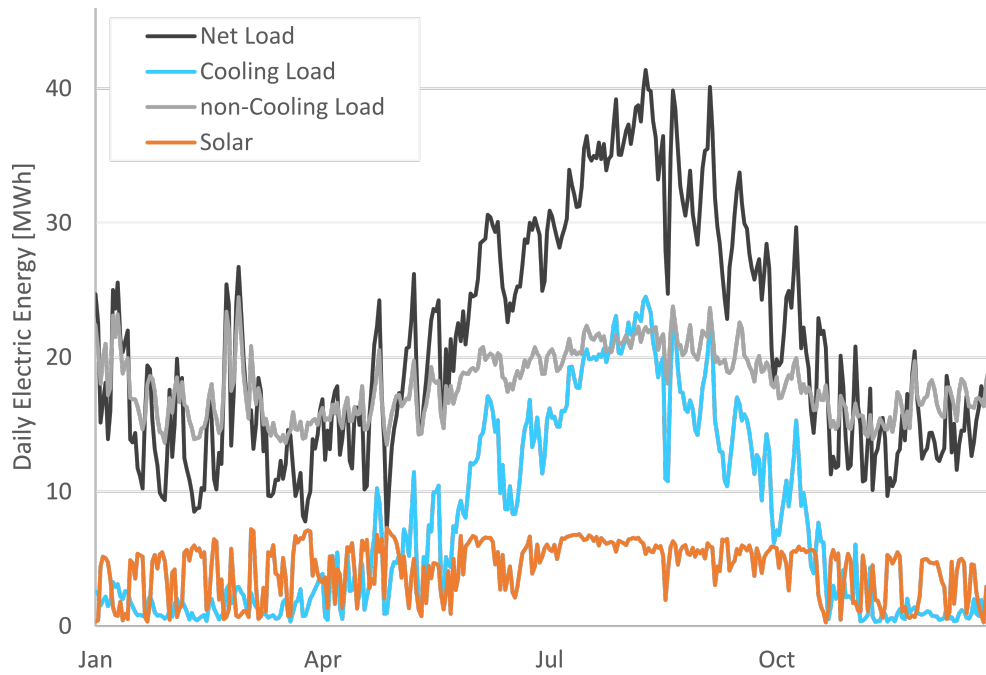


Figure 6.1: Daily sums for the 750-house neighborhood model with 1.2 MW solar.

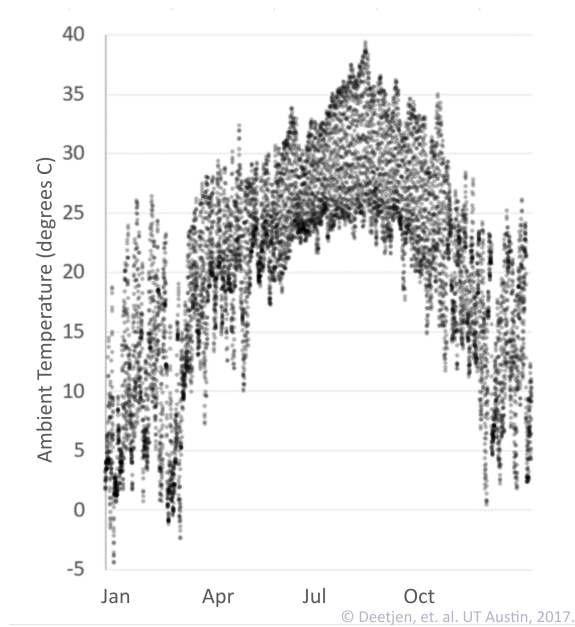


Figure 6.2: Hourly ambient temperature in Austin, TX, USA in 2015.

for each house’s cooling equipment, it is necessary to convert that data from electrical to thermal demand to more accurately represent the cooling needs of the neighborhood. The coefficient of performance (COP) describes an air conditioner’s efficiency at converting electrical energy into cooling energy in units of $\text{MWh}_{th}/\text{MWh}$. Since COP varies with ambient temperature, this study uses a prior COP model [28] along with weather data [186] to estimate each house’s hourly thermal cooling demand from the electrical demand dataset.

The thermal demand data can be used to estimate the cooling equipment capacity at each house. This estimation assumes that the cooling equipment capacity equals the peak thermal cooling demand rounded up to the nearest half-ton. This calculation estimates 7.3 MW_{th} of total installed cooling capacity for the neighbor-

hood.

The capital cost of the neighborhood’s outdoor condenser units (the equipment that would be replaced by a central chiller plant) is not used in the optimization model, but is helpful for comparing the results with a neighborhood baseline. This capital cost is estimated using construction cost data from [157]. This method estimates condenser capital cost at \$1.85 Million overnight or \$175,000 per year when amortized at 7% interest over 20 years (per *R* description in Tables 6.1 and 6.2).

Solar capital cost for the Austin case study is estimated at 1.65 Million \$/MW based on [75] and assuming a 30% Investment Tax Credit [31]. Annual fixed maintenance cost is modeled as 23,000 \$/MW [170].

6.1.2 Central utility plant equipment models

This study utilizes a central utility plant (CUP) to act as an intermediary between the neighborhood and the electric grid. The CUP design includes a gas microturbine generator, battery, chiller plant, and cooling thermal energy storage (CTES). It uses this equipment, supplemented by neighborhood solar generation and electricity purchased from the grid, to meet the neighborhood’s demand for cooling and electricity, as shown in Fig 6.3.

While the literature contains many detailed models of microturbines, batteries, and chilled water production and storage systems, especially when the equipment capacity is specified (as in a case study), the equations used for this CUP model need to be more generalized to allow the optimization program to choose different equipment capacities. The remainder of this section presents models for each piece of CUP

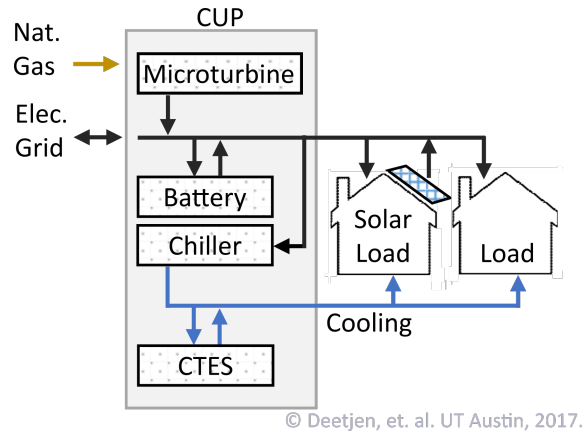


Figure 6.3: CUP flowchart. A microturbine, battery, chiller plant, and CTES system comprise a CUP that acts as an intermediary between the electric grid and the neighborhood’s electric demand, cooling demand, and solar generation.

equipment. The models are general enough to be scalable with equipment capacity but still capture the most important aspects of the equipments’ operation. Tables 6.4 and 6.5 summarize the equipment operation and cost models.

Note that this generalized model uses continuous variables for equipment capacity though the actual capacity options available to a central utility plant might depend on manufacturer offerings. The model also assumes that CUP equipment can reduce its part-load operation or state-of-charge to nearly zero though actual equipment might be subject to stricter operational limitations. When developing a specific CUP design, the modular combination of different equipment sizes might be able to achieve a variety of operational capabilities and total system capacities.

Though each CUP component might have a different lifetime, this study assumes that the entire CUP will be financed with a single loan, and amortizes its capital costs over a period of 20 years with an interest rate of 7% [77]. These pa-

rameters reflect costs associated with financing the entire CUP over the plausible lifetime of a microgrid using lower medium grade corporate bonds [77].

Table 6.4: CUP operation and efficiency equations.

Relationship	Equation	R ² fit
Generator fuel consumption vs. electricity output	$F_{gen,on}^h = 0.137HM_{gen} + 0.863HP_{e,gen}^h$	0.988
Generator capacity de-rating factor vs. ambient temperature	$D_{gen,cap} = 1.136 - 0.00907T$	0.939
Generator heat rate de-rating factor vs. ambient temperature	$D_{gen,hr} = 1 + 0.000768T + 0.00768T^2$	0.982
Battery round trip (charge-discharge) energy efficiency	$\eta_{bat} = 0.85$	-
Chiller COP vs. ambient temperature during cooling mode	$COP_{cool} = 6.35 - 0.0985T$	0.967
Chiller COP vs. ambient temperature during ice-making mode	$COP_{ice} = 5.41 - 0.0985T$	-
CTES round trip (charge-discharge) energy efficiency	$\eta_{ctes} = 0.97$	-

Table 6.5: CUP capital cost and the operation and maintenance (O&M).

Equipment	Capital Cost [\$]	Annual O&M Cost [\$]
Microturbine generator	1,280,000 M_{gen}	$O_{gen} = 0.0105\Sigma_{h=0}^{8760}P_{e,gen}^h$
Lithium-ion battery	375,000 M_{bat}	-
Chiller plant	48,120 + 174,245 M_{ch}	$O_{ch} = 12,750 + 268M_{ch}$
Ice CTES	42,650 M_{ctes}	-
Chilled water piping	2,900,000	-
Rooftop solar	1,650,000 M_{solar}	$O_{solar} = 23,000M_{solar}$

Gas microturbine generator:

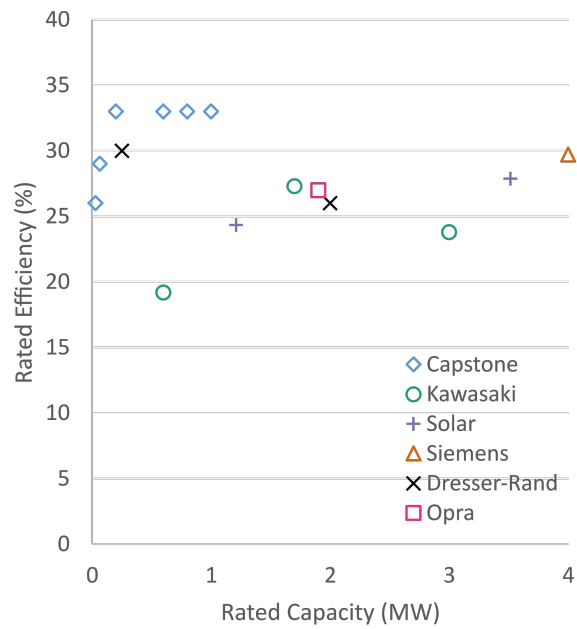
The term “microturbine” describes a subset of open-cycle gas turbine technology that burns fuel to produce electricity and heat for individual buildings or small distribution networks [23]. The fuel required to produce a certain amount of electricity depends on the microturbine’s heat rate, an efficiency metric with units of $Btu_{fuel}/kWh_{electricity}$. A microturbine’s heat rate worsens when it generates less electricity than its rated capacity (“part-load” operation) and when ambient temperature increases. Similarly, its output capacity decreases at higher ambient temperatures.

The microturbine model in this study converts natural gas fuel into electric energy that can be used to meet neighborhood electric demand, operate the chiller plant, charge the battery, or sell energy to the grid. The microturbine’s fuel-to-electricity conversion depends on the heat rate and capacity equations described below. For illustrative purposes, this study prices natural gas λ_{ng} at 3.04 \$/MMBtu based on the average Henry Hub spot price since 2012 [180].

Initially, the microturbine is assigned a rated or baseline heat rate. Manufacturer data from Capstone [2], Kawasaki [5], Solar Turbines [8], Siemens [7], Dresser-Rand [3], and Opra [6] are plotted in Fig 6.4. The data show that, for microturbines with a rated capacity of 0 to 4 MW, the rated efficiency does not correlate strongly with rated capacity. As an illustrative value, the microturbine model assumes a rated efficiency of 25% (a heat rate of 13,648 Btu/kWh) for microturbines of any capacity.

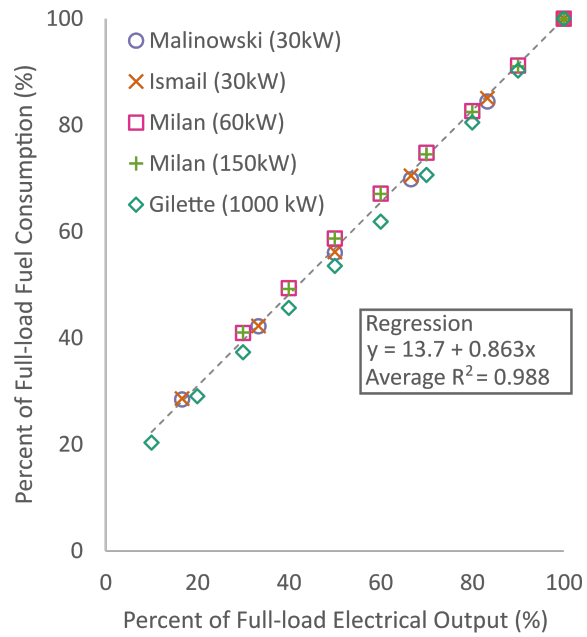
The microturbine’s heat rate worsens when operating at part-load output. From the academic literature, data showing the relationship between normalized fuel consumption and normalized electrical output under part-load operation for microturbines of 30kW [117], 30kW [99], 60kW [121], 150kW [121], and 1000kW [73] capacities are shown in Fig 6.5 along with a linear regression. The positive y-intercept indicates larger heat rates (more fuel burnt per electric energy generated) at lower outputs.

The regression equation in Fig 6.5 is converted to a form in terms of hourly fuel consumption $F_{gen,on}^h$, rated heat rate H , rated capacity M_{gen} , and hourly generator output P_{gen}^h as $F_{gen,on}^h = 0.137HM_{gen} + 0.863HP_{e,gen}^h$. This form interfaces better with the optimization program, allowing fuel consumption to be calculated directly



© Deetjen, et. al. UT Austin, 2017.

Figure 6.4: Manufacturer data indicate a lack of correlation between rated capacity and rated efficiency for microturbines in the 0 to 4 MW capacity range.



© Deetjen, et. al. UT Austin, 2017.

Figure 6.5: Microturbine normalized fuel consumption versus normalized electrical output under part-load operation. Results from Malinowski [117], Ismail [99], Milan [121], and Gillette [73] support a linear relationship between fuel consumption and electrical output.

from the rated capacity and generator output parameters.

The microturbine's heat rate increases and capacity decreases when operating at higher ambient temperatures. These capacity and heat rate de-rating factors are approximated by as $D_{gen,cap} = 1.136 - 0.00907T$ and $D_{gen,hr} = 1 + 0.000768T + 0.000077T^2$. These approximations are regressions of ambient temperature performance data for Kawasaki microturbines with capacities ranging from 1.4 to 5.4 MW [5]. The regressions have average R^2 values of 0.939 and 0.982, respectively, when compared to the original performance data.

A microturbine's capital cost increases directly with its capacity, ranging from 910 to 1650 \$/kW when including installation [23]. Variable maintenance costs range from 0.005 to 0.016 \$/kWh [23]. This study uses 1280 \$/kW and 0.0105 \$/kWh for capital and maintenance costs, respectively, for the Austin case study.

Battery:

Batteries use the chemical potential between anode and cathode materials to store and discharge electrical energy. Lithium-ion batteries, in particular, are becoming the preferred battery technology for utility grid electrical storage due to their high energy density, voltage rating, cycle life, and efficiency [4].

The battery model in this study consumes electric energy, stores it, and discharges that energy later to meet neighborhood electric demand, chiller plant demand, or sell energy to the grid.

The battery's charge-discharge cycle incurs energy losses due to battery inef-

iciencies. Its hourly dispatch can be modeled linearly by assuming a constant energy efficiency for charging and discharging the battery cells [169]. Based on a 92% d.c.-to-d.c. battery efficiency and a 96% d.c.-to-a.c. inverter efficiency, this study gives the battery a roundtrip a.c.-to-a.c. efficiency η_{bat} of 85% [61] as an illustrative value.

Historically, grid-level batteries have been relatively expensive [30], but recent trends show a steady reduction in cost [150]. The balance of system (BOS) costs for installation, which include battery modules, soft costs, and engineering and procurement, can range from 670 \$/kWh [137] in 2015 to 350 [30] or 400 \$/kWh [137] in 2020. This study uses a BOS cost of 375 \$/kWh in anticipation of the lower prices expected in 2020.

Chiller plant and cooling storage:

Air conditioning moves heat from the interior of a building to the outdoors via the vapor-compression refrigeration cycle [26]. A chiller plant accomplishes this heat transfer by raising the temperature of a working fluid above ambient conditions, cooling the working fluid by rejecting heat to the atmosphere via a condenser coil, and returning that working fluid to the building to absorb heat from the the building interior [118].

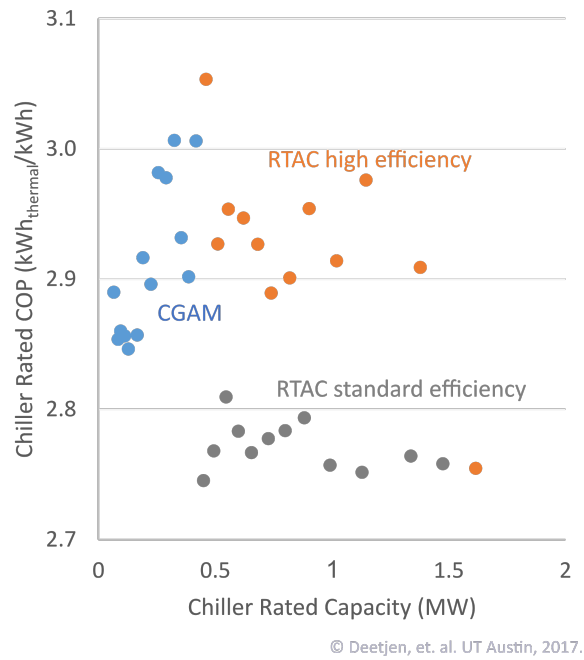
These “air-cooled” chillers operate more efficiently at lower temperatures, though cooling demand is often greatest during the hottest parts of the day (when the chiller is least efficient). Cooling thermal energy storage (CTES), however, can decouple chiller operation from cooling demand. It accomplishes this decoupling by

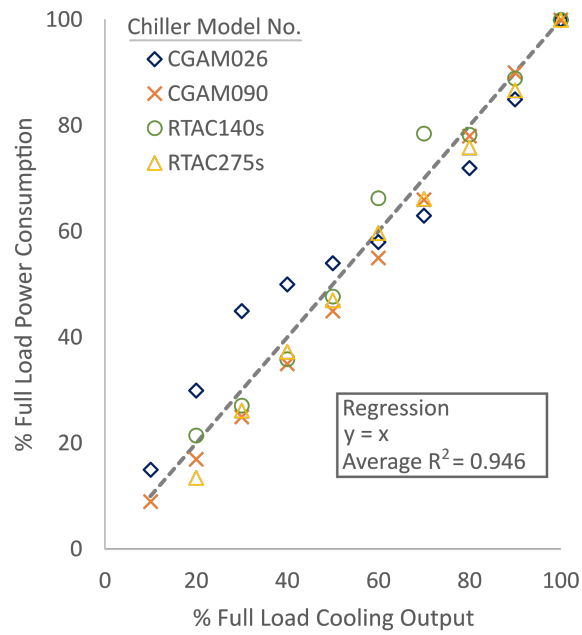
storing a block of ice produced by the chiller early in the day when temperatures are lower and chiller efficiency is higher, and by melting that ice later in the day to help meet cooling demand, which allows chiller output to be lower than cooling demand. (Though not used in this model, note that an alternate CTES method stores cooling in a large, thermally-stratified, tank of chilled water).

In a typical “internal melt”, ice-based, CTES design, the chiller cools a water-glycol working fluid down to 25 °F (-3.9 °C). This fluid flows through a heat exchanger coil in a small water tank to generate ice. Once the ice tank is fully “charged”, the chiller can operate in normal cooling mode, or it can shut off, allowing the CTES to “discharge” and provide cooling to the building without consuming electricity at the chiller [60].

The chiller model in this study converts electric energy into cooling for satisfying the neighborhood’s cooling demand or charging the CTES system. The efficiency of that conversion process depends on the chiller plant’s coefficient of performance (COP), expressed in units of kWh_{th}/kWh. Based on chiller performance data [172] and curves [173] from the Trane Corporation, Fig 6.6 shows that a chiller’s rated COP does not correlate with its capacity, and Fig 6.7 supports a one-to-one relationship between cooling output and power consumption. As an illustrative value, this study assumes a rated COP of 2.9 at 95 °F (35 °C) for the air-cooled chiller, regardless of chiller capacity or part-load operation.

Ambient temperature greatly influences chiller COP. Fig 6.8 shows performance data for a variety of Trane, air-cooled chiller models [173] and supports a linear relationship between ambient temperature and COP.





© Deetjen, et. al. UT Austin, 2017.

Figure 6.7: Data support a one-to-one relationship between part-load chiller cooling output and power demand [173].

Charging the ice-storage system also influences chiller COP. When a chiller switches from cooling to ice-making mode, it must cool the working fluid to a lower temperature, which requires more energy. This study assumes working fluid temperatures of 42 °F (5.55 °C) for cooling (with a return temperature of 56 °F (13.33 °C)) and 25 °F (-3.89 °C) for ice-making [172]. It adjusts the ice-making COP curve, accordingly, as shown in Fig 6.8.

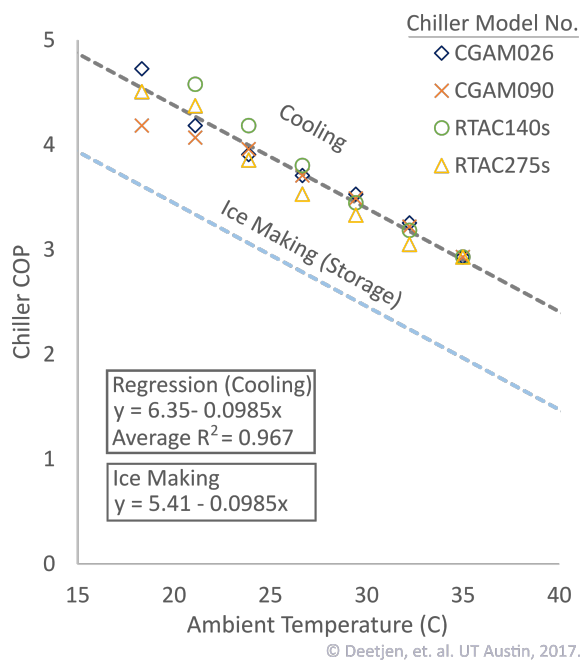


Figure 6.8: Chiller COP varies directly with ambient temperature [173] and whether the chiller is in cooling or ice-making mode [97].

Though ice-making consumes more electricity than cooling at the same ambient temperature, making ice at night when ambient conditions are cooler and chiller COP is higher can compensate for this adverse effect [40]. In Fig 6.8, for example, cooling at ambient temperatures of 30 °C (daytime) has the same COP as ice-making

at ambient temperatures of 20.5 °C (nighttime).

The CTES model in this study consumes cooling energy, stores it, and discharges that energy later to meet neighborhood cooling demand.

Internal melt, ice-based, thermal energy storage systems operate at very high efficiencies, with losses mainly due to heat transfer from the atmosphere to the ice block. While the round trip, charge-discharge efficiency of these CTES systems depends on the storage operational strategy and the ambient temperature, efficiency varies from 97% to 99% under most conditions [115]. This study assumes that CTES efficiency dynamics will have limited impact on the solution, and uses a constant, round trip efficiency of 97% for the ice-storage CTES system.

Chiller plant costs include capital cost and fixed maintenance cost, which both depend on the chiller plant capacity. Overnight capital cost is modeled as $48,120 + 174,245M_{ch}$ using construction cost data from [157]. Annual fixed maintenance cost is modeled as $12,750 + 268M_{ch}$ using data from [126]. Ice storage system capital cost is modeled as $42,650M_{ctes}$ [95].

Another capital cost component of a centralized cooling system is the underground distribution piping that connects the chiller plant with the individual buildings. Heuristics or actual examples of chilled water piping network costs are not widely available in the literature. This study estimates the chilled water piping network capital cost by designing a rudimentary network for an Austin, TX neighborhood representative of the 750-house neighborhood model (see Section 6.1.1). The design is shown in Fig 6.9 and assumes a centrally-located chiller plant. It is

sized for peak cooling demand, assumes that each house contributes an equal share to the peak neighborhood cooling demand, and chooses pipe diameters according to the design guidelines in [165]. The design requires 1130, 1300, 1940, and 14790 linear feet of 6", 4", 3", and 2" diameter insulated, steel, hydronic distribution piping at a total cost of \$2.9 Million (including design, procurement, and construction costs) [157]. The uncertainty of this cost is non-trivial as actual costs might depend on neighborhood density, construction, network design, and other factors.



Figure 6.9: A rudimentary design for the neighborhood chilled water distribution system using design guidelines from [165] helps estimate the capital cost of the piping network at \$2.9 Million.

6.1.3 Electricity rate structures

Observing the response of the CUP to different electricity rate structures is an important analysis component of this study. Residential rate structures are normally “flat,” meaning that price does not change with season or time of day. However, “time-of-use” (TOU) rate structures, where prices do change with season and time of day, are becoming more common, especially in the commercial and industrial

sectors. California requires these sectors to be on a TOU plan and offers TOU rate structures to its residential customers [22]. Another price mechanism, “real time pricing” (RTP), mimics the wholesale prices paid to power plants that can change every 15 minutes. While RTP structures are not generally available to residential customers, this study includes it to illustrate the effects of a pricing structure that is more dynamic than what is typically available.

Switching from flat to TOU or RTP rate structures encourages customers to reduce their peak demand and shift their consumption to times of the day when electric grid costs are lower. These dynamic rate structures might help utilities achieve lower costs, greater reliability, and better renewable energy integration [171].

More dynamic pricing structures might be more effective at accomplishing these goals, and this study uses 5 different energy-only rate structures to test this hypothesis. Three TOU rates are designed to mimic the seasonal and daily timing of a TOU rate structure in Austin, TX, USA with off-peak, mid-peak, and on-peak prices [14]. Each TOU rate has a different spread between those three prices. An RTP rate, mimicking the historic 2015 energy prices in the Texas electricity market, is also used in the analysis. Though constantly changing, real-time prices might be difficult for an actual residential CUP to forecast and respond to, the RTP rate used in this study assumes that the CUP has perfect foreknowledge and tests whether such a volatile rate structure would provide better incentives than a TOU rate.

The rates are designed so a 1 MW constant load would pay the same total annual energy cost under any of the rate structures, at an average price of 120 \$/MWh, based on the average US residential electricity rate [179]. Figs 6.10 and 6.11

summarize the timing and price values of the different rate structures.

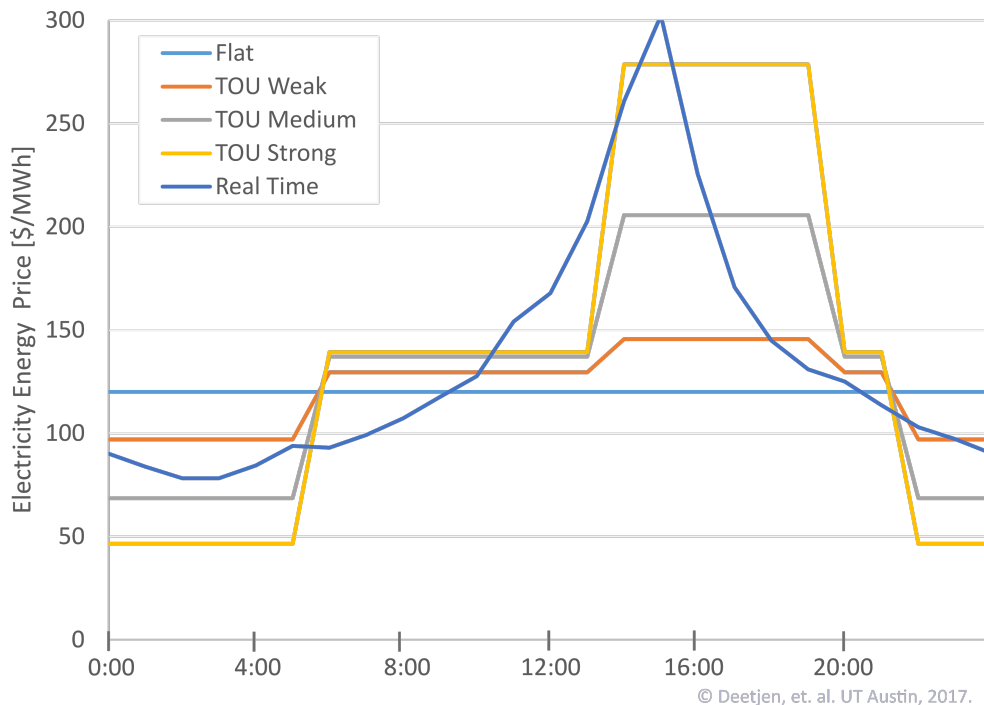


Figure 6.10: Energy only rate structures for electricity purchased during peak season (June 1–September 30). Real time prices vary hourly, based on the historic wholesale market.

Beyond energy-only prices, electricity rate structure can also include demand charges that apply a price to a customer’s peak instantaneous consumption. These charges might encourage lower peak demand and flatter demand profiles [74]. This study tests that hypothesis by adding an increasing demand charge to a TOU rate with a moderate spread between off-peak and on-peak prices, as shown in Table 6.6, where the demand charge is multiplied by the annual maximum amount of electricity bought or sold by the CUP during any hour of the simulation. The demand charge rate structures in Table 6.6 are designed by reducing the energy price in 10% incre-

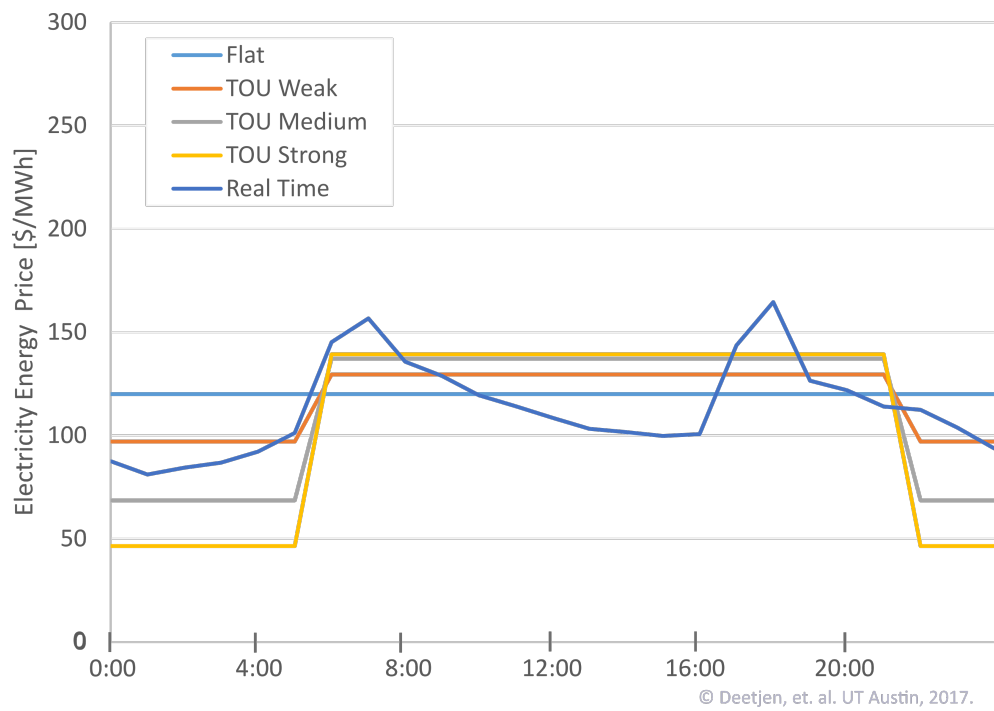


Figure 6.11: Energy only rate structures for electricity purchased during off-peak season (October 1–May 31). Real time prices vary hourly, based on the historic wholesale market.

ments and choosing the demand charge that allows a 1 MW constant load to pay the same annual cost under each rate structure.

Table 6.6: Rate structures with demand charges are created by lowering the energy price of a medium TOU rate and introducing a demand charge. A 1 MW constant load will pay the same annual cost under each rate structure.

	Demand 0	Demand 1	Demand 2	Demand 3	Demand 4
Annual Demand Charge [\$/MW]	0	43,900	106,800	169,800	232,700
Energy Price Reduction [%]	0	10	20	30	40
Energy Price (Off-Peak) [\$/MWh]	61.69	59.11	55.42	51.72	48.03
Energy Price (Mid-Peak) [\$/MWh]	142.46	136.51	127.98	119.4	110.92
Energy Price (On-Peak) [\$/MWh]	195.89	187.72	175.98	164.5	152.52

Another aspect of electricity rate design is the remuneration structure for selling power back to the grid. Net energy metering, a common method for US utilities, subtracts a customer’s monthly generation from their monthly consumption and bases their bill on that net energy amount. Utilities have raised concerns, however, that net metering fails to capture the true costs and benefits of distributed solar [16]. In this study, the CUP can sell electricity at the wholesale market price, but cannot sell it for more than the local electricity rate [120].

The 2015 ERCOT wholesale market prices range from 5 to 2200 \$/MWh with an average price of 26.05 \$/MWh. Prices exceeded 50 \$/MWh for 271 hours of the year, mostly in the spring and summer, and exceeded 250 \$/MWh for only 18 hours of the year. See Fig 6.12 for a profile of the ERCOT wholesale prices in 2015.

6.1.4 CO₂ emissions calculations

Emitting CO₂ into the atmosphere is an important consequence of burning fossil fuels to generate electricity, especially in connection with climate change and

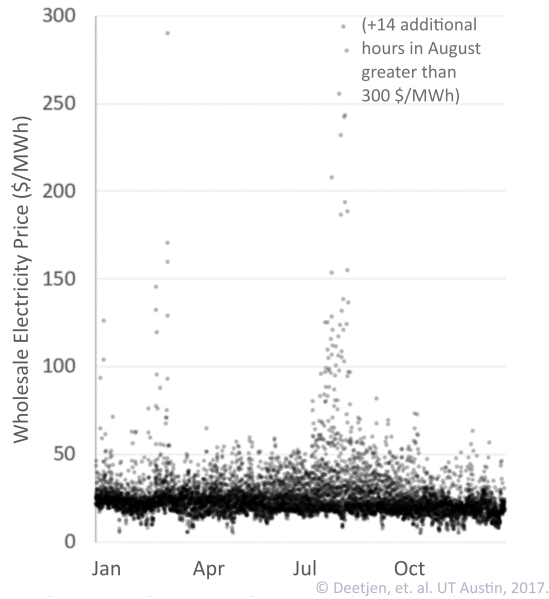


Figure 6.12: Hourly wholesale prices for the ERCOT market, 2015.

climate policies. While this study’s optimization model does not include CO₂ prices or policies when solving, it is useful to calculate the annual CO₂ emissions generated under different model scenarios.

This study assumes that CO₂ emissions come from either the CUP’s microturbine generator or the power plants operating in the electric grid. The microturbine’s CO₂ emissions are calculated by multiplying its annual fuel consumption by the amount of CO₂ generated from burning one unit of natural gas (117 lbs/MMBtu) [181]. The microturbine’s CO₂ emissions average 1820 lbs/MWh and range from 1590 to 3000+ lbs/MWh, depending on the microturbine’s efficiency as influenced by part-load operation and ambient temperature.

The power sector’s CO₂ emissions are estimated by projecting a merit order

curve (power plants organized by increasing marginal cost) onto Texas' 2015 hourly load to estimate which power plant is the marginal generator during each hour of the year [69]. The study assumes that the CO₂ emissions intensity of that marginal power plant can be applied to the CUP's electricity consumption during the same hour. The electric grid's marginal CO₂ emissions average 1460 lbs/MWh and range from 775 to 2520 lbs/MWh, depending on whether the marginal producer is a coal plant or a cleaner technology.

6.2 Optimization description

This study uses a linear optimization program to analyze how a CUP can reduce electricity sales, lower the peak demand, and decrease net load ramp rates in a residential neighborhood. In the optimization model, the CUP responds to an electricity rate structure by choosing the capacity and hourly dispatch for each piece of CUP equipment to maximize its annual profit. The model's decisions about how much equipment to buy and how that equipment should be operated depend on the costs and efficiencies described in Section 6.1.2 and the operational constraints in Section 6.2.1.

This paper's main interest lies in whether electricity rate structures incentivize the CUP to operate in ways that improve rooftop solar integration. Thus, the optimization scenarios are created by applying the different rate structures and demand charges discussed in Section 6.1.3.

6.2.1 Linear program description

The CUP optimization model is a mixed integer linear program (MILP) written using the *Pyomo* [81] optimization package for the *Python* [147] programming language and solved using the *CPLEX* optimizer [96]. The combined-heat-and-power program developed by Mitra et. al. [122] provided a helpful framework for incorporating the Section 6.1.2 equipment models into a linear program form.

The objective function of the model, shown in Eq 6.1, maximizes the system profit by considering the net sum of electricity sales, electricity purchases, fuel cost, variable O&M cost, demand charge cost, and annualized equipment cost. Annualized equipment cost (Eq 6.2) is the sum of the equipment's amortized capital cost and its annual, fixed O&M cost. The linear program is subject to the constraints in Table 6.7. Electricity sold Δ_{e+}^h , electricity bought Δ_{e-}^h , fuel consumption F^h , microturbine output $P_{e,gen}^h$, and peak demand M_Δ all impact the objective function and depend on the hourly dispatch of the CUP equipment (see Table 6.7). Annualized equipment cost A (Eq 6.2) is the sum of the equipment's amortized capital cost and its annual, fixed O&M cost and depends on the CUP equipment capacities.

$$\max(\sum_h (\Delta_{e+}^h \lambda_{e+}^h - \Delta_{e-}^h \lambda_{e-}^h - F^h \lambda_{ng} - P_{e,gen}^h O_{gen}) - M_\Delta \lambda_d - A \quad (6.1)$$

$$\begin{aligned}
Capital &= C_{gen}^1 M_{gen} + C_{bat}^1 M_{bat} + C_{ch}^0 + C_{ch}^1 M_{ch} + C_{piping}^0 + C_{ctes}^1 M_{ctes} + C_{solar}^1 M_{solar} \\
O\&M &= O_{ch} M_{ch} + O_{solar} M_{solar} \\
A &= Capital \times R + O\&M
\end{aligned} \tag{6.2}$$

This study assumes data for electricity prices and net demand are known with perfect foresight, and that the community-system optimally dispatches equipment based on these conditions. Because future day-ahead conditions are not known with certainty, results from this approach establish an upper-bound or “best-case” scenario [49]. Previous work has shown that the value of perfect information is relatively small compared to approaches that incorporate historical information for daily load patterns and weekend/weekday relationships, which supports using optimization with perfect foresight to compute reasonable approximations of CUP operations [164].

6.3 Results and discussion

Table 6.8 summarizes the results from optimizing the CUP in response to the different energy-only rate structures from Section 6.1.3. It shows that a residential neighborhood can reduce its annual cost under all rate structure scenarios by investing capital in a CUP to reduce its energy costs.

The CUP’s success in improving solar integration, however, is mixed. It reduces electricity sales and peak demand for all rate structures, when compared to the “No CUP” scenario. However, ramp rates increase significantly due to the

Table 6.7: Linear program constraints

Constraint	Description
Energy balance	
$\Delta_e^h = \Delta_{e-}^h - \Delta_{e+}^h$	Net demand = electricity bought – electricity sold
$\Delta_e^h = P_e^h - d_e^h$	Net demand = net electricity production – electric demand
$\Delta_{e-}^h \leq M_\Delta$	Electricity bought \leq peak demand
$\Delta_{e+}^h \leq M_\Delta$	Electricity sold \leq peak demand
$P_e^h = P_{e,gen}^h - P_{e,ch}^h - P_{e,ice}^h + P_{e,bat,d}^h - P_{e,bat,c}^h + P_{e,solar}^h$	Net electricity production = generator output – chiller electricity demand – chiller ice-making mode penalty + battery discharge – battery charge + solar output
$0 = P_c^h - d_c^h$	Net cooling production = cooling demand
$P_c^h = P_{c,ch}^h + P_{c,ctes,d}^h - P_{c,ctes,c}^h$	Net cooling production = chiller cooling output + CTES discharge – CTES charge
Microturbine generator	
$P_{e,gen}^h \leq M_{gen} D_{gen,cap}^h$	Generator output \leq generator capacity \times de-rating factor
$P_{e,gen}^h \leq B y_{gen,on}^h$	Generator output is 0 unless generator binary is “on”
$y_{gen,on}^h + y_{gen,off}^h = 1$	Generator binary must be “on” or “off”
$F_{gen,on}^h = H D_{gen,hr}^h (0.137 M_{gen} D_{gen,cap}^h + 0.863 P_{gen}^h)$	Generator “on-mode fuel consumption” depends on the de-rated heat rate, de-rated capacity, and generator output
$F^h \geq -B y_{gen,off}^h + F_{gen,on}^h$	Generator fuel consumption is 0 if the generator binary is “off”, or the “on-mode fuel consumption” otherwise
Battery	
$S_{bat}^h \leq M_{bat}$	Stored battery energy \leq battery capacity
$S_{bat}^{h=0} = M_{bat}$	Stored battery energy = battery capacity at time $h = 0$
$S_{bat}^h = S_{bat}^{h-1} + P_{e,bat,c}^{h-1} \sqrt{\eta_{bat}} - P_{e,bat,d}^{h-1} / \sqrt{\eta_{bat}}$	Stored battery energy in hour h = stored battery energy + battery charge - battery discharge in hour $h - 1$, considering the battery efficiency
Chiller plant	
$P_{ch}^h \leq M_{ch}$	Chiller output \leq chiller capacity
$COP_{cool}^h = 6.35 - 0.0985 T^h$ and $COP_{ice}^h = 5.41 - 0.0985 T^h$	Chiller COP depends on the ambient temperature
$P_{e,ch}^h = P_{c,ch}^h / COP_{cool}^h$	Chiller electric demand depends on cooling output and COP
$P_{e,ice}^h = P_{c,ctes,c}^h / COP_{ice}^h - P_{c,ctes,c}^h / COP_{cool}^h$	Additional electricity for ice production depends on CTES charge and chiller COP
CTES	
$S_{ctes}^h \leq M_{ctes}$	Stored CTES energy \leq CTES capacity
$S_{ctes}^{h=0} = 0$	Stored CTES energy = 0 at the beginning of the simulation
$S_{ctes}^h = S_{ctes}^{h-1} + P_{c,ctes,c}^{h-1} \sqrt{\eta_{ctes}} - P_{c,ctes,d}^{h-1} / \sqrt{\eta_{ctes}}$	Stored CTES energy in hour h = stored CTES energy + CTES charge - CTES discharge in hour $h - 1$, considering the CTES efficiency
Neighborhood solar	
$P_{e,solar}^h \leq M_{solar} K_{solar}^h$	Solar output \leq solar capacity \times solar capacity factor

Table 6.8: Results for optimal CUP operation under flat, time-of-use (TOU), and real-time-price (RTP) electricity rate structures (see Section 6.1.3).

	Flat, No CUP	Flat	TOU Weak	TOU Med	TOU Strong	RTP
Annual Capital Cost [\$M]	0.39	0.67	0.67	0.69	0.71	0.69
Annual Energy Cost [\$M]	0.93	0.52	0.52	0.51	0.46	0.50
Annual Cost [\$M]	1.32	1.19	1.19	1.20	1.17	1.19
Annual CO ₂ Emissions [tons]	5920	6410	6410	6420	5890	6360
Electricity Bought [MWh]	7770	1210	1080	1010	3560	1220
Electricity Sold [MWh]	56.5	34.9	29.8	32.3	38.6	32.8
Peak Demand [MW]	2.98	1.72	1.59	1.46	2.30	1.75
Minimum Ramp [MW/hr]	-0.51	-0.91	-0.81	-0.81	-1.86	-1.65
Maximum Ramp [MW/hr]	0.70	1.28	1.28	1.29	2.00	1.55
Microturbine Capacity [MW]	0.00	1.02	1.04	1.05	1.01	1.03
Battery Capacity [MWh]	0.0	0.0	0.0	0.0	0.0	0.0
Chiller Capacity [MW _{th}]	0.00	3.74	3.38	3.00	3.55	3.44
CTES Capacity [MWh _{th}]	0.0	4.0	7.0	11.0	15.0	11.0
Solar Capacity [MW]	1.2	1.2	1.2	1.2	1.2	1.2
Microturb. Annual Capacity Factor	-	0.72	0.73	0.73	0.44	0.72

CUP's operation. Microturbine generation and CTES load shifting both contribute to lowering peak demand and reducing electricity sales. With a CUP, electricity sales can happen more purposefully in response to high wholesale prices, rather than just as a consequence of solar output exceeding demand. The larger ramp rates are the consequence of volatile chiller plant operation, as the chiller reduces its capacity significantly to avoid the hottest 1 or 2 hours of the day (when it is least efficient).

The “weak” and “medium” TOU structures perform better in reducing electricity sales, peak demand, and ramp rates than the flat, “strong” TOU, or RTP rates. This result suggests that even small steps from flat rates to TOU rates can improve solar integration, but that large differences between off-peak and on-peak prices or the high time-resolution of RTP might not be necessary. The medium TOU provides, perhaps, the best balance between the output parameters, reducing electricity sales by 43%, peak demand by 51%, and annual cost by 9.1% versus the “No CUP” base case while limiting net demand ramp rate increase to 84% more than the base case.

The microturbine marginal operating cost (fuel + O&M) averages 57.30 \$/MWh with a minimum of 51.90 \$/MWh, providing an important pivot point for the CUP's operation. Whenever the CUP can buy electricity for less or sell electricity for more than the microturbine's operating cost, it usually will, depending on other model constraints. This interaction explains the low microturbine capacity factor and large amount of electricity bought under the strong TOU structure, where the 49.00 \$/MWh off-peak price always undercuts the generator, causing the CUP to purchase electricity from the grid.

Electricity purchases also correlate negatively with CO₂ emissions. Though microturbine emissions are sometimes lower than the grid's generation fleet, it ends up emitting more CO₂ on average.

Figs 6.13 and 6.14 provide a more detailed look at the hourly CUP dispatch in the summer and shoulder seasons under the medium TOU rate. Fig 6.13 shows the CUP dispatch for August 14, 2015, one of the hottest days of the year. The microturbine and rooftop solar operate at full output with electric grid purchases (i.e. the “net demand”) making up the difference. CTES is used to balance the difference between the cooling profile and the chiller plant output. This balancing allows the chiller plant to pursue three beneficial, operational strategies. First, it can shift energy demand from on-peak/mid-peak to off-peak energy prices. Second, it augments the chiller's maximum output, enabling the chiller capacity to be lower than the peak cooling demand, which reduces capital costs. (Note that the chiller operates at full output at 14:00, 15:00, and 18:00–23:00 with the CTES discharging to meet cooling demand.) Third, any CTES storage not used for augmenting chiller capacity can discharge during on-peak prices. In this figure, since chiller efficiency degrades with higher ambient temperatures, the chiller reduces its consumption during 17:00, the hottest hour during on-peak prices, until net demand (electric grid purchases) is zero. Then it uses the remaining excess CTES storage to reduce its consumption during 16:00, the next hottest hour.

In comparison to the neighborhood's demand without a CUP (see Fig 1.1), peak net demand falls from 2.65 to 1.25 MW, but the maximum ramp rate rises from 0.52 to 0.94 MW/hr. The chiller's avoidance of the on-peak price hours with

the highest ambient temperatures creates the sudden demand changes that lead to larger ramp rates. While avoiding these high-temperature, low-efficiency hours is technically optimal, the chiller could plausibly produce a smoother net demand curve without significantly impacting the CUP’s annual profit.

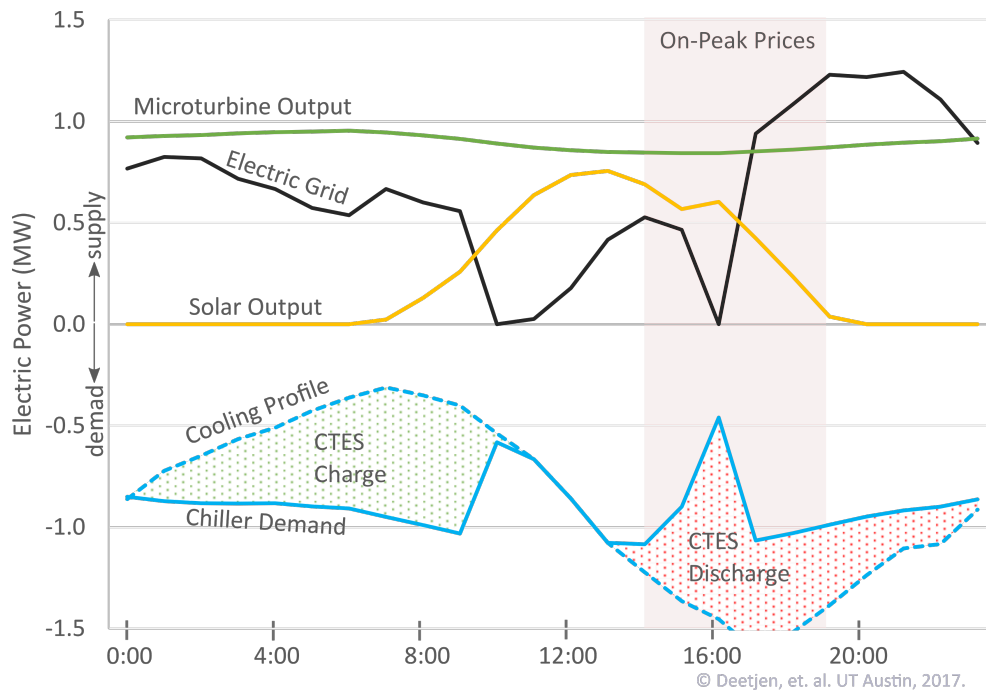


Figure 6.13: Dispatch of the CUP equipment for August 14, 2015, one of the hottest days of the summer (see Fig 1.1). The “Electric Grid” series is equivalent to the net demand.

Fig 6.14 shows the CUP dispatch for October 26, 2015, a shoulder-season day where solar output exceeds total neighborhood demand. The microturbine output matches total neighborhood demand, except when solar is producing, and the turbine adjusts its output to try and keep electricity purchases (net demand) at zero. The CTES charges from 13:00 to 15:00 to avoid selling electricity to the grid, and

discharges from 18:00 to 21:00 to avoid buying electricity when the microturbine is at maximum capacity.

In comparison with the neighborhood’s demand without a CUP (see Fig 1.2), the CUP is able to completely eliminate electricity purchases and reverse power flow. Even though cooling demand is quite low, the CTES is still able to absorb the excess solar energy, using some of its storage that evening, and discharging the remainder of its storage the following day.

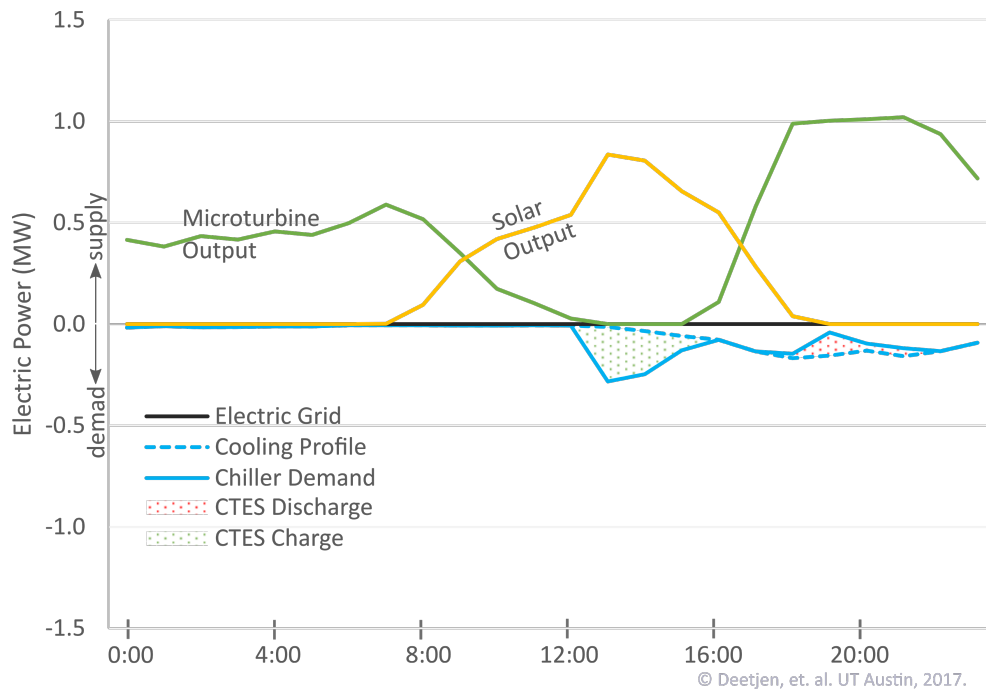


Figure 6.14: Dispatch of the CUP equipment for October 26, 2015, a day where solar output exceeds total neighborhood demand and should lead to reverse power flow (see Fig 1.2). The “Electric Grid” series is equivalent to the net demand.

Including a demand charge in the rate structure also influences the operation of the CUP. Table 6.9 and Fig 6.15 summarize the results for the different demand

charge scenarios.

Table 6.9: Results for 1.2 MW solar under different demand charges.

	Flat, No CUP	Demand 0	Demand 1	Demand 2	Demand 3	Demand 4
Annual Capital Cost [\$M]	0.39	0.68	0.70	0.75	0.79	0.84
Annual Energy Cost [\$M]	0.93	0.52	0.54	0.54	0.53	0.48
Annual Cost [\$M]	1.32	1.20	1.24	1.29	1.32	1.32
Annual CO ₂ Emissions [Tons]	5920	6360	6330	6320	6900	7170
Electricity Bought [MWh]	7770	1190	1260	1330	160	0
Electricity Sold [MWh]	56.5	29	41	54	69	0
Peak Demand [MW]	2.98	1.52	1.10	0.67	0.35	0.00
Minimum Ramp [MW/hr]	-0.51	-0.89	-1.08	-1.30	-0.49	0.00
Maximum Ramp [MW/hr]	0.70	1.32	1.37	1.21	0.49	0.00
Microturbine Capacity [MW]	0.00	1.02	1.10	1.28	1.61	2.03
Battery Capacity [MWh]	0.0	0.0	0.0	0.0	0.0	0.0
Chiller Capacity [MW _{th}]	0.00	3.09	3.14	3.29	3.40	3.36
CTES Capacity [MWh _{th}]	0.0	10.0	13.0	18.0	19.0	19.0
Solar Capacity [MW]	1.2	1.2	1.2	1.2	1.2	1.2
Microturb. Annual Capacity Factor	-	0.74	0.68	0.59	0.55	0.44

Demand charges generally lead to lower peak demand, but more reverse power flow. Larger demand charges incentivize the CUP to invest in larger equipment to reduce its peak demand and lower its annual demand charge cost. That larger equipment improves the CUP’s ability to produce more energy than is needed, giving it more opportunities to sell power and take advantage of price spikes in the wholesale market.

Consequently, the increased ability to sell power can lead to larger ramp rates. The largest ramp rates in these scenarios occur when the CUP switches from buying in one hour to selling in the next (or vice versa). Incentivizing a lower peak demand counteracts the intensity of this switching by limiting the buying and selling

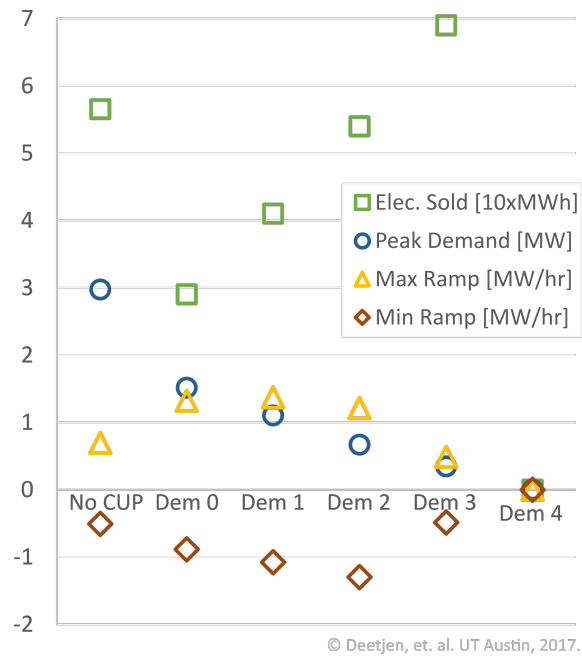


Figure 6.15: Sensitivity of the results to demand charges. “No CUP” is the neighborhood at flat energy rates and no CUP. “Demand 0” through “Demand 4” are TOU energy rates with increasing demand charges as shown in Table 6.6.

magnitude. Thus, small demand charges tend to increase ramp rates, but medium demand charges can reduce them.

Large demand charges lead to the “Demand 4” case, where the charge is high enough to incentivize islanding. In this case, no electricity is bought or sold and all energy costs go towards purchasing natural gas for the microturbine.

Comparing the energy-only rate results (Table 6.8) with the demand-charge rate results (Table 6.9), demand charges tend to increase both capital and energy cost. Small demand charges tend to increase electricity sold and ramp rates, and reduce peak demand and microturbine capacity factor. Large demand charges push the neighborhood towards islanding. Only the “Demand 3” rate structure reduces ramp rates more than any of the energy-only rate structures without moving the neighborhood towards islanding, but is at least 10% more expensive to operate, annually.

Finally, it is helpful to consider the equipments’ part-load operation results, given that manufacturer limitations might prevent different equipment from operating at very low output. Figure 6.16 presents a normalized duration curve for the microturbine, chiller plant, and CTES. For example, the microturbine produces electricity for 8180 hours per year operating at 40% of rated capacity or greater for 6960 of those hours (85% of the time) and at 20% of rated capacity or greater for 7990 of those hours (98% of the time) per year. Thus, a single microturbine capable of operating at 20% part load could meet the majority of the results’ operation schedule. However, the chiller plant regularly operates at low part-load output and might benefit from a CUP design that uses multiple chiller units to efficiently meet the

results' operation schedule.

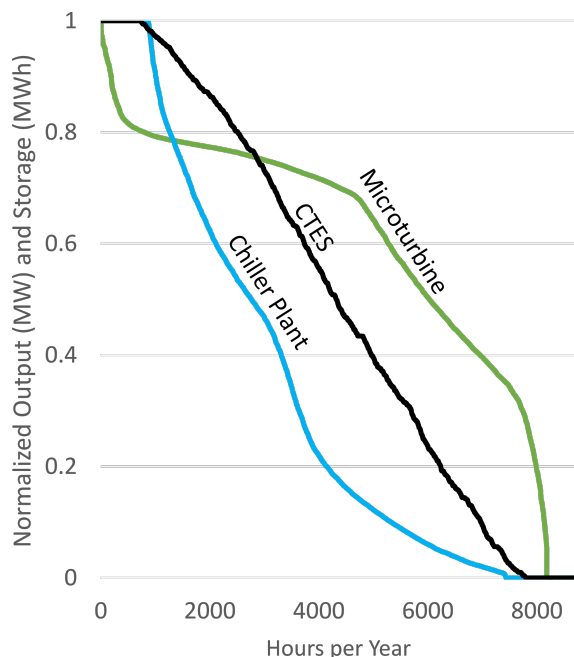


Figure 6.16: Hours per year that each CUP component spends at different output levels under the Medium TOU scenario. While the microturbine seldom operates at low part-loads, the chiller plant regularly operates at low output. An actual CUP design might use multiple chiller units to achieve the dispatch schedule in these results.

6.4 Conclusions

This study uses a MILP optimization model to test the hypothesis that a residential central utility plant can improve the integration of rooftop solar in the electric grid and provide economic benefit to the community. It models a 750-house neighborhood with 1.2 MW of rooftop solar and optimizes a CUP's equipment capacities and hourly dispatch to maximize profit in response to various electricity rate

structures.

Results suggest that a central utility plant could be economically constructed and operated in a residential neighborhood, reducing annual costs by 9.1% under the medium TOU rate. This strategy requires a large up-front capital investment in exchange for lower energy costs in the long run. Though the piping network capital cost estimate is uncertain, the plant's economic benefit is large enough that a more expensive piping network estimation might still be economically feasible, especially in denser neighborhoods being developed at greenfield sites (where underground piping construction might be more manageable than in an existing community).

The optimization does not build a battery under any circumstances, preferring to use a microturbine and CTES storage to provide similar flexibility at a considerably lower capital cost. However, this study uses an hourly time resolution, which undervalues the sub-second flexibility that a battery can provide for voltage support and other beneficial services. In addition, battery costs might drop low enough to make them economically competitive, or a residential neighborhood might not want to operate a microturbine and opt for some battery capacity as a substitute. Thus, batteries might be justifiable in real-world circumstances and should not be excluded from future analyses.

Regarding the study's primary hypothesis, the results indicate that a residential CUP can economically improve some aspects of rooftop solar integration and might be a viable strategy for improving the flexibility of the distribution grid. A variety of rate structures seem to support CUP operation that reduces peak demand and lowers electricity sales. Net demand ramp rates, however, tend to increase except

under rate structures with large demand charges (and high annual costs).

The largest ramp rates result from quickly changing the chiller plant's output to avoid the hottest, least efficient hours of the day. Though this operational strategy is economically optimal, it is unclear if an actual chiller control strategy would place as much emphasis on avoiding peak daily temperature. It seems plausible that a chiller plant could produce a smoother net demand profile without much loss in profit. In any case, the results still suggest that a CUP is a much more flexible system than an uncoordinated neighborhood of houses, and it is capable of large net demand ramp rates that might complicate the operation of the grid. Thus, CUPs might provide new opportunities for solar integration, but they might also provide new challenges depending on the utility's incentives or signals.

Utilities in cooling climates with significant solar integration might find value in supporting microgrid and utility district development, though they should anticipate erratic behavior that leads to increased net demand ramp rates. Electricity rates should be designed carefully to achieve the utility's goals. A time-of-use rate with a medium spread between off-peak and on-peak prices provides a good balance between reducing electricity sales by 43%, peak demand by 51%, and annual cost by 9.1% versus the "No CUP" base case, while increasing ramp rates less than most of the other dynamic rates (an 84% increase over the base case). Adding a demand charge can reduce peak demand further, though it increases annual CUP cost and can incentivize islanding. Additional measures could help manage ramp rates, such as rewarding microgrids for keeping a flatter demand profile.

Chapter 7

Summary

This dissertation explores the integration of renewable energy in the electric grid by studying its impact on the dispatch of power plants, its influence on net load flexibility requirements, and its regional representation in capacity expansion models. It also explores how demand-side management in the form of a residential utility plant can help integrate renewable energy resources. The following objectives were used to frame the research:

- *Objective 1: Explore the effects of adding large amounts of solar generation to the grid and assess the importance of array orientation and geographic location*
- *Objective 2: Determine how growing wind and solar capacities correlate with increasing flexibility requirements*
- *Objective 3: Project the amount of wind and solar capacity that should be installed in different regions of the electric grid*
- *Objective 4: Analyze opportunities for system integration and demand-side management to add flexibility to the electric grid.*

7.1 Solar PV integration cost variation due to array orientation and geographic location in the Electric Reliability Council of Texas

Chapter 3 uses unit commitment and dispatch techniques to provide a holistic study of how generator dispatch, system flexibility requirements, and market dispatch costs are influenced by the orientation and geographic location of solar generation assets. Increased solar generation reduces overall costs, emissions, and water use in the electric grid but intensifies the flexibility requirements needed to match dispatchable generation with the net load. Solar generation also changes how generators are dispatched in the electric grid, because it displaces generation during the day but requires dispatchable ramping in the evening as solar power drops off.

7.2 The impacts of wind and solar on grid flexibility requirements in the Electric Reliability Council of Texas

Chapter 4 uses a data-driven approach to quantify the correlation of increasing wind and solar generation with grid flexibility requirements. The results show that increasing solar capacity correlates strongly with a number of flexibility requirements. Increasing wind capacity correlates slightly with some flexibility requirements, but its main correlation is with reduced 1-hr and 3-hr ramp downs. Wind and solar do not show significant confounding, except that a grid with wind and solar has much greater 1-day volatility than a system with only wind or solar alone. These trends provide meaningful insight for grid planners as they anticipate the growth of renewable energy resources and the strategies they should implement to maintain

reliability and manage integration costs.

7.3 Modeling the optimal mix and location of wind and solar with transmission and carbon pricing considerations

Chapter 5 develops a regionally-sensitive capacity expansion model that recommends the optimal investment of wind, solar, and transmission capacity in the different regions of an electric grid. It also develops a framework for balancing system costs, flexibility requirements, and CO₂ emissions when considering CO₂ prices or other policies. The results show regional wind and solar resources might be developed based not only on their capacity factors but on the timing coincidence of their generation with load and with renewable generation in other regions. The results show that increased CO₂ prices yield diminishing returns for reducing emissions, that some curtailment of wind and solar is economically appropriate, and provide some insights into the scale of the flexibility requirements that will be required to maintain the stability of a system with large, regionally-dispersed, renewable energy assets.

7.4 Optimal dispatch and equipment sizing of a residential central utility plant for improving rooftop solar integration

Chapter 6 develops a capacity and dispatch optimization model to show how a central utility plant (CUP) might economically improve rooftop solar integration in a residential neighborhood. The simulation results show that the CUP allows the neighborhood to operate much more flexibly, but that the CUP operational strategy

depends on electricity rate structure and other market policies. The optimization program does not select the option to build a battery under any scenario but chooses to use less expensive cooling thermal energy storage to accomplish some of the same load shifting tasks at a smaller capital cost. In cooling climates with significant solar integration, CUPs might provide a reasonable way to reduce neighborhood costs and increase neighborhood flexibility for integrating rooftop solar if the right markets and policies are employed.

7.5 Overall considerations

The insights gained from the studies within this dissertation build on each other in the following ways. Chapter 3 looks holistically at the integration of renewable energy in the electric grid and identifies an important drawback of increased renewable energy penetration - that it requires the dispatchable generator fleet to operate much more flexibly, which could increase some operational costs and complicate the grid's ability to balance supply and demand. Chapter 4 explores the correlation of increasing flexibility requirements with larger wind and solar capacity to help characterize the magnitude, severity, and frequency of increased flexibility requirements due to renewable generation. Chapter 5 quantifies the location and scale of potential renewable energy resources in the electric grid. These three chapters together provide a cohesive look of the different aspects of integrating renewable energy into the electric grid and call for some solutions for providing the increased flexibility needed for improving that integration. Chapter 6 examines on-site generation and thermal energy storage in the residential cooling sector as a potential

avenue for increasing grid flexibility by leveraging demand-side technology, energy aggregation, and consumer behavior.

As a whole, this body of work communicates the importance of improving the flexibility of the electric grid if large amounts of renewable energy capacity are to be developed and properly integrated. It examines demand-side management as an important contributor for providing that flexibility. It sets a trajectory of looking further into the technologies, consumer behavior, electricity rates, and policies that will transition electricity demand from being a mostly passive portion of the electricity system to being a dynamic asset that can modulate its energy consumption patterns to respond to needs in the electric grid, reduce system costs, and increase reliability and resilience, especially in the context of greater renewable energy capacity.

7.6 Future work

Future work will expand the research scope beyond some of the assumptions that have been used throughout this dissertation. In particular, this dissertation assumes that supply and demand balancing issues are handled on a grid-wide basis without local or nodal variations and that energy demand is a static input variable that responds inelastically to market conditions. It also excludes utility-scale storage and power plant retirements in the scope of its analyses.

For addressing local variations in supply and demand issues, future work might include representations of transmission congestion when modeling unit commitment and dispatch of the grid's power plant fleet. Future projects will also explore renewable energy integration at the local distribution level, allowing distributed en-

ergy resources and dispatchable loads to help balance supply and demand in feeders with high solar penetration and allowing local utility-scale renewables to be utilized at a higher transmission efficiency and lower congestion rate than resources located far from load centers.

For addressing the static portrayal of electricity demand, future projects will explore demand from the perspective of human decisions and needs, and model demand as an extension of consumer behavior, including the “rebound effect” where consumers might demand more of an energy product after efficiency investments have reduced its apparent cost. This new trajectory can also include technology deployment in urban areas that enable demand to be more dynamic, including energy storage, smart appliances, and central utility plants and will explore how local dynamic pricing structures can encourage flexible demand behavior that benefits the stability, reliability, and resilience of the electric grid.

For addressing the exclusion of storage and power plant retirements at the utility level, future models could incorporate these aspects by making energy storage a possible technology in capacity expansion planning and by creating criteria that removes generators from the generation fleet whenever their profits are too low to justify their continued operation.

Appendices

Appendix A

Statistical Tables for Chapter 4

The following tables contains some statistical information about the 2008-2025 scenarios discussed in Chapter 4. The tables show the maximum, 95th percentile, median, 5th percentile, and minimum values for each of the flexibility requirements over every 15-minute interval per year. Table A.1 shows the calculated values used for the majority of the study. Table A.2 shows the same results if wind generation is removed from the analysis to test for any confounding between the influence of wind and solar on flexibility requirements. It is informative to read across the rows and see how different aspects of the flexibility requirements change with increasing wind and solar peak output.

Table A.1: The following table shows the maximum, 95th percentile, median, 5th percentile, and minimum values for each flexibility requirement over each year.

		Wind Era								Solar Era									
		2008	2009	2010	2011	2012	2013	2014	2015	2016	2017	2018	2019	2020	2021	2022	2023	2024	2025
1-Hr Ramp Rate	Max	6,548	6,023	6,538	6,013	6,426	6,334	6,484	6,223	6,364	7,157	8,125	9,089	10,050	11,010	11,971	12,932	13,893	14,854
	95%	3,049	3,188	3,243	3,471	3,302	3,338	3,327	3,268	3,369	3,397	3,442	3,507	3,613	3,730	3,883	4,035	4,186	4,323
	Med	-14	-25	-48	-37	0	-22	-15	21	25	25	14	-3	-14	-40	-65	-80	-94	-114
	5%	-3,026	-3,034	-3,121	-3,318	-3,253	-3,279	-3,280	-3,340	-3,442	-3,449	-3,468	-3,491	-3,542	-3,596	-3,657	-3,734	-3,819	-3,936
	Min	-5,594	-5,739	-6,024	-6,006	-6,645	-5,739	-6,006	-7,844	-8,241	-8,260	-8,277	-8,293	-8,305	-8,319	-8,333	-8,347	-8,360	-8,873
3-Hr Ramp Rate	Max	12,714	13,300	14,498	15,765	14,975	14,341	14,437	16,380	16,675	16,739	16,796	16,810	16,798	16,809	17,879	18,951	20,023	21,096
	95%	7,859	8,069	8,285	9,079	8,460	8,504	8,356	8,688	8,866	8,805	8,799	8,885	8,999	9,166	9,347	9,571	9,834	10,196
	Med	126	129	16	88	175	72	127	184	222	281	312	315	326	301	261	200	131	55
	5%	-8,182	-8,262	-8,556	-9,258	-8,990	-8,950	-9,006	-9,250	-9,482	-9,509	-9,542	-9,586	-9,645	-9,703	-9,803	-9,937	-10,097	-10,221
	Min	-14,248	-14,078	-15,260	-16,043	-15,565	-15,180	-15,383	-17,337	-17,919	-18,008	-18,089	-18,156	-18,216	-18,277	-18,338	-18,400	-18,462	-18,523
Ramp Factor	Max	0.0770	0.0799	0.0747	0.0840	0.0674	0.0840	0.0904	0.0839	0.1076	0.1049	0.1020	0.1088	0.1216	0.1439	0.1672	0.1916	0.2171	0.2438
	95%	0.0241	0.0251	0.0256	0.0259	0.0258	0.0259	0.0255	0.0254	0.0267	0.0268	0.0272	0.0275	0.0282	0.0289	0.0296	0.0302	0.0308	0.0316
	Med	-0.0002	-0.0003	-0.0004	-0.0004	-0.0002	-0.0003	-0.0003	0.0001	0.0001	0.0001	-0.0001	-0.0003	-0.0005	-0.0007	-0.0009	-0.0010	-0.0012	-0.0014
	5%	-0.0234	-0.0237	-0.0241	-0.0247	-0.0248	-0.0247	-0.0245	-0.0252	-0.0264	-0.0260	-0.0257	-0.0254	-0.0255	-0.0257	-0.0261	-0.0265	-0.0271	-0.0275
	Min	-0.0537	-0.0600	-0.0581	-0.0560	-0.0555	-0.1128	-0.0917	-0.0620	-0.0750	-0.0733	-0.0714	-0.0692	-0.0732	-0.0859	-0.0983	-0.1102	-0.1219	-0.1332
1-Hr Volatility	Max	3,132	3,776	4,280	6,866	3,284	4,608	4,773	4,875	5,188	5,187	5,187	5,186	5,874	6,780	7,686	8,593	9,499	10,405
	95%	1,316	1,299	1,343	1,469	1,281	1,275	1,316	1,136	1,281	1,400	1,589	1,826	2,089	2,349	2,629	2,905	3,196	3,491
	Med	566	528	570	602	566	559	576	450	497	522	542	559	575	592	608	622	637	651
	5%	209	187	207	226	214	216	228	149	163	169	176	183	187	193	196	200	203	206
	Min	23	23	19	22	37	20	17	7	7	7	7	7	7	7	8	7	7	7
1-Day Volatility	Max	24,168	26,740	26,907	43,328	25,067	24,663	25,560	29,585	34,145	34,544	35,269	36,022	36,942	38,066	39,461	40,942	42,570	44,268
	95%	19,080	19,565	20,138	25,288	18,934	18,763	19,798	18,019	20,782	21,556	22,511	23,575	24,781	26,128	27,640	29,145	30,663	32,323
	Med	15,279	14,629	15,328	15,902	15,155	15,052	15,275	12,204	13,525	14,412	15,413	16,482	17,620	18,805	20,034	21,280	22,584	23,852
	5%	11,764	9,981	11,303	11,912	11,499	11,589	12,087	7,724	8,423	9,336	10,421	11,433	12,370	13,365	14,296	15,286	16,266	17,206
	Min	8,176	7,384	7,188	6,975	7,455	7,514	8,421	4,893	5,175	5,701	6,297	7,085	7,917	8,434	8,858	9,278	9,763	10,253

Table A.2: The following table shows the maximum, 95th percentile, median, 5th percentile, and minimum values for each flexibility requirement over each year if wind generation is removed from the analysis.

		Wind Era								Solar Era									
		2008	2009	2010	2011	2012	2013	2014	2015	2016	2017	2018	2019	2020	2021	2022	2023	2024	2025
1-Hr Ramp Rate	Max	6,020	5,797	5,685	5,774	5,360	5,429	5,338	5,725	5,816	6,239	6,715	7,417	8,089	8,719	9,362	10,006	10,663	11,295
	95%	2,973	3,070	3,118	3,300	3,136	3,191	3,133	3,343	3,369	3,403	3,460	3,552	3,642	3,724	3,855	3,995	4,155	4,287
	Med	-34	-44	-69	-58	-43	-44	-53	-50	-48	-43	-39	-41	-53	-63	-71	-86	-101	-113
	5%	-2,914	-2,882	-2,911	-3,103	-3,027	-3,011	-3,009	-3,235	-3,274	-3,320	-3,383	-3,474	-3,546	-3,616	-3,723	-3,835	-3,948	-4,054
	Min	-4,930	-4,981	-5,008	-5,706	-5,316	-5,171	-5,300	-5,678	-5,754	-5,831	-5,929	-6,066	-6,167	-6,221	-6,670	-7,252	-7,842	-8,418
3-Hr Ramp Rate	Max	12,077	12,305	12,949	14,819	14,366	13,145	13,247	15,332	15,478	15,558	15,694	15,935	16,079	16,097	16,153	16,211	16,481	17,372
	95%	7,648	7,771	8,024	8,649	8,003	8,111	7,914	8,533	8,569	8,562	8,605	8,715	8,835	8,934	9,119	9,314	9,596	9,873
	Med	89	65	-30	27	85	85	24	81	130	180	236	281	305	292	285	264	207	136
	5%	-7,870	-7,849	-7,970	-8,646	-8,428	-8,369	-8,327	-9,008	-9,121	-9,244	-9,406	-9,631	-9,807	-9,918	-10,046	-10,197	-10,352	-10,476
	Min	-12,882	-13,140	-13,374	-13,625	-13,835	-13,403	-14,414	-14,776	-14,974	-15,175	-15,430	-15,786	-16,049	-16,190	-16,368	-16,548	-16,768	-16,915
Ramp Factor	Max	0.0669	0.0598	0.0648	0.0633	0.0586	0.0577	0.0604	0.0586	0.0586	0.0586	0.0586	0.0639	0.0750	0.0914	0.1083	0.1257	0.1433	0.1623
	95%	0.0221	0.0224	0.0222	0.0217	0.0215	0.0215	0.0208	0.0215	0.0215	0.0216	0.0220	0.0225	0.0232	0.0240	0.0246	0.0251	0.0257	0.0262
	Med	-0.0003	-0.0004	-0.0005	-0.0005	-0.0003	-0.0003	-0.0004	-0.0004	-0.0003	-0.0003	-0.0003	-0.0004	-0.0006	-0.0007	-0.0008	-0.0009	-0.0011	-0.0012
	5%	-0.0209	-0.0207	-0.0203	-0.0202	-0.0205	-0.0200	-0.0198	-0.0205	-0.0205	-0.0205	-0.0207	-0.0210	-0.0212	-0.0215	-0.0219	-0.0222	-0.0226	-0.0230
	Min	-0.0469	-0.0417	-0.0417	-0.0385	-0.0411	-0.0804	-0.0595	-0.0411	-0.0411	-0.0411	-0.0411	-0.0740	-0.0520	-0.0616	-0.0709	-0.0800	-0.0887	-0.0977
1-Hr Volatility	Max	2,691	2,887	2,650	2,788	2,350	4,362	4,840	2,489	2,492	2,912	3,500	4,483	5,107	5,947	6,790	7,633	8,480	9,320
	95%	1,195	1,116	1,174	1,152	1,151	1,141	1,180	1,230	1,255	1,379	1,547	1,761	1,991	2,248	2,528	2,806	3,102	3,392
	Med	507	436	465	486	473	471	491	507	523	545	570	599	625	644	666	688	710	730
	5%	179	149	163	180	171	175	187	182	187	194	202	211	217	222	227	233	238	242
	Min	0	23	26	18	18	13	28	0	0	0	0	38	0	0	0	0	0	0
1-Day Volatility	Max	21,532	18,805	19,299	18,565	19,471	19,406	21,644	20,800	21,611	23,284	25,203	27,276	29,307	31,176	33,093	35,014	37,004	38,946
	95%	17,078	15,827	16,764	16,366	16,340	16,061	17,027	17,470	17,897	18,859	20,102	21,635	23,227	24,740	26,355	28,067	29,877	31,656
	Med	13,880	12,558	13,300	13,550	13,240	13,157	13,634	14,171	14,549	15,472	16,664	18,047	19,390	20,663	21,964	23,281	24,650	25,960
	5%	10,317	8,230	8,685	9,857	9,847	10,072	10,164	10,551	10,865	11,489	12,314	13,402	14,202	15,163	16,180	17,117	18,082	19,043
	Min	0	6,201	5,437	5,828	6,229	6,821	6,142	4,913	6,850	7,563	8,304	9,273	10,221	10,639	11,668	12,234	12,745	13,252

Appendix B

Interest Rate Sensitivity Figures for Chapter 5

The following figures illustrate the sensitivity of the model solution presented in Chapter 5 to the interest rate used for wind and solar for capital investment using a 60 \$/ton CO₂ price.

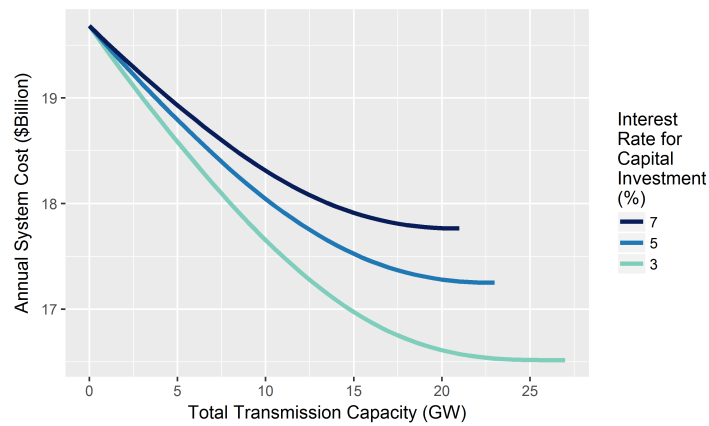


Figure B.1: Annual system cost for different capital investment interest rates.

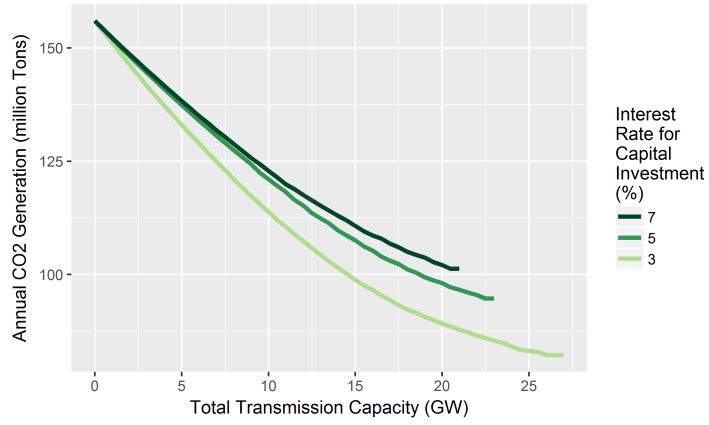


Figure B.2: Annual CO₂ emissions for different capital investment interest rates.

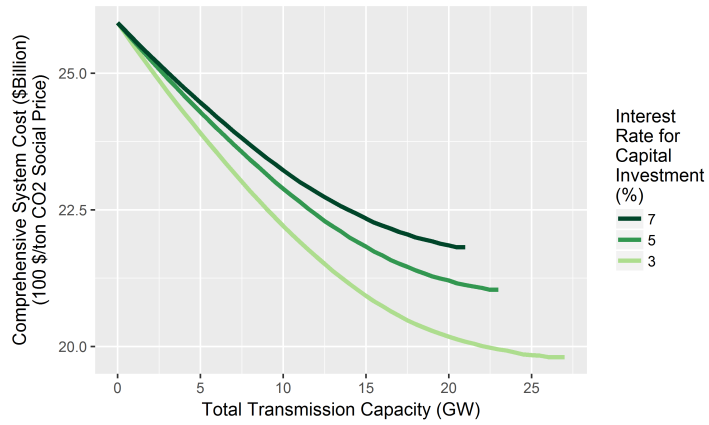


Figure B.3: Comprehensive system cost at a 100 \$/ton social price of CO₂ for different capital investment interest rates.

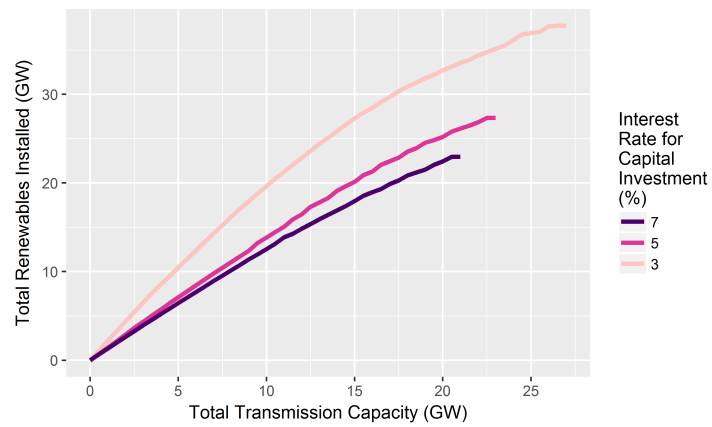


Figure B.4: Renewable capacity installed for different capital investment interest rates.

Bibliography

- [1] Balancing and frequency control a technical document.
- [2] Capstone Turbine Corporation. <https://www.capstoneturbine.com/>. Accessed: August, 2017.
- [3] Dresser-Rand. <http://www.dresser-rand.com/products-solutions/0-15-mw/>. Accessed: August, 2017.
- [4] Integrated resource plan: Appendix I. Puget Sound Energy. 2015.
- [5] Kawasaki gas turbine generator sets. Kawasaki. 2010.
- [6] Opra Turbines. <http://www.opraturbines.com/en/>. Accessed: August, 2017.
- [7] Siemens power generation gas turbines. <https://www.siemens.com/global/en/home/products/energy/power-generation/gas-turbines.html>. Accessed: August, 2017.
- [8] Solar turbines. <https://mysolar.cat.com/>. Accessed: August, 2017.
- [9] MJE Alam, KM Muttaqi, and Darmawan Sutanto. Mitigation of rooftop solar PV impacts and evening peak support by managing available capacity of distributed energy storage systems. *IEEE Transactions on Power Systems*, 28(4):3874–3884, 2013.

- [10] Walid Ouled Amor, Hassen Ben Amar, and Moez Ghariani. Grid stability study after the integration of a wind farm. In *2015 16th International Conference on Sciences and Techniques of Automatic Control and Computer Engineering (STA)*, pages 678–683. IEEE, 2015.
- [11] Casey Anderson. California solar penetration reaches 7.2% in 2016. *Ohm Home*: <https://www.ohmhomenow.com/california-solar-penetration-reaches-7-2-in-2016/> (2016), 2016.
- [12] Kerstine Appunn. Setting the power price: the merit order effect. *Clean Energy Wire* (2015).
- [13] Alessia Arteconi, Neil J Hewitt, and Fabio Polonara. State of the art of thermal storage for demand-side management. *Applied Energy*, 93:371–389, 2012.
- [14] Austin Energy. City of Austin Electric Tariff: Available from <http://austinen-energy.com/wps/wcm/connect/e269c3f9-e09b-40eb-9afc-3b9abc24b67c/secondary-voltage.pdf?mod=ajperes>. 2016.
- [15] Delaram Azari, Shahab Shariat Torbaghan, Hans Cappon, Madeleine Gibescu, Karel Keesman, and Huub Rijnaarts. Assessing the flexibility potential of the residential load in smart electricity grids: a data-driven approach. In *European Energy Market (EEM), 2017 14th International Conference on the*, pages 1–6. IEEE, 2017.

- [16] B. Palmintier, et. al. On the path to sunshot: emerging issues and challenges in integrating solar with the distribution system. *National Renewable Energy Laboratory*, 2016.
- [17] Andrea Baranzini, Jeroen CJM van den Bergh, Stefano Carattini, Richard B Howarth, Emilio Padilla, and Jordi Roca. Carbon pricing in climate policy: seven reasons, complementary instruments, and political economy considerations. *Wiley Interdisciplinary Reviews: Climate Change*, 8(4), 2017.
- [18] Mehmet Bilgili, Arif Ozbek, Besir Sahin, and Ali Kahraman. An overview of renewable electric power capacity and progress in new technologies in the world. *Renewable and Sustainable Energy Reviews*, 49:323–334, 2015.
- [19] Jens C Boemer, Karsten Burges, Pavel Zolotarev, Joachim Lehner, Patrick Wajant, Markus Fürst, Rainer Brohm, and Thomas Kumm. Overview of German grid issues and retrofit of photovoltaic power plants in Germany for the prevention of frequency stability problems in abnormal system conditions of the ENTSO-E region continental Europe. In *1st International Workshop on Integration of Solar Power into Power Systems*, volume 24, 2011.
- [20] Severin Borenstein. The market value and cost of solar photovoltaic electricity production. *Center for the Study of Energy Markets (2008)*.
- [21] California Independent System Operator. What the duck curve tells us about managing a green grid. (2013).

- [22] California Public Utilities Commission. What are TOU rates?: Available from <http://www.cpuc.ca.gov/general.aspx?id=12194>.
- [23] Barney L. Capehart. Microturbines. *Whole Building Design Guide: available at <https://www.wbdg.org/resources/microturbines>*, 2016.
- [24] Peter Cappers, Charles Goldman, and David Kathan. Demand response in us electricity markets: Empirical evidence. *Energy*, 35(4):1526–1535, 2010.
- [25] Berk Celik, Robin Roche, David Bouquain, and Abdellatif Miraoui. Coordinated neighborhood energy sharing using game theory and multi-agent systems. In *PowerTech, 2017 IEEE Manchester*, pages 1–6. IEEE, 2017.
- [26] Yunus A Cengel and Michael A Boles. Thermodynamics: an engineering approach (refrigeration cycles chapter). *McGraw-Hill Higher Education*, 2006.
- [27] Central Air Conditioner Prices. Avg ac unit prices by size or capacity: Available from <http://www.centralairconditionerprice.com/>. Accessed on February, 2017.
- [28] Kristin Sara Cetin. *Smart Technology Enabled Residential Building Energy Use and Peak Load Reduction and Their Effects on Occupant Thermal Comfort: Paper 5*. PhD thesis, 2015.
- [29] YungChung Chang, TienShun Chan, and WenShing Lee. Economic dispatch of chiller plant by gradient method for saving energy. *Applied Energy*, 87(4):1096–1101, 2010.

- [30] Chang, Judy et. al. The value of distributed electricity storage in Texas. *The Brattle Group (2014)*, 2014.
- [31] Charles Y. Chen. The geographic disparity of the PTC & ITC. *Energy Central (2016)*.
- [32] Cédric Clastres, TT Ha Pham, Frédéric Wurtz, and Seddik Bacha. Ancillary services and optimal household energy management with photovoltaic production. *Energy*, 35(1):55–64, 2010.
- [33] Mary E Clayton, Ashlynn S Stillwell, and Michael E Webber. Implementation of brackish groundwater desalination using wind-generated electricity: A case study of the energy-water nexus in Texas. *Sustainability*, 6(2):758–778, 2014.
- [34] Stefano Clò, Alessandra Cataldi, and Pietro Zoppoli. The merit-order effect in the Italian power market: The impact of solar and wind generation on national wholesale electricity prices. *Energy Policy*, 77:79–88, 2015.
- [35] David Connolly, Henrik Lund, Brian Vad Mathiesen, Emmanuel Pican, and Martin Leahy. The technical and economic implications of integrating fluctuating renewable energy using energy storage. *Renewable Energy*, 43:47–60, 2012.
- [36] Maria da Graça Carvalho. EU energy and climate change strategy. *Energy*, 40(1):19–22, 2012.

- [37] David Dallinger, Sct Gerda, and Martin Wietschel. Integration of intermittent renewable power supply using grid-connected vehicles—a 2030 case study for california and germany. *Applied Energy*, 104:666–682, 2013.
- [38] Thomas A Deetjen, Jared B Garrison, Joshua D Rhodes, and Michael E Webber. Solar PV integration cost variation due to array orientation and geographic location in the Electric Reliability Council of Texas. *Applied Energy*, 180:607–616, 2016.
- [39] Thomas A Deetjen, Henry Martin, Joshua D Rhodes, and Michael E Webber. Modeling the optimal mix and location of wind and solar with transmission and carbon pricing considerations. *Renewable Energy*, 120:35–50, 2018.
- [40] Thomas A. Deetjen, Andrew S. Reimers, and Michael E. Webber. Can storage reduce electricity consumption? a general equation for the grid-wide efficiency impacts of using cooling thermal energy storage for load shifting. *Environmental Research Letters*, (In press).
- [41] Thomas A Deetjen, Joshua D Rhodes, and Michael E Webber. The impacts of wind and solar on grid flexibility requirements in the electric reliability council of texas. *Energy*, 123:637–654, 2017.
- [42] Thomas A Deetjen, J Scott Vitter, Andrew S Reimers, and Michael E Webber. Optimal dispatch and equipment sizing of a residential central utility plant for improving rooftop solar integration. *Energy*, (In review).

- [43] Thomas A. Deetjen and Michael E. Webber. Costs associated with grid-level solar integration. In *2016 World Energy Engineering Congress Proceedings*. Association of Energy Engineers, 2016.
- [44] Paul Denholm and Maureen Hand. Grid flexibility and storage required to achieve very high penetration of variable renewable electricity. *Energy Policy*, 39(3):1817–1830, 2011.
- [45] Paul Denholm and R. M. Margolis. Supply curves for rooftop solar PV-generated electricity for the United States. *National Renewable Energy Laboratory (2008)*.
- [46] Paul Denholm and Robert M Margolis. Evaluating the limits of solar photovoltaics (PV) in traditional electric power systems. *Energy policy*, 35(5):2852–2861, 2007.
- [47] Nikolaos A Diangelakis and Efstratios N Pistikopoulos. A multi-scale energy systems engineering approach to residential combined heat and power systems. *Computers & Chemical Engineering (2016)*, 2016.
- [48] M. A. R. do Nascimento and et. al. Central energy plants. *Intech*, 2014.
- [49] Easan Drury, Paul Denholm, and Ramteen Sioshansi. The value of compressed air energy storage in energy and reserve markets. *Energy*, 36(8):4959–4973, aug 2011.

- [50] IM Dudurych, M Holly, and M Power. Integration of wind power generation in the irish grid. In *Power Engineering Society General Meeting, 2006. IEEE*, pages 8–pp. IEEE, 2006.
- [51] Mark Dyson and Amory Lovins. the grid needs a symphony, not a shouting match. *Rocky Mountain Institute*, 2017.
- [52] Eftekharnejad S. et. al. Impact of increased penetration of photovoltaic generation on power systems. *IEEE Transactions on Power Systems (2013)*, 2013.
- [53] Erik Ela. Impacts of solar power on operating reserve requirements. *National Renewable Energy Laboratory*, 2012.
- [54] Electric Reliability Council of Texas. 15 minute interval generation by fuel type for the ERCOT electric grid. *(2008-2014)*.
- [55] Electric Reliability Council of Texas. 2014 long-term system assessment for the ERCOT region. *(December 2014)*.
- [56] Electric Reliability Council of Texas. (august 2016). interview by thomas a. deetjen.
- [57] Electric Reliability Council of Texas. Ercot fundamentals training manual. *(2011)*.
- [58] Electric Reliability Council of Texas. Quick Facts 2016. *(2017)*.

- [59] Electric Reliability Council of Texas. ERCOT generation by resource type in 2016: Available via ERCOT dataport: <https://mis.ercot.com>. Accessed on April, 2017.
- [60] Evapco Inc. Thermal ice storage application & design guide. *Published by Evapco, Inc. (2007)*, 2007.
- [61] Robert L. Fares and Michael E. Webber. The impacts of storing solar energy in the home to reduce reliance on the utility. *Nature Energy*, 2:17001, 2017.
- [62] Ahmad Faruqui. A global perspective on time-varying rates. *The Brattle Group (2015)*, 2015.
- [63] Helder Lopes Ferreira, Raquel Garde, Gianluca Fulli, Wil Kling, and Joao Pecas Lopes. Characterisation of electrical energy storage technologies. *Energy*, 53:288–298, 2013.
- [64] Alessandro Franco and Pasquale Salza. Strategies for optimal penetration of intermittent renewables in complex energy systems based on techno-operational objectives. *Renewable energy*, 36(2):743–753, 2011.
- [65] Carlos J. Pereira Freitas. Evaluation of dynamic pass-through of carbon prices into electricity prices—a cointegrated vecm analysis. *International Journal of Public Policy* 14, 9(1-2):65–85, 2013.
- [66] Vasilis Fthenakis, James E Mason, and Ken Zweibel. The technical, geographical, and economic feasibility for solar energy to supply the energy needs of the US. *Energy Policy*, 37(2):387–399, 2009.

- [67] Ran Fu. U.S. solar photovoltaic system cost benchmark: Q1 2016. *National Renewable Energy Laboratory (2016)*.
- [68] Michaela Fürsch, Simeon Hagspiel, Cosima Jägemann, Stephan Nagl, Dietmar Lindenberger, and Eckehard Tröster. The role of grid extensions in a cost-efficient transformation of the european electricity system until 2050. *Applied Energy*, 104:642–652, 2013.
- [69] J B Garrison. A grid-level unit commitment assessment of high wind penetration and utilization of compressed air energy storage in ERCOT. *Ph.D. dissertation, The University of Texas at Austin (2014)*.
- [70] J B Garrison, S M Cohen, A K Townsend, and M E Webber. Development and benchmarking of a unit commitment model for a modern electricity market (Under review). *International Journal of Electric Power and Energy Systems*, 2015.
- [71] Gas Turbine World. 2014-2015 handbook. 2015.
- [72] GE Energy. Analysis of wind generation impact on ERCOT ancillary services requirements. *Prepared for the Electricity Reliability Council of Texas. Schenectady, New York: GE Energy (2008)*.
- [73] Stephen Gilette. Microturbine technology matures. *Power Magazine*, 2010.
- [74] Caroline Golin. A troubling trend in rate design: proposed rate design alternatives to harmful fixed charges. *Southern Environmental Law Center (2015)*, 2015.

- [75] Howard Gruenspecht. Renewable generation technologies: costs and market outlook. *US Energy Information Administration (2016)*.
- [76] Max Hall. German renewables pushing wholesale electricity further into negative territory. *PV Magazine (2015)*.
- [77] Ryan Hanna, Mohamed Ghonima, Jan Kleissl, George Tynan, and David G Victor. Evaluating business models for microgrids: Interactions of technology and policy. *Energy Policy*, 103:47–61, 2017.
- [78] He Hao, Yashen Lin, Anupama S Kowli, Prabir Barooah, and Sean Meyn. Ancillary service to the grid through control of fans in commercial building HVAC systems. *IEEE Transactions on Smart Grid*, 5(4):2066–2074, 2014.
- [79] Chioke Harris, Jeremy P Meyers, and Michael E Webber. A unit commitment study of the application of energy storage toward the integration of renewable generation. *Journal of Renewable and Sustainable Energy*, 4(1):013120, 2012.
- [80] William E Hart, Carl Laird, Jean-Paul Watson, and David L Woodruff. Pyomo optimization modeling in python. 67, 2012.
- [81] William E Hart, Jean-Paul Watson, and David L Woodruff. Pyomo: modeling and solving mathematical programs in python. *Mathematical Programming Computation*, 3(3):219–260, 2011.
- [82] A D Hawkes and M A Leach. Modelling high level system design and unit commitment for a microgrid. *Applied Energy*, 86(7):1253–1265, 2009.

- [83] Kent Hawkins. Evaluating wind impact (part ii - ramping). *MasterResource* (2016).
- [84] Dominik Heide, Martin Greiner, Lueder Von Bremen, and Clemens Hoffmann. Reduced storage and balancing needs in a fully renewable European power system with excess wind and solar power generation. *Renewable Energy*, 36(9):2515–2523, 2011.
- [85] Dominik Heide, Lueder Von Bremen, Martin Greiner, Clemens Hoffmann, Markus Speckmann, and Stefan Bofinger. Seasonal optimal mix of wind and solar power in a future, highly renewable Europe. *Renewable Energy*, 35(11):2483–2489, 2010.
- [86] Eric Hirst and Jeffrey Hild. The value of wind energy as a function of wind capacity. *The Electricity Journal*, 17(6):11–20, 2004.
- [87] Lion Hirth. The market value of variable renewables: The effect of solar wind power variability on their relative price. *Energy economics*, 38:218–236, 2013.
- [88] Lion Hirth. The optimal share of variable renewables: How the variability of wind and solar power affects their welfare-optimal deployment. *Energy Journal*, 36(1), 2015.
- [89] Lion Hirth, Falko Ueckerdt, and Ottmar Edenhofer. Integration costs revisited—an economic framework for wind and solar variability. *Renewable Energy*, 74:925–939, 2015.

- [90] Hannele Holttinen, Juha Kiviluoma, Ana Estanqueiro, Tobias Aigner, Yih-Huei Wan, and Michael Milligan. Variability of load and net load in case of large scale distributed wind power. In *10th International Workshop on Large-Scale Integration of Wind Power into Power Systems as well as on Transmission Networks for Offshore Wind Power Farms, August 2010.*, 2010.
- [91] Hannele Holttinen, Aidan Tuohy, Michael Milligan, Eamonn Lannoye, Vera Silva, Simon Mu, Lennart Söder, et al. The flexibility workout: managing variable resources and assessing the need for power system modification. *IEEE Power and Energy Magazine*, 11(6):53–62, 2013.
- [92] Matthias Hüber, Desislava Dimkova, and Thomas Hamacher. Integration of wind and solar power in Europe: Assessment of flexibility requirements. *Energy*, 69:236–246, 2014.
- [93] Matthias Huber, Thomas Hamacher, Christian Ziem, and Harald Weber. Combining LP and MIP approaches to model the impacts of renewable energy generation on individual thermal power plant operation. In *Power and Energy Society General Meeting (PES) (2013)*, pages 1–5. IEEE, 2013.
- [94] T. Hunt. Swansons law and making US solar scale like Germany. *Greentech Media: <https://www.greentechmedia.com/articles/read/Is-there-really-a-Swansons-Law> (2014)*, 2014.
- [95] Joss Hurford. How cool is this? ice storage systems. *Strang, Inc.*, 2013.
- [96] IBM. ILOG CPLEX optimizer (last 2010).

- [97] ICE-CEL. Integrated System Product Catalog: Available from: https://dbamericas.com/products/pdf/Integrated_System_Product_Catalog.pdf (Accessed on April, 2017).
- [98] International Energy Agency. PVPS report snapshot of global PV 1992-2013. *IEA-PVPS T1-24:2014*.
- [99] MS Ismail, M Moghavvemi, and TMI Mahlia. Design of an optimized photovoltaic and microturbine hybrid power system for a remote small community: case study of palestine. *Energy Conversion and Management*, 75:271–281, 2013.
- [100] Tryggvi Jonsson, Pierre Pinson, and Henrik Madsen. On the market impact of wind energy forecasts. *Energy Economics*, 32(2):313–320, 2010.
- [101] Paul L Joskow. Comparing the costs of intermittent and dispatchable electricity generating technologies. *The American Economic Review*, pages 238–241, 2011.
- [102] Willett Kempton and Jasna Tomić. Vehicle-to-grid power implementation: From stabilizing the grid to supporting large-scale renewable energy. *Journal of power sources*, 144(1):280–294, 2005.
- [103] B Shiva Kumar and K Sudhakar. Performance evaluation of 10 MW grid connected solar photovoltaic power plant in india. *Energy Reports*, 1:184–192, 2015.

- [104] S. Lacey. This is what the utility death spiral looks like. *Greentech Media*: <https://www.greentechmedia.com/articles/read/this-is-what-the-utility-death-spiral-looks-like> (2014), 2014.
- [105] Doerte Laing, WolfDieter Steinmann, Rainer Tamme, and Christoph Richter. Solid media thermal storage for parabolic trough power plants. *Solar energy*, 80(10):1283–1289, 2006.
- [106] Warren Lasher. The competitive renewable energy zones process. *ERCOT* (2014).
- [107] S Letendre, M Makhyoun, and M Taylor. Predicting solar power production: irradiance forecasting models, applications and future prospects. *Solar Electric Power Association, Tech. Rep*, 2014.
- [108] Wen Liu, Henrik Lund, Brian Vad Mathiesen, and Xiliang Zhang. Potential of renewable energy systems in china. *Applied Energy*, 88(2):518–525, 2011.
- [109] Y Liu, Jovan Bebic, B Kroposki, J De Bedout, and W Ren. Distribution system voltage performance analysis for high-penetration PV. In *Energy 2030 Conference, 2008. ENERGY 2008. IEEE*, pages 1–8. IEEE, 2008.
- [110] Patrick Luckow. 2015 carbon dioxide price forecast. *Synapse Energy Economics, Inc. (2015)*.
- [111] Henrik Lund. Renewable energy strategies for sustainable development. *Energy*, 32(6):912–919, 2007.

- [112] Henrik Lund and E Münster. Management of surplus electricity-production from a fluctuating renewable-energy source. *Applied Energy*, 76(1):65–74, 2003.
- [113] Peter D Lund, Juuso Lindgren, Jani Mikkola, and Jyri Salpakari. Review of energy system flexibility measures to enable high levels of variable renewable electricity. *Renewable and Sustainable Energy Reviews*, 45:785–807, 2015.
- [114] John MacCormack, Aidan Hollis, Hamidreza Zareipour, and William Rosehart. The large-scale integration of wind generation: Impacts on price, reliability and dispatchable conventional suppliers. *Energy Policy*, 38(7):3837–3846, 2010.
- [115] David MacPhee and Ibrahim Dincer. Performance assessment of some ice tes systems. *International Journal of Thermal Sciences*, 48(12):2288–2299, 2009.
- [116] Jim Malewitz. 7 billion CREZ project nears finish, aiding wind power. *The Texas Tribune (2013)*.
- [117] Leszek Malinowski and Monika Lewandowska. Analytical model-based energy and exergy analysis of a gas microturbine at part-load operation. *Applied Thermal Engineering*, 57(1):125–132, 2013.
- [118] R. Matulka. Energy saver 101 infographic: Home cooling. *Department of Energy*. Available at <https://energy.gov/articles/energy-saver-101-infographic-home-cooling> (2014), 2014.
- [119] Paul Meister, Haiping Jia, Jie Li, Richard Kloepsch, Martin Winter, and Tobias Placke. Best practice: performance and cost evaluation of lithium ion battery

- active materials with special emphasis on energy efficiency. *Chemistry of Materials*, 28(20):7203–7217, 2016.
- [120] Esther Mengelkamp, Johannes Garttner, and Christof Weinhardt. The role of energy storage in local energy markets. In *European Energy Market (EEM), 2017 14th International Conference on the*, pages 1–6. IEEE, 2017.
- [121] Christian Milan, Michael Stadler, Gonçalo Cardoso, and Salman Mashayekh. Modeling of non-linear chp efficiency curves in distributed energy systems. *Applied Energy*, 148:334–347, 2015.
- [122] Sumit Mitra, Lige Sun, and Ignacio E Grossmann. Optimal scheduling of industrial combined heat and power plants under time-sensitive electricity prices. *Energy*, 54:194–211, 2013.
- [123] Christopher Mone. 2014 cost of wind energy review. *National Renewable Energy Laboratory (2014)*.
- [124] Pedro S Moura and Anibal T De Almeida. The role of demand-side management in the grid integration of wind power. *Applied Energy*, 87(8):2581–2588, 2010.
- [125] M. Munsell. US solar growth continues: 1.3 gigawatts of PV installed in Q3. *Greentech Media: <http://www.greentechmedia.com/articles/read/growth-spurt>* (2014), 2014.
- [126] Ramez Naguib. Total cost of ownership for air-cooled and water-cooled chiller systems. *ASHRAE(2009)*, 2009.

- [127] National Renewable Energy Laboratory. System Advisor Model. Available from <https://sam.nrel.gov/>.
- [128] National Renewable Energy Laboratory. Texas Wind and Solar Resource Maps. Available from <http://www.nrel.gov/gis/mapsearch/>. Accessed on December, 2016.
- [129] National Renewable Energy Laboratory. PVWatts®Calculator. Available from <http://pvwatts.nrel.gov/>. Accessed on May, 2015.
- [130] National Renewable Energy Laboratory. National Solar Radiation Database. Available from <https://nsrdb.nrel.gov/>. Accessed on May, 2016.
- [131] National Renewable Energy Laboratory. Annual Technology Baseline. Available from <https://atb.nrel.gov/electricity/2017/>. Accessed on October, 2017.
- [132] Newcomb and Boyd. Central energy plants. *Newcomb and Boyd Consultants and Engineers: available at <http://www.newcomb-boyd.com/solutions/central-energy-plants/>*, 2017.
- [133] Marco Nicolosi. Wind power integration and power system flexibility—an empirical analysis of extreme events in Germany under the new negative price regime. *Energy Policy*, 38(11):7257–7268, 2010.
- [134] Marco Nicolosi and Michaela Fürsch. The impact of an increasing share of RES-E on the conventional power market—the example of Germany. *Zeitschrift für Energiewirtschaft*, 33(3):246–254, 2009.

- [135] Public Utility Commission of Texas. Generic transmission and distribution rates: Centerpoint - docket 38339/41072 transmission charge. *Available from: <http://www.puc.texas.gov/industry/electric/rates/Trans/TDGenericRateSummary.pdf>*, 2016.
- [136] Abigail D Ondeck, Thomas F Edgar, and Michael Baldea. Optimal operation of a residential district-level combined photovoltaic/natural gas power and cooling system. *Applied Energy*, 156:593–606, 2015.
- [137] L. Ortiz and R. Manghani. Grid-scale energy storage balance of systems 2015-2020 architectures, costs and players. *GTM Research*, 2016.
- [138] Pacific Northwest National Laboratory. Thermal energy storage for space cooling. *produced for the US Department of Energy (2000)*, 2000.
- [139] Peter Palensky and Dietmar Dietrich. Demand side management: Demand response, intelligent energy systems, and smart loads. *IEEE transactions on industrial informatics*, 7(3):381–388, 2011.
- [140] NL Panwar, SC Kaushik, and Surendra Kothari. Role of renewable energy sources in environmental protection: a review. *Renewable and Sustainable Energy Reviews*, 15(3):1513–1524, 2011.
- [141] Paratus Rentals (2007). Quick reference for efficient chiller system design. 2007.
- [142] Pecan Street Incorporated. Pecan Street Dataport: Available from <https://dataport.pecanstreet.org>. Accessed on October, 2016.

- [143] André Pina, Carlos Silva, and Paulo Ferrão. The impact of demand side management strategies in the penetration of renewable electricity. *Energy*, 41(1):128–137, 2012.
- [144] Ryan Pletka. Capital costs for transmission and substations. *Western Electricity Coordinating Council (2014)*.
- [145] Cameron W Potter, Allison Archambault, and Kenneth Westrick. Building a smarter smart grid through better renewable energy information. In *Power Systems Conference and Exposition, 2009. PSCE'09. IEEE/PES*, pages 1–5. IEEE, 2009.
- [146] Kody M Powell, Wesley J Cole, Udememfon F Ekarika, and Thomas F Edgar. Optimal chiller loading in a district cooling system with thermal energy storage. *Energy*, 50:445–453, 2013.
- [147] Python Software Foundation. Python language reference, version 2.7. available at <http://www.python.org>.
- [148] Daniel Querejazu. Carbon pricing around the world. *The Environmental and Energy Study Institute (2012)*.
- [149] R. Searcy. New pilot program offers incentives to reduce electric use during summer peaks, Electric Reliability Council of Texas Press Release. March 25, 2015.

- [150] T. Randall. No one saw Tesla's solar roof coming. *Bloomberg Technology*: <https://www.bloomberg.com/news/articles/2016-10-31/no-one-saw-tesla-s-solar-roof-coming> (2016), 2016.
- [151] Hongbo Ren, Qiong Wu, Weijun Gao, and Weisheng Zhou. Optimal operation of a grid-connected hybrid PV/fuel cell/battery energy system for residential applications. *Energy*, 113:702–712, 2016.
- [152] Zhenggen Ren, George Grozev, and Andrew Higgins. Modelling impact of PV battery systems on energy consumption and bill savings of australian houses under alternative tariff structures. *Renewable Energy*, 89:317–330, 2016.
- [153] Joshua D Rhodes, Charles R Upshaw, Wesley J Cole, Chris L Holcomb, and Michael E Webber. A multi-objective assessment of the effect of solar PV array orientation and tilt on energy production and system economics. *Solar Energy*, 108:28–40, 2014.
- [154] Joshua D Rhodes, Charles R Upshaw, Chioke B Harris, Colin M Meehan, David A Walling, Paul A Navrátil, Ariane L Beck, Kazunori Nagasawa, Robert L Fares, Wesley J Cole, et al. Experimental and data collection methods for a large-scale smart grid deployment: Methods and first results. *Energy*, 65:462–471, 2014.
- [155] Amy Rose, Robert Stoner, and Ignacio Pérez-Arriaga. Prospects for grid-connected solar pv in kenya: A systems approach. *Applied Energy*, 161:583–590, 2016.

- [156] Ian H Rowlands, Briana Paige Kemery, and Ian Beausoleil-Morrison. Optimal solar-PV tilt angle and azimuth: An Ontario (Canada) case-study. *Energy Policy*, 39(3):1397–1409, 2011.
- [157] RS Means Company. *Mechanical cost data*, volume 39. 2016.
- [158] Suresh B Sadineni, Fady Atallah, and Robert F Boehm. Impact of roof integrated PV orientation on the residential electricity peak demand. *Applied Energy*, 92:204–210, 2012.
- [159] Katrin Schaber, Florian Steinke, and Thomas Hamacher. Transmission grid extensions for the integration of variable renewable energies in Europe: Who benefits where? *Energy Policy*, 43:123–135, 2012.
- [160] Katrin Schaber, Florian Steinke, Pascal Mühlich, and Thomas Hamacher. Parametric study of variable renewable energy integration in Europe: Advantages and costs of transmission grid extensions. *Energy Policy*, 42:498–508, 2012.
- [161] Frank Sensfuss, Mario Ragwitz, and Massimo Genoese. The merit-order effect: A detailed analysis of the price effect of renewable electricity generation on spot market prices in Germany. *Energy policy*, 36(8):3086–3094, 2008.
- [162] Kyle Siler-Evans, M Granger Morgan, and Inês Lima Azevedo. Distributed cogeneration for commercial buildings: Can we make the economics work? *Energy Policy*, 42:580–590, 2012.

- [163] Sunanda Sinha and SS Chandel. Review of recent trends in optimization techniques for solar photovoltaic–wind based hybrid energy systems. *Renewable and Sustainable Energy Reviews*, 50:755–769, 2015.
- [164] Ramteen Sioshansi and Walter Short. Evaluating the impacts of real-time pricing on the usage of wind generation. *IEEE Transactions on Power Systems*, 24(2):516–524, 2009.
- [165] Paul K. Skoglund. Deltapvalue system design manual. *Published by Flow Control Industries, Inc. (2015)*, 2015.
- [166] Smith J.W. et. al. Smart inverter volt/var control functions for high penetration of PV on distribution systems. *IEEE (2011)*, 2011.
- [167] P Sreedharan, J Farbes, E Cutter, CK Woo, and J Wang. Microgrid and renewable generation integration: University of california, san diego. *Applied Energy*, 169:709–720, 2016.
- [168] Goran Strbac. Demand side management: Benefits and challenges. *Energy policy*, 36(12):4419–4426, 2008.
- [169] Daniel Tenfen and Erlon Cristian Finardi. A mixed integer linear programming model for the energy management problem of microgrids. *Electric Power Systems Research*, 122:19–28, 2015.
- [170] The University of Texas at Austin Energy Institute. LCOE calculator with environmental costs. Available from <https://nsrdb.nrel.gov/>. Accessed on December, 2016.

- [171] Herman K. Trabish. Beyond TOU: Is more dynamic pricing the future of rate design? *Utility Dive*: <http://www.utilitydive.com/news/beyond-tou-is-more-dynamic-pricing-the-future-of-rate-design/447171/> (2017), 2017.
- [172] Trane Corporation. Ice-enhanced air-cooled chiller plant: an earthwise system from trane. 2011.
- [173] Trane Corporation. Trane TRACE 700 software with chiller performance curves: Available from <http://www.trane.com/commercial/north-america/us/en/products-systems/design-and-analysis-tools/analysis-tools/trace-700.html>. Accessed on April, 2017.
- [174] Niamh Troy, Eleanor Denny, and Mark O'Malley. Base-load cycling on a system with significant wind penetration. *IEEE Transactions on Power Systems*, 25(2):1088–1097, 2010.
- [175] David P Tuttle and Kara M Kockelman. Electrified vehicle technology trends, infrastructure implications, and cost comparisons. In *Journal of the Transportation Research Forum*, volume 51, 2012.
- [176] Katherine Tweed. California's fowl problem: 10 ways to address the renewable duck curve. *Greentech Media* (2014).
- [177] Katherine Tweed. Texas to overhaul its grid-balancing services with energy storage. *Greentech Media* (2014).
- [178] US Energy Information Administration. Electric Power Monthly, table 5.4b. 2017.

- [179] US Energy Information Administration. Electric Power Monthly, table 5.6a. 2017.
- [180] US Energy Information Administration. Henry Hub Natural Gas Spot Price. Available from: <https://www.eia.gov/dnav/ng/hist/rngwhhdm.htm>. 2017.
- [181] US Energy Information Administration. How much carbon dioxide is produced when different fuels are burned? 2017.
- [182] Thijs van der Klauw, Gerwin Hoogsteen, Marco ET Gerards, Johann L Hurink, Xianyong Feng, and Robert E Hebner. Assessing the potential of residential hvac systems for demand-side management. In *Innovative Smart Grid Technologies Conference (ISGT), 2016 IEEE Power & Energy Society*, pages 1–5. IEEE, 2016.
- [183] M Wagh and V Kulkarni. Modeling and optimization of integration of renewable energy resources (RER) for minimum energy cost, minimum CO₂ emissions and sustainable development, in recent years: A review. *Proceedings for the International Conference on Processing of Materials, Minerals and Energy*, 2016.
- [184] Adrian Wals. How will a CO₂ price affect the playing field in the northwest european power sector? *Research Symposium European Electricity Markets (2003)*.
- [185] Yih-huei Wan. Analysis of wind power ramping behavior in ERCOT. *Contract*, 303:275–3000, 2011.

- [186] Weather Underground. Weather history for katt: Available from <https://www.wunderground.com/cgi-bin/findweather/getforecast?query=katt>. Accessed on October, 2016.
- [187] Xiupeng Wei, Guanglin Xu, and Andrew Kusiak. Modeling and optimization of a chiller plant. *Energy*, 73:898–907, 2014.
- [188] Joakim Widén. Correlations between large-scale solar and wind power in a future scenario for Sweden. *IEEE transactions on sustainable energy*, 2(2):177–184, 2011.
- [189] David M Wogan, Michael E Webber, and Alexandre K da Silva. A framework and methodology for reporting geographically and temporally resolved solar: A case study of Texas. *Renewable and Sustainable Energy*, 2(5):053107, 2010.
- [190] C Woo, I Horowitz, J Moore, and A Pacheco. The impact of wind generation on the electricity spot-market price level and variance: The Texas experience. *Energy Policy*, 39(7):3939–3944, 2011.
- [191] Tiffany Wu. EPA’s valuation of environmental externalities from electricity production. *The University of Texas at Austin Energy Institute (2016)*.
- [192] Zhiqin Zhang, William D Turner, Qiang Chen, Chen Xu, and Song Deng. Tank size and operating strategy optimization of a stratified chilled water storage system. *Applied Thermal Engineering*, 31(14):2656–2664, 2011.

- [193] Wei Zhou, Chengzhi Lou, Zhongshi Li, Lin Lu, and Hongxing Yang. Current status of research on optimum sizing of stand-alone hybrid solar–wind power generation systems. *Applied Energy*, 87(2):380–389, 2010.